Fall 2013

Structural and Functional Characterization of the Endosome-associated Deubiquitinating Enzyme AMSH

Christopher Williamson Davies
Purdue University

Graduate School ETD Form 9
(Revised 12/07)

PURDUE UNIVERSITY
GRADUATE SCHOOL
Thesis/Dissertation Acceptance

This is to certify that the thesis/dissertation prepared

By Christopher W. Davies

Entitled STRUCTURAL AND FUNCTIONAL CHARACTERIZATION OF THE ENDOSOME-ASSOCIATED DEUBIQUITINATING ENZYME AMSH

For the degree of Doctor of Philosophy

Is approved by the final examining committee:

Chittaranjan Das
Chair

Suzanne Bart

Philip Low

Cynthia Stauffacher

To the best of my knowledge and as understood by the student in the *Research Integrity and Copyright Disclaimer (Graduate School Form 20)*, this thesis/dissertation adheres to the provisions of Purdue University's "Policy on Integrity in Research" and the use of copyrighted material.

Approved by Major Professor(s): Chittaranjan Das

Approved by: R. E. Wild 9/05/2013
Head of the Graduate Program Date

STRUCTURAL AND FUNCTIONAL CHARACTERIZATION OF THE ENDOSOME-ASSOCIATED DEUBIQUITINATING ENZYME AMSH

A Dissertation

Submitted to the Faculty

of

Purdue University

by

Christopher W. Davies

In partial Fulfillment of the

Requirements of the Degree

of

Doctor of Philosophy

December 2013

Purdue University

West Lafayette, Indiana

To My Family

ACKNOWLEDGMENTS

To YOUR spoken WORD through Pastor John:

There is a great influence in the place He's taking you. Lean on that influence as you continue to learn and grow. You may have to risk everything that He has brought to you at this point. As He leads you and guides you by His Spirit in your heart you will have peace. When you make that step, you will see the treasure like you've never seen them before. Progression by faith. You are about to have to take another step. Do what God asks you to do when He asks you to. Step out; His hand will be there. The Kingdom of God will be yours. He will provide and make a way for you. Opportunity will chase you. He will cause those things that others chase after to chase you. You will have an opportunity to speak, you will have opportunity to share, opportunity to enlighten. You will have wisdom and knowledge beyond your years, ability, and it will all come from the Spirit and throne room of God, and He will pour it out to a vessel who says, "I will buy the whole field!" As you put your heart toward the Kingdom of God, He will unfold all those things for you in your life. (Pastor John 2/12/12)

TABLE OF CONTENTS

Page

Page

LIST OF TABLES

LIST OF FIGURES

Figure Page

ABSTRACT

Davies, Christopher W. Ph.D., Purdue University, December 2013. Structural and Functional Characterization of the Endosome-Associated Deubiquitinating Enzyme AMSH. Major Professor: Chittaranjan Das.

The endosomal sorting complexes required for transport (ESCRT) machinery is a ubiquitin-dependent molecular mechanism made of up of four individual complexes: ESCRT-0, -I, -II, III, that is necessary for regulating the degradation of cell surface receptors directed towards the lysosome. Not only are the ESCRTs implicated in endosomal sorting and trafficking of proteins, its members also have roles in other important biological processes such as: cytokinesis, HIV budding, transcriptional regulation, and autophagy. As a function of its involvement in several processes throughout the cell, the ESCRT machinery is implicated in a wide variety of diseases including cancer, neurological disease, bacterial infections, cardiovascular disease, and retroviral infection. Proteins marked for lysosomal degradation (cargo) are first ubiquitinated, and then, shuttled in a sequential mechanism through the complexes. In the last step, ubiquitin is removed from the cargo, which is subsequently encapsulated into intralumenal vesicles (ILV) that will ultimately be transported to and fuse with lysosome, degrading and recycling its contents. Deubiquitination is the removal of

ubiquitin, catalyzed by deubiquitinating enzymes (DUBs). The human ESCRT machinery recruits two DUBs: AMSH (associated molecule with a Src homology 3 (SH3) domain of signal transducing adaptor molecule (STAM) or simply, STAM-binding protein (STAMBP)), and UBPY/USP8 (ubiquitin specific protease 8). Both AMSH and USP8 have the same ESCRT-recognition domains facilitating recruitment to ESCRT-0 and ESCRT-III. The *Saccharmyces cerevisiae* (*S. cerevisiae*) version of the ESCRT complex employs only one DUB, Doa4 (degradation of alpha 4) that serves to recycle ubiquitin at ESCRT-III, just prior to ILV formation. Therefore, it is not fully understood why the human ESCRT system requires the function of both AMSH and USP8.

The focus of this thesis is to understand the role of AMSH recruitment at ESCRT-0 with hopes of providing further insight into its role within the ESCRT complex. In doing so, I crystallized and determined the structure of catalytic domain of AMSH. Using this structure, I structurally and thermodynamically compared AMSH to the homologous protein, AMSH-LP. Secondly, I characterized AMSH kinetically by introducing individual point mutations within the catalytic domain and carried out a detailed kinetic analysis to understand the catalytic mechanism of AMSH. Finally, using a combination of biophysical and biochemical experiments, I investigated how AMSH is recruited and recognized at ESCRT-0. My studies show that AMSH is structurally identical to AMSH-LP, however, thermodynamically less stable. Also, AMSH has exquisite specificity for Lys63-linked ubiquitin chains because it recognizes a three-residue sequence within its proximal ubiquitin-binding site. Furthermore, two residues within the distal ubiquitin-binding site (Thr313 and Glu316) play significant roles within AMSH's catalytic mechanism, one of which, Thr313, is mutated to Ile in children with microcephaly

capillary malformation (MIC-CAP) syndrome. Finally, I proposed a mechanism for how the activity of AMSH is stimulated at ESCRT-0 in which the proximal ubiquitin is held by the ubiquitin-interacting motif (UIM) from STAM (ESCRT-0), while the enzyme holds the distal ubiquitin, thus stabilizing the chain, enhancing the enzyme's activity. From this mechanism, I assigned a role for AMSH at ESCRT-0 in which the enzyme facilitates the transfer of cargo from ESCRT-0 to the subsequent complexes. These data taken together further supports that AMSH has an important, specific, and non-redundant function within the ESCRT machinery.

CHAPTER 1: INTRODUCTION

1.1 Ubiquitin and Ubiquitination

Ubiquitination is a highly dynamic post-translational modification within the cell that is conserved in eukaryotes. Ubiquitin is a small, basic protein, that is widely known to be used for directing proteins to the 26S proteasome for degradation (Figure 1.1).[1] Several studies now have shown that ubiquitin modification serve several other processes as well including: DNA repair, endosomal sorting, and protein signaling.[2] Ubiquitination is an energy-dependent process occurring by the action of three classes of enzymes termed E1, E2, and E3 (Figure 1.2).[3; 4; 5] E1s are ubiquitin-activating enzymes, E2s are ubiquitin-conjugating enzymes, and E3s are ubiquitin ligase enzymes.[3; 4; 5] These three enzyme classes in tandem can form a single ubiquitin moiety attached directly to a protein via an isopeptide bond (lysine of the target protein is covalently attached to the C-terminal glycine of ubiquitin), or polymeric chains of ubiquitin attached directly to protein targets.[1] Polymeric chains of ubiquitin are formed from one of the seven lysine residues from ubiquitin (6, 11, 27, 29, 33, 48, and 63), or the N-terminal methionine amine group forming linear ubiquitin chains, all of which have been detected in cells (Figure 1.1).[2; 6; 7] The complexity of ubiquitination has greatly increased in the recent years. Ubiquitin chains can be in the form of monoubiquitin, multi-monoubiquitination, homogenous linkages, mixed ubiquitin linkages, and finally, branched ubiquitin chains.[2]

Increasing complexity occurs with the different linkages and their roles within the cell. Lys48 is the most abundant ubiquitin linkage found in cells,[6; 7] and it is known as a degradation signal by the 26S proteasome.[1] Lys63 is the next most characterized ubiquitin linkage, directing cell surface receptors for degradation by the lysosome.[8] Other roles for Lys63 chains include DNA damage repair[9; 10; 11] and proteasomal degradation.[12; 13] Lys11 linkages have emerging roles as a proteasomal target, largely because Lys11 linked ubiquitin have been shown to bind proteasomal receptors and causes cell cycle regulators to be degraded during mitosis.[14; 15; 16] Lys29 is implicated in substrate turnover within the ubiquitin-fusion degradation pathway.[2] Linear ubiquitin chains are involved in regulation of protein activity as done by LUBAC (linear ubiquitin chain assembly complex).[17] Little is known about the physiological relevance of the four remaining ubiquitin linkages: Lys6, Lys27, Lys29, and Lys33.

1.2 Deubiquitination and Deubiquitinating Enzymes

Deubiquitination, carried out by deubiquitinating enzymes (DUBs), opposes the activity of E3 ligases (Figure 1.2).[18] The human genome codes for ~90 DUBs, of which, 79 are predicted to be active.[18; 19; 20; 21] DUB activity is categorized into three functions: (1) to generate free ubiquitin from the linear fusion of multiple ubiquitin moieties after translation, (2) to reverse the post-translational modification of proteins by ubiquitin, promoting protein stability or to recycle ubiquitin, maintaining the cellular pool of ubiquitin, and (3) to edit the form of ubiquitin modification by trimming ubiquitin chains.[19] DUBs have an important role in ubiquitin regulation because de-regulation of DUB activity is implicated in hereditary cancer, inflammation, immune response, and

neurodegenerative disorders; the current trend is to regulate DUB activity by targeted design of pharmacological therapeutics.[18; 21]

There are five subclasses of DUBs: Ubiquitin C-terminal Hydrolases (UCH), Ubiquitin Specific Proteases (USPs), Machado-Joseph Disease Domain Proteases (MJDs), Ovarian Tumor Proteases (OTUs), and JAB1/MPN/Mov34 metalloproteases (JAMM).[18] Of the five classes of DUBs, all are cysteine proteases except the JAMM family, which are zinc metalloproteases.[18] The USP family is the largest with 56 individual members, with another 11 from the UPS17 multigene family,[22] OTU family has 15 members, the JAMM family has 8 members, and then, the UCH and MJD families each have 4 members.[18; 19; 21]

Just as ubiquitination is implicated in a wide variety of roles throughout the cell, deubiquitination is just as complex. The specificity of DUBs can be determined by sub-cellular localization, specific binding interactions, or the preference for a specific ubiquitin chain linkage.[20] Increasing functions for DUBs have been found throughout the cell; cytosolic functions such as endosomal trafficking, organelle-specific functions as seen in the mitochondria, Golgi, and endoplasmic reticulum (ER), and the nucleus.[20] DUBs bind E3 ligases, regulating E3 autoubiquitination, allowing the E3 to regulate the target and its DUB simultaneously, or confering specificity to the DUB.[18] The diversity in the ubiquitin linkages bring about the diversity in DUB linkage specificities, anywhere from recognition of a specific type of isopeptide bond to linkage promiscuity, all of which has been extensively reviewed previously.[21]

1.3 ESCRT Complex

The endosomal sorting complexes required for transport (ESCRT) is a multi-subunit machinery that is an essential part of the multivesicular body (MVB) pathway in which cargo is sequestered and sorted into endosomal membranes to create MVBs (Figure 1.3).[23; 24] The ESCRT complex was initially discovered in yeast as a part of the vacuolar protein-sorting (vps) mutants, which were unable to deliver proteins to the vacuole.[23] 13 of 46 vps mutants (class E) lacked the ability to deliver membrane proteins to the vacuole, giving rise to the discovery in 2001 of ESCRT-I (the second ESCRT complex) resulting from biochemical characterization of those vps mutants.[23; 24] The ESCRT machinery is a ubiquitin-dependent entity that is involved in several cellular processes including endosomal sorting, endosomal trafficking, viral budding, cytokinesis, transcriptional regulation, and autophagy.[25] As a function of its involvement in several processes throughout the cell, the ESCRT machinery is implicated in a wide variety of diseases including cancer, neurological disease, bacterial infections, cardiovascular disease, and retroviral infection.[26; 27] The ESCRT machinery is subdivided into four complexes: ESCRT-0, -I, -II, -III, that work in a sequential mechanism to sort membrane proteins to the lysosome (vacuole in yeast),[24] other cellular process do not require all four of the complexes to carry out its function.

1.3.1 ESCRT-0

ESCRT-0, the initial ESCRT complex, was not originally classified as a member of the ESCRT complexes; studies later showed that it should be considered apart of the ESCRT machinery.[8; 28; 29; 30] Of all the ESCRTs, ESCRT-0 is the least conserved, not

found in plants and protists, but yet, the ESCRT-dependent MVB pathway for protein degradation is still functional.[8; 23] ESCRT-0 consists of two subunits, hepatocyte growth factor-regulated tyrosine kinase substrate (Hrs) and signal transducing adaptor molecule (STAM) (Vps27 and Hse1 in yeast respectively) (Figure 1.4).[8; 23; 24; 31] Hrs/STAM form a 1:1 heterodimer that localizes to the endosomal membrane via the Hrs Fab1/YOTB/Vac1/EEA1 (FYVE) domain that specifically recognizes phosphatidylinositol 3-phosphate (PI3P).[8; 24; 31; 32; 33] *In vivo*, Hrs/STAM aggregate at the endosomal membrane, forming a stable 2:2 heterotetramer.[32] Giant unilamellar vesicles followed by fluorescent probes showed that ESCRT-0 serves to cluster ubiquitinated cargo at the membrane, supporting the aggregation event seen previously.[34] The stoichiometry of ESCRT-0 becomes important in its ubiquitin binding capabilities. Hrs alone has a VHS (Vps27/Hrs/STAM) domain and a double-sided ubiquitin-interacting motif (DUIM); STAM has its own VHS domain and a UIM, thus, the complete ESCRT-0 has five ubiquitin binding domains (UBDs).[23; 31; 32; 35] Therefore, if ESCRT-0 has five UBDs, the heterotetramer that forms on the endosomal membrane should theoretically bind up to ten ubiquitin moieties simultaneously, especially since it has been shown that ubiquitin chains bind cooperatively at ESCRT-0.[35] However, there are discrepancies in literature over the accepted amount of ubiquitin moieties that bind at ESCRT-0. Mayers *et al.* stated that the ESCRT-0 heterodimer has the capacity to bind four ubiquitin molecules, and their model suggests that the heterotetramer will bind eight ubiquitin molecules once localized to the membrane.[32] Ren *et al.* did detect ubiquitin binding by the VHS domain of Hrs, but, were surprised by its low affinity.[35] Now adding the VHS domain from Hrs, ESCRT-0 will cooperatively bind 10 ubiquitin moieties at the

membrane as first hypothesized. Recently, Lange *et al.* found that the SH3 domain of STAM specifically and independently binds ubiquitin.[36] With the addition of these new data, ESCRT-0 would have six UBDs, which when localizes to the membrane, forming the heterotetramer, would simultaneously bind 12 ubiquitin moieties.

1.3.2 ESCRT-I

ESCRT-I is recruited to the membrane by direct interaction with ESCRT-0 via the PSAP-like motif from Hrs to ubiquitin E2 variant (UEV) domain of ESCRT-I member, Tsg101 (Vps23 in yeast).[8; 23; 24] The ESCRT-I core is made up of a heterotetrameric complex in a 1:1:1:1 ratio of Tsg101, Vps28, Vps37 (A, B, C), and Mvb12 (A, B) or ubiquitin-associated protein 1 (UBAP1) (Vps23, Vps28, Vps37, and Mvb12 in yeast).[8; 23; 24; 37; 38] The x-ray crystal structure of the core ESCRT-I has been determined, revealing an asymmetric complex that spans 18 nm in length and consists of a headpiece attached to a 13 nm stalk (Figure 1.5).[38] Further structural characterization of ESCRT-I using a combination of small angle X-ray scattering (SAXS) and double electron-electron resonance spectroscopy (DEER), circumventing the issues of crystallizing the entire ESCRT-I due to flexibility, showed that ESCRT-I adopts equal populations of a closed and open conformation in solution.[37]

Like ESCRT-0, ESCRT-I binds ubiquitin using the UEV domain of Tsg101, thus facilitating the passage of ubiquitinated cargo from ESCRT-0 to ESCRT-I.[37] Structural characterization of UBAP1 revealed another ESCRT-I UBD.[39] The ubiquitin-association (UBA) domain within UBAP1 binds ubiquitin with a K_D of 70 μM; an intact ESCRT-I

with full-length UBAP1 and Tsg101 (UEV domain deleted to measure ubiquitin binding by simply the UBA domain of UBAP1) showed an apparent K_D of 140 μM.[39] Lys63-linked diubiquitin binds to the UBA domain with a similar affinity as ubiquitin.[39] Taken together, ESCRT-I can bind a minimum of two ubiquitin moieties. [23] No data has shown if ubiquitin binds cooperatively as was seen at ESCRT-0.[35] ESCRT-I works in tandem with ESCRT-II to induce bud formation, confining the cargo within the nascent bud.[34] Not only is ESCRT-I necessary for MVB biogenesis, it adopts important roles in HIV-1 budding from infected cells and midbody localization in cytokinesis.[40; 41; 42; 43; 44; 45]

1.3.3 ESCRT-II

ESCRT-II is composed of EAP30 (ELL-associated protein of 30kDa), EAP45, and two molecules of EAP20 (Vps22, Vps36, and Vps25 in yeast, respectively) forming a 'Y' shaped complex where EAP30 and EAP45 form the base, each bound by one copy of EAP20, which are the branches (Figure 1.6).[46; 47] ESCRT-II recruitment to the membrane is a result of ESCRT-I; recruitment of ESCRT-II by ESCRT-I is well characterized in yeast, but poorly understood in mammals. In yeast, the GLUE (GRAM-like ubiquitin-binding in EAP45) domain of Vps36 binds with nanomolar affinity to the C-terminus of Vps28.[24; 48] The yeast Vps36 GLUE domain has two Npl4 type zinc finger (NZF) domains, one binds to Vps28 (ESCRT-I), and the other binds ubiquitin.[48] Human EAP45 retains the GLUE domain, without the NZF domains. Therefore, the GLUE domain has the ability to bind ubiquitin, but not much is understood about the ESCRT-I binding.[24] A study probed ESCRT-I-II binding in humans and found that residues 149-169 within

EAP45 (VPS36, nomenclature used in publication) is necessary, but not sufficient for binding to Vps28 (ESCRT-I), suggesting that there maybe more than one point of contact between ESCRT-I and II.[49]

As stated previously, ESCRT-I and II work together to deform and stabilize bud necks in which cargo is confined.[34] This localization and deformation of the membrane is further supported by the ability of ESCRT-II to bind with high affinity to PI3P via the GLUE domain, similar to the FYVE domain of ESCRT-0.[24] Structural insight into this mechanism of how ESCRT-I and II working together to deform membranes was provided in a study that combined solution data from SAXS, DEER, and small-molecule Forster resonance energy transfer (smFRET).[50] It was found that the ESCRT-I-II supercomplex forms a crescent shape, which is common for proteins that work at the membrane to induce curvature.[50; 51] This study has provided a structural basis for the mechanism of cargo transfer within MVB biogenesis.[50]

1.3.4 ESCRT-III

ESCRT-III, the final ESCRT member, catalyzes the scission of the bud necks created by ESCRT-I and II, creating intralumenal vesicles (ILVs) that will ultimately fuse with the lysosome (vacuole in yeast) for degradation.[52] Unlike the previous three ESCRT complexes, ESCRT-III does not exist as a pre-formed complex in the cytosol; its members exist in an autoinhibited form prior to its polymerization on the endosomal membrane.[23; 24; 53; 54] ESCRT-II member, Vps25, binds directly to Vps20, initiating recruitment of ESCRT-III proteins in yeast.[8; 24] Subsequently, Vps20 promotes the

sequential recruitment of Snf7, building the main polymer consisting of Vps24 and Vps2, which together cap the polymer and control disassembly.[55; 56; 57] Snf7 is the component with the highest stoichiometry of all the ESCRT-III proteins, and has been found to be absolutely necessary for membrane severing.[58] Recently, a study elucidated Snf7 mechanism of activation in which it exists in its inactive "closed" state in solution, and then, Vps20 gets activated, causing a movement of helix 5 and linker region away from the core domain of Snf7, facilitating interaction with the membrane and downstream ESCRT-III subunits.[59] In humans however, the ESCRT-III complex expands to include 12 members, termed charged multivesicular body proteins (CHMPs).[57; 58; 60] CHMPs have the potential to form analogous complexes to that of yeast using CHMP6 (Vps20), one of three isoforms of Snf7 (CHMP4 A, B, or C), CHMP3 (Vps24) (Figure 1.7), and finally, one of two isoforms of Vps2 (CHMP2 A or B).[58; 60] There are also other CHMPs that serve regulatory roles within ESCRT-III including: two isoforms of CHMP1 (A and B, Vps46 in yeast), CHMP5 (Vps60 in yeast), CHMP7 (no yeast homologue), and increased sodium tolerance-1 (IST-1, Ist-1 in yeast).[58; 60]

Research has been done and models have been proposed attempting to elucidate how ESCRT-III catalyzes membrane scission, forming ILVs. When the four yeast ESCRT-III subunits were added at submicromolar levels in their correct order, ILV formation was observed. However, the activity was less active compared to when a mutant of Vps20 was added in which the C-terminus was deleted, supporting the autoinhibited nature of the subunits prior to membrane localization.[52] Further studies showed that efficient ILV formation and detachment requires the activated from of Vps20, Snf7, and Vps24, but also, lipid composition has some importance to ILV

formation.[52] Several models were proposed as a result of these studies. One model suggests that the ESCRT-III proteins make filaments that form an inward-directed curvature, resulting in its constrictive force.[56] Another model speculates that the ATPase Vps4 plays an important role by remodeling the ESCRT-III components once filament spirals are formed.[56] A third possibility for membrane cleavage could be due to the lipid composition, stabilized by the ESCRT-III polymers.[56] Finally, a dome-like structure has been proposed in which ESCRT-III polymers acquired a dome-like configuration, exposing membrane-binding interfaces, which theoretically has a higher binding energy than required for the membrane to wrap around the dome, thus causing membrane scission.[56]

Upon membrane constriction, the ESCRT-III subunits have to be recycled to carry out multiple rounds of ILV detachment.[52] Vps4 is an ATPase associated with various cellular activities (AAA) ATPase that requires ATP hydrolysis to completely recycle ESCRT-III subunits.[24] Vps4 is a dodecamer of two hexameric rings that has an N-terminal microtubule interacting and trafficking (MIT) domain that interacts with the C-terminal microtubule interacting motifs (MIMs) of ESCRT-III members.[24; 58] Vps4 works in tandem with Vta1, for which a structural basis has been determined, causing an enhancement of ATPase activity, promoting oligomerization, and helping in ESCRT-III disassembly.[61] Formation of this complex is thought to facilitate disassembly of subunits by threading them through the central pore of the ATPase, however, this model is only suggested because its not known how the refolding process would occur.[24]

1.4 Deubiquitination Within the ESCRT Complex

Since the ESCRT machinery is a ubiquitin-dependent process, deubiquitination and DUBs become regulators of this entire machinery. The model ESCRT system within *Saccharmyces cerevisiae* (*S. cerevisiae*) uses the DUB, Degradation of alpha 4 (Doa4), to recycle ubiquitin from ubiquitinated cargo that has been shuttled through the upstream ESCRT complexes and are committed to ILVs.[62] Doa4 has also been shown to interact directly with ESCRT-III subunit, Snf7, thus promoting its localization to the last complex, further supporting its DUB role, however, direct deubiquitination of cargo is not required for MVB sorting in yeast.[62; 63; 64]

Similarly, the human ESCRT system requires DUBs. In humans, there are two DUBs employed, associated molecule with a Src homology 3 (SH3) domain of STAM (or STAM-binding protein (STAMBP) or simply AMSH), and ubiquitin-specific protease Y (UBPY or ubiquitin-specific protease 8 (USP8)).[62; 65; 66; 67; 68] Both AMSH and UBPY have functional SH3-binding motifs (SBMs) that facilitate recruitment to ESCRT-0 via STAM's SH3 domain, and functional MIT domains that allow for recruitment to various CHMPs of ESCRT-III.[62; 67; 69; 70; 71] ESCRT-0 SH3 recruitment is carried out using a conserved consensus sequence, PX(V/I)(D/N)RXXKP (X is any residue).[62; 67] Linking the *S. cerevisiae* and human ESCRTs, there are three yeast proteins with similar domain structures to UBPY, Doa4, Ubp7, and Ubp5, and of the three, Doa4 has a seemingly analogous role to UBPY at ESCRT-III. Interestingly, Ubp7 interacts with Hse1, mimicking UBPY binding to ESCRT-0.[62] There is no direct AMSH homolog within *S. cerevisiae*.

1.4.1 AMSH

AMSH is a 424-amino acid member of the JAMM family of DUBs that binds Zn^{2+} at the active site coordinated by two histidines, an aspartate, and a glutamate bridged by the catalytic water molecule; a second Zn^{2+} is bound ~14Å away from the active-site zinc for structural integrity.[72; 73] AMSH is involved in the regulation of several receptors including: epidermal growth factor (EGFR) receptor, calcium-sensing receptor, δ-opioid receptor, protease-activated receptor (PAR), and the chemokine receptor CXCR4.[65; 74; 75; 76; 77; 78; 79; 80] Not only is AMSH implicated in receptor down-regulation, but also has roles within mitosis, cytokinesis, and HIV budding.[44; 45; 81; 82] More recently, whole-exome sequencing analysis has shown that recessive mutations in AMSH lead to microcephaly-capillary malformation (MIC-CAP) syndrome.[83] MIC-CAP is discovered at or shortly after birth in which children diagnosed with the disease have severe microcephaly with progressive cortical atrophy, intractable epilepsy, profound developmental delay and multiple small capillary malformations on the skin.[83; 84; 85; 86] Out of the ten patients that were screened, six had missense mutations, two had nonsense mutations, two translational frameshift mutations, and three intronic mutations.[83] Interestingly, five out of the six missense mutations were found within AMSH's MIT domain, and the sixth, Thr313Ile, found within the JAMM domain.[83]

AMSH has exquisite specificity for Lys63-linked polyubiquitin chains.[65] The structural basis for specifically recognizing Lys63-linked polyubiquitin chains by the AMSH family of DUBs has been elucidated with the x-ray crystal structure of AMSH-LP bound to a Lys63 ubiquitin dimer.[87] The structure revealed that specificity arises from

recognition of a tripeptide sequence (Gln62-Lys63-Glu64) within the proximal ubiquitin by four residues within the enzyme (Thr, Phe, Ser, and Phe).[87]

AMSH localization to ESCRT-0 is facilitated by the SH3 domain of STAM binding to the SBM of AMSH.[62] Previous work has shown that clathrin, not the SH3 domain of STAM is required for AMSH to be localized to the endosome, suggesting that binding clathrin allows AMSH to be in close proximity to bind the SH3 domain of STAM.[88] Similarly, ESCRT-0 localizes to the endosome because of its interaction with clathrin via the C-terminal domain of Hrs.[89] Furthermore, the recruitment of AMSH to ESCRT-0 enhances the enzyme's activity. One study showed that in the presence of STAM, AMSH processed Lys63 ubiquitin chains better than without STAM, or with mutations disrupting the enzyme's ability to bind STAM.[66] Also, it was found that mutations within the UIM domain of STAM greatly reduced this enhancement of activity, suggesting the UIM has a K_M effect.[66] Another study showed that when Lys63-linked diubiquitin was bound to STAM, the enzyme processed the chains better than when not bound to STAM; AMSH mutants lacking the SBM showed no activity towards diubiquitin bound STAM.[90]

AMSH recruitment to ESCRT-III is facilitated through direct interaction with CHMPs.[69; 70; 71] A yeast-two hybrid system found that AMSH interacts with several CHMP members: CHMP1A, CHMP1B, CHMP2A, and CHMP3; all of these CHMPs did not interact with AMSH-LP, suggesting specific AMSH-CHMP interactions.[71] A more detailed study of AMSH-ESCRT-III binding using a glutathione S-transferase (GST)-pull down assay suggests that AMSH interacts most prominently with CHMP1A, followed by CHMP3 and then, CHMP4C. However, CHMP1A only plays a regulatory role, whereas

CHMP3 is one of the proteins necessary for capping the ESCRT-III polymer in the scission process.[60; 69] Further structural and biophysical studies have been done on the AMSH-CHMP3 interaction. Some initial studies using SAXS found that CHMP3 existed in multiple conformations ranging from a closed conformation in a no-salt buffer to an open conformation in a high-salt condition.[53] This study also determined using isothermal titration calorimetry (ITC) that the AMSH-CHMP3 binding affinity changes as a function of salt concentration ranging from 5.6 nM in no salt to 392 nM in 500 mM NaCl.[53]

More recently, the structural basis of AMSH recruitment by CHMP3 was elucidated with the X-ray crystal structure of a complex including the MIT domain of AMSH (residues 1-146) and a C-terminal fragment of CHMP3 (residues 183-22) (Figure 1.9).[91] In great agreement with the previous study, the K_D of the MIT-MIM interaction was found to be 60 nM using ITC and 113 nM using Surface Plasmon Resonance (SPR).[91] The extraordinarily tight complex is mainly stabilized by polar interactions, which is novel compared to previous crystal structures of MIT-MIM interactions, which showed the importance of hydrophobic interactions.[91] Furthermore, the interaction of AMSH and CHMP1A was analyzed by SPR revealing a K_D of 1.49 mM, suggesting a different mode of interaction between the two subunits and AMSH.[53; 91] Since ESCRT-III is necessary for the final scission step in MVB biogenesis, it is important to comment on how AMSH relates to the role of Vps4 disassembly. Overexpression of Vps4 resulted in weakened affinity of CHMP1B for AMSH, suggesting that the MIT domain of Vps4 competes for the same binding spot on CHMPs.[71] Though Vps4 competed off AMSH from CHMP1B, it is not well understood how Vps4 would compete of CHMP3 because of the low nanomolar affinity that AMSH-CHMP3 has, whereas Vps4-CHMP

interactions have micromolar affinities.[91; 92] Further studies need to be done to elucidate how AMSH is released from ESCRT-III after deubiquitination prior to Vps4-mediated recycling.

1.5 References

1. Pickart, C. M. & Raasi, S. (2005). Controlled synthesis of polyubiquitin chains. *Methods Enzymol* **399**, 21-36.

2. Komander, D. & Rape, M. (2012). The ubiquitin code. *Annu Rev Biochem* **81**, 203-29.

3. Schulman, B. A. & Harper, J. W. (2009). Ubiquitin-like protein activation by E1 enzymes: the apex for downstream signalling pathways. *Nat Rev Mol Cell Biol* **10**, 319-31.

4. Ye, Y. & Rape, M. (2009). Building ubiquitin chains: E2 enzymes at work. *Nat Rev Mol Cell Biol* **10**, 755-64.

5. Deshaies, R. J. & Joazeiro, C. A. (2009). RING domain E3 ubiquitin ligases. *Annu Rev Biochem* **78**, 399-434.

6. Peng, J., Schwartz, D., Elias, J. E., Thoreen, C. C., Cheng, D., Marsischky, G., Roelofs, J., Finley, D. & Gygi, S. P. (2003). A proteomics approach to understanding protein ubiquitination. *Nat Biotechnol* **21**, 921-6.

7. Xu, P., Duong, D. M., Seyfried, N. T., Cheng, D., Xie, Y., Robert, J., Rush, J., Hochstrasser, M., Finley, D. & Peng, J. (2009). Quantitative proteomics reveals the function of unconventional ubiquitin chains in proteasomal degradation. *Cell* **137**, 133-45.

8. Raiborg, C. & Stenmark, H. (2009). The ESCRT machinery in endosomal sorting of ubiquitylated membrane proteins. *Nature* **458**, 445-52.

9. Al-Hakim, A., Escribano-Diaz, C., Landry, M. C., O'Donnell, L., Panier, S., Szilard, R. K. & Durocher, D. (2010). The ubiquitous role of ubiquitin in the DNA damage response. *DNA Repair (Amst)* **9**, 1229-40.

10. Stewart, G. S., Panier, S., Townsend, K., Al-Hakim, A. K., Kolas, N. K., Miller, E. S., Nakada, S., Ylanko, J., Olivarius, S., Mendez, M., Oldreive, C., Wildenhain, J., Tagliaferro, A., Pelletier, L., Taubenheim, N., Durandy, A., Byrd, P. J., Stankovic, T., Taylor, A. M. & Durocher, D. (2009). The RIDDLE syndrome protein mediates a ubiquitin-dependent signaling cascade at sites of DNA damage. *Cell* **136**, 420-34.

11. Sobhian, B., Shao, G., Lilli, D. R., Culhane, A. C., Moreau, L. A., Xia, B., Livingston, D. M. & Greenberg, R. A. (2007). RAP80 targets BRCA1 to specific ubiquitin structures at DNA damage sites. *Science* **316**, 1198-202.

12. Kim, H. T., Kim, K. P., Lledias, F., Kisselev, A. F., Scaglione, K. M., Skowyra, D., Gygi, S. P. & Goldberg, A. L. (2007). Certain pairs of ubiquitin-conjugating enzymes (E2s) and ubiquitin-protein ligases (E3s) synthesize nondegradable forked ubiquitin chains containing all possible isopeptide linkages. *J Biol Chem* **282**, 17375-86.

13. Saeki, Y., Kudo, T., Sone, T., Kikuchi, Y., Yokosawa, H., Toh-e, A. & Tanaka, K. (2009). Lysine 63-linked polyubiquitin chain may serve as a targeting signal for the 26S proteasome. *EMBO J* **28**, 359-71.

14. Jin, L., Williamson, A., Banerjee, S., Philipp, I. & Rape, M. (2008). Mechanism of ubiquitin-chain formation by the human anaphase-promoting complex. *Cell* **133**, 653-65.

15. Matsumoto, M. L., Wickliffe, K. E., Dong, K. C., Yu, C., Bosanac, I., Bustos, D., Phu, L., Kirkpatrick, D. S., Hymowitz, S. G., Rape, M., Kelley, R. F. & Dixit, V. M. (2010). K11-linked polyubiquitination in cell cycle control revealed by a K11 linkage-specific antibody. *Mol Cell* **39**, 477-84.

16. Williamson, A., Wickliffe, K. E., Mellone, B. G., Song, L., Karpen, G. H. & Rape, M. (2009). Identification of a physiological E2 module for the human anaphase-promoting complex. *Proc Natl Acad Sci U S A* **106**, 18213-8.

17. Tokunaga, F., Sakata, S., Saeki, Y., Satomi, Y., Kirisako, T., Kamei, K., Nakagawa, T., Kato, M., Murata, S., Yamaoka, S., Yamamoto, M., Akira, S., Takao, T., Tanaka, K. & Iwai, K. (2009). Involvement of linear polyubiquitylation of NEMO in NF-kappaB activation. *Nat Cell Biol* **11**, 123-32.

18. Nijman, S. M., Luna-Vargas, M. P., Velds, A., Brummelkamp, T. R., Dirac, A. M., Sixma, T. K. & Bernards, R. (2005). A genomic and functional inventory of deubiquitinating enzymes. *Cell* **123**, 773-86.

19. Komander, D., Clague, M. J. & Urbe, S. (2009). Breaking the chains: structure and function of the deubiquitinases. *Nat Rev Mol Cell Biol* **10**, 550-63.

20. Clague, M. J., Coulson, J. M. & Urbe, S. (2012). Cellular functions of the DUBs. *J Cell Sci* **125**, 277-86.

21. Komander, D. (2010). Mechanism, specificity and structure of the deubiquitinases. *Subcell Biochem* **54**, 69-87.

22. Burrows, J. F., McGrattan, M. J. & Johnston, J. A. (2005). The DUB/USP17 deubiquitinating enzymes, a multigene family within a tandemly repeated sequence. *Genomics* **85**, 524-9.

23. Schmidt, O. & Teis, D. (2012). The ESCRT machinery. *Curr Biol* **22**, R116-20.

24. Henne, W. M., Buchkovich, N. J. & Emr, S. D. (2011). The ESCRT pathway. *Dev Cell* **21**, 77-91.

25. Roxrud, I., Stenmark, H. & Malerod, L. (2010). ESCRT & Co. *Biol Cell* **102**, 293-318.

26. Saksena, S. & Emr, S. D. (2009). ESCRTs and human disease. *Biochem Soc Trans* **37**, 167-72.

27. Stuffers, S., Brech, A. & Stenmark, H. (2009). ESCRT proteins in physiology and disease. *Exp Cell Res* **315**, 1619-26.

28. Bache, K. G., Brech, A., Mehlum, A. & Stenmark, H. (2003). Hrs regulates multivesicular body formation via ESCRT recruitment to endosomes. *J Cell Biol* **162**, 435-42.

29. Katzmann, D. J., Stefan, C. J., Babst, M. & Emr, S. D. (2003). Vps27 recruits ESCRT machinery to endosomes during MVB sorting. *J Cell Biol* **162**, 413-23.

30. Lu, Q., Hope, L. W., Brasch, M., Reinhard, C. & Cohen, S. N. (2003). TSG101 interaction with HRS mediates endosomal trafficking and receptor down-regulation. *Proc Natl Acad Sci U S A* **100**, 7626-31.

31. Ren, X., Kloer, D. P., Kim, Y. C., Ghirlando, R., Saidi, L. F., Hummer, G. & Hurley, J. H. (2009). Hybrid structural model of the complete human ESCRT-0 complex. *Structure* **17**, 406-16.

32. Mayers, J. R., Fyfe, I., Schuh, A. L., Chapman, E. R., Edwardson, J. M. & Audhya, A. (2010). ESCRT-0 assembles as a heterotetrameric complex on membranes and binds multiple ubiquitinylated cargoes simultaneously. *J Biol Chem*.

33. Raiborg, C., Bremnes, B., Mehlum, A., Gillooly, D. J., D'Arrigo, A., Stang, E. & Stenmark, H. (2001). FYVE and coiled-coil domains determine the specific localisation of Hrs to early endosomes. *J Cell Sci* **114**, 2255-63.

34. Wollert, T. & Hurley, J. H. (2010). Molecular mechanism of multivesicular body biogenesis by ESCRT complexes. *Nature* **464**, 864-9.

35. Ren, X. & Hurley, J. H. (2010). VHS domains of ESCRT-0 cooperate in high-avidity binding to polyubiquitinated cargo. *EMBO J*.

36. Lange, A., Ismail, M. B., Riviere, G., Hologne, M., Lacabanne, D., Guilliere, F., Lancelin, J. M., Krimm, I. & Walker, O. (2012). Competitive binding of UBPY and ubiquitin to the STAM2 SH3 domain revealed by NMR. *FEBS Lett*.

37. Boura, E., Rozycki, B., Herrick, D. Z., Chung, H. S., Vecer, J., Eaton, W. A., Cafiso, D. S., Hummer, G. & Hurley, J. H. (2011). Solution structure of the ESCRT-I complex by small-angle X-ray scattering, EPR, and FRET spectroscopy. *Proc Natl Acad Sci U S A* **108**, 9437-42.

38. Kostelansky, M. S., Schluter, C., Tam, Y. Y., Lee, S., Ghirlando, R., Beach, B., Conibear, E. & Hurley, J. H. (2007). Molecular architecture and functional model of the complete yeast ESCRT-I heterotetramer. *Cell* **129**, 485-98.

39. Agromayor, M., Soler, N., Caballe, A., Kueck, T., Freund, S. M., Allen, M. D., Bycroft, M., Perisic, O., Ye, Y., McDonald, B., Scheel, H., Hofmann, K., Neil, S. J., Martin-Serrano, J. & Williams, R. L. (2012). The UBAP1 subunit of ESCRT-I interacts with ubiquitin via a SOUBA domain. *Structure* **20**, 414-28.

40. Garrus, J. E., von Schwedler, U. K., Pornillos, O. W., Morham, S. G., Zavitz, K. H., Wang, H. E., Wettstein, D. A., Stray, K. M., Cote, M., Rich, R. L., Myszka, D. G. & Sundquist, W. I. (2001). Tsg101 and the vacuolar protein sorting pathway are essential for HIV-1 budding. *Cell* **107**, 55-65.

41. VerPlank, L., Bouamr, F., LaGrassa, T. J., Agresta, B., Kikonyogo, A., Leis, J. & Carter, C. A. (2001). Tsg101, a homologue of ubiquitin-conjugating (E2) enzymes, binds the L domain in HIV type 1 Pr55(Gag). *Proc Natl Acad Sci U S A* **98**, 7724-9.

42. Martin-Serrano, J., Zang, T. & Bieniasz, P. D. (2001). HIV-1 and Ebola virus encode small peptide motifs that recruit Tsg101 to sites of particle assembly to facilitate egress. *Nat Med* **7**, 1313-9.

43. Demirov, D. G., Ono, A., Orenstein, J. M. & Freed, E. O. (2002). Overexpression of the N-terminal domain of TSG101 inhibits HIV-1 budding by blocking late domain function. *Proc Natl Acad Sci U S A* **99**, 955-60.

44. Carlton, J. G. & Martin-Serrano, J. (2007). Parallels between cytokinesis and retroviral budding: a role for the ESCRT machinery. *Science* **316**, 1908-12.

45. Morita, E., Sandrin, V., Chung, H. Y., Morham, S. G., Gygi, S. P., Rodesch, C. K. & Sundquist, W. I. (2007). Human ESCRT and ALIX proteins interact with proteins of the midbody and function in cytokinesis. *EMBO J* **26**, 4215-27.

46. Hierro, A., Sun, J., Rusnak, A. S., Kim, J., Prag, G., Emr, S. D. & Hurley, J. H. (2004). Structure of the ESCRT-II endosomal trafficking complex. *Nature* **431**, 221-5.

47. Teo, H., Perisic, O., Gonzalez, B. & Williams, R. L. (2004). ESCRT-II, an endosome-associated complex required for protein sorting: crystal structure and interactions with ESCRT-III and membranes. *Dev Cell* **7**, 559-69.

48. Teo, H., Gill, D. J., Sun, J., Perisic, O., Veprintsev, D. B., Vallis, Y., Emr, S. D. & Williams, R. L. (2006). ESCRT-I core and ESCRT-II GLUE domain structures reveal role for GLUE in linking to ESCRT-I and membranes. *Cell* **125**, 99-111.

49. Im, Y. J. & Hurley, J. H. (2008). Integrated structural model and membrane targeting mechanism of the human ESCRT-II complex. *Dev Cell* **14**, 902-13.

50. Boura, E., Rozycki, B., Chung, H. S., Herrick, D. Z., Canagarajah, B., Cafiso, D. S., Eaton, W. A., Hummer, G. & Hurley, J. H. (2012). Solution structure of the ESCRT-I and -II supercomplex: implications for membrane budding and scission. *Structure* **20**, 874-86.

51. Shibata, Y., Hu, J., Kozlov, M. M. & Rapoport, T. A. (2009). Mechanisms shaping the membranes of cellular organelles. *Annu Rev Cell Dev Biol* **25**, 329-54.

52. Wollert, T., Wunder, C., Lippincott-Schwartz, J. & Hurley, J. H. (2009). Membrane scission by the ESCRT-III complex. *Nature* **458**, 172-7.

53. Lata, S., Roessle, M., Solomons, J., Jamin, M., Gottlinger, H. G., Svergun, D. I. & Weissenhorn, W. (2008). Structural basis for autoinhibition of ESCRT-III CHMP3. *J Mol Biol* **378**, 818-27.

54. Bajorek, M., Schubert, H. L., McCullough, J., Langelier, C., Eckert, D. M., Stubblefield, W. M., Uter, N. T., Myszka, D. G., Hill, C. P. & Sundquist, W. I. (2009). Structural basis for ESCRT-III protein autoinhibition. *Nat Struct Mol Biol* **16**, 754-62.

55. Teis, D., Saksena, S. & Emr, S. D. (2008). Ordered assembly of the ESCRT-III complex on endosomes is required to sequester cargo during MVB formation. *Dev Cell* **15**, 578-89.

56. Guizetti, J. & Gerlich, D. W. (2012). ESCRT-III polymers in membrane neck constriction. *Trends Cell Biol* **22**, 133-40.

57. Lata, S., Schoehn, G., Solomons, J., Pires, R., Gottlinger, H. G. & Weissenhorn, W. (2009). Structure and function of ESCRT-III. *Biochem Soc Trans* **37**, 156-60.

58. Hurley, J. H. & Hanson, P. I. (2010). Membrane budding and scission by the ESCRT machinery: it's all in the neck. *Nat Rev Mol Cell Biol* **11**, 556-66.

59. Henne, W. M., Buchkovich, N. J., Zhao, Y. & Emr, S. D. (2012). The endosomal sorting complex ESCRT-II mediates the assembly and architecture of ESCRT-III helices. *Cell* **151**, 356-71.

60. Effantin, G., Dordor, A., Sandrin, V., Martinelli, N., Sundquist, W. I., Schoehn, G. & Weissenhorn, W. (2012). ESCRT-III CHMP2A and CHMP3 form variable helical polymers in vitro and act synergistically during HIV-1 budding. *Cell Microbiol*.

61. Yang, D. & Hurley, J. H. (2010). Structural role of the Vps4-Vta1 interface in ESCRT-III recycling. *Structure* **18**, 976-84.

62. Clague, M. J. & Urbe, S. (2006). Endocytosis: the DUB version. *Trends Cell Biol* **16**, 551-9.

63. Bowers, K., Lottridge, J., Helliwell, S. B., Goldthwaite, L. M., Luzio, J. P. & Stevens, T. H. (2004). Protein-protein interactions of ESCRT complexes in the yeast Saccharomyces cerevisiae. *Traffic* **5**, 194-210.

64. Reggiori, F. & Pelham, H. R. (2001). Sorting of proteins into multivesicular bodies: ubiquitin-dependent and -independent targeting. *EMBO J* **20**, 5176-86.

65. McCullough, J., Clague, M. J. & Urbe, S. (2004). AMSH is an endosome-associated ubiquitin isopeptidase. *J Cell Biol* **166**, 487-92.

66. McCullough, J., Row, P. E., Lorenzo, O., Doherty, M., Beynon, R., Clague, M. J. & Urbe, S. (2006). Activation of the endosome-associated ubiquitin isopeptidase AMSH by STAM, a component of the multivesicular body-sorting machinery. *Curr Biol* **16**, 160-5.

67. Kato, M., Miyazawa, K. & Kitamura, N. (2000). A deubiquitinating enzyme UBPY interacts with the Src homology 3 domain of Hrs-binding protein via a novel binding motif PX(V/I)(D/N)RXXKP. *J Biol Chem* **275**, 37481-7.

68. Row, P. E., Prior, I. A., McCullough, J., Clague, M. J. & Urbe, S. (2006). The ubiquitin isopeptidase UBPY regulates endosomal ubiquitin dynamics and is essential for receptor down-regulation. *J Biol Chem* **281**, 12618-24.

69. Row, P. E., Liu, H., Hayes, S., Welchman, R., Charalabous, P., Hofmann, K., Clague, M. J., Sanderson, C. M. & Urbe, S. (2007). The MIT domain of UBPY constitutes a CHMP binding and endosomal localization signal required for efficient epidermal growth factor receptor degradation. *J Biol Chem* **282**, 30929-37.

70. Tsang, H. T., Connell, J. W., Brown, S. E., Thompson, A., Reid, E. & Sanderson, C. M. (2006). A systematic analysis of human CHMP protein interactions: additional MIT domain-containing proteins bind to multiple components of the human ESCRT III complex. *Genomics* **88**, 333-46.

71. Agromayor, M. & Martin-Serrano, J. (2006). Interaction of AMSH with ESCRT-III and deubiquitination of endosomal cargo. *J Biol Chem* **281**, 23083-91.

72. Maytal-Kivity, V., Reis, N., Hofmann, K. & Glickman, M. H. (2002). MPN+, a putative catalytic motif found in a subset of MPN domain proteins from eukaryotes and prokaryotes, is critical for Rpn11 function. *BMC Biochem* **3**, 28.

73. Davies, C. W., Paul, L. N., Kim, M. I. & Das, C. (2011). Structural and thermodynamic comparison of the catalytic domain of AMSH and AMSH-LP: nearly identical fold but different stability. *J Mol Biol* **413**, 416-29.

74. Sierra, M. I., Wright, M. H. & Nash, P. (2010). AMSH interacts with ESCRT-0 to regulate the stability and trafficking of CXCR4. *J Biol Chem*.

75. Kyuuma, M., Kikuchi, K., Kojima, K., Sugawara, Y., Sato, M., Mano, N., Goto, J., Takeshita, T., Yamamoto, A., Sugamura, K. & Tanaka, N. (2007). AMSH, an ESCRT-III associated enzyme, deubiquitinates cargo on MVB/late endosomes. *Cell Struct Funct* **31**, 159-72.

76. Ma, Y. M., Boucrot, E., Villen, J., Affar el, B., Gygi, S. P., Gottlinger, H. G. & Kirchhausen, T. (2007). Targeting of AMSH to endosomes is required for epidermal growth factor receptor degradation. *J Biol Chem* **282**, 9805-12.

77. Herrera-Vigenor, F., Hernandez-Garcia, R., Valadez-Sanchez, M., Vazquez-Prado, J. & Reyes-Cruz, G. (2006). AMSH regulates calcium-sensing receptor signaling through direct interactions. *Biochem Biophys Res Commun* **347**, 924-30.

78. Reyes-Ibarra, A. P., Garcia-Regalado, A., Ramirez-Rangel, I., Esparza-Silva, A. L., Valadez-Sanchez, M., Vazquez-Prado, J. & Reyes-Cruz, G. (2007). Calcium-sensing receptor endocytosis links extracellular calcium signaling to parathyroid hormone-related peptide secretion via a Rab11a-dependent and AMSH-sensitive mechanism. *Mol Endocrinol* **21**, 1394-407.

79. Hislop, J. N., Henry, A. G., Marchese, A. & von Zastrow, M. (2009). Ubiquitination regulates proteolytic processing of G protein-coupled receptors after their sorting to lysosomes. *J Biol Chem* **284**, 19361-70.

80. Hasdemir, B., Murphy, J. E., Cottrell, G. S. & Bunnett, N. W. (2009). Endosomal deubiquitinating enzymes control ubiquitination and down-regulation of protease-activated receptor 2. *J Biol Chem* **284**, 28453-66.

81. Mukai, A., Mizuno, E., Kobayashi, K., Matsumoto, M., Nakayama, K. I., Kitamura, N. & Komada, M. (2008). Dynamic regulation of ubiquitylation and deubiquitylation at the central spindle during cytokinesis. *J Cell Sci* **121**, 1325-33.

82. Tanaka, N., Kaneko, K., Asao, H., Kasai, H., Endo, Y., Fujita, T., Takeshita, T. & Sugamura, K. (1999). Possible involvement of a novel STAM-associated molecule "AMSH" in intracellular signal transduction mediated by cytokines. *J Biol Chem* **274**, 19129-35.

83. McDonell, L. M., Mirzaa, G. M., Alcantara, D., Schwartzentruber, J., Carter, M. T., Lee, L. J., Clericuzio, C. L., Graham, J. M., Jr., Morris-Rosendahl, D. J., Polster, T., Acsadi, G., Townshend, S., Williams, S., Halbert, A., Isidor, B., David, A., Smyser, C. D., Paciorkowski, A. R., Willing, M., Woulfe, J., Das, S., Beaulieu, C. L., Marcadier, J., Geraghty, M. T., Frey, B. J., Majewski, J., Bulman, D. E., Dobyns, W. B., O'Driscoll, M. & Boycott, K. M. (2013). Mutations in STAMBP, encoding a deubiquitinating enzyme, cause microcephaly-capillary malformation syndrome. *Nat Genet* **45**, 556-62.

84. Carter, M. T. & Boycott, K. M. (2011). Microcephaly-capillary malformation syndrome: a story of rapid emergence of a new recognizable entity. *Am J Med Genet A* **155A**, 2078-9.

85. Mirzaa, G. M., Paciorkowski, A. R., Smyser, C. D., Willing, M. C., Lind, A. C. & Dobyns, W. B. (2011). The microcephaly-capillary malformation syndrome. *Am J Med Genet A* **155A**, 2080-7.

86. Isidor, B., Barbarot, S., Beneteau, C., Le Caignec, C. & David, A. (2011). Multiple capillary skin malformations, epilepsy, microcephaly, mental retardation, hypoplasia of the distal phalanges: report of a new case and further delineation of a new syndrome. *Am J Med Genet A* **155A**, 1458-60.

87. Sato, Y., Yoshikawa, A., Yamagata, A., Mimura, H., Yamashita, M., Ookata, K., Nureki, O., Iwai, K., Komada, M. & Fukai, S. (2008). Structural basis for specific cleavage of Lys 63-linked polyubiquitin chains. *Nature* **455**, 358-62.

88. Nakamura, M., Tanaka, N., Kitamura, N. & Komada, M. (2006). Clathrin anchors deubiquitinating enzymes, AMSH and AMSH-like protein, on early endosomes. *Genes Cells* **11**, 593-606.

89. Raiborg, C., Bache, K. G., Mehlum, A., Stang, E. & Stenmark, H. (2001). Hrs recruits clathrin to early endosomes. *EMBO J* **20**, 5008-21.

90. Kim, M. S., Kim, J. A., Song, H. K. & Jeon, H. (2006). STAM-AMSH interaction facilitates the deubiquitination activity in the C-terminal AMSH. *Biochem Biophys Res Commun* **351**, 612-8.

91. Solomons, J., Sabin, C., Poudevigne, E., Usami, Y., Hulsik, D. L., Macheboeuf, P., Hartlieb, B., Gottlinger, H. & Weissenhorn, W. (2011). Structural basis for ESCRT-III CHMP3 recruitment of AMSH. *Structure* **19**, 1149-59

92. Stuchell-Brereton, M. D., Skalicky, J. J., Kieffer, C., Karren, M. A., Ghaffarian, S. & Sundquist, W. I. (2007). ESCRT-III recognition by VPS4 ATPases. *Nature* **449**, 740-4.

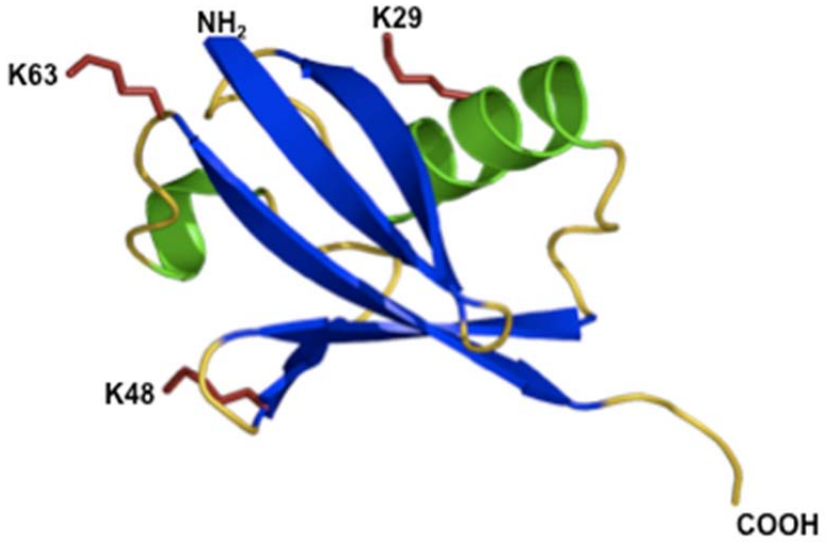

^{1}MQIFVKTLTG KTITLEVEPS DTIENVKAK^{29}I
QDKEGIPPDQ QRLIFAGK^{48}QL EDGRTLSDYN
IQK^{63}ESTLHL VLRLRGG^{76}

Figure 1.1. X-ray crystal structure and primary sequence of human ubiquitin.

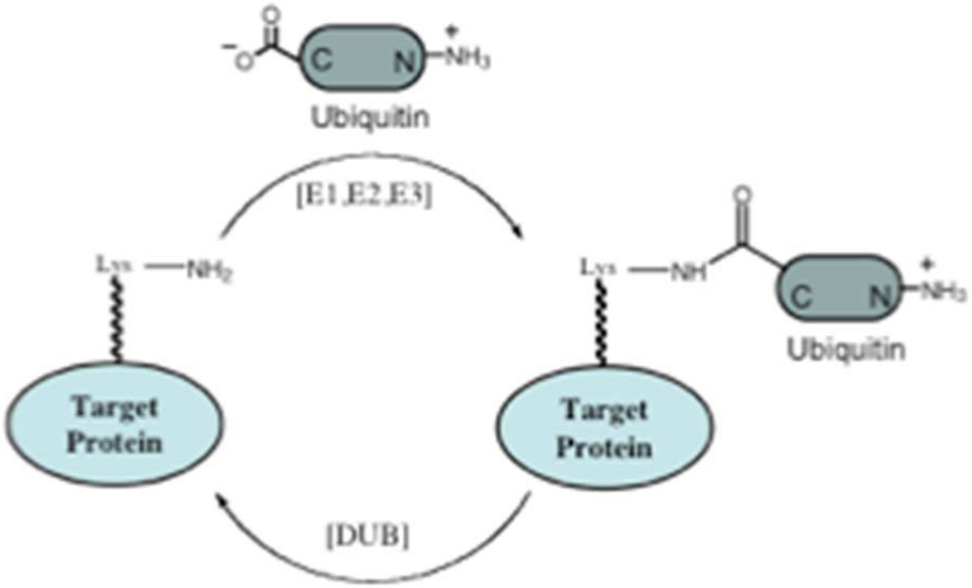

Figure 1.2. Diagram of the ubiquitination and deubiquitination process.

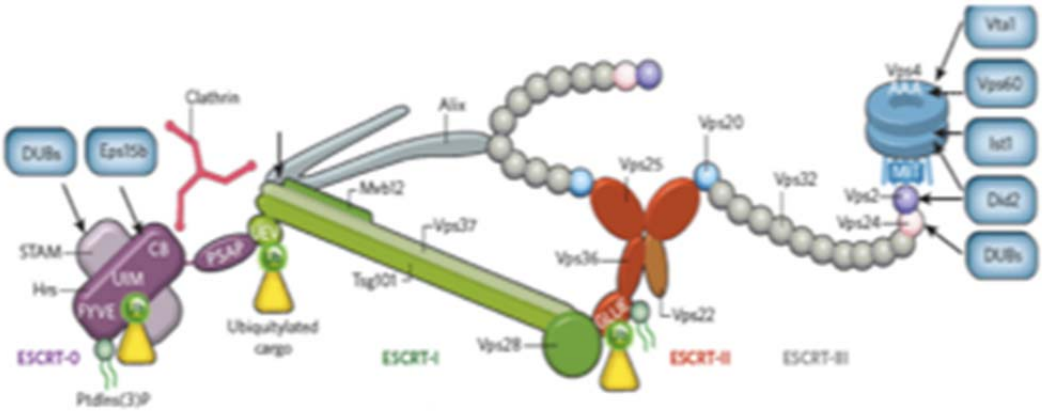

Figure 1.3. Cartoon representation of the ESCRT complexes taken from Railborg, C., et al. (2009) *Nature*.

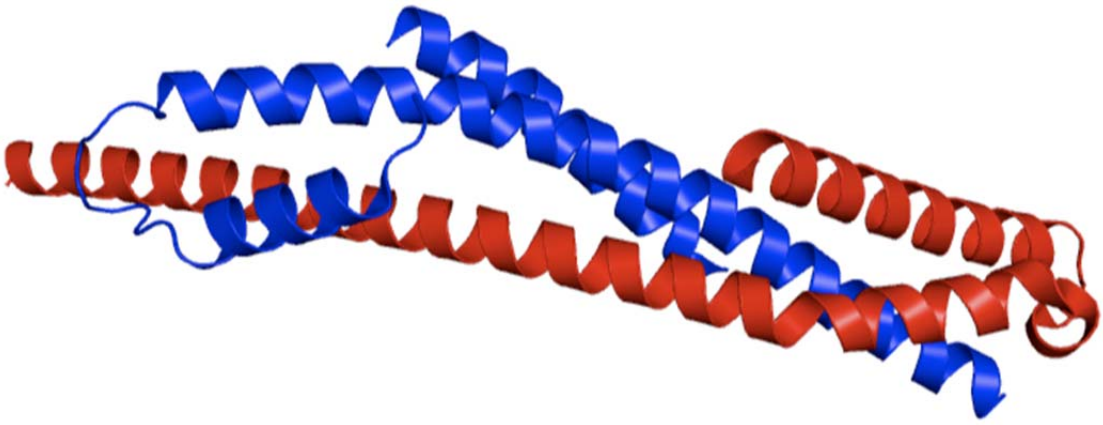

Figure 1.4. X-ray crystal structure of the human core ESCRT-0 heterodimer determined to 2.3Å resolution (PDB ID: 3F1I). Hrs is shown as red ribbon and STAM as blue ribbon.

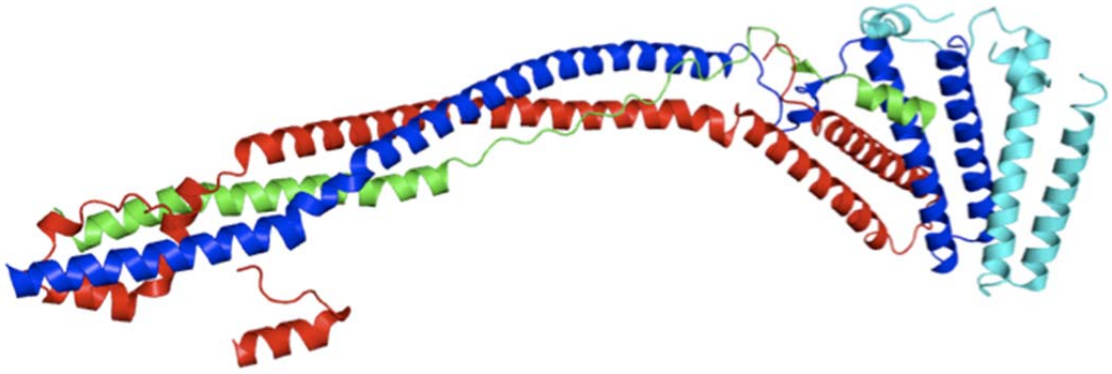

Figure 1.5. X-ray crystal structure of the yeast heterotetrameric ESCRT-I complex. (PDB ID: 2P22) Vps23 is shown as blue ribbon, vps28 as cyan ribbon, vps37 as red ribbon, and Mvb12 as green ribbon.

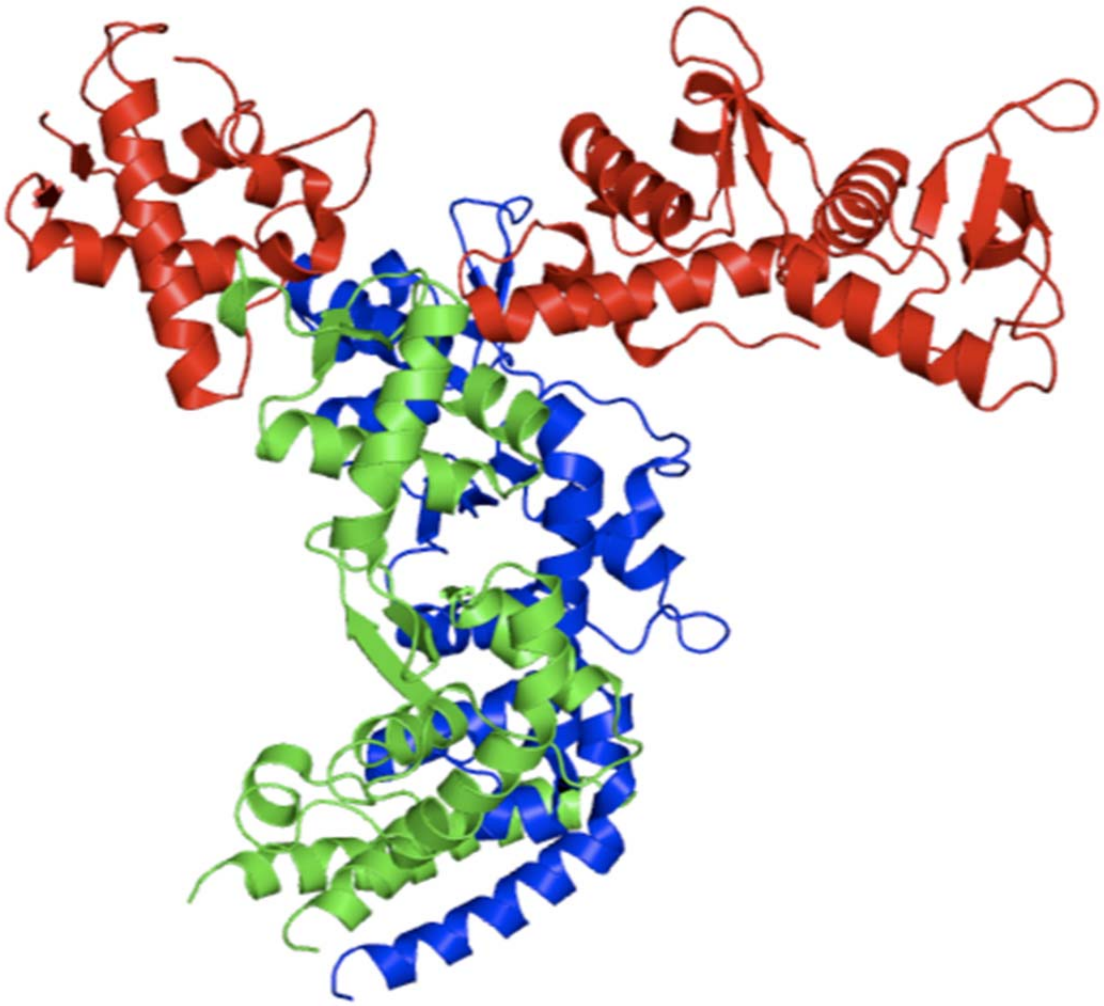

Figure 1.6. X-ray crystal structure of human ESCRT-II. The structure is the complex ESCRT-II lacking the GLUE domain (PDB ID: 3CUQ). VPS36 is shown as green ribbon, VPS22 as blue ribbon, and VPS25 in red ribbon.

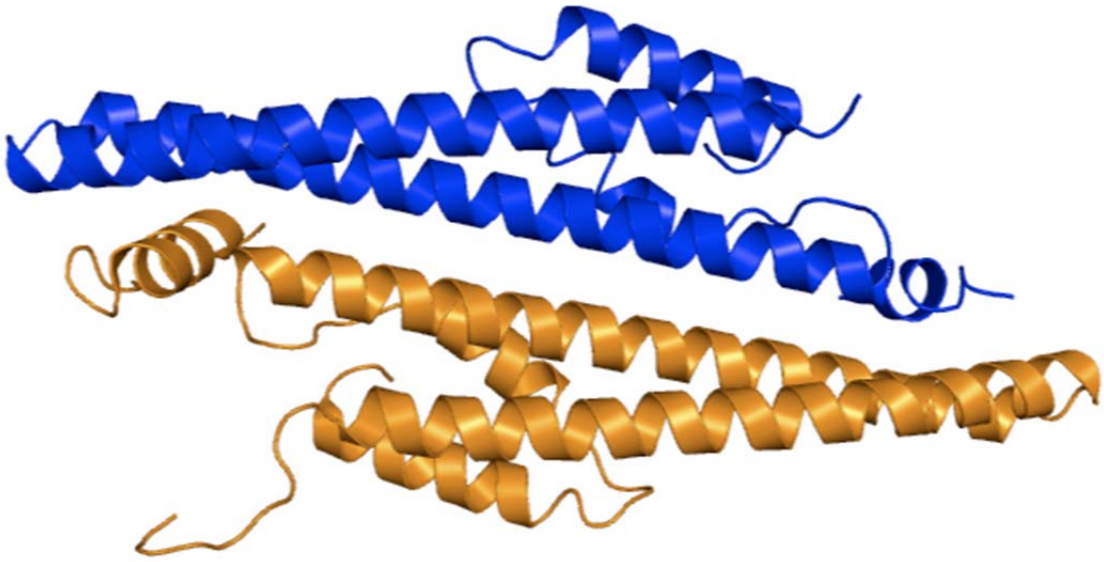

Figure 1.7. X-ray crystal structure of the human CHMP3 dimer (PDB ID: 2GD5).

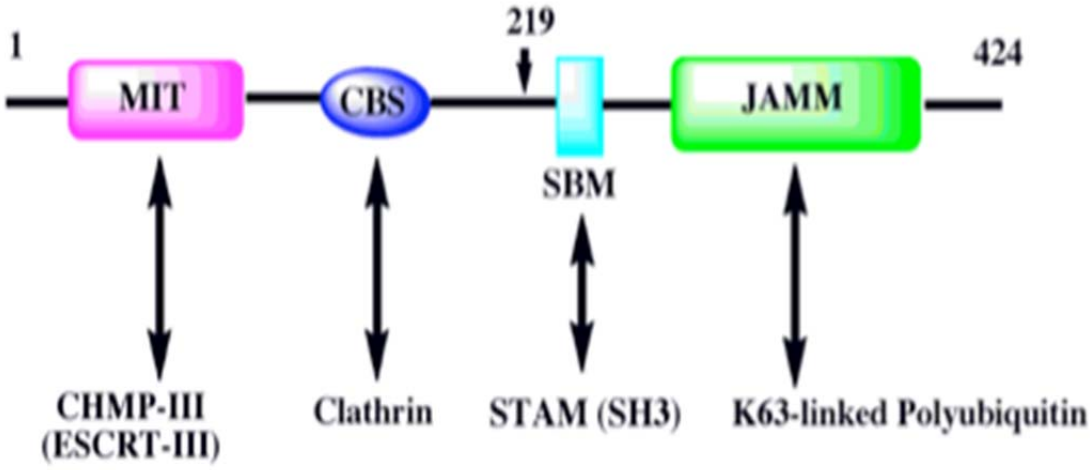

Figure 1.8. AMSH domain diagram.

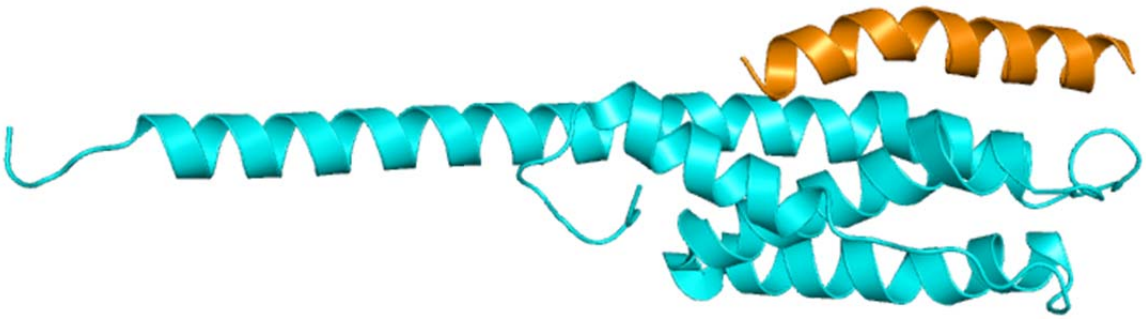

Figure 1.9. X-ray crystal structure of the AMSH MIT domain bound to CHMP3 (PDB ID: 2XZE). The MIT domain of AMSH is shown in cyan ribbon and CHMP3 is shown in orange ribbon.

CHAPTER 2: STRUCTURAL AND THERMODYNAMIC COMPARISON OF AMSH AND AMSH-LP

2.1 Introduction

This chapter describes the structural and thermodynamic comparison of the catalytic domains of AMSH and AMSH-LP. I have determined x-ray crystal structures of two constructs representing the catalytic domain of AMSH: AMSH244-424, the JAMM-domain-containing polypeptide segment from residues 244 to 424 (hereafter referred to simply as AMSH244) and AMSH219^{E280A}, an active-site mutant, Glu280 to Ala, of the segment 219-424, which, in addition to the JAMM domain, also features the SH3-domain-binding motif (SBM) at its N-terminus. When comparing the x-ray crystal structures of AMSH and AMSH-LP, we see that while the overall folds of the two proteins are nearly identical, as expected, the catalytic domain of AMSH is thermodynamically less stable than of AMSH-LP under guanidine hydrochloride (GdHCl)-induced unfolding. Moreover, to further understand the disease basis of MIC-CAP syndrome, the disease-associated mutation, Thr313Ile, was analyzed for its thermodynamic stability. It was determined that the mutation does not significantly alter AMSH's thermodynamic stability, suggesting that the basis of the disease lies elsewhere. Together, these results suggest that the catalytic domain of AMSH is structurally more plastic than AMSH-LP, a property that may endow specific advantage to AMSH enabling it to adapt to a variety of working environments within the context of ESCRT machinery.

2.2 Materials and Methods

2.2.1 Cloning, Expression, and Purification

AMSH244 was subcloned from the full-length plasmid following standard PCR protocols. The resulting gene encoding the catalytic domain was subcloned into pGEX-6p1 (GE Biosciences) by using standard cloning protocols. The resulting N-terminally fused glutathione S-transferase (GST)-tagged protein was expressed in *Escherichia coli* Rosetta cells (Novagen) and purified with a glutathione-Sepharose column (GE Biosciences) following manufacturer's instructions.

AMSH219 was subcloned into a pGEX-6p1 expression vector as before. The Glu280Ala and Thre313Ile mutations was introduced into the gene by site-directed mutagenesis using QuikChange Site-Directed Mutagenesis Kit (Stratagene) following the manufacturer's protocol. DNA sequencing confirmed the presence of the mutation. AMSH219^{E280A} and AMSH219^{T313I} were purified using standard GST affinity chromatography. The DUB domain of AMSH-LP (a kind gift from Prof. Shuya Fukai, The University of Tokyo, Japan) was purified as described before.[1]

2.2.2 Crystallization and Structure Determination

Crystals of AMSH244 were grown at room temperature by the sitting drop vapor diffusion method from a mother liquor containing 0.2M sodium malonate pH 7.0, 20% PEG 3350, and 5% PEG 400. Crystals of AMSH219^{E280A} were grown at room temperature by the sitting drop vapor diffusion method from a mother liquor containing

0.1M 2-(*N*-morpholino)ethanesulfonic acid (MES) pH 6.5, 15% PEG 6000, and 5% 2-methyl-2,4-pentanediol (MPD). Crystals were briefly soaked in cryoprotectant solution (20% ethylene glycol) and then plunged into liquid nitrogen for flash cooling. X-ray diffraction data were collected at 100 K on a Mar300 CCD detector (Mar USA) at the beamline 23-ID-D at the Advanced Photon Source at Argonne National Laboratory. The data were processed using HKL2000.

AMSH244 was determined by molecular replacement using a homology modeled catalytic domain of AMSH based on the catalytic domain of AMSH-LP, from SWISS-MODEL homology modeling server,[2] as a search model. Refinement and multiple rounds of model building were carried out using Phenix[3] and Coot,[4] respectively, yielding a final model with a crystallographic R_{fac} of 19.3% and free R of 22.9%. Residues Thr250 of chain C, Ile251 of chain D, Pro402 of chain E, and Glu314, Asn315, and Glu316 of chain G are within disallowed regions of the Ramachandran plot. All of these residues were in weak or no density at 1σ except Glu314 and Thr250. The structure of $AMSH219^{E280A}$ was also determined by molecular replacement using the previous structure as a search model. Refinement and model building were carried out in the same method yielding a crystallographic R_{fac} of 18.0% and free R of 20.5% (Table 1). Graphical analysis was carried out using PyMOL (DeLano Scientific).

2.2.3 Analytical Ultracentrifugation

To characterize the oligomeric state of AMSH and AMSH-LP, sedimentation velocity experiments were conducted at 50,000 rpm using both the Beckman-Coulter XLI

and XLA (Beckman-Coulter, Fullerton, CA, USA). The samples were monitored by both absorbance and interference optics at 280 and 675 nm, respectively. The proteins were dialyzed in 50 mM TRIS-HCl pH 7.6, 50 mM NaCl and 1 mM DTT. Three concentration series were conducted to evaluate the formation of higher order species, AMSH244 at 30, 60, and 120 μM, AMSH-LP at 25, 47, and 94 μM. The sedimentation coefficients and apparent molecular weights were calculated from size distribution analyses (c(s)) using SEDFIT v. 12.0.[5; 6] The solvent density, viscosity and partial specific volume of the proteins were calculated using SEDNTERP v. 1.09 (http://www.rasmb.bbri.org/rasmb/windows/sednterp-philo).

2.2.4 Guanidine Melt Using Circular Dichroism Spectroscopy

The stability of the folded state of AMSH244, AMSH219^{T313I}, and AMSH-LP towards GdHCl was determined using 8M stock concentrations of GdHCl (Sigma). Varying concentrations of GdHCl were added to the protein (0.2 mg.mL^{-1}) diluted in 100 mM phosphate buffer pH 7.4 and allowed to sit at room temperature overnight to allow for complete equilibration. Changes in the folded state of the proteins were monitored using circular dichroism by following changes in ellipticity at 220 nm. CD spectra were recorded in a Jasco J-810 Spectropolarimeter in the far UV region (195-260 nm) in a 0.1 cm path length cuvette. Each spectrum was averaged over 4 scans (50 nm.min^{-1} scan speed, with a 8 second time constant) and corrected by subtraction of a spectrum of the buffer alone. Mean residue molar ellipticity values were calculated using the following equation:

$$[\theta] = \frac{\theta * 100 * M}{C * l * n} \quad \text{(EQN 1)}$$

Where θ is the ellipticity in degrees, *l* is the optical path in cm, *C* is the concentration in mg/ml, *M* is the molecular mass and *n* is in the number of residues in the protein.

The mean residue molar ellipticity [θ] is given in $deg.cm^2.dmol^{-1}$. Unfolding curves were analyzed using a two-state unfolding model, using linear extrapolation to obtain the ΔG value in the absence of GdHCl.[7]

2.3 Results

2.3.1 Structure of the Catalytic Domain of AMSH

AMSH244 crystallized in the *C*2 space group, with seven monomers in the asymmetric unit (Figure 2.1). The structure was solved by molecular replacement (MR) with the catalytic domain of AMSH-LP as the search model.[1] The MR search identified a model with seven subunits in the asymmetric unit. Rigid-body followed by restrained refinement of this model yielded a crystallographic R factor (R_{crys}) and free R factor (R_{free}) of 25.4 and 34.8 %, respectively. Electron density map at this stage was interpretable and showed clear density for the two Zn^{2+} ions where they should be located, indicating that the MR search was successful. Refinement using Phenix[3] after rounds of model building yielded a final R_{crys} and R_{free} of 19.3 and 22.9 %, respectively

(Table 2.1). The structure of the polypeptide in different subunits is nearly identical except for the N-terminal residues, Asn244 to Asp252, which were ordered to different extent in different subunits.

The observation of seven monomers in the asymmetric unit prompted us to investigate the oligomeric state of the catalytic domain of AMSH in solution. AMSH244 was subjected to analytical ultracentrifugation (AUC) experiments, along with the catalytic domain of AMSH-LP for comparison. The AUC data indicate that in solution, the catalytic domains of both AMSH and AMSH-LP exist as predominantly globular, monomeric proteins with a sedimentation coefficient (s_{20}) value of 2.1 and 2.03, respectively (Figure 2.2). However, this data does not rule out the possibility that the full-length protein can exist as a multimer in solution, through self-association of the part missing in our construct.

Like the DUB domain of AMSH-LP, the structure of AMSH244 consists of the JAMM core with two characteristic insertions, insertion 1 (Ins-1, residues 302-327) and insertion 2 (Ins-2, residues 381-403). The JAMM core comprises a mixed β-sheet in the shape of a partially unfurled β-barrel sandwiched by two α-helices, one on top (α1) and one on the bottom (α3) (Figure 2.3), a feature found in other JAMM domain proteins, such as *Af*JAMM and Prp8.[8; 9; 10; 11] As seen in AMSH-LP, the catalytic site is lined mostly by residues from the JAMM core, from the loop between α1 and β2, α3, β6 and the loop following it (Figure 2.3a). Residues from the β-hairpin turn segment in Ins-1 also contribute to the catalytic site. The catalytic zinc is coordinated by His335, His337 (located on β6 and immediately following it), Asp348 (located on α3) and a water

molecule that is hydrogen bonded to Glu280 (located on the loop following α1) (Figure 2.3b). In addition to these zinc-coordinating residues, the oxyanion-stabilizing side chain from Ser345 (on α3) completes the set of catalytic residues required for peptide bond hydrolysis by a thermolysin-type, mechanistically speaking, zinc metalloprotease.[12; 13] We confirmed the presence of a second zinc ion, 14Å away from the active site, by the presence of strong electron density in the 2fo-fc map in the area coordinated by the residues His350 from the JAMM core, and His396, His398, and Cys390 from Ins-2 (Figure 2.3c), the same set of residues that coordinate the second zinc ion in AMSH-LP.[24]

As seen in the structure of the DUB domain of AMSH-LP, the active-site of AMSH is in a closed configuration, covered by two side chains, that of an asparate (Asp309) in Ins-1 and a phenylalanine (Phe395) in Ins-2, with their van der Waals surface touching each other (Figure 2.3a). The side chains of these two residues have to move away from each other to let the scissile isopeptide bond on the substrate access the active site, suggesting that there is considerable flexibility either in these side chains or in the polypeptide backbone bearing them. Interestingly, in the structure of AMSH-LP DUB domain bound to Lys63-linked ubiquitin dimer, the corresponding residue pair is still seen in a similar position as the substrate-free form,[1] suggesting that these residues close the active site during catalysis as well, perhaps to help position the scissile peptide bond or stabilize the transition state or both. Both these residues are absolutely conserved in all AMSH sequences analyzed so far (data not shown) and in AMSH-LP as well suggesting a functional role.

In our efforts to structurally characterize AMSH's recruitment to the ESCRT-0 complex, we generated an N-terminally longer construct of the catalytic domain that has, in addition to AMSH's DUB domain, the peptide sequence which AMSH uses to bind to STAM's SH3 domain.[14] An active-site mutant of this construct, AMSH219^{E280A}, in which Glu280 is mutated to alanine, crystallized in the tetragonal space group, $P4_32_12$, with a single molecule in the asymmetric unit, consistent with the monomeric state of AMSH244 found in solution. The structure of this mutant was solved by MR using the structure of AMSH244 as the search probe (Table 1). The overall fold of the two structures is very similar with a root mean square deviation (rmsd) between Cα atoms of 0.84Å. The N-terminal SH3-binding peptide segment was not visualized in the structure perhaps because of disorder in the crystal, suggesting that this peptide segment is flexible and is easily accessible for binding to the SH3 domain of STAM. We speculate that the flexibility of this segment may allow it to serve as apart of a linker that connects the JAMM domain to the N-terminal portion of the protein. The structure of the mutant does confirm the presence of the E280A mutation; however, clear density in the vicinity of the active-site metal-coordinating residues was still observed, which was interpreted as the density corresponding to a Zn^{2+} ion (Figure 2.4). Thus, despite having lost the catalytic glutamate, and consequently the water molecule bound to it, the active-site Zn^{2+} is still present. Further inspection reveals that the side chain of a nearby aspartate, Asp309, has swung by nearly 120 degrees from its position in the wild-type structure positioning itself such that one of its Oδ atoms can coordinate to the zinc, thereby restoring the tetrahedral coordination around it (Figure 2.4).

2.3.2 A Potential Disulfide Bond in the Catalytic Domain of AMSH

The overall structure of AMSH244 and AMSH219^{E280A} are nearly identical, however, further inspection during model building revealed the presence of a potential disulfide bond 7.4Å away from the catalytic zinc in the latter. Rounds of refinement showed positive density around Cys282 within which we modeled in three alternate conformations, one of which placed this cysteine side chain within disulfide-bonding distance from Cys311 (Sγ-Sγ distance of 2.0Å) (Figure 2.5). The presence of dithiothreitol (DTT) throughout purification and in the crystallization buffer presents a possible reason for the multiple conformations observed in the crystals, preventing the cysteine pair from achieving 100% occupancy in its oxidized form (Figure 2.5). It is possible that this disulfide may exist in AMSH244 as well, but its observation is precluded because of DTT, whose reducing effect is perhaps more in this construct than in AMSH219^{E280A}. Interestingly, sequence alignment analysis shows that these cysteines are conserved between AMSH and AMSH-LP;[1] however, we do not see the equivalent cysteine pair within disulfide-bonding distance in AMSH-LP (Sγ-Sγ distance is 4.2Å in this case).

2.3.3 Comparison of Thermodynamic Stability of the Catalytic Domains of AMSH and AMSH-LP

The overall three-dimensional fold of the catalytic domain of AMSH is very similar to the previously determined DUB domain of AMSH-LP (PDB code: 2ZNR) [1] with a rmsd of 1.49Å of Cα atoms as determined by the superposition program SuperPose.[15] The architecture of both the active site and the second zinc-binding site of

both the proteins are nearly identical (Figure 2.6). To explore further the similarity or the lack thereof between the catalytic domains of AMSH and AMSH-LP, we wondered if there would be any difference in thermodynamic stability between the two proteins. The unfolding of the catalytic constructs of both AMSH (AMSH244) and AMSH-LP was induced by guanidine hydrochloride (GdHCl) and monitored at 220 nm using circular dichroism spectroscopy (CD). Both proteins reveal a loss in secondary structure with increasing concentration of GdHCl (Figure 2.7); however, it was observed that AMSH244 is less stable towards GdHCl than AMSH-LP, with a midpoint of transition at 2.7 and 3.5 M GdHCl for AMSH and AMSH-LP, respectively (Table 2.2). Using the linear extrapolation method described previously,[7] ΔG_{H2O} of AMSH244 was found to be 1.2 kcal.mol^{-1} less than that of the DUB domain of AMSH-LP, indicating the former is thermodynamically less stable than the latter (Figure 2.8 and Table 2).

To assess the thermodynamic stability of the MIC-CAP-associated mutation, Thr313Ile, in hopes to understand the basis of the disease, another GdHCl-induced melting experiment was done. It was determined that the MIC-CAP-associated mutation has similar thermodynamic stability to the wild type AMSH219 with a ΔG_{H2O} of 2.9 kcal.mol^{-1} compared to the wild type construct at 3.6 kcal.mol^{-}1, with both having similar midpoints of transition at 2.7 and 2.5 M GdHCl respectively (Figure 2.8 and Table 2).

2.4 Discussion

We have determined the structure of two constructs representing the catalytic domain of AMSH, AMSH244 and AMSH219^{E280A}. The structure of AMSH244 confirms

that AMSH is indeed a zinc metalloprotease of the JAMM family of DUBs with two Zn^{2+} ions, one at active site and the other playing a structural role in supporting the placement of ubiquitin-binding residues in Ins-2 in a position appropriate for isopeptide bond recognition. The structure of $AMSH219^{E280A}$ provided a surprising observation. We anticipated the loss of the active-site zinc due to the E280A mutation, because Glu280, according to the known mechanism of thermolysin-type zinc-dependent-metalloproteases, is responsible for holding a water molecule, the one that functions as the nucleophile, at a position such that it is able to serve as the fourth ligand in the coordination sphere of the catalytic zinc. Instead, we see clear density for the zinc. Asp309, on an adjacent loop (from Ins-1), has moved in place to become the fourth residue to coordinate the zinc. The observation that Asp309 moves in the mutant to coordinate zinc is suggestive of the dynamic nature of the hairpin loop in Ins-1. The ability of the enzyme to counteract the loss of the glutamate by still retaining its zinc suggests a form of structural plasticity, allowing for conformational freedom. A similar mutation was incorporated in AMSH-LP for the purpose of co-crystallization with diubiquitin, and the authors stated that they do not see any electron density corresponding to the active site zinc.[1] Interestingly, Asp309 and its equivalent residue in AMSH-LP have to have a certain amount of flexibility; otherwise, the active site will not be accessible for the diubiquitin substrate. The question that if the observation pertaining to Aps309 in $AMSH219^{E280A}$ is due to more flexibility of Ins-1 in AMSH than in AMSH-LP cannot be answered from the data presented here. It is possible that the same rearrangement of the equivalent asparate in AMSH-LP might have been observed in the structure of ubiquitin-free $AMSH^{E292A}$.

Another interesting finding we see from the structure of AMSH219^{E280A} is the presence of a potential disulfide bond adjacent to the active site. It should be noted that a disulfide bond next to the putative active-site zinc was also observed in the structure the JAMM-domain protein AfJAMM, a cytosolic protein from *Archaeoglobus fulgidus.*[10] The possibility that the cysteine pair in AMSH is capable of existing in reduced and oxidized forms, reduced when in cytosol and oxidized when associated with endosomes, cannot be ruled out. This feature may contribute to or result from the structural plasticity of the enzyme. However, we cannot say with any degree of certainty if this reversible disulfide bridge is unique to AMSH, and if it is, whether it contributes to the biological difference between AMSH and AMSH-LP, two very similar proteins. It is not clear why the DUB domain of AMSH not AMSH-LP should have a disulfide, or is it common to both of them (DTT was also present in the crystallization buffer and throughout purification in the case of the AMSH-LP DUB domain). If it happens to be unique to AMSH, it could perhaps be linked to its association with endosomes, which have been shown to be oxidizing.[16]

Lastly, we sought to compare the structural and thermodynamic properties of the catalytic domains of AMSH and AMSH-LP. It is expected that homologous proteins that share 75% sequence similarity to have a similar fold and overall architecture. On par with this expectation, the catalytic domains of AMSH and AMSH-LP have a nearly identical fold and superimposable zinc coordination sites. Furthermore, AUC experiments confirmed that both the proteins are globular and monomeric in solution. Thus, structurally, we cannot separate the two proteins from one another. Thermodynamically, however, we see a difference between the two. Chaotrope-induced

unfolding with GdHCl indicates that the catalytic domain of AMSH is thermodynamically less stable than that of AMSH-LP. Analysis of primary sequences of the proteins does reveal some differences in certain key positions, such as in the hydrophobic core (residues Val259, Val363, and Phe376 in AMSH are substituted by residues Leu271, Ile375, Ile388 in AMSH-LP, respectively), which could contribute to the difference in thermodynamic stability; however, this needs to be investigated in future.

Furthermore, to understand the basis for the onset of MIC-CAP syndrome in children, we further assessed stability using GdHCl. Surprisingly, we do not see a significant difference in thermodynamic stability between the T313I mutant and the wild type, amounting to a minimal 0.4 kcal.mol^{-1} difference. This data suggests that the onset of the disease lies beyond protein folding, perhaps because the original threonine residue is surface-exposed, therefore, a substitution to isoleucine would present minimal changes to the overall three-dimensional structure.

Overall, we propose that the difference in thermodynamic stability between AMSH and AMSH-LP implies more plasticity in case of AMSH, a property that is consistent with its ability to function in the context of diverse environments such as within ESCRT-0 and ESCRT-III. We propose that this difference in stability implies a difference in flexibility between the catalytic domains of the AMSH and AMSH-LP. A more stable protein is likely to have better close packing of side chains making it more rigid, whereas a less stable protein, presumably because it has lesser amount of close packing, can tend to be more plastic, a property that may make AMSH more suitable for working in the context of a number different type of protein-protein complexes, such as

ESCRT-0 and ESCRT-III. Whether this has anything to do with the biological differences between the two proteins is worth investigating in future.

This chapter presents structurally and thermodynamic evidence that further separates the functional significance of AMSH and AMSH-LP. The two x-ray crystal structures of the catalytic domain of AMSH reveal an identical fold to AMSH-LP, however, two differences were discovered: (1) the E280A mutation did not lose Zn^{2+} at the active site, but instead had Asp309 complete the tetrahedron around Zn^{2+}, and (2) there are two cysteines at the peripheral of the active site in which one orientation formed a disulfide bridge. Finally, the most significant difference between AMSH and AMSH-LP was in their thermodynamic stability, where AMSH was significantly less stable than AMSH-LP. These data together suggest that AMSH has a clear, yet undefined, role within the ESCRT machinery, much different than the homologous, ESCRT-independent, AMSH-LP.

2.5 References

1. Sato, Y., Yoshikawa, A., Yamagata, A., Mimura, H., Yamashita, M., Ookata, K., Nureki, O., Iwai, K., Komada, M. & Fukai, S. (2008). Structural basis for specific cleavage of Lys 63-linked polyubiquitin chains. *Nature* **455**, 358-62.

2. Arnold, K., Bordoli, L., Kopp, J. & Schwede, T. (2006). The SWISS-MODEL workspace: a web-based environment for protein structure homology modelling. *Bioinformatics* **22**, 195-201.

3. Adams, P. D., Grosse-Kunstleve, R. W., Hung, L. W., Ioerger, T. R., McCoy, A. J., Moriarty, N. W., Read, R. J., Sacchettini, J. C., Sauter, N. K. & Terwilliger, T. C. (2002). PHENIX: building new software for automated crystallographic structure determination. *Acta Crystallogr D Biol Crystallogr* **58**, 1948-54.

4. Emsley, P., Lohkamp, B., Scott, W. G. & Cowtan, K. (2010). Features and development of Coot. *Acta Crystallogr D Biol Crystallogr* **66**, 486-501.

5. Brown, P. H. & Schuck, P. (2006). Macromolecular size-and-shape distributions by sedimentation velocity analytical ultracentrifugation. *Biophys J* **90**, 4651-61.

6. Schuck, P. (2000). Size-distribution analysis of macromolecules by sedimentation velocity ultracentrifugation and lamm equation modeling. *Biophys J* **78**, 1606-19.

7. Pace, C. N. (1986). Determination and analysis of urea and guanidine hydrochloride denaturation curves. *Methods Enzymol* **131**, 266-80.

8. Pena, V., Liu, S., Bujnicki, J. M., Luhrmann, R. & Wahl, M. C. (2007). Structure of a multipartite protein-protein interaction domain in splicing factor prp8 and its link to retinitis pigmentosa. *Mol Cell* **25**, 615-24.

9. Zhang, L., Shen, J., Guarnieri, M. T., Heroux, A., Yang, K. & Zhao, R. (2007). Crystal structure of the C-terminal domain of splicing factor Prp8 carrying retinitis pigmentosa mutants. *Protein Sci* **16**, 1024-31.

10. Ambroggio, X. I., Rees, D. C. & Deshaies, R. J. (2004). JAMM: a metalloprotease-like zinc site in the proteasome and signalosome. *PLoS Biol* **2**, E2.

11. Tran, H. J., Allen, M. D., Lowe, J. & Bycroft, M. (2003). Structure of the Jab1/MPN domain and its implications for proteasome function. *Biochemistry* **42**, 11460-5.

12. Gupta, S. P. (2007). Quantitative structure-activity relationship studies on zinc-containing metalloproteinase inhibitors. *Chem Rev* **107**, 3042-87.

13. Lipscomb, W. N. & Strater, N. (1996). Recent Advances in Zinc Enzymology. *Chem Rev* **96**, 2375-2434.

14. Clague, M. J. & Urbe, S. (2006). Endocytosis: the DUB version. *Trends Cell Biol* **16**, 551-9.

15. Maiti, R., Van Domselaar, G. H., Zhang, H. & Wishart, D. S. (2004). SuperPose: a simple server for sophisticated structural superposition. *Nucleic Acids Res* **32**, W590-4.

16. Austin, C. D., Wen, X., Gazzard, L., Nelson, C., Scheller, R. H. & Scales, S. J. (2005). Oxidizing potential of endosomes and lysosomes limits intracellular cleavage of disulfide-based antibody-drug conjugates. *Proc Natl Acad Sci U S A* **102**, 17987-92.

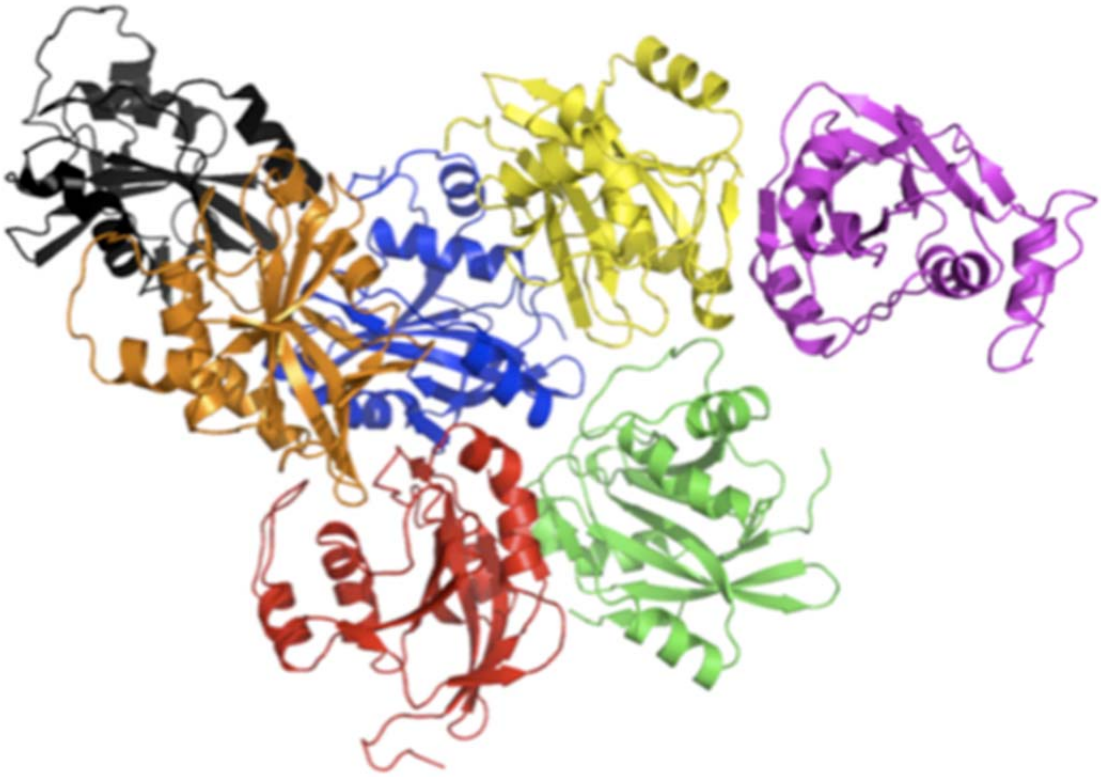

Figure 2.1. Asymmetric unit of AMSH244. The crystallographic heptamer present in the asymmetric unit of AMSH244 crystal structure. Each of the seven monomers of AMSH44 is represented in a different color.

Table 2.1. Crystallographic data and refinement statistics

	AMSH244	AMSH219^{E280A}
Residues	244-424	219-424
Data Collection		
Space Group	C 1 2 1	P 4_32_12
Cell dimensions		
a, b, c (Å)	203.5, 67.4, 113.2	53.4, 53.4, 128.8
α, β, γ (°)	90, 112.4, 90	90, 90, 90
Resolution (Å)	50.0 - 2.50 (2.59 - 2.50)*	50 – 1.68 (1.71- 1.68)*
Rsym or Rmerge	8.5 (54.3)*	7.1 (60.4)*
I/ σI	12.6 (2.04)*	28.3 (3.7)*
Completeness (%)	99.5 (97.8)*	99.6 (100.0)*
Redundancy	3.5 (3.0)*	12.1 (12.2)*
Refinement		
Resolution	47.2 - 2.50	33.5 – 1.67
No. of reflections	49,373 (48,880)+	22,665 (22,375)+
Rwork/Rfree	19.2/24.1	18.0/20.5
rmsd		
Bond lengths (Å)	0.002	0.006
Bond angles (°)	0.495	0.993
Ramachandran Plot		
Preferred (%)	94.4	98.9
Allowed (%)	4.5	1.1
Disallowed (%)	1.2	0.0

*$R_{sym} = \Sigma\Sigma |I_{hkl} - I_{hkl(j)}| / \Sigma I_{hkl}$, where $I_{hkl(j)}$ is the observed intensity and I_{hkl} is the final average intensity.

[1]$R_{crys} = \Sigma ||F_{obs}| - |F_{calc}|| / \Sigma |F_{obs}|$ and $R_{free} = \Sigma ||F_{obs}| - |F_{calc}|| / \Sigma |F_{obs}|$, where R_{free} and R_{crys} are calculated using a randomly selected test set of 5% of the data and all reflections excluding the 5% test data, respectively. Numbers in parentheses are for the high-resolution shell.

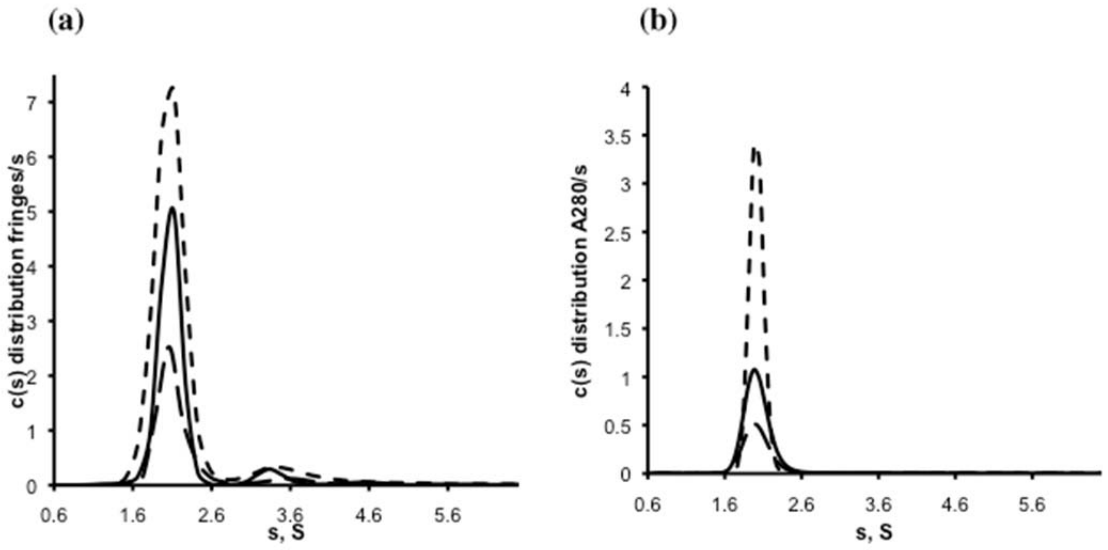

Figure 2.2. c(s) distribution plots of the DUB domains of AMSH244 and AMSH-LP as determined by AUC. (a) c(s) distribution plot of AMSH244 using interference optics shows that the majority discrete species at 2.1S is a globular, monomeric protein. The protein concentrations used were 30μM (large dashes), 60μM (solid line), and 120μM (small dashes). (b) c(s) distribution plot of AMSH-LP using absorbance at 280nm shows that the majority discrete species at 2.03S is a globular, monomeric protein. The protein concentrations used were 25μM (large dashes), 47μM (solid line), 94μM (small dashes).

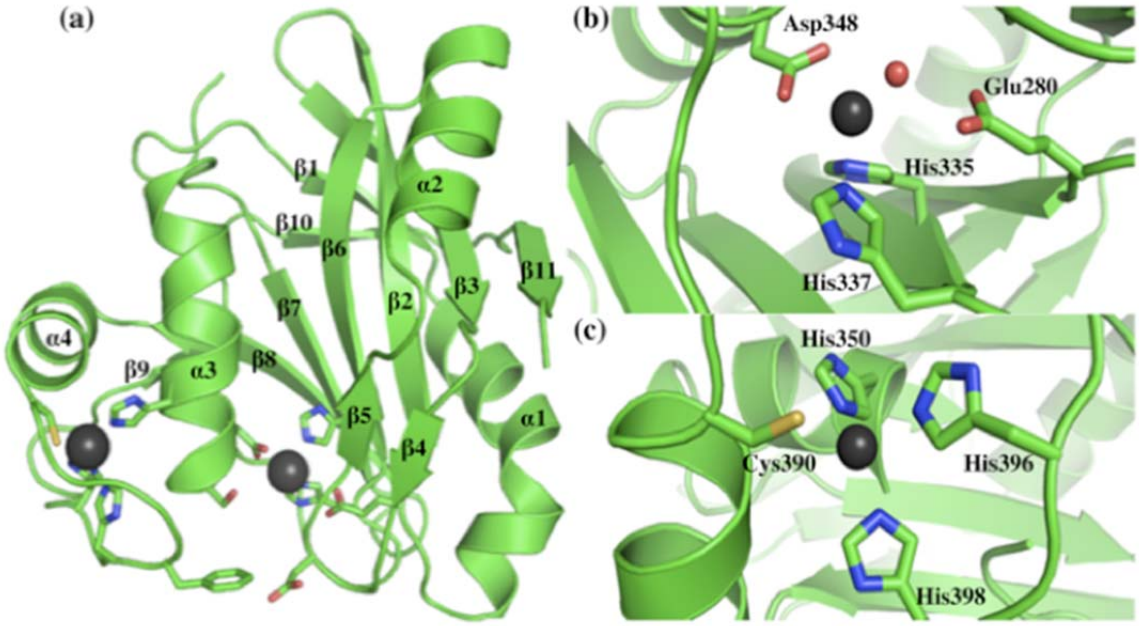

Figure 2.3. The structure of the catalytic domain of AMSH. (a) Ribbon representation of the X-ray structure of AMSH244. (b) Expanded view of the active-site zinc coordination. (c) Expanded view of the second zinc coordination site. The coordinating residues are shown as sticks, with carbon shown in green, oxygen in red, nitrogen in blue and sulfur in yellow. Zinc is shown as grey sphere.

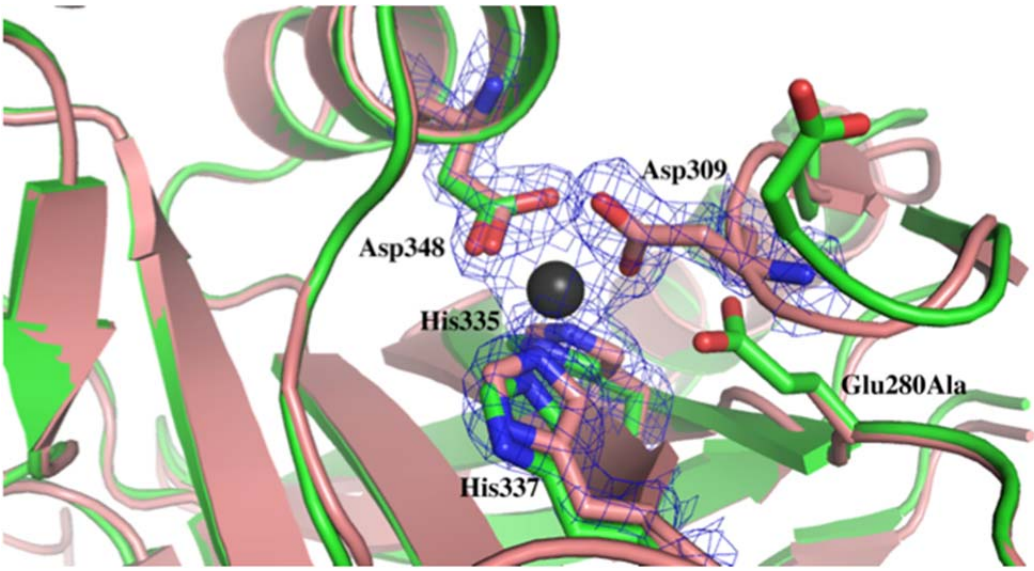

Figure 2.4. Superposition of the active sites of AMSH244 and AMSH219^{E280A}. AMSH244 is shown in green and AMSH219^{E280A} in pink. The zinc-coordinating residues in AMSH219^{E280A} are outlined in electron density ($2F_o$-F_c) at 1σ.

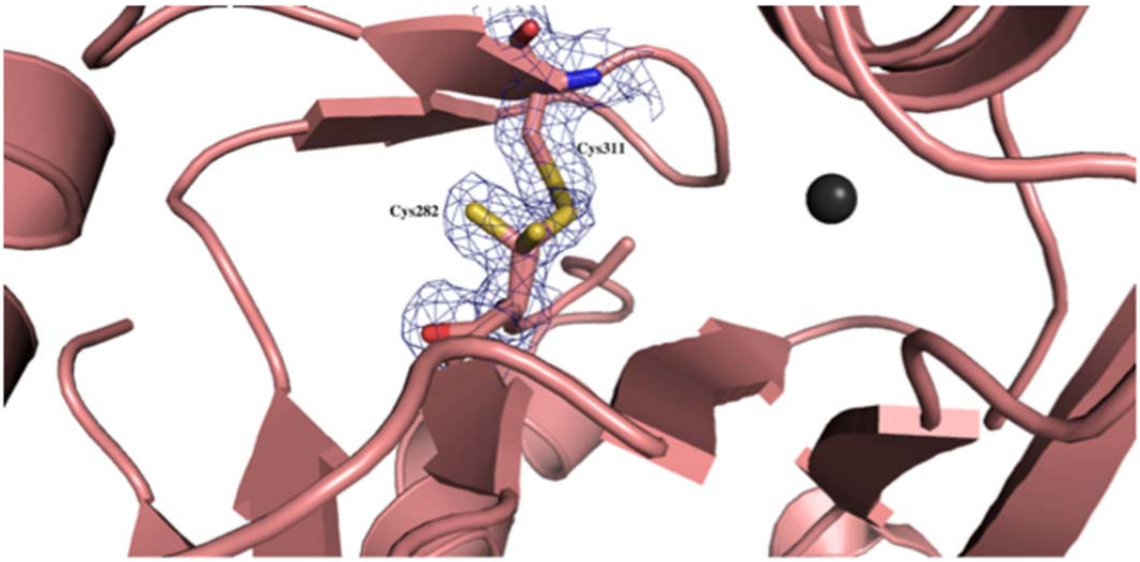

Figure 2.5. A potential disulfide bond in AMSH219^{E280A}. Expanded view of Cys282 modeled in three alternate conformations, one of which makes a disulfide bond with Cys311, adjacent to the active site zinc. Electron density ($2F_o$-F_c) at 1σ is shown in blue mesh.

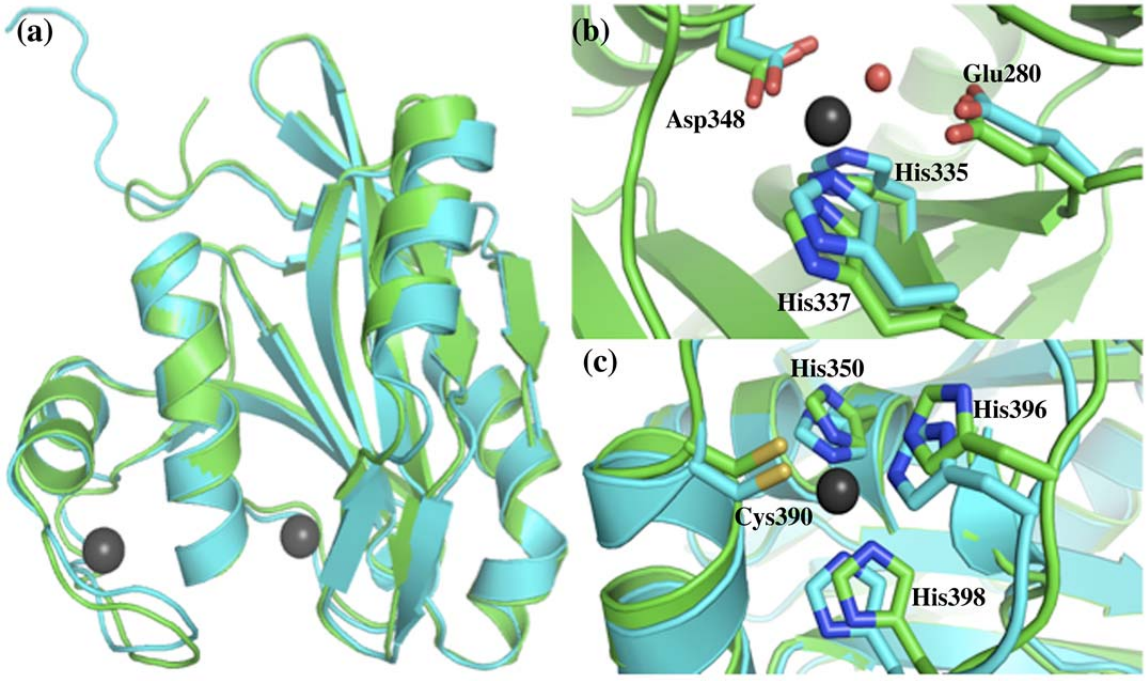

Figure 2.6. Structural comparison of the catalytic domains of AMSH and AMSH-LP. (a) Backbone superposition of AMSH (shown in green) and AMSH-LP (shown in cyan). (b) Expanded view of the zinc-coordinating residues in the active site. (c) Expanded view of the residues coordinating the second zinc. The coordinating residues are shown as sticks, with carbon shown in green and cyan, oxygen in red, nitrogen in blue and sulfur in yellow. Zinc is shown as grey sphere.

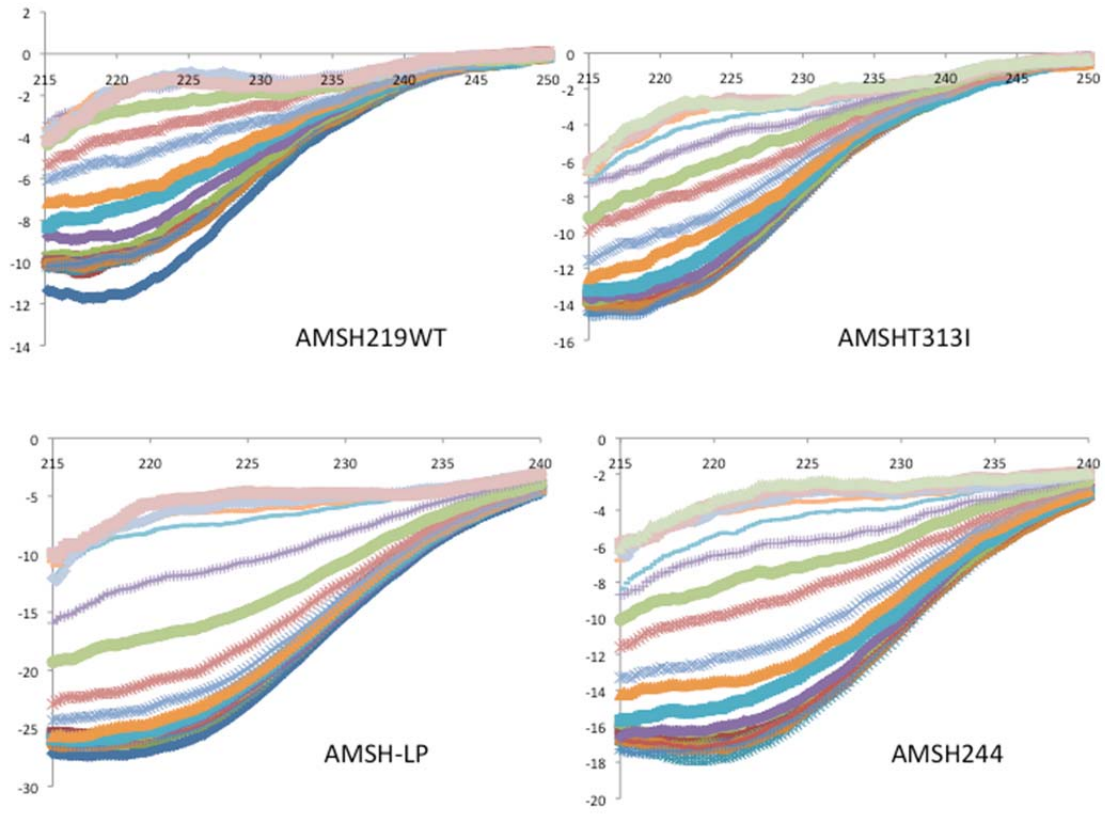

Figure 2.7. Circular dichroism spectra of guanidine hydrochloride induced melting. Raw data of the guanindine hydrochloride induced melting experiment for (a) AMSH and (b) AMSH-LP. Both spectra show a decrease in signal with increasing concentration of guanidine. Spectra has reported as mean molar ellipticity.

Table 2.2. Stability Data

	ΔG_{H20} (kcal.mol^{-1})	$[GdHCl]_{0.5}$ (M)	m (kcal.mol^{-1}.M^{-1})
AMSH244	**3.7**	**2.7**	**-1.4**
AMSH219	**3.6**	**2.5**	**-1.4**
AMSHT313I	**2.9**	**2.7**	**-1.1**
AMSH-LP DUB	**4.9**	**3.5**	**-1.4**

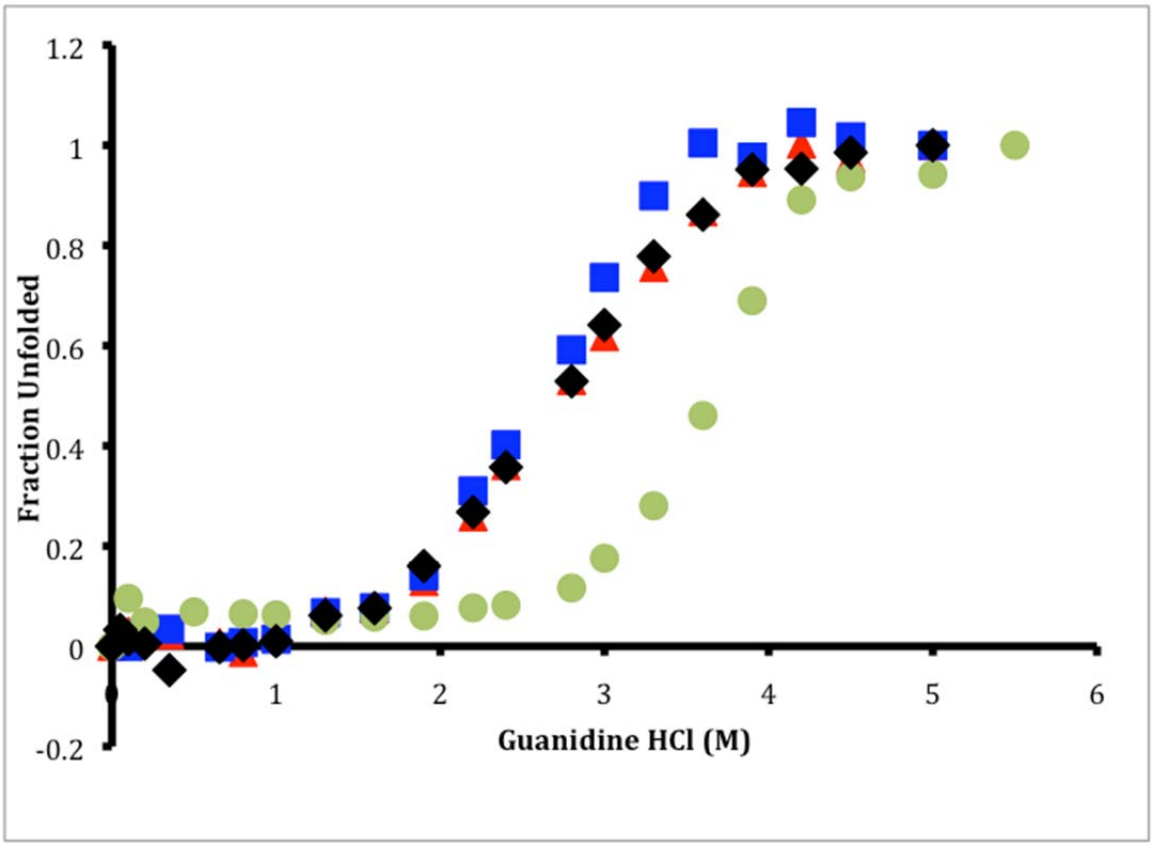

Figure 2.8. Fraction unfolded curves comparing the stability of two wild-type AMSH catalytic domain segments: AMSH244 (black diamonds) and AMSH219 (blue squares), the DUB domain of AMSH-LP (green circles), and the MIC-CAP mutants, T313I (red triangles) with increasing concentrations of GdHCl followed by circular dichroism spectroscopy (CD) at 220nm.

CHAPTER 3: COMPARISON OF KINETIC PROPERTIES OF AMSH AND AMSH-LP

3.1 Introduction

This chapter's aim is to provide further insight into the differences between AMSH and AMSH-LP by comparing their kinetic properties. We have carried out a DUB diubiquitin cleavage assay in which we have determined the Michaelis-Menten kinetic parameters. We see that AMSH-LP is ~4-fold more active compared to AMSH mainly due to a 10-fold increase in k_{cat}. To help understand this difference in catalytic activity, we modeled the structure of the catalytic domain of AMSH onto the previously determined co-crystal structure of AMSH-LP bound to a Lys63-linked ubiquitin dimer.[1] We see that the proximal ubiquitin recognition between the two enzymes is completely conserved, however, the distal ubiquitin recognition is the main difference between the two enzymes, arising from three residue substitutions, one of which (Thr313) is mutated in microcephaly capillary malformation (MIC-CAP) syndrome.[2] To assess the role of these residues within AMSH, we carried out extensive mutational and kinetic analyses introducing individual point mutations within the active site, proximal, and distal ubiquitin binding sites to determine their individual kinetic parameters. Our results confirm that AMSH's proximal ubiquitin recognition reveals similar effects as was seen in AMSH-LP, but much to our surprise, the distal ubiquitin site differed from AMSH-LP with the most significant effects seen when residues Thr313 and Glu316 were modified.

These data further separate the catalytic mechanisms of AMSH and AMSH-LP, which could correlate to AMSH, not AMSH-LP, recruitment to regulate the ESCRT machinery.

3.2 Materials and Methods

3.2.1 Cloning, Expression, and Purification

The DNA encoding the catalytic domain of AMSH was amplified by PCR using a plasmid that contained full-length DNA as the template (pGEX-6p1-AMSH, a kind gift from Sylvie Urbe, University of Liverpool, UK) and was subcloned into pGEX-6p1 (GE Biosciences) by using standard cloning protocols. The resulting N-terminally fused glutathione S-transferase (GST)-tagged protein was expressed in *Escherichia coli* Rosetta cells (Novagen) and purified with a glutathione-Sepharose column (GE Biosciences) following manufacturer's instructions. After removal of the tag by PreScission protease (GE Biosciences), the protein was further purified by size-exclusion chromatography (SEC) using Superdex S75 column (GE Biosciences).

The series of individual point mutations were introduced into the AMSH catalytic domain gene by site-directed mutagenesis using QuikChange Site-Directed Mutagenesis Kit (Stratagene) following manufacturer's protocol. DNA sequencing confirmed the presence of the mutations. The resulting proteins were purified using standard GST-affinity chromatography followed by SEC (Superdex S75 column).

Human ubiquitin (residues 1-75) was subcloned into pGEX-6p1 and purified using GST affinity chromatography, and the GST tag was removed by PreScission

Protease. The protein was further purified using SEC (Superdex S75 column). Lys63-diubiquitin was enzymatically synthesized from ubiquitin using ATP, human E1, and the E2 complex (Ubc13 and Uev1a) following previously reported procedures.[1] The reaction was incubated at 37°C for 2 h and then quenched by dilution with buffer A (50 mM sodium acetate, pH 4.5). The quenched reaction mixture was subjected to ion-exchange chromatography on a Mono-S column (GE Biosciences) to obtain Lys63-diubiquitin.

3.2.2 Determination of Kinetic Parameters

The qualitative *in vitro* DUB assay was carried out by incubating wild-type AMSH244, wild-type AMSH219, wild-type AMSH219 (expressed and purified in the absence of DTT) ($AMSH219^{-DTT}$), $AMSH219^{C282A}$ (expressed and purified in the absence of DTT), and $AMSH219^{E280A}$ to a final enzyme concentration of 100 nM with 20 μM K63-linked diubiquitin in a total reaction volume of 20 μL. All reactions were carried out in reaction buffer (50 mM TRIS-HCl pH 7.0, 25 mM KCl, 5 mM $MgCl_2$, and 1 mM DTT) for one hour at 20°C, except $AMSH219^{-DTT}$ and $AMSH219^{C282A}$ were incubated in the same reaction buffer without the 1 mM DTT. The reaction was quenched by the addition of 5X SDS-PAGE sample buffer followed by boiling, and then analyzed by SDS-PAGE.

The kinetic parameters of AMSH244 were determined by incubating 100 nM of enzyme with four concentrations of diubiquitin ranging from 20-100 μM in reaction buffer (50 mM TRIS-HCl pH 7.0, 25 mM KCl, 5 mM $MgCl_2$, and 1 mM DTT) along with ubiquitin standards ranging from 4-12.3 μg. The reaction was carried out at 20°C for 15

minutes for initial velocity measurements. Reaction tubes were quenched by the addition of 5X SDS-PAGE sample Buffer followed by boiling. The reaction mixtures were visualized by SDS-PAGE gels and scanned. Bands corresponding to ubiquitin were integrated using ImageJ software (http://rsb.info.nih.gov/ij/). Kinetic parameters were calculated by fitting the data in SigmaPlot.

The kinetic parameters were determined by incubating the enzymes (25 nM T313A, 100 nM C282A, N312A, T313I, E317A, and F320A, 2 μM E316A and F395A, 3 μM T341A and S346A, and 10 μM F343A and S345A) with four concentrations of diubiquitin, ranging from 20 to 177μM, in reaction buffer (50 mM TRIS-HCl (pH 7.0), 20 mM KCl, 5 mM $MgCl_2$ and 1 mM DTT). The reaction was carried out at 20°C for 10-75 min depending on activity for initial velocity measurements. Reaction tubes were quenched as described above. Ubiquitin quantification and kinetic parameters were calculated as described before.

3.3 Results

3.3.1 Qualitative Analysis of the Kinetic Activity of AMSH

The previous chapter discusses the crystal structures of two constructs of the catalytic domain of AMSH, AMSH244 and AMSH219^{E280A}. Within the AMSH219^{E280A} structure we found a potential disulfide bridge between Cys282 and Cys311 that is 7.4Å away from the active-site Zn^{2+}. In order to understand if the varying lengths of AMSH and if Cys282 has any effect on the activity of the enzyme, we carried out a qualitative

Lys63-linked diubiquitin cleavage assay. It was found that the catalytic activities of AMSH244 and AMSH219 are similar (Figure 3.1), suggesting that the SH3 domain-binding peptide segment does not fold onto the catalytic domain, at least not in way to influence diubiquitin binding. As expected, the E280A mutant is still catalytically inactive despite having the zinc in place (Figure 3.1), as determined from the x-ray crystal structure. To probe if the oxidation state of Cys282 is important for the catalytic activity of the enzyme, a mutant that would lack the disulfide bond (the Cys282 to Ala mutant) was introduced and purified without DTT at all steps. The catalytic activity of the Cys282Ala mutant appears to be similar to the wild-type protein's activity (the mutant retains ~80 % of activity seen with the wild type) (Figure 3.1).

3.3.2 Comparison of the Kinetic Activities of AMSH and AMSH-LP

The overall three-dimensional fold of the catalytic domains of AMSH and AMSH-LP are structurally identical, having conserved active-site residues and architecture; we proceeded to understand if there are differences between the two enzymes kinetically. We found that AMSH244 is catalytically less efficient than the DUB domain of AMSH-LP, with most of the difference being contributed by a k_{cat} that is 10-fold less, but with a slightly better K_M (2-fold lower) (Table 3.1 and Figure 3.2).

3.3.3 Mutational and Kinetic Analysis of the Catalytic Domain of AMSH

To gain insight into how AMSH would recognize Lys63-linked diubiquitin, a model of AMSH244 bound to Lys63-linked ubiquitin dimer was generated by

superimposing AMSH244 onto the previously determined X-ray structure of the DUB domain of AMSH-LP^{E292A} bound to Lys63-linked ubiquitin dimer (PDB code: 2ZNV) (Figure 3.3).[1] The overall structure of AMSH244 is similar to ubiquitin-bound DUB domain of AMSH-LP with an rmsd (root mean square deviation) of 0.93Å of Cα atoms. This level of structural similarity suggests that the mode of diubiquitin binding seen in the model would be preserved in the actual structure of AMSH244 bound to Lys63-linked diubiquitin. To further validate that AMSH does indeed have a very different catalytic mechanism compared to AMSH-LP based on the difference in catalytic activity, we introduced individual point mutations within the AMSH catalytic domain gene and carried out an extensive kinetic analysis.

3.3.3.1 Active Site

The active site of AMSH consists of a Zn^{2+} ion, coordinated directly by three residues (Asp348, His 335, and His337) and a water molecule that is hydrogen bonded to Glu280, and a putative oxy-anion stabilizing residue (Ser345) (Figure 3.4). In order to probe the roles of Asp348 and Glu280, we generated two aspartate mutants (D348A and D348N) and a glutamate mutant (E280A) and, as expected, found that there was no detectable activity in these mutants (Table 3.2), most likely due to the loss of Zn^{2+} for the aspartate mutations and the loss of the water molecule in the glutamate mutation.

Next, we probed the function of the putative oxy-anion hole-stabilizing residue, Ser345. Mutating serine to alanine resulted in a significantly impaired enzyme with a 1000-fold reduction in k_{cat} (Table 3.2). As described with other families of hydrolases, the

oxy-anion hole-stabilizing residue plays a critical role in donating a hydrogen bond to the negatively charged tetrahedral intermediate formed after the initial nucleophilic attack. Substantial reduction of k_{cat} alone upon mutation to alanine, with K_M remaining nearly the same, is consistent with Ser345 playing the role as the oxy-anion stabilizing residue in AMSH.

In our previous structural analysis, we noted a potential disulfide bridge between Cys282 and Cys311, 7.4Å away from the active-site Zn^{2+}.[3] Previous studies have shown that N-ethylmaleimide (NEM) inhibits AMSH activity (IC_{50} of 16.2± 3.2 μM),[4; 5] presumably by modifying one of these two cysteines, perhaps Cys282 because it is proximal to the active-site cleft. Its modification might introduce some steric hindrance for substrate binding thus explaining the inhibitory effect. We sought to determine if Cys282 has any role in the catalytic activity of the enzyme. Previously, when Cys282 was mutated to alanine, we noticed a loss of activity,[3] however, a more detailed kinetic analysis of this mutant revealed a more significant reduction in activity, a 6-fold loss in k_{cat} (Table 3.2), which would suggest that Cys282 does indeed have a role in catalysis. Cys282 is seen making a van der Waals contact with Leu73 of the distal ubiquitin, which may explain the reduction in activity observed here.

3.3.3.2 Proximal Ubiquitin Site

Modeling of the catalytic domain of AMSH onto the structure of AMSH-LP bound to Lys63-linked diubiquitin revealed four residues within AMSH (Thr341, Phe343, Ser346, and Phe395) that could determine its specificity for Lys63-linked polyubiquitin chains by recognizing the tri-peptide sequence motif Gln62-Lys63-Glu64

within the proximal ubiquitin, which encompasses the acceptor Lys63 and its two immediate flanking residues. Individual point mutants (to alanine) were generated and kinetic analysis was performed to probe the functional significance of these residues. Overall, the four resides within AMSH showed a drastic reduction in k_{cat} with similar K_M values compared to the wild-type enzyme, confirming their utmost importance to the enzyme's catalytic mechanism (Figure 3.5 and Table 3.2), especially during the rate-determining step of isopeptide bond hydrolysis.

3.3.3.3 Distal Ubiquitin Site

The distal site is where AMSH significantly differs from AMSH-LP in diubiquitin recognition. Three substitutions are found going from AMSH-LP to AMSH: an aspartate to asparagine, a methionine to a threonine, and a valine to glutamate. Two other important residues within the distal site are completely conserved between AMSH and AMSH-LP, a phenylalanine (Phe320, AMSH numbering) and a glutamate (Glu317) (Figure 3.6). The conserved Phe320 when mutated to alanine exhibited a 4-fold reduction in k_{cat} and 3-fold increase in K_M, whereas, the Glu317Ala mutant exhibits somewhat similar activity to the wild type, with only a modest 2-fold reduction in k_{cat} (Table 3.2).

Moving forward, individual point mutations of the three substitutions between AMSH and AMSH-LP revealed some interesting results. Mutating Asn312 to alanine yielded only an approximate 3-fold reduction in k_{cat} (Table 3.2). Surprisingly, a qualitative diubiquitin cleavage assay revealed that Thr313Ala was apparently more

active than the wild type (Figure 3.7), however, detailed kinetic analysis showed simply an approximate 2-fold increase in k_{cat}, with a ~3-fold loss in K_M (Table 3.2).

Mutating the Glu316 to alanine proved to cause the most significant change in enzymatic activity amongst the distal site residues. Glu316Ala showed a substantial 74-fold reduction in k_{cat} (Table 3.2). This k_{cat} effect differs strikingly from the distal site residues from AMSH-LP whose mutation to Ala showed a loss primarily in K_M.[1] The effect of the glutamate mutation in AMSH mirrors that of residues from the proximal site. Inspection of the AMSH-diubiquitin model reveals that Glu316 is within hydrogen-bonding distance from two distal ubiquitin residues: Arg42 is within 3.1Å (εN of Arg42 and εO of Glu316), and Gln49 is within 2.8Å, if the side chain is flipped by 180° (Figure 3.6). A significant loss in k_{cat} but not in K_M is consistent with these hydrogen-bonding interactions contributing to the stabilization of the transition state, perhaps by playing a role in orienting the scissile peptide bond for nucleophilic attack.

3.3.4 Kinetic Characterization of the Effect of the MIC-CAP-associated Mutation, Thr313Ile

To better understand the molecular basis of the MIC-CAP syndrome, the Thr313Ile (T313I) mutant was generated and analyzed for its catalytic activity towards Lys63-diubiquitin. In the absence of a structure, a modeled AMSH-diubiquitin structure suggests that the side-chain hydroxyl from threonine is hydrogen bonded to the backbone NH group of Leu73 in the distal ubiquitin (Figure 3.7). The T313I mutant was found to suffer a 6-fold reduction in k_{cat}, with a comparable K_M (Table 3.2). This result indicates

that the reduced catalytic activity of the mutant, with a similar thermodynamic stability, could lead to a loss of function of AMSH translating into the disease state.

3.4 Discussion

Our kinetic analysis using site-directed mutants of conserved residues in the proximal ubiquitin binding site has shown that AMSH's specificity for Lys63-linked polyubiquitin chains arises from its recognition of the proximal ubiquitin, similar to the case of AMSH-LP.[1] Lys63-linked chain specificity for AMSH plays a significant role in understanding its function as an ESCRT-DUB. Since Lys63-linked polyubiquitin chains are targeting signals for ESCRT-mediated degradation, the specific DUB activity of AMSH may play a central role in the persistent functionality of the ESCRT machinery. Mutation of the proximal ubiquitin binding residues causes drastic reduction in k_{cat}, suggesting that recognition of the tri-peptide sequence motif Gln62-Lys63-Glu64 within the proximal ubiquitin plays a significant role AMSH's ability to cleave Lys63-linked polyubiquitin chains. Recognition of Lys63 isopeptide bond and its two flanking residues in the proximal ubiquitin would mean that AMSH could only efficiently hydrolyze bonds between successive ubiquitins in a polymeric chain, and not the last ubiquitin directly attached to a protein receptor (the cargo). This impediment toward completely deubiquitinating a ubiquitinated receptor could have multiple functional implications. At the outset, it calls into question the functional role of AMSH when it is recruited to ESCRT-III, where complete deconjugation of a ubiquitinated cargo is the absolute desire, since ubiquitin will otherwise end up in intralumenal vesicles (ILVs) attached to the cargo and will be subsequently degraded in the lysosome. It seems

unlikely that AMSH can have a significant catalytic role with respect to hydrolyzing the last ubiquitin attached to the cargo, yet, AMSH binds to ESCRT-III component CHMP3 with relatively high affinity.

Our data on mutational analysis of the distal ubiquitin binding residues offer some interesting insights. Of the three residues different between AMSH and AMSH-LP, two of them, Glu316 and Thr313, contribute significantly to catalysis playing different roles than the corresponding residues in AMSH-LP. The AMSH residue Glu316 contributes to stabilization of the transition state as indicated by the largely k_{cat} effect when it is mutated to Ala, in contrast to mostly a K_M effect observed when the corresponding residues Val in AMSH-LP mutated to Ala.[1] Thr313 in our AMSH-diubiquitin model is seen making a hydrogen bonding contact with the backbone NH group of Leu73 of the distal ubiquitin using its side-chain hydroxyl group and its methyl group is engaged in van der Waals contact with the aliphatic side groups of Leu73 from ubiquitin. Its substitution with Ile as seen in children with the MIC-CAP syndrome is expected to preserve the van der Waals contact but loose the hydrogen bond. Our data show that the substitution of the Thr to an Ile has minimal effect on protein folding and stability, but results in a significantly reduced catalytic efficiency. Going from AMSH to AMSH-LP, the Thr residue is replaced by Met, which could contribute only van der Waals interaction with the substrate. Thus, it appears that the hydrogen-bonding interaction of Thr in AMSH has a unique role whose loss leads to a dramatic effect resulting in a loss of function substantial enough to cause the disease. Overall, these results indicate that subtle differences between very similar enzymes can have profound functional effect.[6] Another important thing that our kinetic data has shown is that AMSH and AMSH-LP are more different

than initially thought. Sharing very close homology and structural similarities usually allow for these two proteins to be used interchangeably. Our distal site mutational and kinetic analysis reveals that the differences are on the scale of individual residue differences. We saw three residue changes between AMSH and AMSH-LP and one of those, Thr313, is found in children with MIC-CAP syndrome. It is interesting to see that a simple modification of the threonine to an isoleucine has minimal effect on protein folding and stability, but has significantly reduced catalytic properties. Then again we see that Glu316 plays a surprisingly downstream catalytic role within AMSH as well. This shows that not only does AMSH-LP lack the functional domains required to be recruited to the ESCRT machinery, but also, that AMSH has inherent catalytic regulatory mechanism that lay within its amino acid sequence, that when modified proves to be very detrimental.

Overall, the kinetic analysis of AMSH reveals that even though AMSH has a similar structural makeup and sequence homology to AMSH-LP, AMSH is hardwired to function significantly different than AMSH-LP. Beginning with the 10-fold difference in the activity of the wild type protein to the three residue differences in the distal ubiquitin binding site, AMSH has the necessary characteristics that promote its function within the ESCRT complex. The most important thing these kinetic analyses have shown is that small residue level changes can translate into significant differences in protein function. These data provide further evidence that AMSH plays an exquisite and necessary function within the ESCRT machinery that absolutely cannot be fulfilled by AMSH-LP.

3.5 References

1. Sato, Y., Yoshikawa, A., Yamagata, A., Mimura, H., Yamashita, M., Ookata, K., Nureki, O., Iwai, K., Komada, M. & Fukai, S. (2008). Structural basis for specific cleavage of Lys 63-linked polyubiquitin chains. *Nature* **455**, 358-62.

2. McDonell, L. M., Mirzaa, G. M., Alcantara, D., Schwartzentruber, J., Carter, M. T., Lee, L. J., Clericuzio, C. L., Graham, J. M., Jr., Morris-Rosendahl, D. J., Polster, T., Acsadi, G., Townshend, S., Williams, S., Halbert, A., Isidor, B., David, A., Smyser, C. D., Paciorkowski, A. R., Willing, M., Woulfe, J., Das, S., Beaulieu, C. L., Marcadier, J., Geraghty, M. T., Frey, B. J., Majewski, J., Bulman, D. E., Dobyns, W. B., O'Driscoll, M. & Boycott, K. M. (2013). Mutations in STAMBP, encoding a deubiquitinating enzyme, cause microcephaly-capillary malformation syndrome. *Nat Genet* **45**, 556-62.

3. Davies, C. W., Paul, L. N., Kim, M. I. & Das, C. (2011). Structural and thermodynamic comparison of the catalytic domain of AMSH and AMSH-LP: nearly identical fold but different stability. *J Mol Biol* **413**, 416-29.

4. McCullough, J., Clague, M. J. & Urbe, S. (2004). AMSH is an endosome-associated ubiquitin isopeptidase. *J Cell Biol* **166**, 487-92.

5. Arnst, J. L., Davies, C. W., Raja, S. M., Das, C. & Natarajan, A. (2013). High-throughput compatible fluorescence resonance energy transfer-based assay to identify small molecule inhibitors of AMSH deubiquitinase activity. *Anal Biochem*.

6. Komander, D., Clague, M. J. & Urbe, S. (2009). Breaking the chains: structure and function of the deubiquitinases. *Nat Rev Mol Cell Biol* **10**, 550-63.

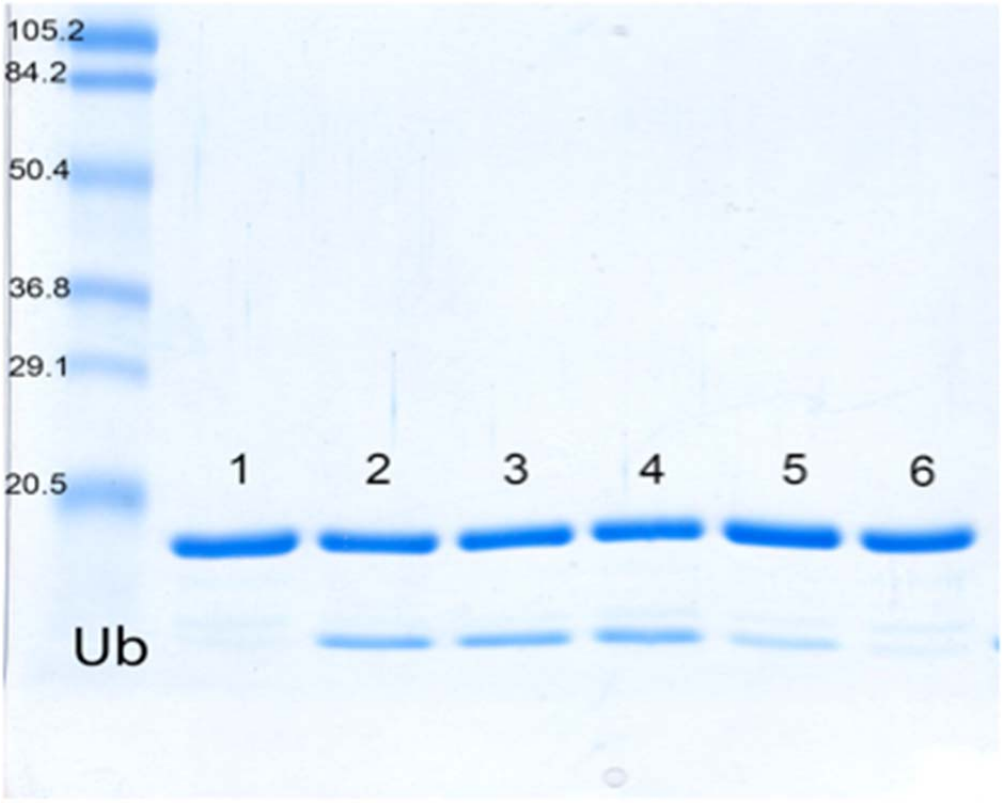

Figure 3.1. K63-linked AMSH Activity Assay. Lane 1. Diubiquitin. Lane 2. AMSH244. Lane 3. AMSH219WT. Lane 4. AMSH219^{-DTT}. Lane 5. AMSH219^{C282A}. Lane 6. AMSH219^{E280A}.

Table 3.1. AMSH and AMSH-LP Kinetic Parameters

Enzyme	k_{cat} (s^{-1})	K_M (μM)	k_{cat} / K_M x 10^{-3} ($\mu M^{-1} s^{-1}$)
AMSH244	1.4 ± 0.1	32.0 ± 5.3	43.8
AMSH-LP DUB	10.3 ±0.3	66.2 ± 4.8	155.6
	0.860 ± 0.0654*	71.8 ± 6.3*	12.0*

*Kinetic parameters reported from Sato et al. Nature (2008). Differences in values are presumably due to the difference in substrates used in the activity assay.

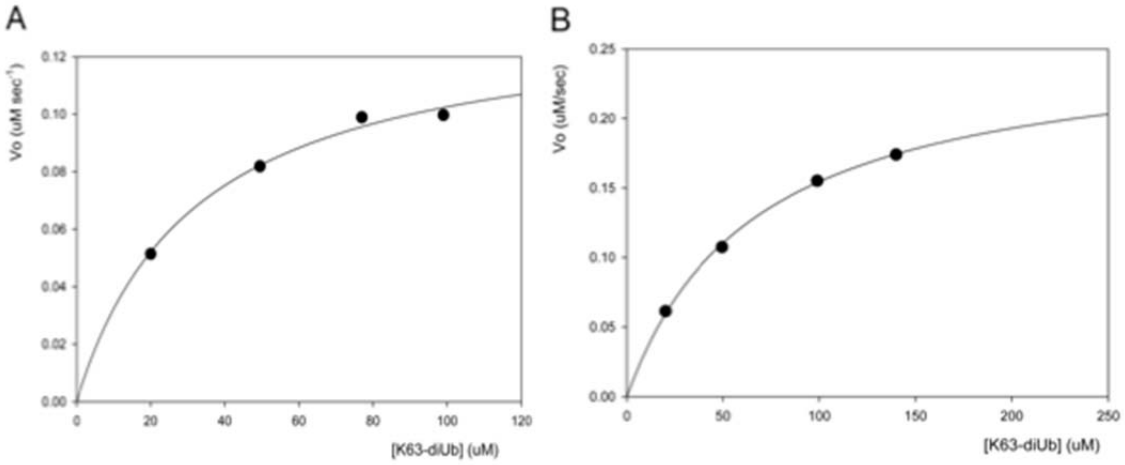

Figure 3.2. Michaelis-Menten curves for AMSH244 and AMSH-LP DUB. Plots of initial velocity versus substrate concentration for which the kinetic parameters of (A) AMSH244 and (B) AMSH-LP DUB Domain were derived.

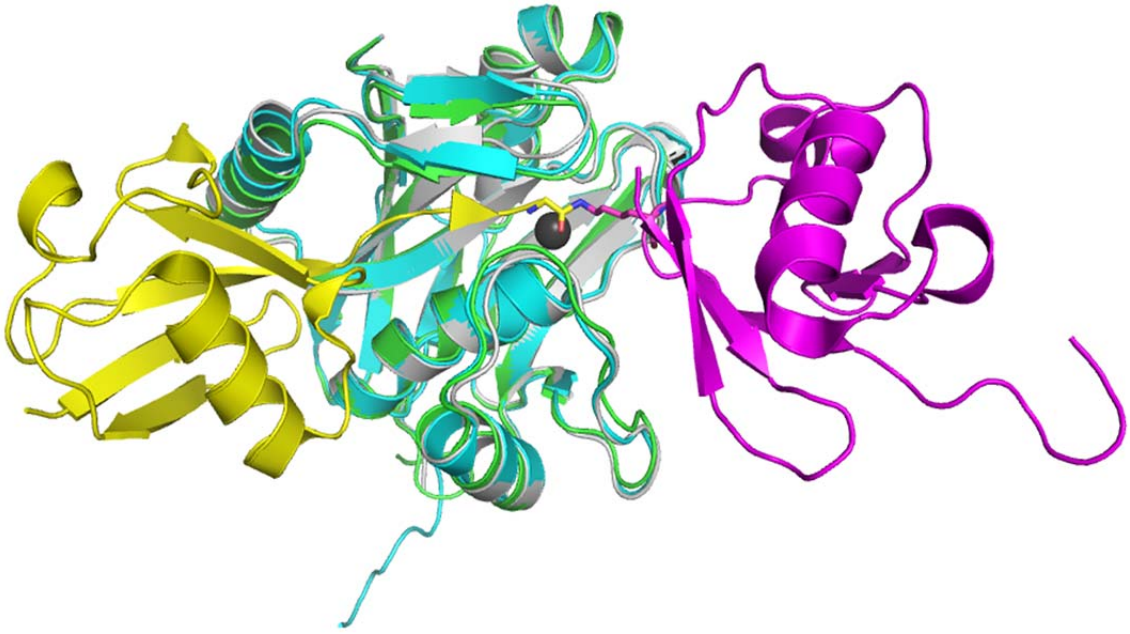

Figure 3.3. A model of AMSH244 bound to Lys63-linked ubiquitin dimer. Backbone superposition of AMSH244 (green), the DUB domain of AMSH-LP (cyan), and the DUB domain of AMSH-LP bound to Lys63-linked diubiquitin (gray). The proximal ubiquitin and distal ubiquitin are shown in magenta and yellow ribbon, respectively.

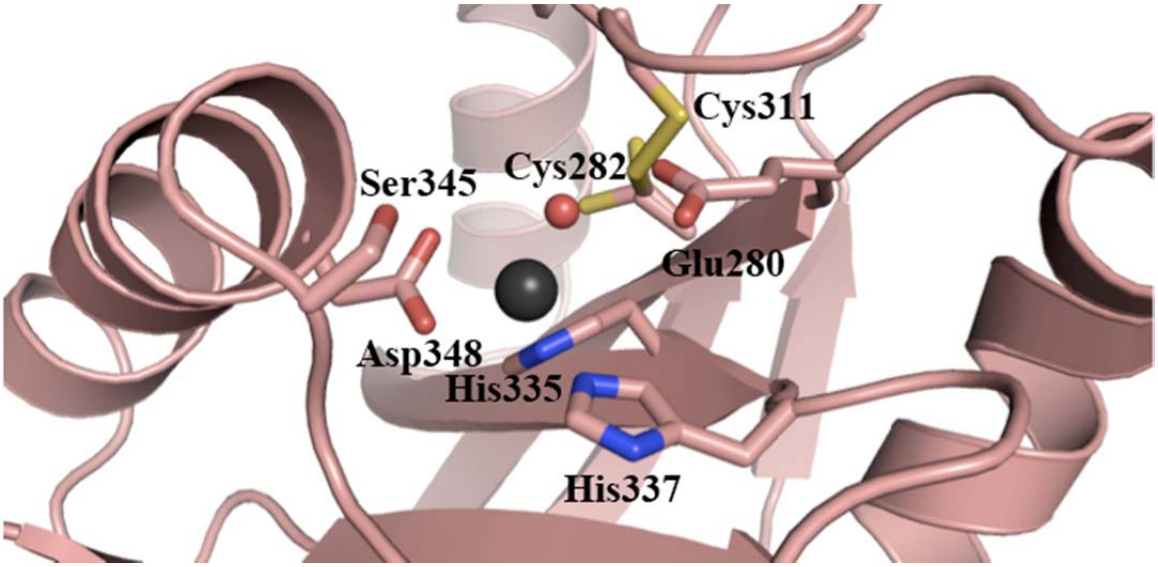

Figure 3.4. A view of the active site of AMSH. The active-site Zn^{2+} is shown as a black sphere and the active-site water molecule is shown as a red sphere.

Table 3.2. AMSH Catalytic Domain Mutants.

Site	Protein	k_{cat} x 10^{-3} (s^{-1})	K_M (μM)
	Wild type	1400 ± 100	32.0 ± 5.3
Active site			
	Glu280Ala	ND	ND
	Cys282Ala	230 ± 140	44.7 ± 7.4
	Ser345Ala	1.4 ± 0.1	38.2 ± 15.3
	Asp348Ala	ND	ND
	Asp348Asn	ND	ND
Proximal			
	Thr341Ala	24 ± 1.0	15.2 ± 2.7
	Phe343Ala	5 ± 3.0	20.8 ± 4.2
	Ser346Ala	13 ± 3.0	23.0 ± 7.6
	Phe395Ala	22 ± 8.0	18.4 ± 9.3
Distal			
	Asn312Ala	430 ± 60	19.0 ± 2.3
	Thr313Ala	2600 ± 600	81.7 ± 5.2
	Glu316Ala	19 ± 4	31.1 ± 8.9
	Glu317Ala	750 ± 200	18.8 ± 6.6
	Phe320Ala	370 ± 20	97.5 ± 14.8
MIC-CAP			
	Thr313Ile	225 ± 39	21.3 ± 4.7

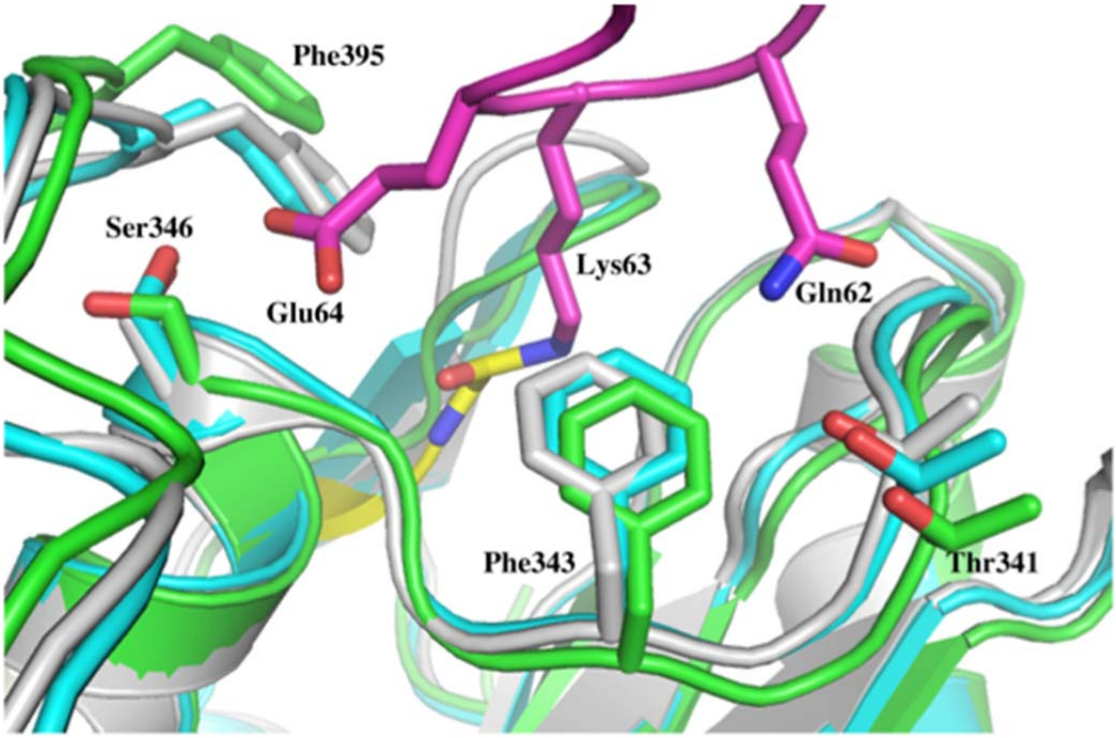

Figure 3.5. View of the residues involved in the proximal ubiquitin recognition. Superposition of AMSH244 (green ribbon), the DUB domain of AMSH-LP (cyan ribbon) and the DUB domain of AMSH-LP bound to Lys63-linked diubiquitin (gray ribbon). Residues from the proximal ubiquitin making contact at the proximal site are shown in magenta.

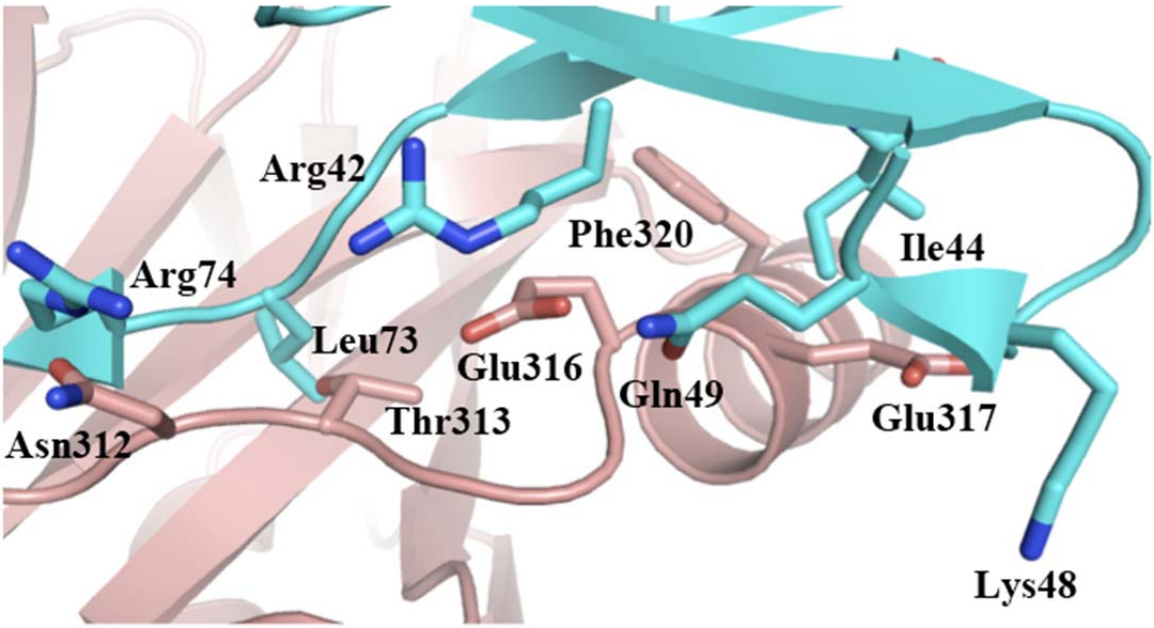

Figure 3.6. View of the residues involved in the distal ubiquitin recognition. Superposition of AMSH244 (green ribbon) and the DUB domain of AMSH-LP bound to Lys63-linked diubiquitin (gray ribbon). The distal ubiquitin is shown in yellow. Hydrogen bonding interactions are shown as black dashes and van der Waals interactions are shown as blue dashes.

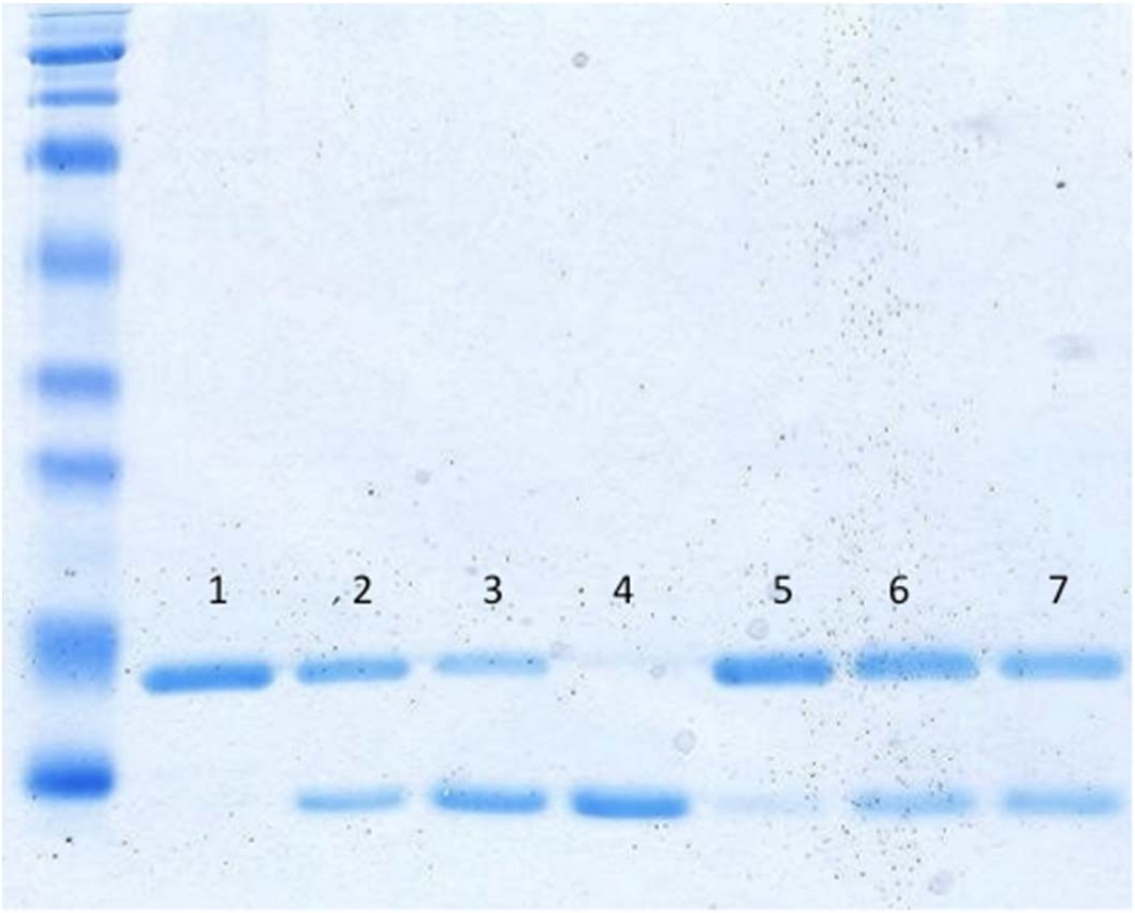

Figure 3.7. Qualitative DUB Lys63-diubiquitin cleavage assay of the residues within AMSH's catalytic domain that recognize the distal ubiquitin. Lane 1: Lys63-diubiquitin. Lane 2: AMSH219WT. Lane 3: N312A. Lane 4: T313A. Lane 5: E316A. Lane 6: E317A. Lane 7: F320A.

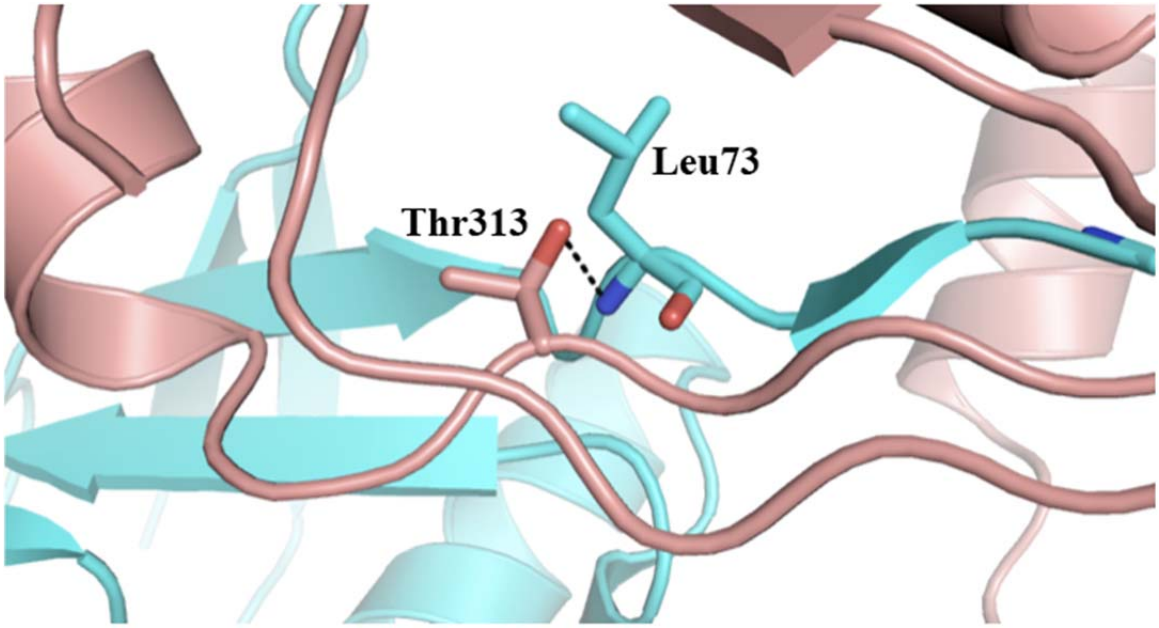

Figure 3.8. Structural modeling of the interaction between Thr313 and the distal ubiquitin to understand the role of the MIC-CAP-associated mutation, Thr313Ile.

CHAPTER 4: MECHANISM OF AMSH RECRUITMENT AND ACTIVATION AT ESCRT-0

4.1 Introduction

The aim of this chapter is to provide further evidence in support of the exquisite role of AMSH as an important regulator of the ESCRT machinery by revealing a mechanism for enzyme activation at ESCRT-0 and to assign a role for AMSH at ESCRT-0. I have employed a biophysical and biochemical approach to probe the function of AMSH at ESCRT-0. It was found that diubiquitin and ubiquitin bind with similar affinities to the catalytic domain of AMSH, suggesting only one binding site for ubiquitin, which sets up a mechanism for how the ESCRT-0 member, STAM, supports AMSH-diubiquitin binding. Using the minimal domains of STAM, the UIM and SH3 domains, both AMSH and ubiquitin binding to STAM were characterized, and then, the ternary complex of AMSH, the SH3 domain fused to its N-terminally adjacent UIM (UIM-SH3), and Lys63-linked diubiquitin were kinetically characterized. The AMSH-SH3 interaction was confirmed by both isothermal titration calorimetry (ITC) and analytical ultracentrifugation (AUC). Furthermore, UIM-ubiquitin binding was assessed by ITC, however, unexpectedly, the SH3 domain of STAM was shown to binds ubiquitin independently, with similar affinity to the UIM. Building up the ternary complex revealed the role of UIM in stimulating AMSH activity in which mutations within the UIM and SH3 domains failed to recapitulate this activation phenomenon, suggesting that

an intact AMSH-SH3 interaction and a functional UIM is required for AMSH activation. These data together suggest a model for how AMSH would work at ESCRT-0 in which diubiquitin is held in tandem by both the enzyme and the UIM of STAM, stabilizing the chain, thus, stimulating the activity of the enzyme. This model suggests that AMSH has the role of promoting cargo shuttling from ESCRT-0 to the subsequent complexes.

4.2 Materials and Methods

4.2.1 Cloning, Expression, and Purification

The DNA encoding the catalytic domain of AMSH was amplified by PCR using a plasmid that contained full-length DNA as the template (pGEX-6p1-AMSH, a kind gift from Sylvie Urbe, University of Liverpool, UK) and was subcloned into pGEX-6p1 (GE Biosciences) by using standard cloning protocols. The resulting N-terminally fused glutathione S-transferase (GST)-tagged protein was expressed in *Escherichia coli* Rosetta cells (Novagen) and purified with a glutathione-Sepharose column (GE Biosciences) following manufacturer's instructions. After removal of the tag by PreScission protease (GE Biosciences), the protein was further purified by size-exclusion chromatography (SEC) using Superdex S75 column (GE Biosciences).

The series of individual point mutations were introduced into the AMSH catalytic domain gene by site-directed mutagenesis using QuikChange Site-Directed Mutagenesis Kit (Stratagene) following manufacturer's protocol. DNA sequencing confirmed the

presence of the mutations. The resulting proteins were purified using standard GST-affinity chromatography followed by SEC (Superdex S75 column).

The DNA encoding the SH3 and UIM-SH3 domains was amplified by PCR using a plasmid that contained the full-length DNA as the template (pGW1Myc2c-STAM2, a kind gift from Craig Blackstone, National Institutes of Neurological Disorders and Stroke (NINDS) at the National Institutes of Health (NIH)) and was subcloned into pGEX-6p1 (GE Biosciences) using standard cloning protocols. The resulting N-terminally fused GST-tagged protein was expressed in *E. coli* Rosetta cells (Novagen) and purified with a glutathione-Sepharose column (GE Biosciences) following manufacturer's instructions. After removal of the tag by PreScission protease (GE Biosciences), the protein was further purified by size-exclusion chromatography (SEC) using Superdex S75 column (GE Biosciences).

The A176G mutation was introduced into the UIM-SH3 gene by site-directed mutagenesis using QuikChange Site-Directed Mutagenesis Kit (Stratagene) following manufacturer's protocol. DNA sequencing confirmed the presence of the mutations. The resulting proteins were purified using standard GST-affinity chromatography followed by SEC (Superdex S75 column).

Human ubiquitin was subcloned into pGEX-6p1 and purified using GST affinity chromatography, and the GST tag was removed by PreScission Protease. The protein was further purified using SEC (Superdex S75 column). Lys63-diubiquitin was enzymatically synthesized from ubiquitin using ATP, human E1, and the E2 complex (Ubc13 and Uev1a) following previously reported procedures.[1] The reaction was

incubated at 37°C for 2 h and then quenched by dilution with buffer A (50mM sodium acetate, pH 4.5). The quenched reaction mixture was subjected to ion-exchange chromatography on a Mono-S column (GE Biosciences) to obtain Lys63-diubiquitin.

4.2.2 DUB Assay

The initial *in vitro* DUB assay was carried out by incubating AMSH (residues 219-424) to a final enzyme concentration of 100 nM with 1 μM of the SH3 domain of STAM2 or UIM-SH3 gene of STAM2, and 20 μM Lys63-diubiquitin in a total reaction volume of 20 μL. All reactions were carried out in reaction buffer (50 mM TRIS-HCl (pH 7.0), 25 mM KCl, 5 mM $MgCl_2$, and 1 mM DTT) for 5 h at 20°C. The reaction was quenched by the addition of 5X SDS-PAGE sample buffer followed by boiling and then analyzed by SDS-PAGE.

The *in vitro* DUB assay to probe the contribution of the SBM and UIM was carried out by incubating AMSH (residues 219-424) to a final enzyme concentration of 1 μM with 5 μM of the STAM binding partner, and 20 μM Lys63-diubiquitin in a total reaction volume of 20 μL. These reactions were carried out in the same reaction buffer as before at 37°C for 15 minutes. The reactions were quenched and visualized as above.

4.2.3 Analytical Ultracentrifugation

Sedimentation velocity experiments were conducted at 50,000 rpm using the Beckman Coulter XLA and XLI (Beckman Coulter, Fullerton, CA, USA). The samples were monitored by both interference and absorbance optics at 254 and 280 nm. The

proteins were dialyzed in 50 mM TRIS-HCl pH 7.6, 50 mM NaCl. Three concentration series for AMSH (residues 219-424) were conducted to evaluate the formation of higher-order species at 24, 48, and 96 μM. The AMSH-SH3 complex was characterized using a constant concentration of 23.5 μM of AMSH and three concentrations of SH3 at 24, 47, and 70 μM. The AMSH-UIM-SH3 complex was characterized using a constant concentration of 23.5 μM of AMSH and three concentrations of 48, 144, and 288 μM. The AMSH-ubiquitin complex was characterized using a constant concentration of 23.5 μM of AMSH and two concentrations of ubiquitin at 23 and 92μM. The AMSH-diubiquitin complex was characterized using a constant concentration of 23.5 μM of AMSH and three diubiquitin concentrations at 24, 48, and 96 μM. The solvent density (1.00170 $g.ml^{-1}$), viscosity (0.01022 poise), and the partial specific volumes that were used for the analyses, 0.73387 $ml.g^{-1}$ (AMSH219), 0.71870 $ml.g^{-1}$ (AMSH-SH3), 0.71701 $ml.g^{-1}$ (AMSH-UIM-SH3), 0.72934 $ml.g^{-1}$ (AMSH-diubiquitin), and 0.72479 $ml.g^{-1}$ (AMSH-ubiquitin), were calculated by SEDNTERP v. 20120828 BETA (http://bitcwiki.sr.unh.edu/index.php/Main_Page).[2] The sedimentation coefficients and apparent molecular weights were calculated from size distribution analyses [c(s)] using SEDFIT v. 14.3e.[3; 4] The figures were prepared using GUSSI v. 1.0.7b beta with the sedimentation coefficients standardized to $s_{20,w}$ and the data was normalized to the peak area of the complexes.

Sedimentation equilibrium experiments were conducted at 20°C using a 6-channel centerpiece in an AN-60 Ti rotor spun at speeds of 13,200, 29,900, and 42,000 rpm for the AMSH-ubiquitin complex and 11,600, 21,000, and 36,000 rpm for the AMSH-

diubiquitin complex. The molar ratios of the AMSH-ubiquitin complex were: 1:2, 1:4, and 1:8, and the molar ratios of the AMSH-diubiquitin complex were: 1:2, 1:4, and 1:5, to determine the molecular weight of the complexes. Absorbance scans at 280 nm were taken every 2 hours for 60 hours. The samples were tested for equilibrium using Sedfit.[3; 4] Calculations of the molecular weights were done by SEDPHAT v. 10.58d [5; 6; 7; 8; 9; 10] using the Species Analysis and Species Analysis with Mass Conservation Constraints. Errors were calculated using 1-dimensional error surface projections. Final figures were generated in GUSSI.

4.2.4 Isothermal Titration Calorimetry

To determine the K_Ds of AMSH binding to ubiquitin, ITC experiments were conducted using the MicroCal ITC200 (GE Healthcare Life Sciences). The proteins were dialyzed in the same buffer as was used for AUC. For the AMSH-diubiquitin experiment, 10 μM AMSH was in the cell and 500 μM of diubiquitin was in the syringe. The AMSH-ubiquitin titration had 100 μM AMSH in the cell, and 1 mM ubiquitin in the syringe. The F320A mutant of AMSH with ubiquitin had 100 μM of the enzyme in the cell, and 1 mM of ubiquitin in the syringe. These experiments were done at 20°C, 18 total injections of 1.4 μL per injection, with 180 seconds in between injections to allow for a return to baseline before the subsequent injection. The data was then baseline corrected by NITPIC [11] and loaded into SEDPHAT [5; 6; 7; 8; 9; 10] for global analysis and fitting using a 1:1 model. Figures were prepared using GUSSI. To determine the K_D for the AMSH-SH3 interaction, 50 μM of AMSH was in the cell and 750 μM of the SH3 domain was in

the syringe. K_D of AMSH-UIM-SH3 interaction was determined using 100 μM AMSH in the cell and 1 mM UIM-SH3 in the syringe. AMSHK238T-UIM-SH3 experiment was conducted using 50 μM of the enzyme in the cell and 1 mM of UIM-SH3 in the syringe. Characterization of ubiquitin binding to UIM-SH3 was done using 50 μM UIM-SH3 was in the cell and 3.1 mM ubiquitin in the syringe. This data was fit to a two-site model. Confirmation of SH3-ubiquitin binding was done with 100 μM of SH3 in the cell and 3.0 mM ubiquitin in the syringe. The UIM-SH3-Lys63-diubiquitin experiment had 50 μM of UIM-SH3 in the cell and 750 μM diubiquitin in the syringe.

4.3 Results

4.3.1 Biophysical Characterization of Ubiquitin Binding to the Catalytic Domain of AMSH

Mutational and kinetic analyses from the previous chapter prompted us to seek a better understanding of AMSH-ubiquitin complex formation in solution. Using isothermal titration calorimetry (ITC), we analyzed the binding of Lys63-linked diubiquitin and the catalytic domain of AMSH (AMSH 219-424^{E280A}, an inactive mutant to ensure diubiquitin is not hydrolyzed), and obtained an equilibrium dissociation constant (K_D) of 19 ± 4 μM (Figure 4.1b and Table 4.1). As a control, ubiquitin and the catalytic domain of AMSH was analyzed and it was determined that it binds AMSH with similar affinity of 19 ± 3 μM (Figure 4.1a and Table 4.1). Both sedimentation velocity and sedimentation equilibrium experiments using analytical ultracentrifugation (AUC)

confirmed the ITC results (Figure 4.2, Figure 4.3, and Table 4.2). Almost identical binding affinities between diubiquitin and ubiquitin to AMSH's catalytic domain suggest that there is only one binding site for ubiquitin. To probe which ubiquitin binding site is used, another ITC experiment was done with $AMSH^{Phe320Ala}$ (Phe320 at the distal site is mutated to Ala) and ubiquitin. We observed a ~4-fold decrease in affinity (K_D of 81 ± 15 μM) (Figure 4.1c and Table 4.1), consistent with what was observed from kinetics, suggesting that the distal ubiquitin makes the most significant contribution to diubiquitin binding, and the single binding site observed in our ITC experiments with ubiquitin corresponds to binding at the distal site. These data suggest that AMSH alone cannot discriminate between its polyubiquitin substrate and its ubiquitin product.

4.3.2 The Intact Minimal STAM Construct UIM-SH3 is Necessary for AMSH Activation

The I44 patch, a hydrophobic surface centered on the Ile44 residue from ubiquitin, is ubiquitously used by proteins that specifically bind to ubiquitin, including DUBs. Inspection of our structural model representing AMSH-diubiquitin complex reveals that the I44 patch of the distal ubiquitin is satisfied, with the Ile44 residue engaged in van der Waals interaction with Phe320; however, Ile44 of the proximal ubiquitin is unoccupied (Figure 4.4). Looking at the domain structure of the ESCRT-0 member, STAM, one finds a UIM (ubiquitin-interacting motif) N-terminally adjacent to its SH3 domain (Figure 4.5). We sought to understand if the UIM, separated from the SH3 domain by a short linker, could act as an adaptor to AMSH by interacting with the proximal ubiquitin while AMSH's engages the distal one. To probe this, we used a

combination of biophysical techniques and biochemical assays to assess three individual events: (1) AMSH recruitment to STAM via the SH3 domain and a longer STAM segment in which the UIM is fused to the SH3 domain (UIM-SH3), (2) ubiquitin binding to UIM-SH3, and finally, (3) the ternary complex of the catalytic domain of AMSH, UIM-SH3, and Lys63-linked diubiquitin.

4.3.2.1 AMSH Binds to the SH3 Domain of STAM2

To confirm that we have the minimal domains required for the AMSH-STAM interaction we carried out ITC and AUC experiments. We determined that the SH3 domain of STAM binds the catalytic domain of AMSH ($AMSH219^{E280A}$) with a K_D of 1.4 ± 0.04 μM (Table 4.1 and Figure 4.6). Using the longer UIM-SH3 construct, we obtained an identical K_D of 1.9 ± 0.1μM (Table 4.1 and Figure 4.6), both of which are consistent with a previous ITC study, which showed that a peptide representing the SBM from AMSH binds the SH3 domain with 7 μM affinity.[12] Using an orthogonal and complementary technique, we confirmed complex formation by sedimentation velocity experiments using AUC and determined that the catalytic domain of AMSH forms a 1:1 complex. The respective $s_{20,w}$ values of 2.5S and 2.6S for the SH3 domain and UIM-SH3 (Figure 4.7a and b) suggest that the UIM has no role in AMSH recruitment to STAM, as expected.

4.3.2.2 Both SH3 Domain and UIM of STAM Bind Ubiquitin Independently

Secondly, we characterized ubiquitin binding to the UIM of STAM. Since UIMs are only 30-residue domains, much too small for bacterial expression, we used UIM-SH3 to investigate UIM-ubiquitin binding by ITC. Somewhat surprisingly, we found that both the UIM and SH3 domains bind ubiquitin independently. This observation was based on two pieces of evidence. (1) The UIM-SH3 construct binds ubiquitin with a K_D of 273 ± 16 μM, in agreement with previous biosensor measurements of a STAM-derived UIM peptide binding to ubiquitin that provided a K_D of 182 μM.[13] (2) Interestingly, our measurement of SH3-ubiquitin binding by ITC resulted in a K_D of 62 ± 7 μM (Figure 4.8b and Table 4.1). It has been shown previously that a subset of SH3 domains bind ubiquitin,[14; 15] and a recent study using NMR titration experiments showed that the SH3 domain of STAM does in fact bind ubiquitin, and that this interaction can be competed off by USP8 binding to the SH3 domain of STAM.[16] Taken together, these data seem to indicate that both the SH3 domain and the UIM bind ubiquitin independently, with the former having higher affinity than the latter, which would explain the overall K_D of 273 ± 15 μM obtained as the binding affinity of the UIM-SH3 construct for ubiquitin. It is possible that the two binding events corresponding to the two binding sites on UIM-SH3 have similar enthalpy of binding, and with binding affinities not drastically different between them, the ITC experiment is unable to resolve them distinctly.

Alternatively, it is possible that the UIM and SH3 domain fold onto each other generating a weaker interface for ubiquitin than either of them alone. This seems unlikely since UIM-SH3 binds to Lys63-linked diubiquitin with a K_D of 54 ± 20 μM (Figure 4.8c

and Table 4.1), an affinity higher than that of UIM-SH3 for ubiquitin. These results are consistent with the principle of avid binding of polyubiquitin chains at ESCRT-0, thus indicating that both the UIM and SH3 domain in UIM-SH3 are accessible for ubiquitin binding.

4.3.2.3 UIM and SH3 Domains are Necessary for Stimulating the Activity of AMSH

Using the catalytic domain of AMSH, UIM-SH3 and Lys63-linked diubiquitin, we attempted to recapitulate AMSH recruitment to ESCRT-0 *in vitro*. We carried out a Lys63-diubiquitin DUB cleavage assay with the AMSH:UIM-SH3 complex. The initial experiment comparing the enzyme's activity alone and in the presence of the SH3 domain and then, UIM-SH3, revealed a remarkable difference in DUB activity of AMSH. In the presence of UIM-SH3, it turned over nearly all of the Lys63-diubiquitin to ubiquitin, whereas, AMSH alone or in the presence of simply the SH3 domain had a significant amount of diubiquitin remaining, suggesting a stimulatory role for UIM-SH3 (Figure 4.9).

Diving deeper into the mechanism of activation, a similar *in vitro* assay was performed, this time using two SBM, and one UIM mutant versions of the UIM-SH3 construct (Figure 4.10). Two individual point mutations within the SBM of AMSH were introduced (Lys238Ala and Lys238Thr) to obliterate the SH3-SBM interaction. Lys238 is a completely conserved residue in the canonical SBM motif known to bind SH3 domains, mutating this to threonine made AMSH look like AMSH-LP in terms of its SBM. AMSH-LP has the conserved set of residues within its SBM, except the critical Lys

replaced by Thr. We confirmed that there was no binding between the AMSH SBM mutants and the SH3 domain using ITC (Figure 4.11). Secondly, we introduced a mutation within the UIM of UIM-SH3 (Ala176Gly) to interrupt ubiquitin binding (Figure 4.10). The Ala to Gly mutation has been shown previously to cause significant reduction in ubiquitin binding.[13] The diubiquitin cleavage reactions were performed at 37°C for 15 minutes using 1 μM enzyme, 20 μM Lys63-linked diubiquitin as the substrate, and 5 μM STAM binding partner (SH3, UIM^{A176G}SH3, or UIM-SH3). SDS-PAGE analysis revealed that only in the presence of the wild-type enzyme and UIM-SH3 is diubiquitin completely hydrolyzed to ubiquitin, hence, an intact SBM-SH3 interaction and a functional UIM are necessary for AMSH activation (Figure 4.10).

Furthermore, we wanted to understand this activation phenomenon in more detail, in terms of k_{cat} and K_M. To this end, we carried out another kinetic assay in which the catalytic domain of AMSH was pre-incubated in the presence of 20-fold excess UIM-SH3 to ensure that equilibrium favors the formation of the AMSH-UIM-SH3 complex. We saw 6-fold activation in AMSH in the presence of UIM-SH3, contributed by a somewhat greater change in k_{cat} than in K_M (Table 4.3). The k_{cat} effect is not entirely surprising because the UIM interacts with the proximal ubiquitin, and as we have shown in our mutational and kinetic analysis, the proximal site plays a significant role in properly aligning the isopeptide bond within AMSH's active-site, as determined by the significant loss in k_{cat} upon mutating the residues involved in binding.

4.4 Discussion

We found the minimal domain of STAM that is required to stimulate AMSH's activity. Previous work has shown that STAM has a role in AMSH activation towards Lys63 polymeric chains;[12; 17] however, these studies were not able to fully elucidate the mechanism of activation. Our study begins to divulge the mechanism underlying activation. This work suggests a simple model invoking simultaneous recognition of two ubiquitin groups in a polyubiquitin chain by AMSH and the UIM of STAM could explain the catalytic activation of the DUB. The UIM of STAM, separated from the SH3 domain by a short linker, could act as an adaptor for AMSH by interacting with the proximal ubiquitin, while AMSH engages the distal one. Such an arrangement would create a more extensive binding interface for diubiquitin in the AMSH:STAM complex than in the enzyme alone, causing catalytic activation. It appears that such activation is necessary since, as our ITC data show, AMSH has no preference for binding to Lys63-linked diubiquitin, therefore by extrapolation to Lys63-linked polyubiquitin chains over the ubiquitin product.

Prior to activation, AMSH is in a more latent state, but when it is recruited to STAM its full activity is unveiled. AMSH is known to have diverse subcellular localization profiles. Perhaps the free form of the enzyme needs to be in a less-active state so as not to hydrolyze the Lys63 chains that are present in the cytosol other than endosomes. Once it is recruited to the endosomes, its true activity comes alive, as seen by the 6-fold enhancement in activity upon binding to the STAM derived UIM-SH3 construct. A significant implication of this mechanism of activation is that the activation will be absent when AMSH is trying to cleave the last ubiquitin attached to the cargo.

While efficiently cleaving between two ubiquitin groups in a Lys63-linked polyubiquitin chain, AMSH might show a severe impediment in hydrolyzing the last ubiquitin attached directly to a cargo, on account of two factors: (1) its high specificity for the Lys63-linked chain between two ubiquitins, which in turn would make it a poor enzyme when ubiquitin is attached to a non-ubiquitin protein, the cargo; and, (2) the lack of an activation effect when cleaving ubiquitin attached to a non-ubiquitin moiety.

Finally, bringing all our data together, we can envision a mechanism for recruitment and activation for AMSH that will ultimately define a function for the enzyme. ESCRT-0 has the defined function of ubiquitinated cargo clustering, capable of harboring up to eight ubiquitin moieties at a time,[18; 19] which now, with the addition of the SH3 domain could be ten ubiquitins. Our ITC data show that the SH3 domain can actually bind ubiquitin tighter than the UIM. Subsequently, AMSH is recruited to STAM. The AMSH-SH3 binding affinity is stronger than SH3-ubiquitin, making it possible for AMSH to effectively displace ubiquitin from the SH3 domain (the binding interface on SH3 domain for the two proteins show substantial overlap) [16] leading to its recruitment to ESCRT-0. With the UIM from STAM acting as an adaptor to the enzyme, facilitating enzyme activity enhancement, AMSH begins to efficiently disassemble the polyubiquitin chain attached to the cargo. Deubiquitination of the chain will continue until the last ubiquitin directly attached to the cargo. Thus, recruitment of AMSH to ESCRT-0 will lead to substantial chain trimming but not complete deconjugation of ubiquitin from the cargo. As discussed in the next paragraph, this would promote the cargo's passage from ESCRT-0 to ESCRT-I and subsequent complexes.

Our proposed mechanism defines AMSH as the DUB that facilitates cargo passage from ESCRT-0 onto the next complex. This idea is supported by previous data that shows that avidly bound ubiquitin chains comprise of a binding affinity of ~20 μM affinity,[20] whereas, ESCRT-I subunit, UBAP1, binds ubiquitin anywhere from 70-140 μM.[21] The affinity of ESCRT-0 for ubiquitin needs to be reduced at least 5-10-fold in order for cargo destined for lysosomal degradation to be transferred to ESCRT-I. When going from Lys63-linked tetra-ubiquitin to diubiquitin, ESCRT-0 has a ~6-fold reduced affinity, and a remarkable, 46-fold reduction in affinity for ubiquitin.[20] Therefore, we presume that because of the specificity and activation of AMSH, this would be the enzyme that would be most suited for promoting cargo passage, all in support of an idea proposed previously.[22] By occupying the binding site on ESCRT-0, AMSH will serve to keep USP8 off the initial ESCRT complex. The recruitment of USP8 at ESCRT-0 would be detrimental to the passage of cargo to lysosome because USP8 has no hindrance in complete deconjugation. We suggest that the role of USP8 is specifically at the ESCRT-III level where complete deconjugation is desired.

In summary, using a combination of biochemical and biophysical studies, guided by a structural model, we are able to learn many important aspects of AMSH: (1) The T313I mutation underlying the MIC-CAP syndrome leads to a significant loss of catalytic activity owing to loss of a hydrogen-bonding interaction with ubiquitin. (2) Recognition of proximal ubiquitin contributes significantly to catalysis. (3) Activation of AMSH is enabled by facile, simultaneous binding to two ubiquitin groups in a polyubiquitin substrate, one by the catalytic domain of the DUB (binding to the distal ubiquitin) and the other (the proximal ubiquitin) by the UIM from STAM. (4) Taken together, the above

two points strongly indicate that AMSH will suffer a severe loss of catalytic efficiency when cleaving the last ubiquitin attached to cargo compared to a Lys63-linked polyubiquitin chain substrate. These studies provide biochemical and biophysical evidence in support of a hypothesis which postulates that AMSH is recruited to the initial ESCRT complex to facilitate transfer of cargo from one ESCRT member to the next, but not to completely deubiquitinate.[23] AMSH recruitment therefore would facilitate cargo shuttling rather than release from ESCRT and subsequent recycling back to the plasma membrane.

4.5 References

1. Sato, Y., Yoshikawa, A., Yamagata, A., Mimura, H., Yamashita, M., Ookata, K., Nureki, O., Iwai, K., Komada, M. & Fukai, S. (2008). Structural basis for specific cleavage of Lys 63-linked polyubiquitin chains. *Nature* **455**, 358-62.

2. Laue, T. M., Shah, B. D., Ridgeway, T. M. & Pelletier, S. L. (1992). Analytical Ultracentrifugation in Biochemistry and Polymer Science. *Royal Society of Chemistry*, 90-125.

3. Brown, P. H. & Schuck, P. (2006). Macromolecular size-and-shape distributions by sedimentation velocity analytical ultracentrifugation. *Biophys J* **90**, 4651-61.

4. Schuck, P. (2000). Size-distribution analysis of macromolecules by sedimentation velocity ultracentrifugation and lamm equation modeling. *Biophys J* **78**, 1606-19.

5. Balbo, A., Minor, K. H., Velikovsky, C. A., Mariuzza, R. A., Peterson, C. B. & Schuck, P. (2005). Studying multiprotein complexes by multisignal sedimentation velocity analytical ultracentrifugation. *Proc Natl Acad Sci U S A* **102**, 81-6.

6. Dam, J. & Schuck, P. (2005). Sedimentation velocity analysis of heterogeneous protein-protein interactions: sedimentation coefficient distributions c(s) and asymptotic boundary profiles from Gilbert-Jenkins theory. *Biophys J* **89**, 651-66.

7. Dam, J., Velikovsky, C. A., Mariuzza, R. A., Urbanke, C. & Schuck, P. (2005). Sedimentation velocity analysis of heterogeneous protein-protein interactions: Lamm equation modeling and sedimentation coefficient distributions c(s). *Biophys J* **89**, 619-34.

8. Houtman, J. C., Brown, P. H., Bowden, B., Yamaguchi, H., Appella, E., Samelson, L. E. & Schuck, P. (2007). Studying multisite binary and ternary protein interactions by global analysis of isothermal titration calorimetry data in SEDPHAT: application to adaptor protein complexes in cell signaling. *Protein Sci* **16**, 30-42.

9. Vistica, J., Dam, J., Balbo, A., Yikilmaz, E., Mariuzza, R. A., Rouault, T. A. & Schuck, P. (2004). Sedimentation equilibrium analysis of protein interactions with global implicit mass conservation constraints and systematic noise decomposition. *Anal Biochem* **326**, 234-56.

10. Schuck, P. (2003). On the analysis of protein self-association by sedimentation velocity analytical ultracentrifugation. *Anal Biochem* **320**, 104-24.

11. Keller, S., Vargas, C., Zhao, H., Piszczek, G., Brautigam, C. A. & Schuck, P. (2012). High-precision isothermal titration calorimetry with automated peak-shape analysis. *Anal Chem* **84**, 5066-73.

12. Kim, M. S., Kim, J. A., Song, H. K. & Jeon, H. (2006). STAM-AMSH interaction facilitates the deubiquitination activity in the C-terminal AMSH. *Biochem Biophys Res Commun* **351**, 612-8.

13. Fisher, R. D., Wang, B., Alam, S. L., Higginson, D. S., Robinson, H., Sundquist, W. I. & Hill, C. P. (2003). Structure and ubiquitin binding of the ubiquitin-interacting motif. *J Biol Chem* **278**, 28976-84.

14. He, Y., Hicke, L. & Radhakrishnan, I. (2007). Structural basis for ubiquitin recognition by SH3 domains. *J Mol Biol* **373**, 190-6.

15. Stamenova, S. D., French, M. E., He, Y., Francis, S. A., Kramer, Z. B. & Hicke, L. (2007). Ubiquitin binds to and regulates a subset of SH3 domains. *Mol Cell* **25**, 273-84.

16. Lange, A., Ismail, M. B., Riviere, G., Hologne, M., Lacabanne, D., Guilliere, F., Lancelin, J. M., Krimm, I. & Walker, O. (2012). Competitive binding of UBPY and ubiquitin to the STAM2 SH3 domain revealed by NMR. *FEBS Lett*.

17. McCullough, J., Row, P. E., Lorenzo, O., Doherty, M., Beynon, R., Clague, M. J. & Urbe, S. (2006). Activation of the endosome-associated ubiquitin isopeptidase AMSH by STAM, a component of the multivesicular body-sorting machinery. *Curr Biol* **16**, 160-5.

18. Mayers, J. R., Fyfe, I., Schuh, A. L., Chapman, E. R., Edwardson, J. M. & Audhya, A. (2010). ESCRT-0 assembles as a heterotetrameric complex on membranes and binds multiple ubiquitinylated cargoes simultaneously. *J Biol Chem*.

19. Wollert, T. & Hurley, J. H. (2010). Molecular mechanism of multivesicular body biogenesis by ESCRT complexes. *Nature* **464**, 864-9.

20. Ren, X. & Hurley, J. H. (2010). VHS domains of ESCRT-0 cooperate in high-avidity binding to polyubiquitinated cargo. *EMBO J*.

21. Agromayor, M., Soler, N., Caballe, A., Kueck, T., Freund, S. M., Allen, M. D., Bycroft, M., Perisic, O., Ye, Y., McDonald, B., Scheel, H., Hofmann, K., Neil, S. J., Martin-Serrano, J. & Williams, R. L. (2012). The UBAP1 subunit of ESCRT-I interacts with ubiquitin via a SOUBA domain. *Structure* **20**, 414-28.

22. Hurley, J. H. (2011). Nipped in the bud: how the AMSH MIT domain helps deubiquitinate lysosome-bound cargo. *Structure* **19**, 1033-5.

23. Clague, M. J. & Urbe, S. (2006). Endocytosis: the DUB version. *Trends Cell Biol* **16**, 551-9.

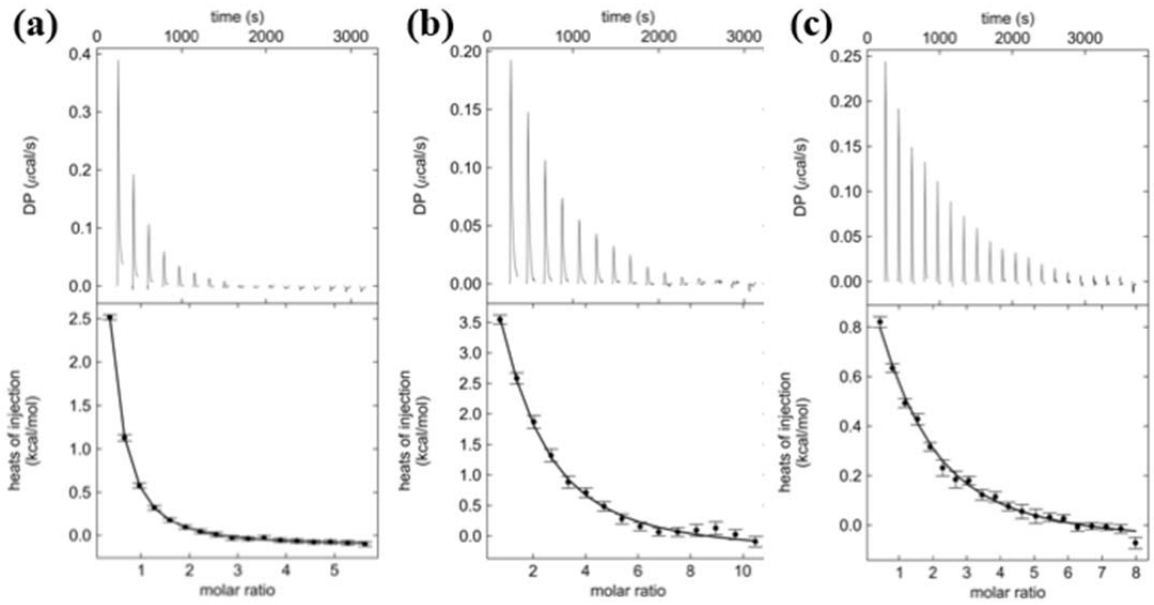

Figure 4.1. Isothermal titration calorimetry (ITC) thermograms of ubiquitin binding to the catalytic domain of AMSH. (a) ITC thermogram of ubiquitin binding to the catalytic domain of AMSH revealing a K_D of 19 ± 3 μM. (b) ITC thermogram of Lys63-linked diubiquitin binding to the catalytic domain of AMSH revealing a K_D of 19 ± 4 μM. (c) ITC thermogram of a Phe320Ala mutant of the catalytic domain of AMSH binding to ubiquitin revealing a K_D of 81 ± 15 μM.

Table 4.1. Kinetic Parameters of AMSH Mutants

Site	Protein	k_{cat} x 10^{-5} (s^{-1})	K_M (μM)
	Wild type	1400 ± 100	32 ± 5
Active site			
	Glu280Ala	ND	ND
	Cys282Ala	230 ± 140	45 ± 7
	Ser345Ala	1.4 ± 0.1	38 ± 15
	Asp348Ala	ND	ND
	Asp348Asn	ND	ND
Proximal			
	Thr341Ala	24 ± 1	15 ± 3
	Phe343Ala	5 ± 3	21 ± 4
	Ser346Ala	13 ± 3	23 ± 8
	Phe395Ala	22 ± 8	18 ± 9
Distal			
	Asn312Ala	430 ± 60	19 ± 2
	Thr313Ala	2600 ± 600	82 ± 5
	Glu316Ala	19 ± 4	31 ± 9
	Glu317Ala	750 ± 200	19 ± 7
	Phe320Ala	370 ± 20	98 ± 15
MIC-CAP			
	Thr313Ile	225 ± 39	21 ± 5

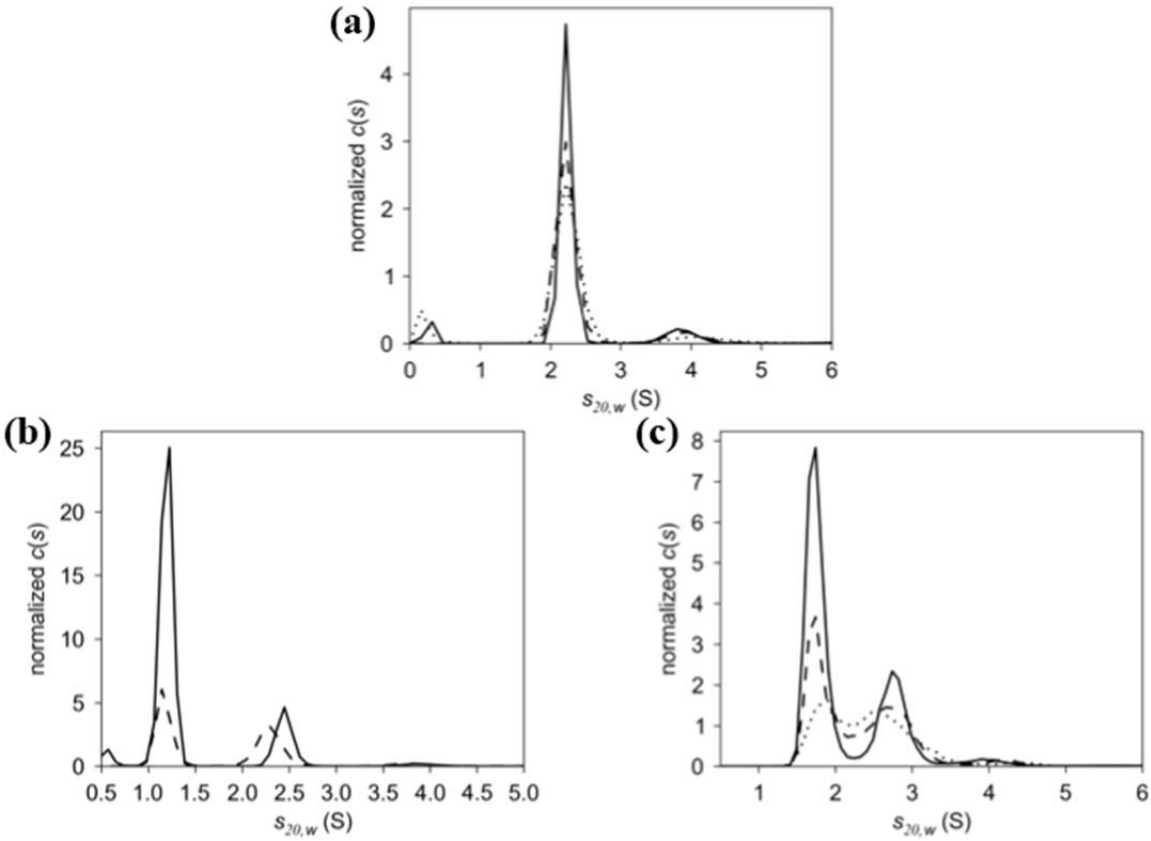

Figure 4.2. c(s) distributions of (a) AMSH219, (b) AMSH:ubiquitin, and (c) AMSH:Lys63-diubiquitin. Three concentration series were used for AMSH219 and AMSH:Lys63-diubiquitin, while two concentrations were used for AMSH:ubiquitin. It was found that AMSH219 sediments at 2.2S, AMSH:ubiquitin complex at 2.4S, and AMSH:Lys63-diubiquitin at 2.8S, with excess ubiquitin and diubiquitin at 1.2S and 1.7S respectively. Plots were normalized to the peak area of AMSH219 or the peak area of the complexes.

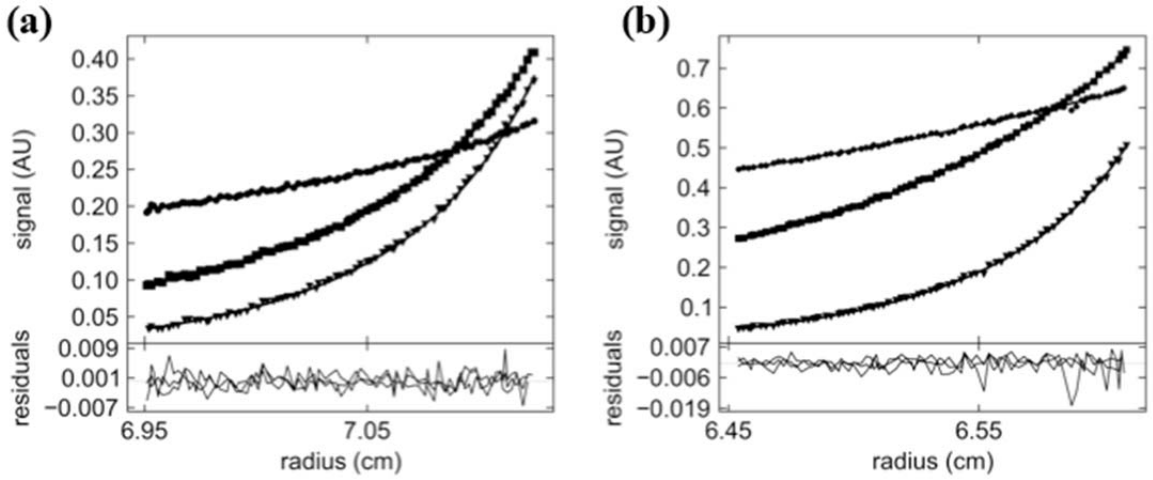

Figure 4.3. Representative sedimentation equilibrium profiles for (a) AMSH:ubiquitin and (b) AMSH:Lys63-diubiquitin to determine the molecular weights of the complexes.

Table 4.2. AUC Data

Protein	$S_{20,w}$ (S)	v-bar ($ml.g^{-1}$)	Theoretical molecular weight (Da)	Calculated molecular weight (Da)
AMSH219	2.2	0.7338	23120	22000 [SV]
AMSH-SH3	1.3, 2.5	0.7187	7561 / 30664	8600 / 23000 [SV]
AMSH-UIM-SH3	1.3, 2.6	0.7170	12588 / 35690	12000 / 34000 [SV]
AMSH-Ub	1.2, 2.4	0.7247	8976 / 32079	8000 / 24000 [SV]
				8900 ± 2900 / 31500 ± 12000 [SE]
AMSH-DiUb	1.7, 2.8	0.7293	17935 / 41037	17000 / 34000 [SV]
				14700 ± 3700 / 44000 ± 10000 [SE]

SE= sedimentation equilibrium
SV= sedimentation velocity

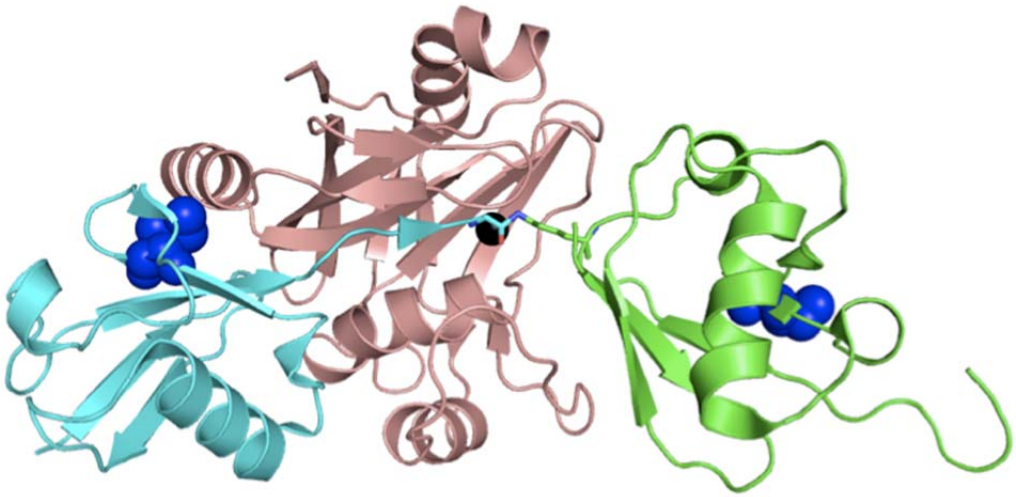

Figure 4.4. Model of AMSH bound to Lys63-diubiquitin. Cartoon representation of AMSH (pink ribbon) bound to a Lys63-linked diubiquitin, showing Ile44 as blue spheres in both the proximal (green ribbon) and distal (cyan ribbon) ubiquitins. The active-site Zn^{2+} is shown as a black sphere.

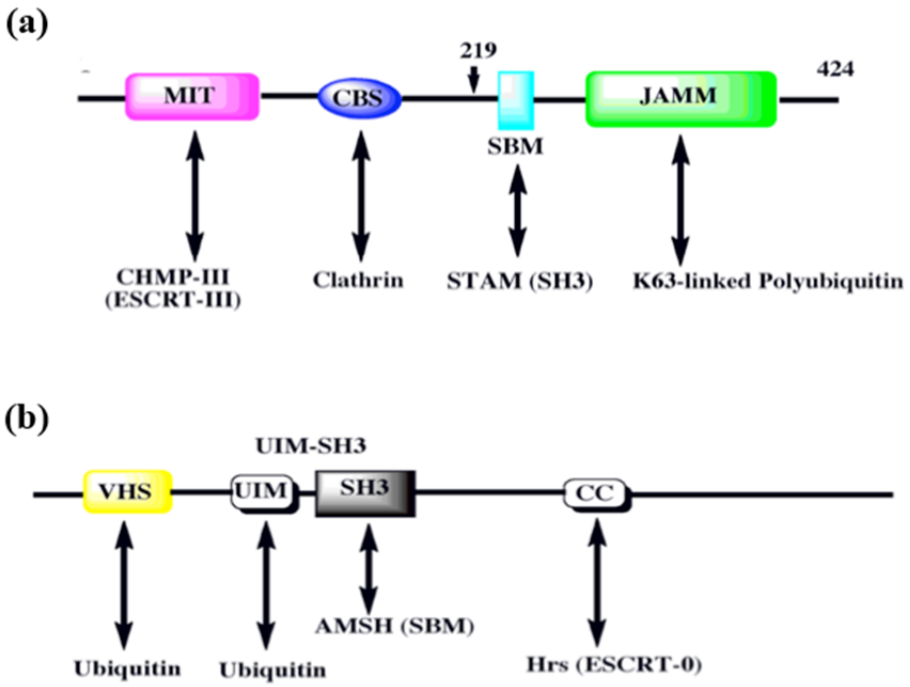

Figure 4.5. Domain diagram of (a) full-length AMSH and (b) full-length STAM indicating the appropriate binding partners associated with each domain. Abbreviations are as follows: MIT (microtubule interacting and transport), CBS (clathrin binding sequence), SBM (SH3-binding motif), JAMM (JAB1/MPN/MOV34), VHS (Vps27, Hrs, STAM), UIM (ubiquitin-interacting motif), SH3 (Src homology 3 domain), Hrs (hepatocyte growth factor (HGF)-regulated tyrosine kinase substrate).

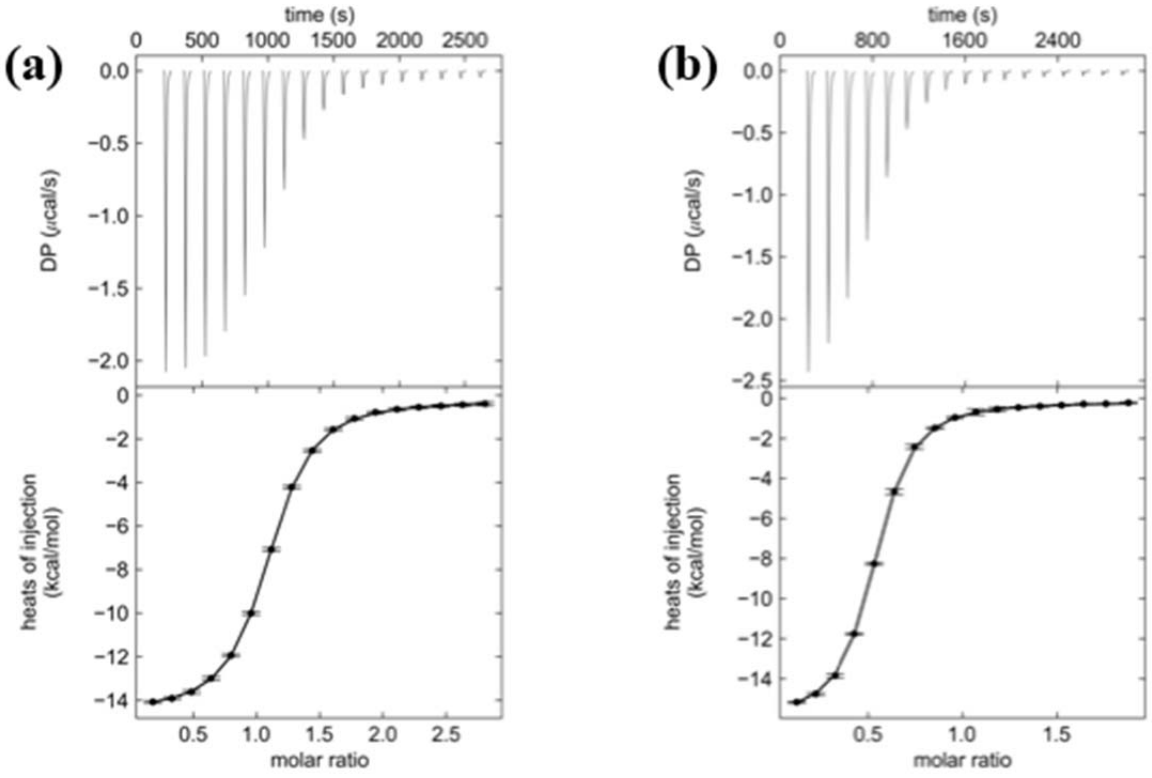

Figure. 4.6. ITC thermograms of (a) SH3 and (b) UIM-SH3 binding to the catalytic domain of AMSH revealing K_Ds of 1.4 ± 0.04 and 1.9 ± 0.1 μM, respectively.

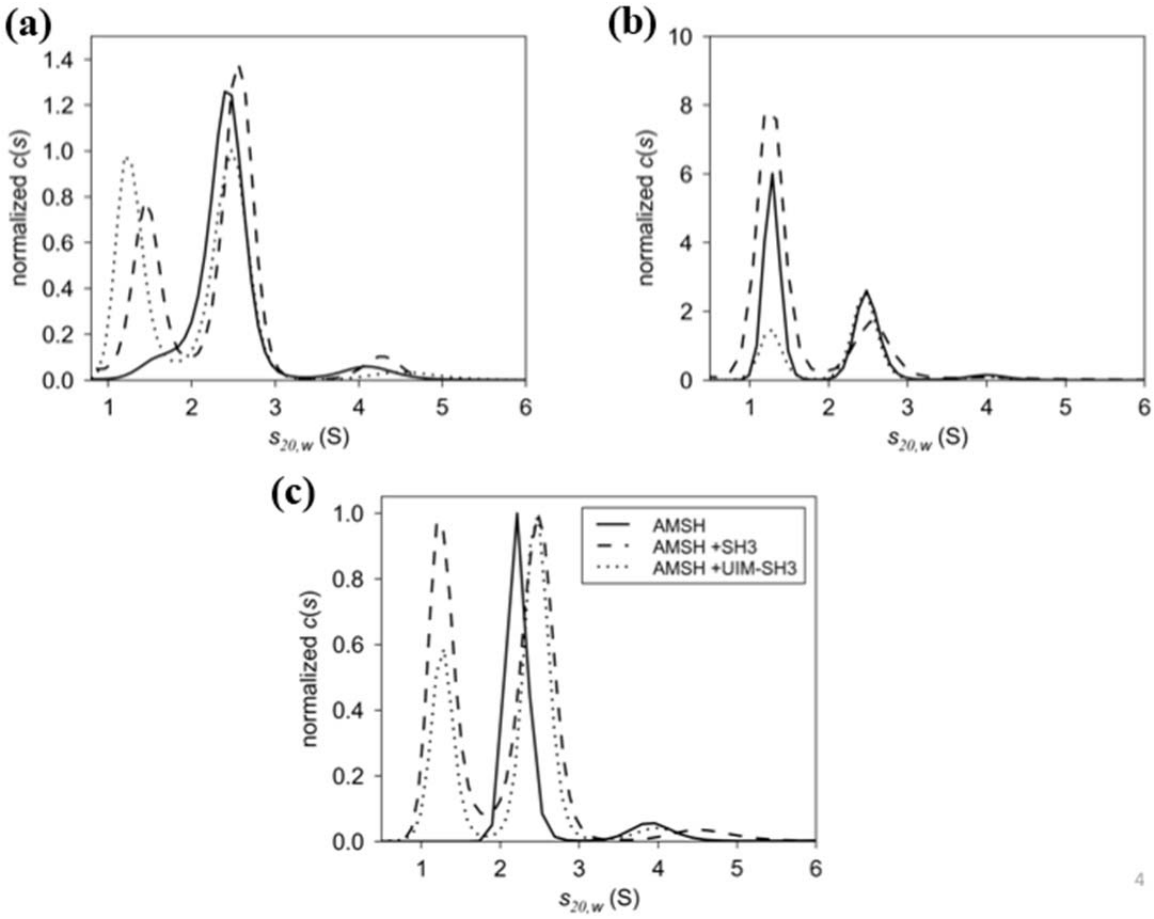

Figure 4.7. c(s) distributions of the catalytic domain of AMSH binding to (a) the SH3 domain of STAM and (b) UIM-SH3. Three concentration series were used to assess the formation of the AMSH:SH3 and AMSH:UIM-SH3 complexes revealing 1:1 complexes at 2.5S and 2.6S, respectively. Excess SH3 and UIM-SH3 are present at 1.3S. The data for both c(s) distributions were normalized to the peak area of the complexes. (C) Overlay of AMSH, AMSH:SH3, and AMSH:UIM-SH3 revealing changes in s-value of the AMSH:SH3 and AMSH:UIM-SH3 complexes compared to AMSH alone at 2.2S. The c(s) distributions were normalized to the peak area of the complexes.

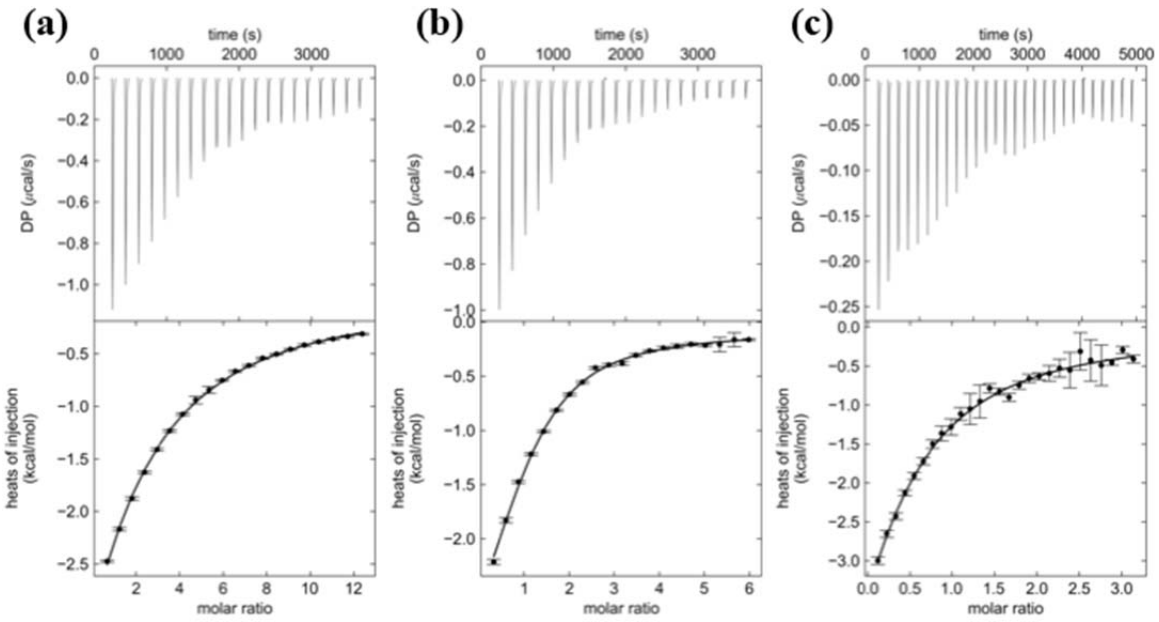

Figure 4.8. ITC thermograms of ubiquitin binding to UIM-SH3 of STAM. (a) Thermogram of ubiquitin binding to UIM-SH3 revealing a K_D of 273 ± 16 μM. (b) Thermogram of ubiquitin binding to the SH3 domain of STAM revealing a K_D of 62 ± 7 μM. (c) Thermogram of Lys63-linked diubiquitin binding to UIM-SH3 revealing a K_D of 54 ± 21 μM.

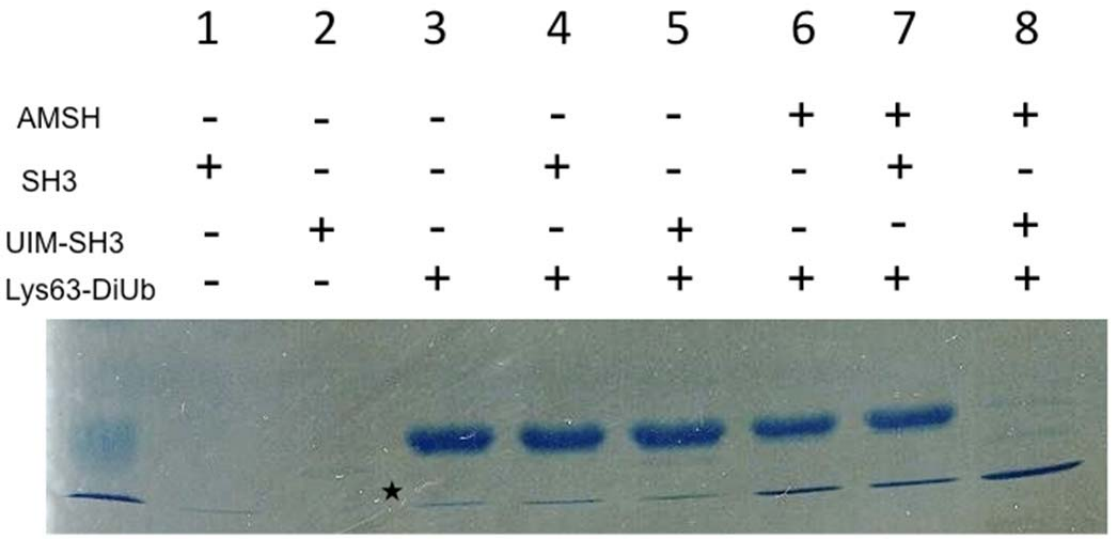

Figure 4.9. DUB activity assay by monitoring diubiquitin cleavage. SDS-PAGE gel comparing the activity of the catalytic domain of AMSH alone and in the presence of STAM's SH3 domain and UIM-SH3. Only the lane with UIM-SH3 reveals activation. The asterisk indicates ubiquitin contamination in the diubiquitin purification.

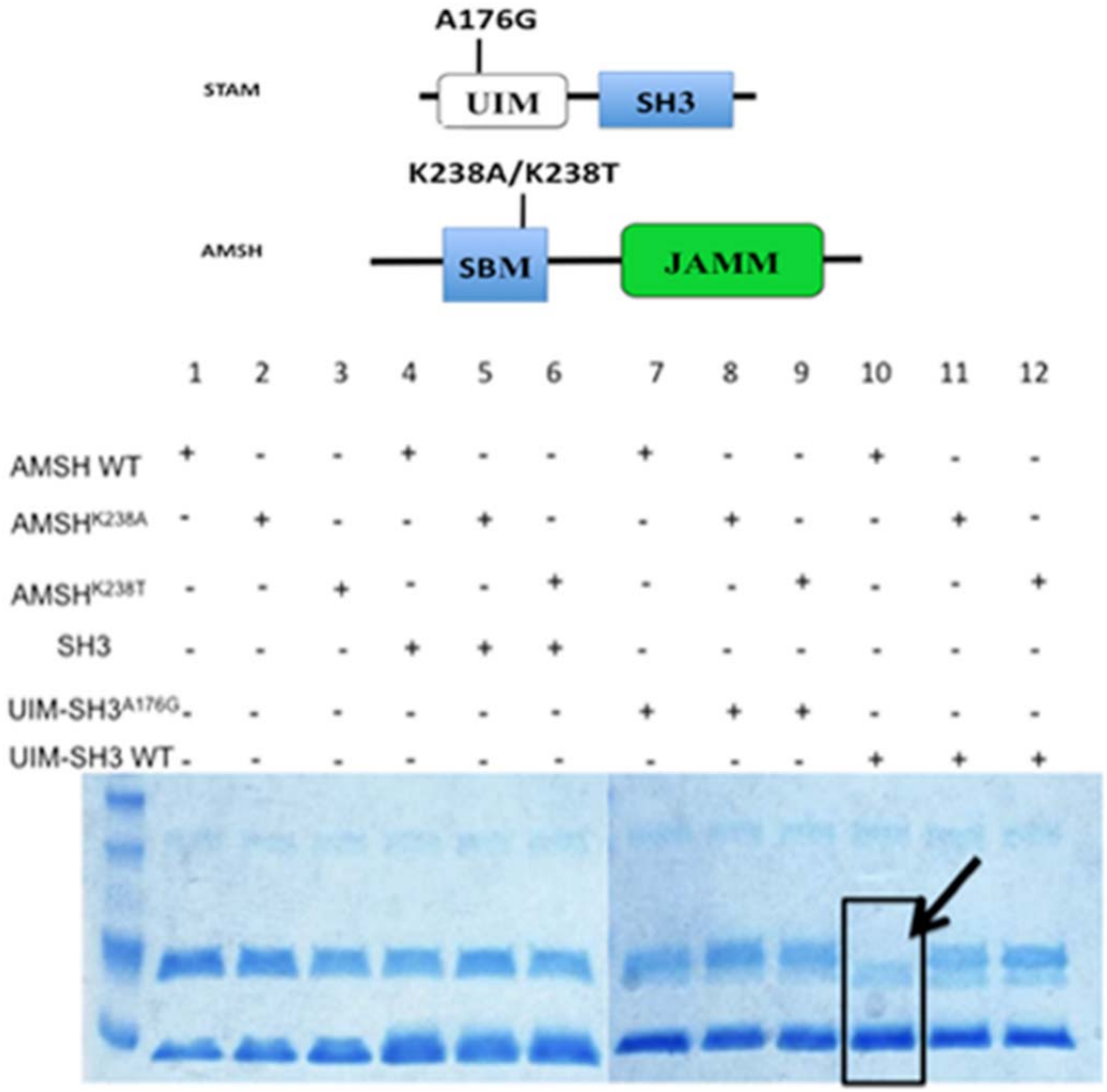

Figure 4.10. Catalytic activation of AMSH in presence of UIM-SH3. (a) Domain diagram of the minimal AMSH and STAM proteins, indicating the locations of the introduced mutations. (b) SDS-PAGE investigating the effects of mutants on the catalytic activation of AMSH. Only in the presence of the wild-type enzyme and wild-type UIM-SH3 is the activity of AMSH enhanced, indicated by complete disappearance of the diubiquitin substrate (black arrow). All lanes have Lys63-linked diubiquitin.

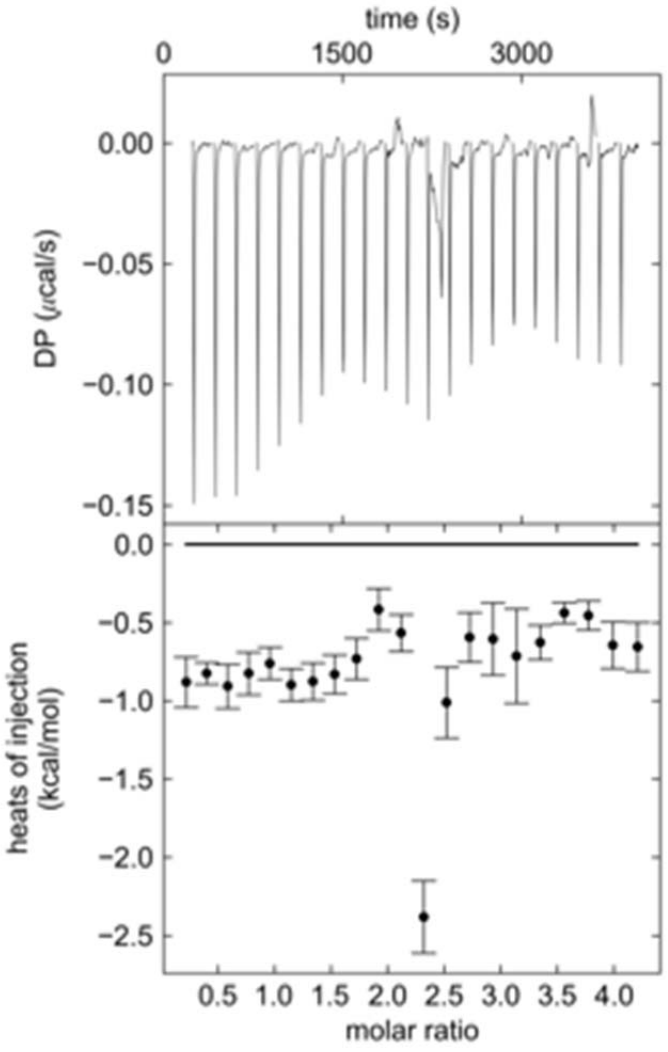

Figure 4.11. Representative ITC thermogram of the titration of UIM-SH3 into the Lys238Thr mutant of the catalytic domain of AMSH showing no binding.

Table 4.3. AMSH Activation Data

Protein	k_{cat} (s^{-1})	K_M (μM)
AMSH	1.4 ± 0.1	32 ± 5
AMSH + UIM-SH3	5 ± 1	19 ± 3

CHAPTER 5: STRUCTURAL AND BIOPHYSICAL INSIGHT INTO THE ROLES OF ESCRT-DUBS

5.1 Introduction

The endosomal sorting complexes required for transport (ESCRT) is a multi-subunit machinery that is an essential part of the multivesicular body (MVB) pathway in which cargo is sequestered and sorted into endosomal membranes.[1; 2] The ESCRT complex was initially discovered in yeast as a part of the vacuolar protein-sorting (vps) mutants, which were unable to deliver proteins to the vacuole.[1] 13 of the 46 vps mutants (class E) lacked the ability to deliver membrane proteins to the vacuole, giving rise to the discovery in 2001 of ESCRT-I (the second ESCRT complex) resulting from biochemical characterization of those vps mutants.[1; 2] The ESCRT machinery is a ubiquitin-dependent process that is involved in several cellular processes including endosomal sorting, endosomal trafficking, viral budding, cytokinesis, transcriptional regulation, and autophagy.[3] As a function of its involvement in several processes throughout the cell, the ESCRT machinery is implicated in a wide variety of diseases including cancer, neurological diseases, bacterial infections, cardiovascular disease, and retroviral infection.[4; 5]

The ESCRT machinery is subdivided into four complexes, ESCRT-0, -I, -II, -III, that work in a sequential manner to sort membrane proteins to the lysosome (vacuole in

yeast);[2] not all cellular process require all four of the complexes to carry out its function. A milestone study deciphered the role of each of the complexes by reconstituting and visualizing the complexes in giant unilamellar vesicles.[6] The study found that ESCRT-0 clusters ubiquitinated cargo and localizes closely to membrane buds that are formed in tandem by ESCRT-I and II, which in turn begin to confine the cargo within the newly formed buds. Finally, ESCRT-III is recruited to the neck of the bud by ESCRT-II to pinch off the membrane, forming intralumenal vesicles (ILVs) that can go off to the lysosome to degrade their contents.[6]

Since the ESCRT machinery works in a ubiquitin-dependent manner, deubiquitination and DUBs become an important mechanism of regulation within this entire machinery. The model ESCRT system, *Saccharmyces cerevisiae* (*S. cerevisiae*), uses the DUB Degradation of alpha 4 (Doa4) to recycle ubiquitin from ubiquitinated cargo that has been shuttled through the upstream ESCRT complexes and are committed to ILVs.[7] Doa4 has also been shown interact directly with ESCRT-III subunit, Snf7, thus promoting its localization to the last complex, further supporting its DUB role. However, direct deubiquitination of cargo is not required for MVB sorting in yeast.[7; 8; 9]

Similarly, the human ESCRT system requires DUBs. In humans, two DUBs are employed to regulate ESCRT-mediated sorting, associated molecule with a Src homology 3 (SH3) domain of STAM (or STAM-binding protein (STAMBP) or simply AMSH), and ubiquitin-specific protease Y (UBPY or ubiquitin-specific protease 8 (USP8)).[7; 10; 11; 12; 13] Both AMSH and UBPY have functional SH3-binding motifs (SBMs) that facilitates recruitment to ESCRT-0, more specifically, the SH3 domain of STAM, and functional MIT domains that allow for recruitment to various CHMPs of ESCRT-III.[7; 12; 14; 15; 16]

ESCRT-0 SH3 recruitment is carried out using a conserved consensus sequence: PX(V/I)(D/N)RXXKP, in which X is any residue.[7; 12] Linking the *S. cerevisiae* and human ESCRTs, there are three yeast proteins with similar domain structures to UBPY, Doa4, Ubp7, and Ubp5, and of the three, Doa4 has a seemingly redundant role to UBPY at ESCRT-III, but interestingly, Ubp7 interacts with Hse1, which mimics UBPY binding to ESCRT-0.[7] There is no direct AMSH homolog within *S. cerevisiae*.

Both AMSH and UBPY have critical roles in receptor down-regulation and other ESCRT functions including cytokinesis, HIV budding, and transcriptional regulation; the exact role of DUBs is not well understood. There is a significant amount of *in vivo* data that have implicated one DUB or the other in the down-regulation of various receptors using siRNA, unfortunately, we do not know the mechanism by which these enzymes work. For the most part, the role of DUBs has been glossed over in ESCRT literature, just accepting that DUBs deubiquitinate cargo, however, diving deeper into the literature suggests that DUBs play a significant regulatory role. More importantly, AMSH and UBPY may not have redundant functions even though in humans they have the same ESCRT-recognition domains. A very good review of ESCRT-DUBs was written back in 2006.[7] The goal of this literature review is to take a more structural and biophysical approach at understanding the roles that AMSH and UBPY could be playing within the ESCRTs.

5.2 AMSH

AMSH is a 424-amino acid member of the JAMM family of DUBs that binds Zn^{2+} at the active site coordinated by two histidines, an aspartate, and a glutamate bridged by the catalytic water molecule; a second Zn^{2+} is bound ~14Å away from the active-site zinc for structural integrity.[17; 18] AMSH is involved in the regulation of several receptors including: epidermal growth factor (EGFR) receptor, calcium-sensing receptor, δ-opioid receptor, protease-activated receptor (PAR), and the chemokine receptor CXCR4.[10; 19; 20; 21; 22; 23; 24; 25] Not only is AMSH implicated in receptor down-regulation, but also has roles within mitosis, cytokinesis, and HIV budding.[26; 27; 28; 29]

The structure of the wild-type catalytic domain of AMSH has been determined to 2.5Å, and a second structure of the catalytic domain including a Glu280Ala active-site mutation to 1.7Å resolution.[18] The structure of the catalytic domain of AMSH is nearly identical to that of the catalytic domain of the homologous (75% sequence similarity in the catalytic domain) AMSH-like protein (AMSH-LP) with a root mean square deviation (RMSD) of C^{α} atoms of 1.49Å, however, AMSH was found to be thermodynamically less stable than AMSH-LP, owing to a structural plasticity.[18] This idea of structural plasticity is consistent with the ability of AMSH to localize to multiple ESCRT complexes, whereas, AMSH-LP is ESCRT-independent. Also, structural analysis has shown the potential for the formation of a disulfide bridge between Cys282 and Cys311 ~7Å away from the active-site Zn^{2+}.[18] A detailed kinetic study shows that when Cys282 is mutated to alanine there is a ~6-fold reduction in k_{cat}, suggesting a role for this residue within the enzyme's catalytic mechanism (Davies, C.W., *et. al* (2013) *Biochemistry*

accepted). Another study found that N-ethylmalemide (NEM) is an inhibitor of AMSH activity due to a possible alkylation of Cys282.[10] In accordance with this study, the IC_{50} for NEM inhibition was determined to be 16.2 ± 3.1 μM.[30]

AMSH has exquisite specificity for Lys63-linked polyubiquitin chains.[10] The structural basis for the AMSH family of DUBs specificity for Lys63-linked chains has been elucidated with the x-ray crystal structure of AMSH-LP bound to a Lys63 ubiquitin dimer.[31] The structure reveals that specificity arises from the specific recognition of a tripeptide sequence (Gln62-Lys63-Glu64) within the proximal ubiquitin by four residues within the enzyme (Thr, Phe, Ser, and Phe).[31] Structural modeling of AMSH onto AMSH-LP bound to diubiquitin reveals that the linkage specificity is completely conserved between AMSH and AMSH-LP; however, there is a three-residue difference in recognition of the distal ubiquitin, a Asn to Asp, a Thr to Met, and a Glu to Val, going from AMSH to AMSH-LP.[18] A more detailed mutational and kinetic analysis probing the role of these residues individually found that the threonine to alanine mutation showed some hyperactivity, however, this was counterbalanced with a loss in K_M. Also, the threonine (Thr313) is mutated to isoleucine in children with microcephaly capillary malformation (MIC-CAP) syndrome. Analyzing the MIC-CAP-associated mutant revealed a significant reduction in catalytic activity, without much change in its thermodynamic stability (Davies, C.W., *et. al* (2013) *Biochemistry* accepted). Mutating the glutamate to alanine revealed the most significant result in which there was an ~74-fold reduction in k_{cat} (Davies, C.W., *et. al* (2013) *Biochemistry* accepted).

AMSH localization to ESCRT-0 is facilitated by the SH3 domain of STAM binding to the SBM of AMSH.[7] It has been shown that clathrin, not the SH3 domain of

STAM, is required for AMSH endosomal localization, suggesting that binding clathrin allows AMSH to be in close proximity to bind the SH3 domain of STAM.[32] Similarly, Hrs-STAM (ESCRT-0) localizes to the endosome because of its interaction with clathrin via the C-terminal domain of Hrs.[33] Furthermore, the recruitment of AMSH to ESCRT-0 enhances the enzyme's activity. One study showed that in the presence of STAM, AMSH processed Lys63 ubiquitin chains better than without STAM, or with mutations disrupting the enzyme's ability to bind STAM.[11] Also, it was found that mutations within the UIM domain of STAM greatly reduced this enhancement of activity, suggesting a K_M effect for the UIM.[11] Another study showed that when diubiquitin was bound to STAM, the enzyme processed the chains better than when not bound to STAM; AMSH mutants lacking the SBM showed no activity towards diubiquitin bound STAM.[34] Using a combination of biophysical and biochemical experiments, this activation mechanism has been further elucidated. It was found that the enzyme has no preference for Lys63-linked diubiquitin over simply ubiquitin based on isothermal titration calorimetry (ITC) experiments that revealed identical binding affinities (19 μM); from this, a role for STAM's UIM was proposed (Davies, C.W., *et. al* (2013) *Biochemistry* accepted). An enzymatic assay using the minimal domains of AMSH and STAM along with Lys63-linked diubiquitin found that the UIM of STAM plays a significant role in stimulating the enzyme's activity by recognizing the proximal ubiquitin, while the enzyme binds the distal ubiquitin (Davies, C.W., *et. al* (2013) *Biochemistry* accepted). As a consequence of these results, it was proposed that AMSH serves to promote the shuttling of ubiquitinated cargo from ESCRT-0 to ESCRT-I and –II by reducing the affinity of ESCRT-0 for ubiquitin (Davies, C.W., *et. al* (2013) *Biochemistry* accepted).

AMSH recruitment to ESCRT-III is facilitated through interactions with ESCRT-III members, CHMPs.[14; 15; 16] A yeast-two hybrid system found that AMSH interacts with several CHMP members: CHMP1A, CHMP1B, CHMP2A, and CHMP3; all of these CHMPs did not interact with AMSH-LP, suggesting that the AMSH-CHMP interaction is specific.[16] A more detailed study of the AMSH-CHMP interaction using a glutathione S-transferase (GST)-pull down assay suggests that AMSH interacts most prominently with CHMP1A, followed by CHMP3 and then, CHMP4C. However, CHMP1A only plays a regulatory role, whereas CHMP3 is one of the proteins necessary for capping the ESCRT-III polymer in the scission process.[14; 35] Further structural and biophysical studies have been done on the AMSH-CHMP3 interaction. Some initial studies using small angle x-ray scattering (SAXS) found that CHMP3 existed in multiple conformations ranging from a closed conformation in a no-salt buffer to an open conformation in a high salt condition.[36] This study also determined using ITC that the AMSH-CHMP3 binding affinity changes as a function of salt concentration ranging from 5.6 nM in no-salt to 392 nM in 500 mM NaCl.[36]

More recently, the structural basis of AMSH recruitment by CHMP3 was elucidated using x-ray structure determination of a complex between the MIT domain of AMSH (residues 1-146) and a C-terminal fragment of CHMP3 (residues 183-22, representing its MIT-interacting motif (MIM) domain).[37] In great agreement with the previous study, the K_D of the MIT-MIM interaction was found to be 60 nM using ITC and 113 nM using Surface Plasmon Resonance (SPR).[37] The extraordinarily tight complex is mainly stabilized by polar interactions, which is novel compared to previous crystal structures of MIT-MIM interactions, showing the importance of hydrophobic

interactions.[37] Furthermore, the interaction of AMSH and CHMP1A was analyzed by SPR and determined a K_D of 1.5 mM, suggesting a different mode of interaction between CHMP1A-AMSH and CHMP3-AMSH, since a C-terminal peptide of CHMP3 binds with micromolar affinity to AMSH, whereas the full-length protein has low nanomolar affinity.[36; 37] Since ESCRT-III is necessary for the final scission step in MVB biogenesis, it is important to comment on how AMSH relates to the role of Vps4 disassembly. Overexpression of Vps4 resulted in weakened affinity of CHMP1B for AMSH, suggesting that the MIT domain of Vps4 competes for the same binding spot on CHMPs.[16] Though Vps4 competed off AMSH from CHMP1B, it is not well understood how Vps4 would compete off CHMP3 because of the low nanomolar affinity between AMSH-CHMP3, whereas the Vps4-CHMP interaction has a micromolar affinity.[37; 38] Further studies are required to elucidate how AMSH is released from ESCRT-III after deubiquitination prior to Vps4-mediated recycling.

5.3 USP8/UBPY

UBPY is an 1118 amino acid member of the USP family of cysteine protease DUBs.[39; 40] The USP family is the largest and the most diverse family of DUBs with 56 distinct members; USPs are large proteins ranging from 300-3400 amino acids, with a ~350 amino acid catalytic domain.[41] UBPY is implicated in the cell cycle by regulating the entry into the S phase.[42] UBPY also interacts with and serves multiple other roles in the cell including: $CDC25^{Mm}$, a GDP/GTP exchange factor for Ras, GRAIL, an E3 ubiquitin ligase involved in energy induction in $CD4^+$ T-cells, and Nrdp1, an E3 enzyme that regulates receptor tyrosine kinases (RTKs).[43; 44; 45] The more widely known role for

UBPY is to regulate the cellular levels of ubiquitin by deubiquitinating ubiquitinated proteins, specifically, ubiquitinated receptors targeted for degradation by the lysosome, much like Doa4.[7] UBPY localizes to early endosomes, regulating the level of protein ubiquitination on endosomes, where inactivation of UBPY caused morphological aberration of endosomes.[46] Also, UBPY activity is necessary for regulating the degradation patterns of specific receptors such as epidermal growth factor receptor (EGFR), MET receptor, the Ca^{2+}-activated K^{+} channel (KCa3.1), and the epithelial Na^{+}channel.[13; 47; 48]

The structure of UBPY has been solved elucidating the many domains that reside within UBPY. The N-terminal domain of UBPY (residues 1-142) was crystallized and its structure was determined up to 2.1Å resolution revealing a helical structure that has a coiled-coil region forming a molecular dimer.[49] This N-terminal region, which was later shown to be a canonical MIT domain,[14] has a large cavity lined with basic residues that are speculated to facilitate ligand binding by a negatively charged molecule; this promotes the N to C-terminal interaction between the basic N-terminal region of UPBY and the acidic C-terminal tail of CHMPs.[49]

Separated by a 40-amino acid linker from the MIT domain of UBPY is the rhodanese domain that facilitates interaction with the RING-finger containing E3 ubiquitin ligase, neureglin receptor degradation protein 1 (Nrdp1).[45; 49] *In vivo* studies show that UBPY specifically interacts with Nrdp1 since UBPY does not bind to cbl, a RING Finger E3 ligase involved in EGFR down-regulation.[45] Also, UBPY promotes the stability of the ligase in which a catalytically inactive mutation within UBPY destabilized endogenous Nrdp1.[45] The crystal structure of the rhodanese domain (residues 181-319) in

complex with Nrdp1 (residues 193-317) was shown to form a 1:1 complex (each migrating as monomeric proteins within size-exclusion chromatography (SEC)) that has a buried surface area of 2100Å^2, mainly comprised of a peptide loop from UBPY (residues 237-242) nestled within a pocket from Nrdp1 centered on residue Ile218.[49] When compared to the unbound proteins, no significant conformational changes were found.[49] It is speculated that the rhodanese domain may contribute to UBPY oligomerization because of a predicted coiled-coil region within Nrdp1 that may promote dimerization of the ligase, therefore, when UBPY is recruited, the enzyme with oligormerizes.[49]

The C-terminal domain, upstream of the rhodanese domain, is the catalytic domain of UBPY, in whose segment comprising of 376-residues was crystallized and determined its x-ray structure at 2Å resolution.[49] The structure of the catalytic domain contains similar domain architecture to other members of the USP family (resembling a right hand with a palm, thumb and fingers); however, the structure of the catalytic domain of UBPY has several structural features that are not present in other USPs.[49] Two loops (blocking loop 1 (BL1) and 2 (BL2)) in a closed conformation appear to be important for capping the active site and recognition of the P site within the substrate, which would ultimately block the peptide bond from being presented to the active site.[49] Also, in accordance with the inhibition of substrate entry, the fingers of UBPY are 9 Å closer to the active site, leaving insufficient room for the binding of ubiquitin when comparing UBPY to previously solved USP family proteins.[49; 50; 51] All the analysis of the closed conformation of UBPY has brought about a speculation that this is a hardwired structural feature that regulates the activity of UBPY where its goes through a substrate-induced activation mechanism.[49] Another structural feature that UBPY has that is not

consistent throughout all USP family members is the presence of a Zn^{2+}-binding motif, present at the end of the fingers.[49] Four cysteines are in a tetrahedral coordination around Zn^{2+}, resembling a Zn^{2+}-ribbon fold.[52] The importance of this Zn^{2+}-ribbon motif is not well understood, however, it is speculated to be important in binding a second ubiquitin, similarly to Zn^{2+}-finger domains, allowing for efficient cleavage of ubiquitin chains.[49]

The role of UBPY within the ESCRT machinery is to regulate the ubiquitination events by deubiquitinating cargo, maintaining the ubiquitin pool within the cell. Unlike AMSH, UBPY is a promiscuous enzyme in its ability to cleave Lys48 and Lys63-linked ubiquitin chains.[13] The original analysis of DUB specificity towards Lys48 and Lys63-linked ubiquitin chains revealed that AMSH cleaved only Lys63 and UBPY cleaved only Lys48, however, the substrate used in this experiment had all the lysines mutated to arginine except for the lysine used to make the specific chain.[10] When the wild-type ubiquitin was used, UBPY processed Lys63-ubiquitin chains to lower units suggesting that one of the six other lysines are necessary for recognition and activity towards Lys63.[13] Furthermore, the activity of UBPY was determined by using the substrate-mimic, ubiquitin 7-amino-4-methylcoumarin (Ub-AMC), obtaining a k_{cat} of 2.4 s^{-1} and a K_M of 10.2 ± 1.4 μM.[49] The ability of UBPY to hydrolyze Ub-AMC suggests the possibility that UBPY can also hydrolyze monoubiquitinated substrates.

Just like AMSH, UBPY recruitment to ESCRT-0 is facilitated through SBM-SH3 domain interactions. The interaction between the SH3 domain of STAM and UBPY was first characterized in 2000 in a study that discovered the nine-amino acid consensus SBM sequence (PX(V/I)(D/N)RXXKP), and that UBPY has two SBM motifs within its gene.[12] Using deletion mutants of mouse UBPY, an *in vitro* binding assay was conducted probing

the binding interactions of the UBPY mutants to GST-STAM SH3 revealing one SBM motif within residues 378-434 and then, another SBM within residues 666-731.[12] Human UBPY has its two SBMs within residues 405-413 and 738-746. Comparing the sequences of the two human UBPY sequences, we see that position three and four are both changed when going from one SBM to the other (^{3}ID^{4} within the first SBM (residues 405-413) and ^{3}VN^{4} in the second SBM (residues 738-746)).

For further insights into the SBM-SH3 domain interactions, alanine-scanning mutagenesis was performed. It was found that mutating the prolines at position one and nine, the arginine at position five, or the lysine at position eight resulted in complete abolishment of binding, whereas, mutating position three (valine /isoleucine) or four (asparagine/aparatic acid) resulted in reduced binding.[12] The structural basis for understanding these interactions has been determined by co-crystallizing the SH3 domain of STAM2 with an 11-mer peptide derived from the sequence of mouse UBPY.[53] The structure of the peptide binding site within STAM2 SH3 is similar to other SH3 domains showing a hydrophobic surface suitable for polyproline type II helix-binding and an adjacent acidic region formed by the RT and n-Src loops.[53] The peptide binds within the predicted site of the SH3 domain, however, the second half of the peptide adopts a novel right-handed 3_{10} helical conformation.[53] Looking at the interactions, the position four residue (asparagine in this structure, but could be substituted by an asparatic acid) facilitated two hydrogen-bonding interactions with the main chain nitrogen atoms of residues in position five and six.[53] The significance of the 3_{10} helix becomes important because this conformation allows for a series of electrostatic interactions to take place between the arginine at position five and the lysine at position eight.[53] Two hydrogen-

bonding interactions are seen between arginine and Glu220, and the lysine residue adopts four distinct interactions, van der Waals interaction with Trp239, and three hydrogen bonding interactions with three oxygen atoms from Glu217, Glu219, and Glu220.[53]

Using tryptophan fluorescence and a mouse UBPY-derived peptide, it was shown that UBPY binds to the SH3 domain of STAM2 with a K_D of 27 μM,[53] similar to the 7 μM affinity that was determined for the AMSH-SH3 interaction [34]. Also, data shows that the activity of UBPY is enhanced towards Lys48 and Lys63-linked tetraubiquitin chains in the presence of STAM.[14] These data suggest that the role of STAM is to recruit and stimulate DUB activity towards polyubiquitin chains.

UBPY, like AMSH, interacts with ESCRT-III proteins, CHMPs, through an MIT-MIM type interaction using its N-terminal basic MIT domain binding to the acidic C-terminal domain of CHMPs. The same study that probed the AMSH-CHMP interaction, assayed the MIT domain of UBPY against 11 CHMPs. The MIT domain of UBPY specifically interacted with CHMP1B, 4C, and 7, and 2A to a lesser extent.[14] Unlike the ability of STAM to stimulate DUB activity, CHMPs had no stimulatory affect on the DUB activity of UBPY.[14]

5.4 Structural and Biophysical Insights into Understanding Previously Described Cellular Data Suggest Roles for AMSH and UBPY

It is widely accepted that the main function of DUBs is to regulate and maintain the cellular pool of ubiquitin since the attachment of ubiquitin to target proteins is an ATP-dependent process. The employment of both AMSH and UBPY within the ESCRT machinery could and should adopt this same role, however, its not well understood the

'other' roles that these enzymes have in regulating ESCRT-mediated degradation. Mammalian ESCRTs recruit two DUBs to two complexes (ESCRT-0 and III) with redundant localization domains between them. At first look, this recruitment and recognition suggests functionally redundant roles, especially since Doa4 is the main regulator of ESCRT-mediated degradation in *S. cerevisiae*. Further insight into understanding these DUBs reveals the difference in ubiquitin-chain specificity, which will be the initial determining factor is showing that AMSH and UBPY are not functionally redundant; in fact, each seem to serve an important and distinct role is regulation and proper functionality of the ESCRT machinery.

5.4.1 The Role of DUBs at ESCRT-0

Two models have been proposed for role of a DUB at ESCRT-0 in which AMSH serves to oppose the action of the E3 ligase by completely deubiquitinating a ubiquitinated receptor, thus promoting the recycling of that receptor back to the plasma membrane. Alternatively, the proposed role of UBPY is to deubiquitinate ESCRT-0 member, STAM, because its been shown that STAM becomes Lys48 ubiquitinated, targeting it for proteasomal degradation.[7] Both DUBs could theoretically localize with similar affinity to ESCRT-0, however, AMSH is recruited mainly by its clathrin-binding domain,[32] but also, has its SBM that binds to the SH3 domain of STAM. Similarly, UBPY has two SBMs, one of which has been shown to bind to the SH3 domain of STAM with 27 μM affinity.[53] Both DUBs have two points of ESCRT-0 recruitment, however, AMSH maybe more apt to be recruited because of the clathrin binding, but the two SBMs

of UBPY may produce avid binding even though there is an ~300 amino acid linker in between SBMs.

The proposed role of AMSH opposing the activity of the E3 ligase, promoting receptor recycling, arose from the observation that small interfering RNA (siRNA) knockdown of AMSH lead to increased degradation of ligand-stimulated EGFR.[10] A recent study has proposed that the decision to recycle receptors back to the plasma membrane is made prior to the localization of the ubiquitinated receptor to ESCRT-0 because they showed that an EGF-stimulated chimera protein of EGFR and ErbB2 and TGFα-stimulated EGFR showed impaired AMSH deubiquitination.[54] Structural modeling shows that AMSH and AMSH-LP have the same mode of Lys63-linked polyubiquitin chain specificity, therefore, taking these results into account, we speculate that AMSH cannot completely deubiquitinate a receptor because of its exquisite chain specificity. The enzyme could cleave a Lys63-linked polymeric chain of ubiquitin, leaving the last ubiquitin still attached to the receptor. These data do not line up with the hypothesis that AMSH opposes E3 ligase activity at ESCRT-0.

Alternatively, we can see how UBPY could be the DUB that opposes the action of the E3 ligase by completely deubiquitinating a receptor before it is 'committed' to the subsequent ESCRTs. This proposed role of UBPY opposing ligase activity has a caveat: if the decision for receptor recycling is made before binding to ESCRT-0, then UBPY would not be needed, however, if a receptor is incorrectly ubiquitinated and brought to ESCRT-0, UBPY could serve the role to correct this by completely removing ubiquitin. UBPY could easily have this role because of its lack of specificity. UBPY cleaves both

Lys48 and Lys63-linked ubiquitin chains,[13] but more importantly, UBPY also cleaves Ub-AMC,[49] serving as a model of a monoubiquitinated receptor.

Though structural and biochemical data do not support the idea that AMSH completely opposes the E3 ligase, these data do suggest that AMSH could work to process Lys63-ubiquitin chains at ESCRT-0 down to the last ubiquitin, which could be important in efficiently passing ubiquitinated receptors onto the subsequent complexes. SPR experiments show that ubiquitin chains bind avidly to ESCRT-0.[55] The binding affinity of ESCRT-0 for ubiquitin is 920 μM, however, through avid binding, the affinity of ESCRT-0 for Lys63-diubiquitin increased ~8-fold to 110 μM, and for Lys63-tetraubiquitin to 18 μM, a 51-fold increase in affinity.[55] Alternatively, when looking at ESCRT-I ubiquitin binding affinity, ubiquitin and Lys63-diubiquitin bind in the range of 70-140 μM.[56] These data suggest that a polyubiquitinated receptor at ESCRT-0 would not be passed on to ESCRT-I/II because it would have a greater affinity for ESCRT-0 than for ESCRT-I/II, unless the ubiquitin chain is trimmed substantially, possibly to the last ubiquitin. Taking all of this into account, we speculate that AMSH could play a role as the DUB that facilitates the passage of ubiquitinated cargo from ESCRT-0 to ESCRT-I/II. As stated above, the structure suggests that AMSH will process Lys63 chains, leaving the last ubiquitin moiety, thus greatly reducing the affinity of ESCRT-0 for the monoubiquitinated receptor, allowing for efficient passage onto ESCRT-I/II. This idea has been mentioned previously in which it was stated that both AMSH and UBPY might be important for disengaging avidly bound K63-linked ubiquitin chains from ESCRT-0 for cargo to be handed off to ESCRT-I and –II.[57] Based on ubiquitin-chain specificity,

both UBPY and AMSH could carry out this role at ESCRT-0 since both are activated at ESCRT-0;[11; 14] both enzymes cleave Lys63-linked chains,[10; 14] however, UBPY is more promiscuous, therefore, this enzyme has the potential to completely deubiquitinate the receptor, thus releasing the cargo from ESCRT-0. Of the two, AMSH would best be served to promote cargo movement from ESCRT-0 to ESCRT-I/II.

The *S. cerevisiae* STAM ortholog, Hse1, has a SBM that interacts with both an E3 ligase and a DUB. A GST pull-down assay found the DUB, Ubp7, interacts via the SH3 domain of Hse1.[58] Ubp7 interacting with Hse1 is synonymous to AMSH because deletion of Ubp7 resulted in an increase in Cps1 sorting; suggesting that DUB activity here regulates ubiquitinated cargo.[58] Ubp7 has some significant differences compared to AMSH. The domain structure of Ubp7 resembles UBPY more than AMSH in that Ubp7 is a 125 kD (1072 amino acids) cysteine protease, however, Ubp7 does have a putative SBM; its predicted SBM is not the canonical SBM sequence that reside within both AMSH and UBPY.[58] Lastly, analysis of Ubp7 activity towards HA-Ub-VME was barely detectable, probably due to low levels of the protein being expressed in yeast [59] even after Hse1 was added, revealing that Hse1 does not activate Ubp7, unlike human ESCRT-DUBs.[58] These results suggest that yeast uses a DUB to carry out a regulatory role early in the endosomal process, similar to mammalian DUBs, alternatively, it is not known whether Ubp7 can be considered adopting an identical role to what was proposed for AMSH at ESCRT-0 because of its expression levels and lack of enzyme stimulation by Hse1.

The proposed function of UBPY regulating the ubiquitination status of the ESCRT-0 members themselves, specifically STAM arose from a study in which UBPY

was knocked out and it was found that >90% of STAM levels were reduced, with only a minimal affect on Hrs.[13] Similarly, another study investigating the ubiquitination status of ESCRT-0 showed that wild-type AMSH and a functional SBM controlled the ubiquitination of both Hrs and STAM.[19] These studies suggest that ESCRT DUBs not only regulate the cargo degradation, but also, the ESCRT-0 members themselves. It is not fully understood why ESCRT-0 becomes ubiquitinated. Two of the possible reasons for ESCRT-0 ubiquitination are: (1) to regulate the steady state levels of both Hrs and STAM, therefore, degrade these proteins once their function is complete and (2) to regulate cargo entry. Proteasome inhibition coupled with UBPY knockout cells had an accumulation of ubiquitinated STAM, suggesting that STAM becomes Lys48-polyubiquitinated.[13] In terms of regulating cargo entry, Hrs does not become ubiquitinated when its UIM is mutated, suggesting that this UBD not only binds ubiquitinated cargo, but also becomes ubiquitinated itself.[60] Looking at the ubiquitination status of ESCRT-0 and attempting to assign a role to AMSH or UBPY, structural and biophysical data supports the model that UBPY regulates STAM proteasomal targeting because of its ability to cleave Lys48-linked ubiquitin chains, a role in which AMSH can not fit.[7] Furthermore, UBPY could in theory control the ubiquitination status of ESCRT-0 in terms of regulation of cargo entry because studies show that ESCRT-0 is multi-ubiquitinated or monoubiquitinated.[60] Looking at AMSH and its structural and biochemical specificity, it could cleave Lys63-linked polyubiquitinated ESCRT-0,[60] but again, a single ubiquitin moiety would be left, thus not fully releasing the regulatory mechanism that blocks cargo entry. Ultimately, the data supports UBPY controlling the ubiquitination of Hrs/STAM as it pertains to proteasomal degradation and ubiquitination.

5.4.2 The Role of DUBs at ESCRT-III

DUB role at ESCRT-III seems to be more clearly understood than at ESCRT-0, however, dissection of these potential roles for DUBs at ESCRT-III have seemingly proven to be more complicated than initially thought. It is widely understood that the ubiquitin has to be removed prior to cargo sequestration into an ILV. The confusing part regarding this role within mammalian ESCRTs is the presence of both AMSH and UBPY. Both DUBs have functional MIT domains that allow for proper recruitment to ESCRT-III, however, as seen with ESCRT-0, their individual ubiquitin chain specificities and a new issue, they specifically interact with different ESCRT-III subunits, may separate their individual functions at ESCRT-III.

Doa4 is the only DUB in *S. cerevisiae* required to regulate MVB sorting by recycling ubiquitin from ubiquitinated cargo destined for the vacuole.[7] Of the two DUBs employed by the human ESCRT system, UBPY displays the highest similarity to Doa4; therefore, it would be easy to assign UBPY a similar role within the mammalian ESCRT system. Structural and biophysical evidence supports this role for UBPY because of the lack of chain specificity between Lys48, Lys63, and monoubiquitin. More evidence in support of UBPY functioning to recycle ubiquitin from receptors prior to confinement to ILVs arises from studies that highlight the specific interaction UBPY has with CHMP4, particularly, CHMP4C.[14] This interaction becomes important because CHMP4 is the human homologue to Snf7, which is the most abundant ESCRT-III subunit and is absolutely necessary for bud severing,[61] suggesting UBPY is recruited in close proximity to the severing bud neck. Also, UBPY-CHMP4 interaction could support the idea of UBPY oligomerization since CHMP4 oligomerizes,[61] but also, UBPY existing in

multiple copies has been suggested from the structure of the N-terminal dimerization domain.[49] If these data are taken together, then multiple copies of UBPY would be present to facilitate deubiquitination.

Again, AMSH would not have a redundant role because of its chain specificity. Even more interesting about AMSH recruitment to ESCRT-III is that its MIT domain interactions do not overlap with the UBPY in terms of the subunits necessary for vesicle formation. Of the subunits speculated to be involved in vesicle formation (CHMP6<CHMP4<CHMP3<CHMP2), AMSH only interacts specifically and tightly with CHMP3.[14; 37] It suggests that AMSH and UBPY could in theory be present at ESCRT-III at the same time. Based on reasons discussed above, UBPY would be more abundant, however, there is no evidence supporting that both enzymes are present at the same time. The tight AMSH-CHMP3 interaction suggests a role for AMSH in HIV-1 budding. The role of AMSH in HIV-1 budding is still poorly understood. One study showed that catalytically inactive AMSH resulted in strong inhibition of virion release, however, the same study showed that AMSH is not essential for viral budding, stating that the initial finding regarding catalytically inactive AMSH inhibiting viral budding could be due to competition or interference with other necessary components.[16] Another study showed that HIV-1 budding has a minimal requirement for CHMP3 as compared to CHMP4B and CHMP2 (A or B).[62] Slight opposition to this study in which SPR measurements showed that CHMP4B binds ~16-fold more tightly to CHMP3 than to CHMP2A, while CHMP2A binds CHMP4B and CHMP3 with similar K_Ds, suggesting that CHMP3 would be recruited to the HIV-1 budding site prior to CHMP2A, after CHMP4B (CHMP4B<CHMP3<CHMP2A).[35] In accordance with these results, AMSH

seems to play some role within HIV-1 budding, whereas UBPY would not because of its inability to interact with the necessary ESCRT-III subunits, however, the exact role AMSH plays is not very clear.

A possible non-catalytic role was proposed for AMSH at ESCRT-III by interfering with cargo sorting by competing with Vps4 for CHMP-binding, possibly inhibiting luminal vesicle budding.[7] Biochemical studies show that Vps4 works to recycle ESCRT-III proteins after membrane scission because omission of Vps2 (CHMP2) completely inhibited a second round of ILV formation.[63] These data suggest that when the cargo is committed into an ILV, and completely deubiquitinated, membrane scission occurs, possibly concurrently to ESCRT-III recycling by Vps4. The idea that AMSH competes with Vps4 for CHMP binding was shown previously in which over-expression of Vps4 resulted in decreased binding of CHMP1B to wild-type and catalytically inactive AMSH, the MIT domain of Vps4 was the minimal domain needed to compete with AMSH for CHMP1B binding.[16] Contrary to these results, AMSH binds to CHMP3 with 63 nM affinity, ~70-fold tighter than the tightest affinity measurement for Vps4-CHMP1A interaction, suggesting that AMSH would be too tightly bound for Vps4 to displace the enzyme.[37; 38] If we take into account that based on sequence homology and functional similarities, CHMP1-3 are grouped together into a class, different from CHMP4-6, containing three conserved leucines,[38] then AMSH's affinity for CHMP3 would be similar to its affinity for CHMP1 proteins, meaning that its affinity for CHMPs would be much greater than Vps4's affinity for CHMPs. Based on these data we cannot see how Vps4 would effectively compete off AMSH for CHMP binding. There must be another mechanism for DUB release prior to Vps4 recycling the ESCRT-III subunits.

5.5 DUB Interaction with Ubiquitin Ligases

Although it is better understood that DUBs oppose E3 ligase action by removing ubiquitin, it is less well understood why some DUBs interact and binding directly to an E3 ligase. It is suggested that a direct interaction between a DUB and an E3 ligase is because many E3 ligases undergo autoubiquitination and DUBs serve to stabilize the ligase by reversing this autoubiquitination, however, in reversing autoubiquitination, this may indirectly destabilize proteins targeted by the E3 ligase because they will get ubiquitinated [64]. Accordingly, AMSH and UBPY have been shown to interact directly with E3 ligases, and we seek to gain understanding as to what role these interactions serve in regards to regulating the ESCRT machinery.

5.5.1 AMSH-E3 Ligase Interaction

A yeast two-hybrid study followed by an immuno-precipitation experiment found that AMSH binds Ring-finger protein 11 (RNF11), a small, ring-finger protein that has a RING H2 domain that facilitates protein-protein interactions involved in ubiquitination events, in particular, HECT-type E3 ligases.[65] RNF11 binds to the HECT-type E3 ligase, Smurf2, using its PY motif, which does not overlap with AMSH binding, suggesting that RNF11 acts as an adaptor protein, mediating the interaction between AMSH and Smurf2.[65] In the presence of RNF11, Smurf2 promotes ubiquitination of AMSH, correlating directly to the observation that within total cell lysates, the steady state level of AMSH was significantly reduced in the presence of both RNF11 and Smurf2.[65] These data suggest a role not spoken of much in terms of ESCRT-mediated degradation, that the

E3 ligase, the direct interaction of Smurf2 with AMSH (via RNF11) is necessary for regulating the steady-state levels of AMSH. This is consistent with Smurf2's function of catalyzing the ubiquitination of target protein substrates destined for proteolysis.[65]

Similarly, RNF11 interacts with another E3 ligase, atrophin-interacting protein 4 (AIP4), through the WW domain of AIP4 and the PY motif in RNF11.[65] AIP4 is a member of the Nedd4-family of E3 ligases in which the prototypic member, Nedd4 has a 350-amino acid HECT domain, a Ca^{2+}-dependent phospholipid binding C2 domain, and three or four WW domains.[66] AIP4 mediates agonist-dependent ubiquitination and degradation of the G-protein couple receptor, CXCR4, which in turn caused the ubiquitination of ESCRT-0 member, Hrs.[66] Not only does AIP4 interact with Hrs, it has been shown that AIP4 specifically binds STAM, mediated through the SH3 domain of STAM because deletion of the SH3 domain reduced AIP4 binding by 50%.[67] In accordance with AIP4 binding to STAM, wild-type AIP4 enhanced the ubiquitination of STAM compared to a catalytically inactive mutant of AIP4.[67] In light of these data, it is suggested that AMSH specifically recruits AIP4 to ubiquitinate STAM, which is stabilized by catalytically inactive AMSH.[13] Supporting this hypothesis, proper sorting of CXCR4 is dependent on AMSH, suggesting a role that AMSH regulates the ubiquitination status of ESCRT-0, which in turns affects the fate of CXCR4.[19] Alternatively, AMSH does not mediate agonist-induced degradation of CXCR4.[68] However, a larger role for STAM in CXCR4 sorting has been proposed in which AIP4 binding to and ubiquitinating STAM mediates CXCR4-induced extracellular signal-regulated kinases-1/2 (ERK-1/2) activation.[67] Just like RNF11, STAM could be an adaptor protein for the interaction of AMSH with the E3 ligase, however, in terms of

AIP4, it seems that this interaction is more involved in regulating CXCR4 sorting as opposed to regulating the enzyme itself.

5.5.2 UBPY-E3 Ligase Interaction

An affinity pull-down assay was conducted to isolate proteins that bound to the E3 ligase, Nrdp1, and UBPY was discovered as a Nrdp1 binding partner.[45] Consistent with the discovery that Nrdp1 is intrinsically unstable in cells due to autoubiquitination and subsequent proteasomal degradation, catalytic activity of UBPY greatly enhances Nrdp1 stability to a similar level as catalytically inactive mutants of Nrdp1.[45] This interaction between UBPY and Nrdp1 has been mapped to the rhodanese domain within UBPY, the structure basis of which was described previously.[45; 49] It is suggested that UBPY and Nrdp1 exist as a highly specific complex for three reasons: (1) UBPY does not bind the E3 ligase that ubiquitinates EGFR, Cbl, (2) USP2, a ubiquitin specific protease family member with the highest sequence homology to UBPY in its catalytic domain, cannot stabilize Nrdp1, and lastly, (3) Nrdp1 mediates subcellular relocalization of UBPY.[45] All these studies have led to the speculation that Nrdp1 regulates steady-state levels of itself and UBPY through autoubiquitination and ubiquitination of UBPY, whereas the activity of UBPY can reverse both of these processes.

Another interesting DUB-E3 ligase interaction that has been described previously involves two DUBs, UBPY and OTU family member, otubain 1, and the E3 ligase, GRAIL (gene related to anergy in lymphocytes).[44] GRAIL is an active RING-type E3 ubiquitin ligase that is crucial in the induction of CD4 T cell anergy.[44] Yeast two-hybrid study found that two isoforms of otubain1, the full length and an inactive splice variant

with the same C-terminal domain as the wild-type protein, shows opposite effects regarding GRAIL stability.[44] Even though the wild type otubain1 has deubiquitinating activity towards polyubiquitin chains, the wild type promotes autoubiquitinated GRAIL, whereas, catalytically inactive otubain1 reduces the amount of autoubiquitinated GRAIL.[44] This result prompted another yeast two-hybrid experiment in which it was found that otubain1 binds the catalytic domain of UBPY, and immuno-precipitation showed that otubain1, GRAIL, and UBPY formed a ternary complex.[44] In an attempt to understand the role of UBPY in the ternary complex, studies show that UBPY can deubiquitinate GRAIL, and in forming the complete complex, a catalytically inactive UBPY leads to increase polyubiquitination of GRAIL, suggesting that otubain1 may regulate UBPY DUB activity, leading to GRAIL autoubiquitination, whereas, inactive otubain1, enhances UBPY activity, thus stabilizing GRAIL.[44]

5.6 Conclusions

A significant body of work has been dedicated toward investigating the mechanism of action for ESCRT-mediated degradation, however, there is still a lot to learn. The ESCRT-DUBs, AMSH and UBPY, have been extensively studied for their structural and *in vivo* functions, in relation to the consequences due to gene knockouts, however, there is still a significant amount of work to be done to understand their exact function within the ESCRT machinery. Using structural and biophysical data we have dissected the proposed roles of AMSH and UBPY in an attempt to test these hypotheses. We see that AMSH is more suited to play a role at ESCRT-0 than at ESCRT-III because of its ubiquitin linkage specificity, however, an experiment to show that AMSH is

incapable of deubiquitinating a monoubiquitinated substrate is still lacking. Furthermore, AMSH activity at ESCRT-III is still a mystery because of its linkage specificity. Interestingly though, AMSH has the highest CHMP binding affinity with CHMP3, which leads one to believe that this tight interaction is of significant importance. Could AMSH really be playing a non-catalytic role at ESCRT-III? It makes sense for UBPY to work similarly to Doa4 in yeast, but is there any other roles for UBPY at ESCRT-III? Finally, the DUB-E3 ligase interaction has not been discussed at great length especially in terms of its role in regulating the ESCRT machinery. Does the DUB-E3 ligase interaction serve to regulate the cellular concentration of ESCRT-DUBs? Overall, the role of DUBs within the ESCRT machinery should be looked at more closely because some of the underlying functions of each DUB maybe beyond their ability to hydrolyze ubiquitin.

5.7 References

1. Schmidt, O. & Teis, D. (2012). The ESCRT machinery. *Curr Biol* **22**, R116-20.

2. Henne, W. M., Buchkovich, N. J. & Emr, S. D. (2011). The ESCRT pathway. *Dev Cell* **21**, 77-91.

3. Roxrud, I., Stenmark, H. & Malerod, L. (2010). ESCRT & Co. *Biol Cell* **102**, 293-318.

4. Saksena, S. & Emr, S. D. (2009). ESCRTs and human disease. *Biochem Soc Trans* **37**, 167-72.

5. Stuffers, S., Brech, A. & Stenmark, H. (2009). ESCRT proteins in physiology and disease. *Exp Cell Res* **315**, 1619-26.

6. Wollert, T. & Hurley, J. H. (2010). Molecular mechanism of multivesicular body biogenesis by ESCRT complexes. *Nature* **464**, 864-9.

7. Clague, M. J. & Urbe, S. (2006). Endocytosis: the DUB version. *Trends Cell Biol* **16**, 551-9.

8. Bowers, K., Lottridge, J., Helliwell, S. B., Goldthwaite, L. M., Luzio, J. P. & Stevens, T. H. (2004). Protein-protein interactions of ESCRT complexes in the yeast Saccharomyces cerevisiae. *Traffic* **5**, 194-210.

9. Reggiori, F. & Pelham, H. R. (2001). Sorting of proteins into multivesicular bodies: ubiquitin-dependent and -independent targeting. *EMBO J* **20**, 5176-86.

10. McCullough, J., Clague, M. J. & Urbe, S. (2004). AMSH is an endosome-associated ubiquitin isopeptidase. *J Cell Biol* **166**, 487-92.

11. McCullough, J., Row, P. E., Lorenzo, O., Doherty, M., Beynon, R., Clague, M. J. & Urbe, S. (2006). Activation of the endosome-associated ubiquitin isopeptidase AMSH by STAM, a component of the multivesicular body-sorting machinery. *Curr Biol* **16**, 160-5.

12. Kato, M., Miyazawa, K. & Kitamura, N. (2000). A deubiquitinating enzyme UBPY interacts with the Src homology 3 domain of Hrs-binding protein via a novel binding motif PX(V/I)(D/N)RXXKP. *J Biol Chem* **275**, 37481-7.

13. Row, P. E., Prior, I. A., McCullough, J., Clague, M. J. & Urbe, S. (2006). The ubiquitin isopeptidase UBPY regulates endosomal ubiquitin dynamics and is essential for receptor down-regulation. *J Biol Chem* **281**, 12618-24.

14. Row, P. E., Liu, H., Hayes, S., Welchman, R., Charalabous, P., Hofmann, K., Clague, M. J., Sanderson, C. M. & Urbe, S. (2007). The MIT domain of UBPY

constitutes a CHMP binding and endosomal localization signal required for efficient epidermal growth factor receptor degradation. *J Biol Chem* **282**, 30929-37.

15. Tsang, H. T., Connell, J. W., Brown, S. E., Thompson, A., Reid, E. & Sanderson, C. M. (2006). A systematic analysis of human CHMP protein interactions: additional MIT domain-containing proteins bind to multiple components of the human ESCRT III complex. *Genomics* **88**, 333-46.

16. Agromayor, M. & Martin-Serrano, J. (2006). Interaction of AMSH with ESCRT-III and deubiquitination of endosomal cargo. *J Biol Chem* **281**, 23083-91.

17. Maytal-Kivity, V., Reis, N., Hofmann, K. & Glickman, M. H. (2002). MPN+, a putative catalytic motif found in a subset of MPN domain proteins from eukaryotes and prokaryotes, is critical for Rpn11 function. *BMC Biochem* **3**, 28.

18. Davies, C. W., Paul, L. N., Kim, M. I. & Das, C. (2011). Structural and thermodynamic comparison of the catalytic domain of AMSH and AMSH-LP: nearly identical fold but different stability. *J Mol Biol* **413**, 416-29.

19. Sierra, M. I., Wright, M. H. & Nash, P. (2010). AMSH interacts with ESCRT-0 to regulate the stability and trafficking of CXCR4. *J Biol Chem*.

20. Kyuuma, M., Kikuchi, K., Kojima, K., Sugawara, Y., Sato, M., Mano, N., Goto, J., Takeshita, T., Yamamoto, A., Sugamura, K. & Tanaka, N. (2007). AMSH, an ESCRT-III associated enzyme, deubiquitinates cargo on MVB/late endosomes. *Cell Struct Funct* **31**, 159-72.

21. Ma, Y. M., Boucrot, E., Villen, J., Affar el, B., Gygi, S. P., Gottlinger, H. G. & Kirchhausen, T. (2007). Targeting of AMSH to endosomes is required for epidermal growth factor receptor degradation. *J Biol Chem* **282**, 9805-12.

22. Herrera-Vigenor, F., Hernandez-Garcia, R., Valadez-Sanchez, M., Vazquez-Prado, J. & Reyes-Cruz, G. (2006). AMSH regulates calcium-sensing receptor signaling through direct interactions. *Biochem Biophys Res Commun* **347**, 924-30.

23. Reyes-Ibarra, A. P., Garcia-Regalado, A., Ramirez-Rangel, I., Esparza-Silva, A. L., Valadez-Sanchez, M., Vazquez-Prado, J. & Reyes-Cruz, G. (2007). Calcium-sensing receptor endocytosis links extracellular calcium signaling to parathyroid hormone-related peptide secretion via a Rab11a-dependent and AMSH-sensitive mechanism. *Mol Endocrinol* **21**, 1394-407.

24. Hislop, J. N., Henry, A. G., Marchese, A. & von Zastrow, M. (2009). Ubiquitination regulates proteolytic processing of G protein-coupled receptors after their sorting to lysosomes. *J Biol Chem* **284**, 19361-70.

25. Hasdemir, B., Murphy, J. E., Cottrell, G. S. & Bunnett, N. W. (2009). Endosomal deubiquitinating enzymes control ubiquitination and down-regulation of protease-activated receptor 2. *J Biol Chem* **284**, 28453-66.

26. Carlton, J. G. & Martin-Serrano, J. (2007). Parallels between cytokinesis and retroviral budding: a role for the ESCRT machinery. *Science* **316**, 1908-12.

27. Morita, E., Sandrin, V., Chung, H. Y., Morham, S. G., Gygi, S. P., Rodesch, C. K. & Sundquist, W. I. (2007). Human ESCRT and ALIX proteins interact with proteins of the midbody and function in cytokinesis. *EMBO J* **26**, 4215-27.

28. Mukai, A., Mizuno, E., Kobayashi, K., Matsumoto, M., Nakayama, K. I., Kitamura, N. & Komada, M. (2008). Dynamic regulation of ubiquitylation and deubiquitylation at the central spindle during cytokinesis. *J Cell Sci* **121**, 1325-33.

29. Tanaka, N., Kaneko, K., Asao, H., Kasai, H., Endo, Y., Fujita, T., Takeshita, T. & Sugamura, K. (1999). Possible involvement of a novel STAM-associated molecule "AMSH" in intracellular signal transduction mediated by cytokines. *J Biol Chem* **274**, 19129-35.

30. Arnst, J. L., Davies, C. W., Raja, S. M., Das, C. & Natarajan, A. (2013). High-throughput compatible fluorescence resonance energy transfer-based assay to identify small molecule inhibitors of AMSH deubiquitinase activity. *Anal Biochem*.

31. Sato, Y., Yoshikawa, A., Yamagata, A., Mimura, H., Yamashita, M., Ookata, K., Nureki, O., Iwai, K., Komada, M. & Fukai, S. (2008). Structural basis for specific cleavage of Lys 63-linked polyubiquitin chains. *Nature* **455**, 358-62.

32. Nakamura, M., Tanaka, N., Kitamura, N. & Komada, M. (2006). Clathrin anchors deubiquitinating enzymes, AMSH and AMSH-like protein, on early endosomes. *Genes Cells* **11**, 593-606.

33. Raiborg, C., Bache, K. G., Mehlum, A., Stang, E. & Stenmark, H. (2001). Hrs recruits clathrin to early endosomes. *EMBO J* **20**, 5008-21.

34. Kim, M. S., Kim, J. A., Song, H. K. & Jeon, H. (2006). STAM-AMSH interaction facilitates the deubiquitination activity in the C-terminal AMSH. *Biochem Biophys Res Commun* **351**, 612-8.

35. Effantin, G., Dordor, A., Sandrin, V., Martinelli, N., Sundquist, W. I., Schoehn, G. & Weissenhorn, W. (2012). ESCRT-III CHMP2A and CHMP3 form variable helical polymers in vitro and act synergistically during HIV-1 budding. *Cell Microbiol*.

36. Lata, S., Roessle, M., Solomons, J., Jamin, M., Gottlinger, H. G., Svergun, D. I. & Weissenhorn, W. (2008). Structural basis for autoinhibition of ESCRT-III CHMP3. *J Mol Biol* **378**, 818-27.

37. Solomons, J., Sabin, C., Poudevigne, E., Usami, Y., Hulsik, D. L., Macheboeuf, P., Hartlieb, B., Gottlinger, H. & Weissenhorn, W. (2011). Structural basis for ESCRT-III CHMP3 recruitment of AMSH. *Structure* **19**, 1149-59.

38. Stuchell-Brereton, M. D., Skalicky, J. J., Kieffer, C., Karren, M. A., Ghaffarian, S. & Sundquist, W. I. (2007). ESCRT-III recognition by VPS4 ATPases. *Nature* **449**, 740-4.

39. Nijman, S. M., Luna-Vargas, M. P., Velds, A., Brummelkamp, T. R., Dirac, A. M., Sixma, T. K. & Bernards, R. (2005). A genomic and functional inventory of deubiquitinating enzymes. *Cell* **123**, 773-86.

40. Komander, D., Clague, M. J. & Urbe, S. (2009). Breaking the chains: structure and function of the deubiquitinases. *Nat Rev Mol Cell Biol* **10**, 550-63.

41. Komander, D. (2010). Mechanism, specificity and structure of the deubiquitinases. *Subcell Biochem* **54**, 69-87.

42. Naviglio, S., Mattecucci, C., Matoskova, B., Nagase, T., Nomura, N., Di Fiore, P. P. & Draetta, G. F. (1998). UBPY: a growth-regulated human ubiquitin isopeptidase. *EMBO J* **17**, 3241-50.

43. Gnesutta, N., Ceriani, M., Innocenti, M., Mauri, I., Zippel, R., Sturani, E., Borgonovo, B., Berruti, G. & Martegani, E. (2001). Cloning and characterization of mouse UBPy, a deubiquitinating enzyme that interacts with the ras guanine nucleotide exchange factor CDC25(Mm)/Ras-GRF1. *J Biol Chem* **276**, 39448-54.

44. Soares, L., Seroogy, C., Skrenta, H., Anandasabapathy, N., Lovelace, P., Chung, C. D., Engleman, E. & Fathman, C. G. (2004). Two isoforms of otubain 1 regulate T cell anergy via GRAIL. *Nat Immunol* **5**, 45-54.

45. Wu, X., Yen, L., Irwin, L., Sweeney, C. & Carraway, K. L., 3rd. (2004). Stabilization of the E3 ubiquitin ligase Nrdp1 by the deubiquitinating enzyme USP8. *Mol Cell Biol* **24**, 7748-57.

46. Mizuno, E., Kobayashi, K., Yamamoto, A., Kitamura, N. & Komada, M. (2006). A deubiquitinating enzyme UBPY regulates the level of protein ubiquitination on endosomes. *Traffic* **7**, 1017-31.

47. Balut, C. M., Loch, C. M. & Devor, D. C. (2011). Role of ubiquitylation and USP8-dependent deubiquitylation in the endocytosis and lysosomal targeting of plasma membrane KCa3.1. *FASEB J* **25**, 3938-48.

48. Zhou, R., Tomkovicz, V. R., Butler, P. L., Ochoa, L. A., Peterson, Z. J. & Snyder, P. M. (2013). Ubiquitin Specific Peptidase 8 (USP8) Regulates Endosomal Trafficking of the Epithelial Na+ Channel. *J Biol Chem*.

49. Avvakumov, G. V., Walker, J. R., Xue, S., Finerty, P. J., Jr., Mackenzie, F., Newman, E. M. & Dhe-Paganon, S. (2006). Amino-terminal dimerization, NRDP1-rhodanese interaction, and inhibited catalytic domain conformation of the ubiquitin-specific protease 8 (USP8). *J Biol Chem* **281**, 38061-70.

50. Hu, M., Li, P., Li, M., Li, W., Yao, T., Wu, J. W., Gu, W., Cohen, R. E. & Shi, Y. (2002). Crystal structure of a UBP-family deubiquitinating enzyme in isolation and in complex with ubiquitin aldehyde. *Cell* **111**, 1041-54.

51. Hu, M., Li, P., Song, L., Jeffrey, P. D., Chenova, T. A., Wilkinson, K. D., Cohen, R. E. & Shi, Y. (2005). Structure and mechanisms of the proteasome-associated deubiquitinating enzyme USP14. *EMBO J* **24**, 3747-56.

52. Krishna, S. S., Majumdar, I. & Grishin, N. V. (2003). Structural classification of zinc fingers: survey and summary. *Nucleic Acids Res* **31**, 532-50.

53. Kaneko, T., Kumasaka, T., Ganbe, T., Sato, T., Miyazawa, K., Kitamura, N. & Tanaka, N. (2003). Structural insight into modest binding of a non-PXXP ligand to the signal transducing adaptor molecule-2 Src homology 3 domain. *J Biol Chem* **278**, 48162-8.

54. Meijer, I. M., van Rotterdam, W., van Zoelen, E. J. & van Leeuwen, J. E. (2012). Recycling of EGFR and ErbB2 is associated with impaired Hrs tyrosine phosphorylation and decreased deubiquitination by AMSH. *Cell Signal* **24**, 1981-8.

55. Ren, X. & Hurley, J. H. (2010). VHS domains of ESCRT-0 cooperate in high-avidity binding to polyubiquitinated cargo. *EMBO J*.

56. Agromayor, M., Soler, N., Caballe, A., Kueck, T., Freund, S. M., Allen, M. D., Bycroft, M., Perisic, O., Ye, Y., McDonald, B., Scheel, H., Hofmann, K., Neil, S. J., Martin-Serrano, J. & Williams, R. L. (2012). The UBAP1 subunit of ESCRT-I interacts with ubiquitin via a SOUBA domain. *Structure* **20**, 414-28.

57. Hurley, J. H. (2011). Nipped in the bud: how the AMSH MIT domain helps deubiquitinate lysosome-bound cargo. *Structure* **19**, 1033-5.

58. Ren, J., Kee, Y., Huibregtse, J. M. & Piper, R. C. (2007). Hse1, a component of the yeast Hrs-STAM ubiquitin-sorting complex, associates with ubiquitin peptidases and a ligase to control sorting efficiency into multivesicular bodies. *Mol Biol Cell* **18**, 324-35.

59. Ghaemmaghami, S., Huh, W. K., Bower, K., Howson, R. W., Belle, A., Dephoure, N., O'Shea, E. K. & Weissman, J. S. (2003). Global analysis of protein expression in yeast. *Nature* **425**, 737-41.

60. Komada, M. & Kitamura, N. (2005). The Hrs/STAM complex in the downregulation of receptor tyrosine kinases. *J Biochem* **137**, 1-8.

61. Hurley, J. H. & Hanson, P. I. (2010). Membrane budding and scission by the ESCRT machinery: it's all in the neck. *Nat Rev Mol Cell Biol* **11**, 556-66.

62. Morita, E., Sandrin, V., McCullough, J., Katsuyama, A., Baci Hamilton, I. & Sundquist, W. I. (2011). ESCRT-III protein requirements for HIV-1 budding. *Cell Host Microbe* **9**, 235-42.

63. Wollert, T., Wunder, C., Lippincott-Schwartz, J. & Hurley, J. H. (2009). Membrane scission by the ESCRT-III complex. *Nature* **458**, 172-7.

64. Clague, M. J., Coulson, J. M. & Urbe, S. (2012). Cellular functions of the DUBs. *J Cell Sci* **125**, 277-86.

65. Li, H. & Seth, A. (2004). An RNF11: Smurf2 complex mediates ubiquitination of the AMSH protein. *Oncogene* **23**, 1801-8.

66. Marchese, A., Raiborg, C., Santini, F., Keen, J. H., Stenmark, H. & Benovic, J. L. (2003). The E3 ubiquitin ligase AIP4 mediates ubiquitination and sorting of the G protein-coupled receptor CXCR4. *Dev Cell* **5**, 709-22.

67. Malik, R., Soh, U. J., Trejo, J. & Marchese, A. (2012). Novel roles for the E3 ubiquitin ligase atrophin-interacting protein 4 and signal transduction adaptor molecule 1 in G protein-coupled receptor signaling. *J Biol Chem* **287**, 9013-27.

68. Malik, R. & Marchese, A. (2010). Arrestin-2 interacts with the endosomal sorting complex required for transport machinery to modulate endosomal sorting of CXCR4. *Mol Biol Cell* **21**, 2529-41.

VITA

VITA

Christopher was born in Bowling Green, KY to Simeon and Frederica Davies on October 8th, 1986. He was the last of three children, the oldest child, Claire, and the middle, Conrad. His parents were both born in Sierra Leone, West Africa, and they came to the United States to finish their schooling, in search of a better life and more opportunities for their three children. Both Simeon and Frederica have Master's degrees from Western Kentucky University, Simeon in Chemistry and Frederica in Library Science and Education, which would set the tone for Christopher's academic career.

Christopher grew up in Frankfort, KY where he attended elementary, middle, and one year of high school. Towards the end of his freshman year in high school, Simeon approached Christopher about the idea of sending him to a private school in Lexington, KY, Lexington Catholic High School, in order to raise the level of his educational and athletic training. He was attending public school in Frankfort, however, due to the minimal amount of advanced placement courses and Christopher's desire to excel in soccer, the decision was made to enroll him at Lexington Catholic High School. Christopher spent his last three years of high school at Lexington Catholic High School becoming a member of the National Honor's Society and a prominent member of the school's soccer team, helping to lead them to two consecutive final four finishes, the second of which was a state runners up.

After graduating in 2004 from Lexington Catholic High School, Christopher maintained a Davies' family tradition of attending Western Kentucky University. Every member of his immediate family has received their degree from Western Kentucky. As much as Christopher entertained the idea of attending other universities, Western Kentucky proved to be the best fit for his academic, athletic, and overall growth. Much of Christopher's success at Western Kentucky stemmed from the discipline and drive that was required of a division I soccer player. Christopher's time at Western Kentucky would prove to be a very significant four years in his life. There were some tough times early on in his college career, mostly stemming from growing up and establishing who he was, but ultimately ended up well. While playing four years of soccer, he managed to be heavily involved in undergraduate research under the direction of Prof. Thandi Buthelezi. Ever semester, including the first two summers, he would work at least 10 hours a week in the lab. His undergraduate research project was to investigate a host-guest relationship using cyclophane molecules to capture polyaromatic hydrocarbons (PAHs) out of solution. As a result of his studies, he regularly attended and presented at national conferences including: the American Chemical Society (ACS) Meeting, the Pittsburg Conference on Analytical Chemistry and Applied Spectroscopy (Pittcon), and the National Organization for the Advancement of Black Chemists and Chemical Engineers (NOBCChE) Meeting. As a result of attending the ACS meeting, Christopher met Dr. James Grainger, a group leader at the Centers for Disease Control and Prevention (CDC) in Atlanta, GA. After meeting Dr. Grainger at the ACS meeting, further contact continued for up to a year later, leading to Christopher being invited to do a summer-long internship at the CDC.

The summer between his junior and senior years, Christopher at age 20, moved to Atlanta, GA as an intern at the CDC. The experiences and the people he met during his internship were remarkable and important in his journey. His project at the CDC was to develop a method for quantifying benzo[a]pyrene adducts to human serum albumin to study the effects of PAH accumulation in smokers versus non-smokers. That summer he learned about proteins and protein purification, which would drive his long-term career interests away from pure chemistry to biochemistry. More importantly, Christopher worked under Dr. Angela Ragin-Wilson, who would mentor him on his path to obtaining his PhD. Dr. Ragin-Wilson is distinguished alum from the Chemistry Department at Purdue University; so naturally, she pushed Christopher towards applying for Purdue. After a long search at schools and professors, Christopher settled on applying for only two schools, Purdue University and University of North Carolina Chapel Hill.

His senior year at Western Kentucky was focused on applying for graduate school and playing his last year of college soccer, but he also continued to work in the lab. After having applied to Purdue in early September, Christopher received his acceptance letter in November; however, the application deadline for North Carolina was not until January. Having been accepted into Purdue's graduate school, he was set on attending Purdue, until the acceptance letter for North Carolina came in the email. Christopher actually had to make a decision on which school to attend, and North Carolina had initially offered him a fellowship package. After visiting and meeting professors at both schools, the much-anticipated decision was made to attend Purdue.

Prior to his arrival in West Lafayette in the fall of 2008, he was invited back to Atlanta for a second summer at CDC. Christopher moved from Atlanta directly to West

Lafayette with much anticipation of what graduate school was all about. It was around this time, that Christopher received an encouraging word from his brother Conrad that would set the foundation for what was to come. Conrad told him that he would be a highly sought out researcher. As the years past, Christopher's graduate career began to align under that encouraging word. Christopher was a co-author of a Proceedings of the National Academy (*PNAS*) paper in his second year, and then, went on to publish his first-author publication at Purdue in 2011. Christopher would then go on to publish four more papers in 2011, 2012, and 2013. He anticipates another two if not three more publications in the near future from his work at Purdue. This publication record would help pave the way for his future scientific career. During his 5th year, Christopher has traveled to Fortune 500 companies, government institutions, and research hospitals to give oral presentations on his work. These presentations built an extraordinary professional network for him that ultimately led to company and post-doc interviews. After much consultation from those important to Christopher, his decision came down to where his heart led him. He accepted a post-doc position at UC Berkeley working for the former National Institutes of Health (NIH) professor, James Hurley. He will be joining a well established, well-known professor to further is structural and biophysical training in hopes to go on to establish his own independent scientific career.

PUBLICATIONS

Ubiquitin vinyl methyl ester binding orients the misaligned active site of the ubiquitin hydrolase UCHL1 into productive conformation

David A. Boudreaux[1], Tushar K. Maiti[1], Christopher W. Davies, and Chittaranjan Das[2]

Department of Chemistry, Purdue University, 560 Oval Drive, West Lafayette, IN 47907

Edited by Gregory A. Petsko, Brandeis University, Waltham, MA, and approved March 30, 2010 (received for review September 21, 2009)

Ubiquitin carboxy-terminal hydrolase L1 (UCHL1) is a Parkinson disease-associated, putative cysteine protease found abundantly and selectively expressed in neurons. The crystal structure of apo UCHL1 showed that the active-site residues are not aligned in a canonical form, with the nucleophilic cysteine being 7.7 Å from the general base histidine, an arrangement consistent with an inactive form of the enzyme. Here we report the crystal structures of the wild type and two Parkinson disease-associated variants of the enzyme, S18Y and I93M, bound to a ubiquitin-based suicide substrate, ubiquitin vinyl methyl ester. These structures reveal that ubiquitin vinyl methyl ester binds primarily at two sites on the enzyme, with its carboxy terminus at the active site and with its amino-terminal β-hairpin at the distal site—a surface-exposed hydrophobic crevice 17 Å away from the active site. Binding at the distal site initiates a cascade of side-chain movements in the enzyme that starts at a highly conserved, surface-exposed phenylalanine and is relayed to the active site resulting in the reorientation and proximal placement of the general base within 4 Å of the catalytic cysteine, an arrangement found in productive cysteine proteases. Mutation of the distal-site, surface-exposed phenylalanine to alanine reduces ubiquitin binding and severely impairs the catalytic activity of the enzyme. These results suggest that the activity of UCHL1 may be regulated by its own substrate.

deubiquitinating enzyme | enzyme suicide substrate complex | neurodegeneration | ubiquitination

UCHL1, a member of the UCH (ubiquitin C-terminal hydrolase) family of deubiquitinating enzymes (DUBs), is a 223-amino acid protein found abundantly and selectively expressed in brain, constituting up to 1–2% of total brain protein (1, 2). In vivo studies suggest that UCHL1 is involved in regulation of ubiquitin pool, apoptosis, and learning and memory, and its absence in mice because of spontaneous intragenic deletions yields phenotypes with neurological defects (3). Mutations in UCHL1 have been implicated in Parkinson disease (PD). A point mutation near the active site that changes Ile93 to Met (I93M) has been linked to an increased risk of developing an autosomal-dominant form of PD (4). Conversely, a common S18Y polymorphism reduces susceptibility to PD (5, 6) and Alzheimer's disease (7). In addition to its association with neurodegenerative diseases, abnormal expression of UCHL1 is found in many forms of cancer, including lung, colorectal, and pancreatic cancers, and may be related to tumor progression (8, 9). The normal function of UCHL1, however, is not known. Also unknown are how the activity of this abundant neuronal enzyme is regulated and what its true physiological substrates are, although biochemical studies have indicated that UCHL1 can accept short-peptide (α or ϵ-amino-linked) or small-molecule C-terminal conjugates of ubiquitin as substrates, cleaving, as its name suggests, the amide bond following immediately after the C-terminal glycine (Gly76) of ubiquitin (10).

Like other members of the UCH family, UCHL1 is a cysteine protease, with a catalytic triad consisting of a cysteine (Cys90), a histidine (His161), and an aspartate (Asp176). The overall structure of UCHL1 is very similar to that of its nearest UCH relative, UCHL3, which shares 51% of sequence identity with UCHL1. However, unlike UCHL3, the catalytic triad in UCHL1 is misaligned. Whereas the His161-Asp176 distance (2.7 Å) is very much within the expected range, the critical Cys90-His161 pair is separated by 7.7 Å (the Sγ atom of Cys90 from the Nδ1 atom of His161), a distance far greater than expected of a productive cysteine protease (11). This observation raises the question as to how this enzyme would catalyze the hydrolysis of an amide bond as a cysteine protease and how it would act as a ubiquitin hydrolase. To resolve this issue, we sought to determine the three-dimensional structure of the enzyme bound to a substrate analog. Here we report the X-ray structures of the wild-type UCHL1 and its two PD-associated variants, S18Y and I93M, hereafter referred to as UCHL1S18Y and UCHL1I93M, bound to a substrate mimic, ubiquitin vinyl methyl ester (UbVMe).

Results

Structure Determination. To prepare a stable complex with ubiquitin, UCHL1 and its variants were allowed to react with UbVMe, a derivative of ubiquitin with a glycyl vinyl methyl ester (GlyVMe) group substituting for Gly76 of ubiquitin (Fig. 1*A*). UbVMe acts as a suicide substrate for cysteine protease DUBs by targeting the active-site cysteine leading to the formation of a covalently bonded DUB–UbVMe complex, in which a thioether bond links the Sγ atom of the active-site cysteine of the DUB to the Cβ atom of the VMe moiety (Fig. 1*A*) (12). The thioether linkage mimics the thioester reaction intermediate proposed to exist during catalysis of the peptide bond hydrolysis by a cysteine protease. UCHL1 and its variants reacted with UbVMe nearly quantitatively, as judged by a mobility shift on a sodium dodecyl sulfate polyacrylamide gel of approximately 8 kDa, the expected molecular mass of ubiquitin (molecular mass, 8564.5 Da), allowing isolation of the complexes by size exclusion chromatography in milligram quantities suitable for crystallization.

The UCHL1S18Y–UbVMe complex structure was solved at 2.4 Å by molecular replacement using the wild-type UCHL1 and ubiquitin (residues 1–75) as search models (11, 12). Cross-rotation followed by translation search identified a single copy of the complex in the asymmetric unit. The electron density

Author contributions: C.D. designed research; D.A.B., T.K.M., C.W.D., and C.D. performed research; D.A.B., T.K.M., C.W.D., and C.D. analyzed data; and D.A.B., T.K.M., and C.D. wrote the paper.

The authors declare no conflict of interest.

This article is a PNAS Direct Submission.

Data deposition: Coordinates and structure factors for the UCHL1S18Y–UbVMe complex, UCHL1–UbVMe complex, UCHL1I93M–UbVMe complex, and apo UCHL1I93M have been deposited in the Protein Data Bank with ID codes 3IFW, 3KW5, 3KVF, and 3IRT, respectively.

[1]D.A.B. and T.K.M. contributed equally to this work.

[2]To whom correspondence should be addressed. E-mail: cdas@purdue.edu.

This article contains supporting information online at www.pnas.org/lookup/suppl/doi:10.1073/pnas.0910870107/-/DCSupplemental.

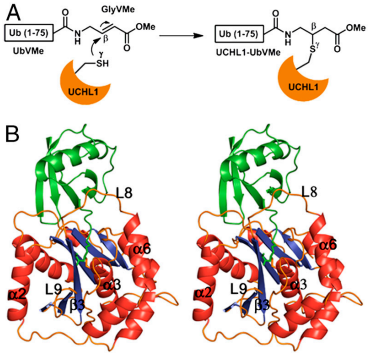

Fig. 1. Structure of UCHL1S18Y bound to the suicide substrate UbVMe. (*A*) Schematic representation of the UCHL1S18Y–UbVMe complex formed by covalent attack of the catalytic cysteine of UCHL1S18Y at the α,β-unsaturated bond of the VMe moiety. (*B*) Ribbon representation of the structure of UCHL1S18Y–UbVMe complex at 2.4 Å resolution. UbVMe is shown in green. Secondary structures of UCHL1S18Y discussed in the text are labeled.

map generated after rigid-body followed by restrained refinement of the model, obtained as the solution to molecular replacement, was interpretable, indicating the success of the molecular replacement search. Refinement using Refmac (13) after rounds of model building in Coot (14) yielded a final model with a crystallographic R factor of 20.9% and an R_{free} of 25.6% (Table S1). The final model contains a complete UCHL1S18Y chain (residues 1–223), a ubiquitin chain (residues 1–75), the GlyVMe group (modeled as 4-amino methyl butanoate), and 51 ordered solvent molecules. More than 98% of nonglycine residues are placed within the most favorable and additionally allowed regions of the Ramachandran plot, and less than 0.5% are located in the disallowed areas, as defined by the program PROCHECK (15). Structure of apo UCHL1I93M (2.80 Å) was solved by molecular replacement using the wild-type UCHL1 as the search model (*SI Methods* and Table S1). Structures of UCHL1-UbVMe (2.85 Å) and UCHL1I93M-UbVMe (2.80 Å) were solved by molecular replacement using the UCHL1S18Y–UbVMe complex as the search model (*SI Methods* and Table S1). The structures of UCHL1-UbVMe and UCHL1I93M-UbVMe are very similar to that of UCHL1S18Y-UbVMe (Fig. S1). We therefore chose to focus our discussion only on the UCHL1S18Y–UbVMe complex because it was determined at the highest resolution.

Overall Structure of UCHL1S18Y in the Complex. UCHL1S18Y is composed of two lobes, one consisting of five α helices (α1, α3, α4, α5, and α6) and the other consisting of two helices (α2 and α7) and a 6-stranded β-sheet (Fig. 1*B*). These secondary structures together form an α-β-α sandwich fold that characterizes most structurally known members of the papain family of cysteine proteases, including UCHL3 (16) and the yeast ubiquitin C-terminal hydrolase Yuh1 (17). Between the two lobes lies a relatively deep cleft that harbors the active site, which is composed of three secondary structure elements: a helix (α3), a strand (β3), and a loop (L9) on which the members of the catalytic triad Cys90, His161, and Asp176 reside, respectively. Tyr18 is located on the solvent-exposed face of the first N-terminal helix (α1). This residue is involved in tight hydrogen-bonding interactions with Arg27 with a distance of 2.8 Å separating the hydroxyl oxygen and one of the guanidinium nitrogens. In contrast, the corresponding residue in the wild-type protein, Ser18, is completely solvent-exposed and is not engaged in any interaction with other protein atoms. The overall architecture of UCHL1S18Y in UbVMe-bound complex is quite similar to that of apo wild-type UCHL1 (11), with C^{α} rmsd of 1.50 Å (Fig. S2). The arrangement of active-site residues, however, is quite different than the apo form, which has the general base His161 at 7.7 Å from the nucleophile Cys90, consistent with an inactive state of the enzyme (16, 18, 19). In the complex, the catalytic residues have adopted a canonical arrangement found in active cysteine proteases with His161 at 3.9 Å from the catalytic Cys90.

Specific Interactions of UbVMe with UCHL1S18Y. Binding of UbVMe with UCHL1S18Y is substantial, burying 2,548 $Å^2$ solvent-accessible surface area. Complex formation involves binding of UbVMe primarily at two sites on the enzyme: the active-site cleft and a solvent-exposed hydrophobic crevice 17 Å away from the active-site cysteine, hereafter referred to as the distal site (Fig. 2*A*). In terms of the buried accessible surface area on UCHL1S18Y, the UbVMe-binding interface is split almost evenly between the two sites, with the contributions from the active site and the distal site being ~45% and ~55%, respectively. The C-terminal segment of UbVMe (Val70 to GlyVMe76) is deeply buried in the active-site cleft, accounting for nearly 46% of the total buried accessible surface. With its backbone in an extended β conformation, this segment of UbVMe is extensively coordinated by hydrogen-bonding and salt-bridge interac-

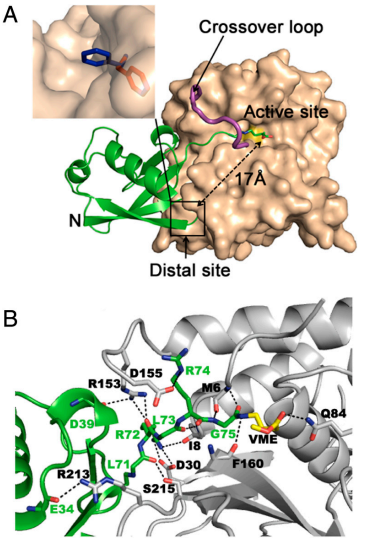

Fig. 2. Intermolecular contacts between UCHL1S18Y and UbVMe. (*A*) Molecular surface representation of UCHL1S18Y structure as observed in the crystal structure of its complex with UbVMe (shown as a green ribbon), illustrating the distal- and active-site binding of UbVMe. The active-site cysteine is indicated in yellow. The cross-over loop of UCHL1S18Y (L8 in Fig. 1*B*) is shown as a purple ribbon. The N terminus of UbVMe is indicated. (*Inset*) An expanded view of the distal binding site on UCHL1S18Y showing the Phe214 side-chain (*Orange*) compared to its position in apo UCHL1 (*Blue*). (*B*) Active-site interactions of the C-terminal segment of UbVMe (*Green Ribbon*) with the UCHL1S18Y (*Gray Ribbon*). Backbone and side chains of interacting residues are shown in stick representation. Oxygen atoms are shown in red, nitrogen atoms in blue, and carbon atoms of UCHL1S18Y and UbVMe (1–75) in gray and green, respectively. Carbon atoms of the GlyVMe residue are shown in yellow. The segment comprising residues 156–159 of UCHL1S18Y is removed for clarity.

tions to residues lining the active-site cleft of the enzyme (Fig. 2*B*), with the active-site cysteine linked to the VMe moiety of the suicide substrate via a thioether bond. In addition to these contacts, intermolecular van der Waals contacts also contribute to the specific recognition of the C-terminal segment of UbVMe. The two hydrophobic residues, Leu71 and Leu73, point into the catalytic cleft by making direct van der Waals contacts to the corresponding UCHL1S18Y residues (Leu71 of UbVMe with Val212 and Arg213 of UCHL1S18Y, and Leu73 of UbVMe with Ile8, Leu52, and Phe160 of UCHL1S18Y). The last two residues of UbVMe, Gly75 and GlyVMe76, fit in the narrowest region of the catalytic cleft (Fig. 2*A*). The space surrounding the backbone C^{α} atoms of these Gly and GlyVMe residues is insufficient to accommodate any other side chain, consistent with the selectivity displayed by UCH enzymes for cleaving the amide bond immediately following the terminal Gly-Gly motif of ubiquitin. The UCHL1S18Y-interacting UbVMe residues determined in this study are mostly in agreement with a previous mutational analysis delineating the side chains of ubiquitin required for its recognition by UCHL1 (20). For example, mutation of residues Leu71, Leu73, and Gly76 to Ala on ubiquitin-tryptophan as the substrate significantly reduced the k_{cat}/K_M value by approximately 50-, 100-, and 300-fold, respectively (20).

The so-called active-site cross-over loop is an important structural feature shared uniquely among the members of the UCH family of DUBs (11, 17). This loop has been proposed to play a pivotal role in substrate selection by UCH enzymes (17, 21). The cross-over loop in UCHL1, comprising of residues Gly150 to Lys157 (loop L8, Fig. 1*B*), connects the helix α6 on one lobe and the strand β3 on the other and strings across the active-site cleft (11) forming an arch directly over the catalytic Cys90 (Fig 2*A*). The position and the dimension of this loop in apo UCHL1 are similar to that in UCHL1S18Y–UbVMe complex (Fig S2), with the diameter of the opening enclosed by the loop (the distance measured between the C^{α} atoms of Glu7 and Val154, the pair of atoms with widest separation across the loop) being approximately 9 and 13 Å in the apo and UbVMe-bound forms, respectively. In the complex, the loop appears to have opened up a little to embrace the C terminus of UbVMe. Comparison of the apo and UbVMe-bound structures suggests that the cross-over loop of UCHL1 is relatively rigid, which may serve the function of a stereochemical gate for selecting substrates; only those ubiquitin conjugates whose C-terminal extension at ubiquitin (the P1' portion of the substrate) can thread through the narrow arch of the loop would be accepted (Fig. 2*A*). This inference is consistent with a previous biochemical analysis showing that UCHL1 can preferentially cleave small leaving groups such as amino acids and polypeptides from the C terminus of ubiquitin (10). In contrast, UCHL3 possesses a longer (residues 146–167) and more flexible cross-over loop, which can adopt a wide range of conformational states allowing the enzyme to accept larger extensions at the C terminus of ubiquitin (12). In addition to its apparent role as a stereochemical gate for substrate selection, the cross-over loop also contributes key interactions to the specific recognition of the C-terminal segment of UbVMe. For example, the side chain of Arg74 of UbVMe is engaged in electrostatic interaction with that of Asp155 of the cross-over loop, and, reciprocally, the side chain of Arg153 of the cross-over loop is hydrogen-bonded to the backbone carbonyl of Arg72 of UbVMe (Fig. 2*B*).

Alignment of Active-Site Residues is Induced by Binding of UbVMe. The distal site on UCHL1S18Y is occupied by the two-residue turn segment (Leu8-Thr9) of the N-terminal β-hairpin of ubiquitin, with Leu8 nestled in the surface-exposed hydrophobic pocket lined by Val31, Leu34, Leu51, Phe214, and Ala216 of the enzyme. Comparison of UCHL1S18Y–UbVMe structure with that of UCHL1 in apo form reveals remarkable differences in the position of the side-chain rings of three residues: Phe214, Phe53, and the general base His161 (Fig. 3*A*). In the apo form of the enzyme, the aromatic ring of Phe214 is solvent-exposed, facing away from the inner core of the protein (Fig. 2*A Inset*). Binding of ubiquitin pushes this ring, causing it to swing inward 7.1 Å (Cζ-Cζ distance) away from its position in the apo form of the enzyme. The displaced ring of Phe214, in turn, causes the aromatic ring of Phe53 to swivel away by 7.8 Å (Cζ-Cζ distance) relative to its unbound position to avoid steric overlap. The aromatic ring of Phe53 is now too close to His161, which, in order to accommodate the Phe53 ring, moves into the free space in the vicinity of Cys90 reorienting itself such that the Nδ1 atom of the imidazole ring faces the Sγ atom of Cys90 with a distance of 3.9 Å between the two. Consequently, the enzyme adopts a catalytically competent, papain-like arrangement of the catalytic triad (Fig. 3*B*). The possibility that the change in the environment surrounding Cys90, brought about by its reaction with the VMe group, might have attracted His161 to its proximity causing the observed rearrangement cannot be ignored. This possibility could be addressed in the future by cocrystallizing UCHL1 with a short vinyl methyl ester such as Gly-VMe.

In addition to the UCHL1S18Y–UbVMe complex, we have also solved the structures of the wild-type UCHL1–UbVMe

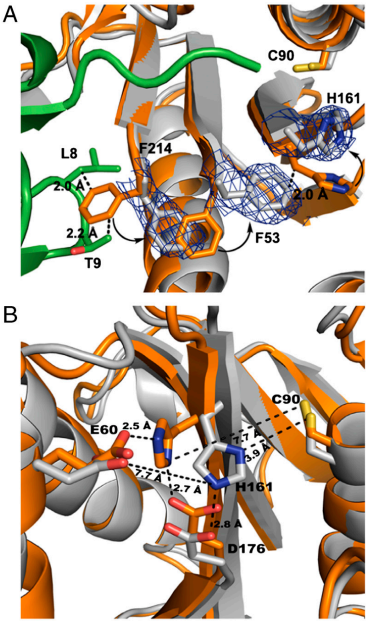

Fig. 3. Binding of ubiquitin induces a conformational relay leading to the alignment of the catalytic triad. (*A*) Conformational changes of three side-chain rings of UCHL1S18Y induced by UbVMe binding. Superposition of apo UCHL1 (*Orange*) and UCHL1S18Y in UbVMe-bound form (*Gray*) showing the relative positions of Phe214, Phe53, His161, and Cys90. Electron density (contoured at 1.0σ) is shown as blue line. UbVMe is shown in green (without the VMe portion). For clarity, the following segments were removed: residues 31–39, 54–57, 147–160, and 207–212 of UCHL1S18Y and apo UCHL1. (*B*) Comparison of the active-site triad of UCHL1S18Y in UbVMe-bound form with that of apo UCHL1. Oxygen atoms are shown in red, nitrogen atoms in blue, sulfur in yellow, and carbon in gray (UCHL1S18Y bound) and orange (apo UCHL1).

(2.85 Å) and UCHL1I93M–UbVMe (2.80 Å). Comparison of structures of these complexes with their respective apo enzymes reveals that the relative movement of Phe214, Phe53, and His161 upon UbVMe binding is a common feature in all the UCHL1 variants studied (Fig. 4). To corroborate the crystallographic observations, we sought to carry out mutational analysis by substituting Phe214 with alanine (the F214A mutant). As shown in Fig. 5, the activity of the F214A mutant in ubiquitin aminomethyl coumarin (UbAMC) hydrolysis assay is significantly reduced relative to the wild-type UCHL1. This difference in the catalytic activity of the F214A mutant relative to the wild-type enzyme is not because of the difference in structures of these proteins; the overall three-dimensional structure of the F214A mutant is nearly identical to that of the wild type as judged by inspection of the far-UV circular dichroism spectra (Fig. S3).

The loss of activity observed upon mutation of Phe214 could be attributed to the impairment of the concerted movements of phenylalanine residues or the disruption of binding at the distal site. To explore this further, we performed isothermal titration calorimetry (ITC) to estimate the binding affinity of ubiquitin toward the wild-type UCHL1 and the F214A mutant (Fig. 6 and Table S2). Analysis of the ITC data showed that UCHL1 binds ubiquitin with a dissociation constant (K_d) of 385 nM, whereas the F214A mutant binds with approximately 60-fold less affinity ($K_d = 22$ μM). This reduced affinity for ubiquitin displayed by the F214A mutant suggests that Phe214 is essential for distal-site substrate binding, and the loss of catalytic activity of the mutant may reflect its reduced affinity toward the substrate. This observation corresponds to the previous biochemical analysis by Luchansky et al. demonstrating that Leu8 of ubiquitin is critically required for its interaction with UCHL1 (20).

Discussion

UCHL1 is a neuron-specific DUB that has been linked to neurodegenerative diseases and cancer. In particular, the two point mutations I93M and S18Y have been linked to the early onset of and protection from PD, respectively (4–6). Yet the normal function of UCHL1 and how the activity of this cysteine protease is regulated remain elusive. The crystal structure of UCHL1 in apo form revealed that the active-site triad is misaligned for catalysis. In traditional cysteine proteases, the nucleophilicity of the catalytic cysteine is enhanced by the abstraction of the proton from the thiol group by a proximal histidine, the general base catalytic residue (22). Such a relationship between the nucleophilic cysteine and the general base histidine would require them to

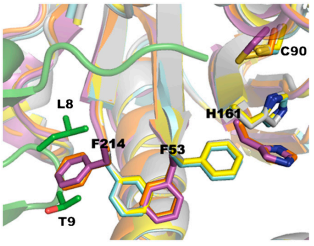

Fig. 4. Concerted movement of Phe214, Phe53, and His161 side chains relative to the apo form is also observed in the crystal structures of the wild-type UCHL1 and its PD-associated variant I93M bound to UbVMe. Superposition of the structures of apo UCHL1 (*Orange*), UCHL1-UbVMe (*Yellow*), apo UCHL1I93M (*magenta*), and UCHL1I93M-UbVMe (*Cyan*) are shown in ribbon representations. UCHL1S18Y-UbVMe is also shown (*Gray Ribbon*) for comparison. UbVMe from the UCHL1S18Y complex is shown in green. For clarity, the following segments were removed from the structures: residues 54–56, 210–213, and 154–160 and the VMe moiety.

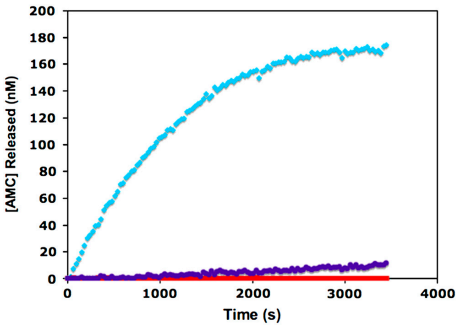

Fig. 5. Comparison of the enzymatic activity of the wild-type UCHL1 and the F214A and C90S mutants. Reaction progress curves showing AMC released vs. time for the cleavage of Ub-AMC by UCHL1 (*Cyan*), UCHL1F214A (*Purple*), and the catalytically inactive mutant UCHL1C90S (*Red*). The substrate and enzyme concentrations for all reactions were 600 and 3 nM, respectively.

be within ~4 Å of each other, allowing effective hydrogen-bonding interactions (16). In the apo UCHL1 structure, this distance (between Cys90 and His161) is 7.7 Å, far greater than expected for any productive interaction. To understand how this enzyme functions as a cysteine protease, we have crystallized and solved the structures of the wild-type UCHL1 and its two PD-associated variants, UCHL1S18Y and UCHL1I93M, bound to the suicide substrate UbVMe. The structures of these complexes reveal a previously unanticipated feature of the enzyme, a substrate-mediated distal-site effect leading to the transition of the active site of the enzyme from an unproductive to its productive form.

The binding of the suicide substrate reveals two dominant substrate binding sites on the enzyme: the active-site cleft and a distal site 17 Å away from the active site. Intermolecular interactions at the active-site cleft ensure that the scissile peptide bond is positioned appropriately relative to the catalytic cysteine. The

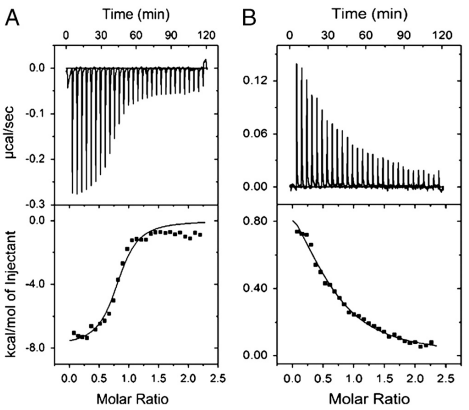

Fig. 6. Binding isotherm of the titration of UCHL1 and UCHL1F214A with ubiquitin. (*A*) Binding of ubiquitin (100 μM) to UCHL1 (10 μM). (*B*) Binding of ubiquitin (576 μM) to UCHL1F214A (56 μM). The top panel for each figure shows the raw data, and the lower panel shows the integrated heat data as enthalpy as a function of molar ratio of ligand to protein. The solid line in the bottom panel represents the best curve fit to the data by using a one-site binding model.

active-site cross-over loop may help select the appropriate substrate—a yet to be identified ubiquitinated species with small-molecule or short/unfolded polypeptide as the C-terminal extension of ubiquitin. However, no useful chemistry can occur without the presence of the general base histidine, properly oriented, in the proximity of the catalytic thiol and the scissile peptide bond. The task of aligning the general base relative to the reactive moieties appears to be left to the interactions at the distal site. A conformational relay, presumably starting at a surface-exposed phenylalanine in the distal site, is triggered by the binding of the N-terminal β-hairpin of ubiquitin resulting in the placement of the active-site histidine in the correct location.

Ligand-dependent alignment of an active-site Cys-His pair has been observed previously in the case of two cysteine proteases: USP7, a DUB in the USP family (18), and μ-calpain, a calcium-activated cysteine protease (19). USP7 is a much larger protein with a very different binding site for ubiquitin. Crystal structures of USP7 in free and ubiquitin-aldehyde (Ubal)-bound form revealed that the C-terminal segment of Ubal induces significant backbone conformational changes in the vicinity of the active site leading to alignment of the catalytic triad (18). In μ-calpain, calcium binding changes the relative orientation of the two domains of the protease leading to the alignment of active-site residues (19). In contrast, ubiquitin-induced conformational changes in UCHL1 appear to originate at a distal site and involve swiveling motion of the side-chain rings of three residues that work in a concerted manner to avoid steric clash, with relatively little backbone reorganization, consistent with the observation that the UCHL1 backbone is extensively knotted (23).

The pair of phenylalanine residues (Phe53 and Phe214) involved in the active-site alignment in UCHL1 is highly conserved in different vertebrates (Fig. S4) as well as in other UCHs (Fig. S5). Although the general mode of ubiquitin binding observed in the UCHL1–UbVMe complex, including the interactions involving ubiquitin's Leu8-Thr9 at the distal site, is very similar to that seen in UCHL3–UbVMe (12) and Yuh1–Ubal complexes (17), the concerted movement of phenylalanines leading to active-site alignment is observed only in the case of UCHL1. Comparison of the structures of UCHL3 in apo (16) and UbVMe-bound form (12) reveals that the orientation and the position of the side-chain rings of the phenylalanine pair and the general base histidine are nearly identical in both forms, overlapping with those observed in the UbVMe-bound form of UCHL1 (Fig. S6). This observation suggests that there is no distal-site conformational relay in UCHL3, consistent with a preorganized active-site triad in this enzyme (16). Considering that UCHL1 and UCHL3 share a high level of sequence and structural similarity and their ubiquitin-binding interfaces are nearly identical (this study and ref. 12), the difference in the way they are regulated is remarkable. Although the biological relevance of this is unclear at the moment, this difference may translate into a different function and could explain their distinct tissue specificity (unlike UCHL1, UCHL3 is expressed ubiquitously in all tissues) (3, 24).

Compared to other UCHs such as UCHL3, whose active-site triad is prearranged in a catalytically productive conformation, UCHL1's active site is misaligned. Therefore, ubiquitin-mediated activation of UCHL1 appears to be necessary for the catalytic activity of this enzyme. The structural studies presented herein provide a mechanism to this end. However, whether this confers an advantage to UCHL1 over the selective mechanism of other ubiquitin hydrolases needs to be investigated in the future.

UCHL1 is abundantly expressed in neurons and has been known to undergo several types of posttranslational modification, such as farnesylation and monoubiquitination, that may regulate its localization and enzymatic activity (25, 26). Our crystallographic results suggest that the activity of UCHL1 is intrinsically regulated by its own substrate and provide a structural basis for the enzyme's specificity for ubiquitin. Interestingly, these studies also indicate that the PD-associated mutants of UCHL1 (I93M and S18Y), like the wild-type enzyme, can adopt productive catalytic triads when bound to ubiquitin. The biochemical basis of how these mutations are linked to PD is yet to be elucidated. By showing that the mutants can have a similar productive triad, and hence similar catalytic properties as the wild type, this study raises an intriguing question as to what could then be the difference between the mutants and the wild-type protein.

The true in vivo function of UCHL1 remains unclear. Although it was proposed to be a deubiquitinating enzyme, primarily because of its sequence similarity with UCHL3, a widely accepted deubiquitinating enzyme, several lines of evidence suggest that UCHL1 may have other alternative functions. For example, a dimerization-dependent ligase activity was previously proposed for UCHL1 (27). More recently, a report suggests that UCHL1 can inhibit microtubule formation in a ubiquitination-dependent manner. The authors of this report suggest that UCHL1 may increase ubiquitination (and hence behave as a ligase) of microtubule components (28). In light of these studies, and others that indicate that UCHL1 may have functions independent of the ubiquitin-proteasome system (29, 30) and the misaligned active site observed in the structure of the apo form of the protein, the demonstration that UCHL1 can adopt a productive conformation as a hydrolase when bound to ubiquitin assumes particular significance.

Although UCHL1 is normally expressed in the brain, abnormal overexpression of this enzyme has been found in many forms of cancer, including lung and colorectal cancer (8, 9). Identification of high-affinity small-molecule inhibitors as pharmacological agents is highly desirable to elucidate the pathophysiological roles of UCHL1. The crystallographic studies along with the mutational data presented here suggest that the perturbation of enzyme–substrate interactions at the distal site of UCHL1 could be detrimental to its enzymatic activity. Targeting the distal site with small-molecule binders that can perturb these interactions could be envisioned as an attractive strategy for UCHL1 inhibition.

Experimental Procedures

Cloning, Expression, and Purification. UCHL1S18Y was subcloned from a pcDNA-UCHL1S18Y vector into a pGex-6P-1 vector (GE Biosciences) by using standard cloning protocols. The resulting N-terminally fused glutathione S-transferase (GST)-tagged UCHL1S18Y protein was expressed in *Escherichia coli* Rosetta cells (Novagen) and purified with a glutathione-Sepharose column (GE Biosciences) following manufacturer's instructions. For expression and purification of other variants of UCHL1 described in this paper, please see *SI Methods*.

The UCHL1S18Y–UbVMe complex was prepared according to the method described by Misaghi et al. with slight modifications (12). In brief, 1 M excess of UbVMe solution (pH adjusted to 8.0 by adding 1 M $NaHCO_3$) was added to the UCHL1S18Y protein solution (in 50 mM Tris.HCl, 150 mM NaCl, pH 7.4). The mixture was incubated for 5 h at room temperature. The formation of the complex was verified by an 8-kDa shift of the UCHL1 protein band in an SDS-PAGE gel. The UCHL1S18Y–UbVMe complex was purified by size exclusion chromatography with a Superdex S75 column (GE Biosciences). UbVMe used in the preparation of the complex was obtained by intein-mediated semisynthesis using a previously published procedure (31, 32).

Crystallization and Structure Determination. The UCHL1S18Y–UbVMe complex was concentrated to ~25 mg/mL in a solution of 50 mM Tris.HCl (pH 7.4), 150 mM NaCl, and 10 mM DTT. Crystals were grown at room temperature by the hanging drop vapor diffusion method from a solution that contained 2.4 M ammonium sulfate and 0.1 M bicine (pH 9.0). Crystals grew

over 2 months to a final dimension of approximately 200 × 200× 100 μm. Crystals were briefly soaked in the cryoprotectant solution (2.9 M sodium malonate, pH 7.5) and plunged into liquid nitrogen for flash cooling. X-ray diffraction data (up to 2.4 Å) were collected at 100 K on a Mar300 CCD detector (Mar USA) at the beam line 23-ID-D at the Advanced Photon Source of Argonne National Laboratory. The data were processed with the program HKL2000 (33). The crystals belong to the space group R32, with unit cell dimensions $a = 87.3$ Å, $b = 87.3$ Å, $c = 193.5$ Å, $\alpha = 90.0°$, $\beta = 90.0°$, and $\gamma = 120.0°$, with one UCHL1S18Y–UbVMe complex per asymmetric unit.

The structure was determined by molecular replacement employing Molrep (34) using the wild-type UCHL1 and human ubiquitin (residues 1–75) as search models. Cross-rotation and translational searches identified a single copy of the complex in the asymmetric unit. Rigid-body refinement of this model followed by restrained refinement brought the crystallographic R factor to 31.7% and R_{free} to 40.5%. The electron density map at this stage showed clear density corresponding to the side chain of Tyr at position 18 on UCHL1S18Y and the VMe part of UbVMe. Subsequent refinement was performed with Refmac (13) and model building with Coot (14). The final crystallographic R factor (R_{cryst}) and R_{free} are 20.9% and 25.6%, respectively (Table S1). The model contains the complete 223-residue UCHL1S18Y chain, 1–75 residues of ubiquitin, the GlyVMe moiety (modeled as 4-amino methyl butanoate), and 51 ordered solvent molecules. More than 98% of the nonglycine residues are placed within the most favorable and additionally allowed areas of Ramachandran plot, and less than 0.5% are located in the disallowed areas, as defined within the program PROCHECK (15). The first five N-terminal residues carried over from the GST-tagged cloning vector were disordered and, therefore, were not included in the model. Graphical analysis was done with the program PYMOL (DeLano Scientific).

Enzymatic Activity Assay. Stock solutions of wild-type UCHL1 and the F214A and C90S mutants were diluted into the reaction buffer (50 mM Tris.HCl, pH 7.4, 1 mM DTT, and 1 mM EDTA) in individual wells of a 96-well plate to the final concentration of 3 nM. UbAMC was added to these wells to yield a final concentration of 600 nM to initiate the enzymatic reaction. The rate of AMC cleavage was monitored at 25 °C by a TECAN Genios microplate spectrofluorometer with excitation at 380 nm and emission at 465 nm.

ITC. ITC was carried out by using a VP-ITC Microcal calorimeter (MicroCal) at 24 °C. Ubiquitin from bovine erythrocytes was purchased from Sigma-Aldrich. Amino acid sequences between human and bovine ubiquitin are identical. Samples of UCHL1, UCHL1F214A, and ubiquitin were extensively dialyzed against the buffer 50 mM Tris-HCl, pH 7.6 (buffer A) and then degassed to remove dissolved air. Titrations consisted of 10-μL injections of ubiquitin into the sample cell containing the protein, at time intervals of 4 min to ensure each peak returned to baseline. Each UCHL1 sample was followed by a background titration of an equal volume of ubiquitin being titrated into a sample cell containing buffer A to account for the heat of dilution, which was subtracted from the UCHL1–ubiquitin data. All data were analyzed by using the program Origin, version 7.0, included with the system. The data were fitted with a one-site binding model (one molecule of ubiquitin binding to one molecule of UCHL1). Binding constants and thermodynamic parameters are given in Table S2.

ACKNOWLEDGMENTS. The authors acknowledge Venugopalan Nagarajan and Michael Becker at beam line 23-ID-D of Advanced Photon Source for assistance with data collection. We thank Dr. Mini Thomas for the critical reading of the manuscript. The General Medicine and Cancer Institutes Collaborative Access Team has been funded in whole or in part with Federal funds from the National Cancer Institute (Y1-CO-1020) and the National Institute of General Medical Science (Y1-GM-1104). Use of the Advanced Photon Source was supported by the U.S. Department of Energy, Basic Energy Sciences, Office of Science, under Contract DE-AC02-06CH11357. Financial support by a Showalter grant and Purdue University (C.D.) is gratefully acknowledged.

1. Doran JF, Jackson P, Kynoch PA, Thompson RJ (1983) Isolation of PGP 9.5, a new human neurone-specific protein detected by high-resolution two-dimensional electrophoresis. *J Neurochem* 40:1542–1547.
2. Wilkinson KD, et al. (1989) The neuron-specific protein PGP 9.5 is a ubiquitin carboxyl-terminal hydrolase. *Science* 246:670–673.
3. Saigoh K, et al. (1999) Intragenic deletion in the gene encoding ubiquitin carboxy-terminal hydrolase in gad mice. *Nat Genet* 23:47–51.
4. Leroy E, et al. (1998) The ubiquitin pathway in Parkinson's disease. *Nature* 395:451–452.
5. Maraganore DM, et al. (1999) Case-control study of the ubiquitin carboxy-terminal hydrolase L1 gene in Parkinson's disease. *Neurology* 53:1858–1860.
6. Maraganore DM, et al. (2004) UCHL1 is a Parkinson's disease susceptibility gene. *Ann Neurol* 55:512–521.
7. Xue S, Jia J (2006) Genetic association between ubiquitin carboxy-terminal hydrolase-L1 gene S18Y polymorphism and sporadic Alzheimer's disease in a Chinese Han population. *Brain Res* 1087:28–32.
8. Hibi K, et al. (1998) Serial analysis of gene expression in non-small cell lung cancer. *Cancer Res* 58:5690–5694.
9. Yamazaki T, et al. (2002) PGP9.5 as a marker for invasive colorectal cancer. *Clin Cancer Res* 8:192–195.
10. Larsen CN, Krantz BA, Wilkinson KD (1998) Substrate specificity of deubiquitinating enzymes: Ubiquitin C-terminal hydrolases. *Biochemistry* 37:3358–3368.
11. Das C, et al. (2006) Structural basis for conformational plasticity of the Parkinson's disease-associated ubiquitin hydrolase UCH-L1. *Proc Natl Acad Sci USA* 103:4675–4680.
12. Misaghi S, et al. (2005) Structure of the ubiquitin hydrolase UCH-L3 complexed with a suicide substrate. *J Biol Chem* 280:1512–1520.
13. Murshudov GN, Vagin AA, Dodson EJ (1997) Refinement of macromolecular structures by the maximum-likelihood method. *Acta Crystallogr D* 53:240–255.
14. Emsley P, Lohkamp B, Scott WG, Cowtan K (2010) Features and development of Coot. *Acta Crystallogr D* 66:486–501.
15. Laskowski RA, MacArthur MW, Moss DS, Thornton JM (1993) PROCHECK: A program to check the stereochemical quality of protein structures. *J Appl Crystallogr* 26:283–291.
16. Johnston SC, et al. (1997) Crystal structure of a deubiquitinating enzyme (human UCH-L3) at 1.8 A resolution. *EMBO J* 16:3787–3796.
17. Johnston SC, Riddle SM, Cohen RE, Hill CP (1999) Structural basis for the specificity of ubiquitin C-terminal hydrolases. *EMBO J* 18:3877–3887.
18. Hu M, et al. (2002) Crystal structure of a UBP-family deubiquitinating enzyme in isolation and in complex with ubiquitin aldehyde. *Cell* 111:1041–1054.
19. Moldoveanu T, et al. (2002) A Ca(2+) switch aligns the active site of calpain. *Cell* 108:649–660.
20. Luchansky SJ, Lansbury PT, Jr, Stein RL (2006) Substrate recognition and catalysis by UCH-L1. *Biochemistry* 45:14717–14725.
21. Popp MW, Artavanis-Tsakonas K, Ploegh HL (2009) Substrate filtering by the active site crossover loop in UCHL3 revealed by sortagging and gain-of-function mutations. *J Biol Chem* 284:3593–3602.
22. Storer AC, Menard R (1994) Catalytic mechanism in papain family of cysteine peptidases. *Methods Enzymol* 244:486–500.
23. Virnau P, Mirny LA, Kardar M (2006) Intricate knots in proteins: Function and evolution. *PLoS Comput Biol* 2:e122.
24. Kurihara LJ, Semenova E, Levorse JM, Tilghman SM (2000) Expression and functional analysis of Uch-L3 during mouse development. *Mol Cell Biol* 20:2498–2504.
25. Liu Z, et al. (2009) Membrane-associated farnesylated UCH-L1 promotes alpha-synuclein neurotoxicity and is a therapeutic target for Parkinson's disease. *Proc Natl Acad Sci USA* 106:4635–4640.
26. Meray RK, Lansbury PT, Jr (2007) Reversible monoubiquitination regulates the Parkinson disease-associated ubiquitin hydrolase UCH-L1. *J Biol Chem* 282:10567–10575.
27. Liu Y, et al. (2002) The UCH-L1 gene encodes two opposing enzymatic activities that affect alpha-synuclein degradation and Parkinson's disease susceptibility. *Cell* 111:209–218.
28. Bheda A, et al. (2010) Ubiquitin editing enzyme UCH L1 and microtubule dynamics: Implication in mitosis. *Cell Cycle* 9:980–994.
29. Walters BJ, et al. (2008) Differential effects of Usp14 and Uch-L1 on the ubiquitin proteasome system and synaptic activity. *Mol Cell Neurosci* 39:539–548.
30. Kyratzi E, Pavlaki M, Stefanis L (2008) The S18Y polymorphic variant of UCH-L1 confers an antioxidant function to neuronal cells. *Hum Mol Genet* 17:2160–2171.
31. Borodovsky A, et al. (2001) A novel active site-directed probe specific for deubiquitylating enzymes reveals proteasome association of USP14. *EMBO J* 20:5187–5196.
32. Borodovsky A, et al. (2002) Chemistry-based functional proteomics reveals novel members of the deubiquitinating enzyme family. *Chem Biol* 9:1149–1159.
33. Otwinowski Z, Minor W () *Methods in Enzymology*, eds CW Carter Jr and RM Sweet Jr (Academic, New York), Vol 276, pp 307–326.
34. Vagin A, Teplyakov A (1997) MOLREP: An automated program for molecular replacement. *J Appl Crystallogr* 30:1022–1025.

doi:10.1016/j.jmb.2011.08.029 J. Mol. Biol. (2011) 413, 416–429

Contents lists available at www.sciencedirect.com

Journal of Molecular Biology

journal homepage: http://ees.elsevier.com.jmb

Structural and Thermodynamic Comparison of the Catalytic Domain of AMSH and AMSH-LP: Nearly Identical Fold but Different Stability

Christopher W. Davies [1], Lake N. Paul [2], Myung-Il Kim [1] and Chittaranjan Das [1]*

[1]*Brown Laboratory of Chemistry, Department of Chemistry, Purdue University, 560 Oval Drive, West Lafayette, IN 47907, USA*
[2]*Bindley Biosciences Center, Discovery Park, Purdue University, West Lafayette, IN 47907, USA*

Received 2 June 2011;
received in revised form
8 August 2011;
accepted 12 August 2011
Available online
24 August 2011

Edited by I. Wilson

Keywords:
endosomal deubiquitinase;
Lys63-linked polyubiquitin-chain-specific deubiquitinase;
JAMM domain deubiquitinase;
metalloprotease;
conformational plasticity

AMSH plays a critical role in the ESCRT (*e*ndosomal *s*orting *c*omplexes *r*equired for *t*ransport) machinery, which facilitates the down-regulation and degradation of cell-surface receptors. It displays a high level of specificity toward cleavage of Lys63-linked polyubiquitin chains, the structural basis of which has been understood recently through the crystal structure of a highly related, but ESCRT-independent, protein AMSH-LP (*AMSH-l*ike *p*rotein). We have determined the X-ray structure of two constructs representing the catalytic domain of AMSH: AMSH244, the JAMM (*JAB1/MPN/MOV34*)-domain-containing polypeptide segment from residues 244 to 424, and AMSH219^{E280A}, an active-site mutant, Glu280 to Ala, of the segment from 219 to 424. In addition to confirming the expected zinc coordination in the protein, the structures reveal that the catalytic domains of AMSH and AMSH-LP are nearly identical; however, guanidine-hydrochloride-induced unfolding studies show that the catalytic domain of AMSH is thermodynamically less stable than that of AMSH-LP, indicating that the former is perhaps structurally more plastic. Much to our surprise, in the AMSH219^{E280A} structure, the catalytic zinc was still held in place, by the compensatory effect of an aspartate from a nearby loop moving into a position where it could coordinate with the zinc, once again suggesting the plasticity of AMSH. Additionally, a model of AMSH244 bound to Lys63-linked diubiquitin reveals a type of interface for the distal ubiquitin significantly different from that seen in AMSH-LP. Altogether, we believe that our data provide important insight into the structural difference between the two proteins that may translate into the difference in their biological function.

*Corresponding author. E-mail address: cdas@purdue.edu.

Abbreviations used: DUB, deubiquitinating enzyme; EGFR, epidermal growth factor receptor; GdHCl, guanidine hydrochloride; AUC, analytical ultracentrifugation; MR, molecular replacement; PDB, Protein Data Bank; GST, glutathione *S*-transferase; SEC, size-exclusion chromatography; PEG, polyethylene glycol.

Introduction

AMSH, associated molecule with the *SH3* (*S*rc *h*omology *3*) domain of STAM (*s*ignal *t*ransducing *a*daptor *m*olecule), is a member of the JAMM (*JAB1/MPN/MOV34*) family of deubiquitinating enzymes (DUBs),[1] which catalyze the hydrolysis of isopeptide or peptide bonds between ubiquitin and target

proteins or between monomers in polymeric chains of ubiquitin. The JAMM family, one of the five classes of DUBs, is composed of metalloproteases, the others being cysteine proteases.[2–5] These metalloproteases, although having very different sequences compared to the quintessential metalloprotease thermolysin, are generally thought to share similar features in their active site and, hence, mechanism with thermolysin. They have a Zn^{2+} in their active site coordinated by two histidines, an aspartate or a glutamate and a water molecule, which, in addition to the metal ion, is held in its place by hydrogen bonding with a different glutamate residue. This water plays two critical roles: (1) it acts as the nucleophile during the hydrolysis of the peptide bond, and (2) in addition to the other coordinating side chains, it stabilizes the bound Zn^{2+}, which is responsible for polarizing the carbonyl group of the scissile peptide bond. However, of the 14 JAMM proteins in the human genome, only 7 contain a complete set of conserved residues needed for Zn^{2+} coordination,[2] 6 of which, AMSH, AMSH-LP (*AMSH-l*ike *p*rotein), BRCC36, RPN11 (POH1), MYSM1 and CSN5, have been shown to exhibit isopeptidase activity toward ubiquitin or ubiquitin-like proteins.[2,6,7]

AMSH is one of the two DUBs, the other being the cysteine protease DUB UBPY (also known as ubiquitin-specific protease 8),[8] known to be involved in receptor down-regulation and turnover mediated by the ESCRT (*e*ndosomal *s*orting *c*omplexes *r*equired for *t*ransport) machinery.[9] The ESCRT machinery, composed of four distinct macromolecular assemblies, ESCRT-0, ESCRT-I, ESCRT-II and ESCRT-III, drives the internalization of ubiquitinated cell-surface receptors,[10] which are shuttled from one ESCRT member to the next (e.g., from ESCRT-0 to ESCRT-I, from ESCRT-I to ESCRT-II and so on) until they are finally degraded by the lysosome or recycled back to the membrane.[11] The initial (ESCRT-0) and the final (ESCRT-III) complexes are the two recognition points for both AMSH and UBPY. ESCRT-0 recruits the DUBs through the SH3 domain of STAM binding to the PX(V/I)(D/N)RXXKP (X is any amino acid) motif present on both DUBs, whereas ESCRT-III recruitment is facilitated by the MIT (*mi*crotubule *i*nteracting and *t*ransport) domain of the DUBs binding to CHMPs (*c*hromatin *m*odifying *p*roteins) of ESCRT-III.[9] The ability of DUBs to deubiquitinate endocytosed receptors at various points in the process, either before or after sequestration of the receptors into multivesicular bodies, may have a role in altering receptor trafficking, regulating their turnover rate.[12]

The exact function of AMSH within the ESCRT machinery is still poorly understood. Studies have shown that AMSH has a role in the regulation of several receptors including epidermal growth factor receptor (EGFR), calcium-sensing receptor, δ-opioid receptor, protease-activated receptor and the chemokine receptor CXCR4.[13–20] Studies have also shown that AMSH serves to regulate endosomal trafficking by counteracting the ubiquitination of ESCRT-0 proteins themselves.[12] Not only does AMSH have a role in endocytosis of receptors, AMSH also plays a role in mitosis and cytokinesis.[21–24] During mitosis, AMSH deubiquitinates v-SNARE and VAMP8 in an ESCRT-dependent manner while also being present in the early phases of cytokinesis, both implicating a potential role of AMSH as a regulator of proliferation and survival.[21–23]

Even though AMSH has no clearly defined role to date, it is well characterized that AMSH has specificity toward Lys63-linked polymeric chains of ubiquitin, which have previously been shown to be the minimal requirement for directing receptors toward lysosomal degradation (in some cases, monoubiquitination instead of polyubiquitination is used as a signal for lysosomal degradation).[13] The structural basis for Lys63-linked polyubiquitin chain cleavage has been elucidated with the crystal structure determination of the DUB (JAMM) domain of AMSH-LP.[25] AMSH and AMSH-LP share 54% identity and 75% sequence similarity in their JAMM domain.[9,25] It is known that both proteins act as regulators of free ubiquitin in the cell, bind clathrin, contain a putative nuclear localization signal and an MIT domain.[9,26,27] Although perceived as functionally redundant, AMSH-LP lacks several key features when compared to AMSH. AMSH contains an SH3-binding motif, which facilitates interaction with STAM of ESCRT-0, while a functional SH3-binding motif is lost in AMSH-LP from primates but present in chicken, cow, dog, frog, mouse and snake.[9,26,27] AMSH's MIT domain interacts with specific ESCRT-III proteins, CHMPs, while it was shown that none of the CHMP proteins interacted with AMSH-LP, suggesting a highly specific interaction with AMSH.[28] In addition to these differences, it is possible that the biological difference between the two proteins may lie also in their catalytic domain, presumed to be very similar based on the similarity of primary structure.

The present study aims at providing a structural and thermodynamic comparison between the catalytic domains of AMSH and AMSH-LP. We have determined the X-ray crystal structures of two constructs representing the catalytic domain of AMSH: AMSH244-424, the JAMM-domain-containing polypeptide segment from residues 244 to 424 (hereafter referred to simply as AMSH244), and $AMSH219^{E280A}$, an active-site mutant, Glu280 to Ala, of the segment 219–424, which, in addition to the JAMM domain, also features the SH3-domain-binding motif at its N-terminus. We see that while the overall folds of the two proteins are nearly identical, as expected, the catalytic domain of AMSH is thermodynamically less stable than that of AMSH-

LP under guanidine hydrochloride (GdHCl)-induced unfolding, based on which we propose that the catalytic domain of AMSH is structurally more plastic than the latter, a property that may endow specific advantage to AMSH, enabling it to adapt to a variety of working environments within the context of ESCRT machinery.

Results

Structure of the catalytic domain of AMSH

AMSH244 crystallized in the *C*2 space group, with seven monomers in the asymmetric unit (Supplementary Fig. 1). The structure was solved by molecular replacement (MR) with the catalytic domain of AMSH-LP as the search model.[25] The MR search identified a model with seven subunits in the asymmetric unit. Rigid body followed by restrained refinement of this model yielded a crystallographic *R*-factor (R_{crys}) and a free *R*-factor (R_{free}) of 25.4% and 34.8%, respectively. Electron density map at this stage was interpretable and showed clear density for the two zinc ions where they should be located, indicating that the MR search was successful. Refinement using PHENIX[29] after rounds of model building yielded a final R_{crys} and R_{free} of 19.3% and 22.9%, respectively (Table 1). The structure of the polypeptide in different subunits is nearly identical except for the N-terminal residues, Asn244 to Asp252, which were ordered to a different extent in different subunits.

The observation of seven monomers in the asymmetric unit prompted us to investigate the oligomeric state of the catalytic domain of AMSH in solution. AMSH244 was subjected to analytical ultracentrifugation (AUC) experiments, along with the catalytic domain of AMSH-LP for comparison. The AUC data indicate that, in solution, the catalytic domains of both AMSH and AMSH-LP exist as predominantly globular, monomeric proteins with sedimentation coefficient (s_{20}) values of 2.1 and 2.03, respectively (Fig. 1). However, these data do not rule out the possibility that the full-length protein can exist as a multimer in solution, through self-association of the part missing in our construct.

Like the DUB domain of AMSH-LP, the structure of AMSH244 consists of the JAMM core with two characteristic insertions, insertion 1 (Ins-1, residues 302–327) and insertion 2 (Ins-2, residues 381–403). The JAMM core comprises a mixed β-sheet in the shape of a partially unfurled β-barrel sandwiched by two α-helices, one on top (α1) and one on the bottom (α3) (Fig. 2a), a feature found in other JAMM domain proteins, such as *Af*JAMM and Prp8.[30–33] As seen in AMSH-LP, the catalytic site is lined mostly by residues from the JAMM core, from the loop between α1 and β2, α3, β6 and the loop following it (Fig. 2a). Residues from the β-hairpin turn segment in Ins-1 also contribute to the catalytic site. The catalytic zinc is coordinated by His335, His337 (located on β6 and immediately following it), Asp348 (located on α3) and a water molecule that is hydrogen bonded to Glu280 (located on the loop following α1) (Fig. 2b). In addition to these zinc-coordinating residues, the oxyanion-stabilizing side chain from Ser345 (on α3) completes the set of catalytic residues required for peptide bond hydrolysis by a thermolysin-type, mechanistically speaking, zinc metalloprotease.[34,35] We confirmed the presence of a second zinc ion, 14 Å away from the active site, by the presence of strong electron density in the $2F_{obs} - F_{calc}$ map in the area coordinated by the residues His350 from the JAMM core and His396, His398 and Cys390 from Ins-2 (Fig. 2c), the same set of residues that coordinate the second zinc ion in AMSH-LP.[25]

As seen in the structure of the DUB domain of AMSH-LP, the active site of AMSH is in a closed configuration, covered by two side chains, those of an aspartate (Asp309) in Ins-1 and a phenylalanine

Table 1. Crystallographic data and refinement statistics

	AMSH244	AMSH219^{E280A}
Residues	244–424	219–424
Data collection		
Space group	*C*121	$P4_32_12$
Cell dimensions		
a, *b*, *c* (Å)	203.5, 67.4, 113.2	53.4, 53.4, 128.8
α, β, γ (°)	90, 112.4, 90	90, 90, 90
Resolution (Å)	50.0–2.50 (2.59–2.50)	50–1.68 (1.71–1.68)
R_{sym}[a]	8.5 (54.3)	7.1 (60.4)
$I/\sigma I$	12.6 (2.04)	28.3 (3.7)
Unique reflections	48,879	22,375
Completeness (%)	99.5 (97.8)	99.6 (100.0)
Redundancy	3.5 (3.0)	12.1 (12.2)
Refinement		
Resolution	47.2–2.50	33.5–1.67
R_{crys}/R_{free}[b]	19.3/22.9	18.0/20.5
Number of atoms	9560	1398
Number of ions	14	2
rmsd		
Bond lengths (Å)	0.008	0.006
Bond angles (°)	1.4	0.99
Ramachandran plot (%)		
Preferred	96.9	98.9
Allowed	2.7	1.1
Disallowed	0.4	0.0
B-factors (Å^2)		
Protein	61.5	36.2
Solvent	49.9	45.4
Ions	54.9	23.5

Numbers in parentheses are for the high-resolution shell.

[a] $R_{sym} = \sum\sum |I_{hkl} - I_{hkl(j)}| / \sum I_{hkl}$, where $I_{hkl(j)}$ is the observed intensity and I_{hkl} is the final average intensity.

[b] $R_{crys} = \sum ||F_{obs}| - |F_{calc}|| / \sum |F_{obs}|$ and $R_{free} = \sum ||F_{obs}| - |F_{calc}|| / \sum |F_{obs}|$, where R_{free} and R_{crys} are calculated using a randomly selected test set of 5% of the data and all reflections excluding the 5% test data, respectively.

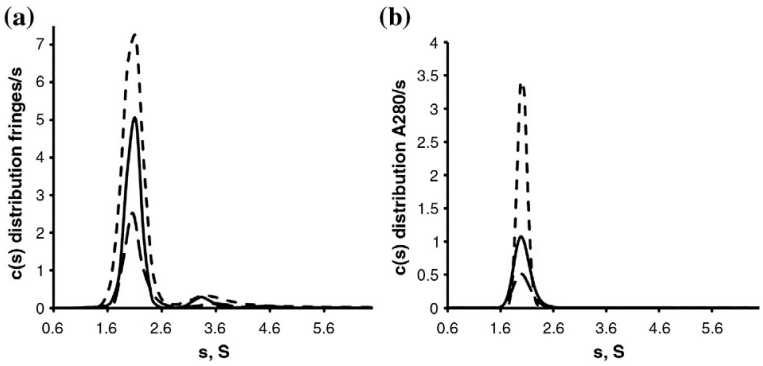

Fig. 1. *c*(*s*) distribution plots of the DUB domains of AMSH244 and AMSH-LP as determined by AUC. (a) *c*(*s*) distribution plot of AMSH244 using interference optics shows that the majority of discrete species at 2.1 S is a globular, monomeric protein. The protein concentrations used were 30 μM (large dashes), 60 μM (continuous line) and 120 μM (small dashes). (b) *c*(*s*) distribution plot of AMSH-LP using absorbance at 280 nm shows that the majority of discrete species at 2.03 S is a globular, monomeric protein. The protein concentrations used were 25 μM (large dashes), 47 μM (continuous line) and 94 μM (small dashes).

(Phe395) in Ins-2, with their van der Waals surfaces touching each other (Fig. 2a). The side chains of these two residues have to move away from each other to let the scissile isopeptide bond on the substrate access the active site, suggesting that there is considerable flexibility either in these side chains or in the polypeptide backbone bearing them. Interestingly, in the structure of AMSH-LP DUB domain bound to Lys63-linked ubiquitin dimer, the corresponding residue pair is still seen in a similar position as the substrate-free form,[25] suggesting that these residues close the active site during catalysis as well, perhaps to help position the scissile peptide bond or stabilize the transition state or both. Both these residues are absolutely conserved in all AMSH sequences analyzed so far (data not shown) and in AMSH-LP as well, suggesting a functional role.

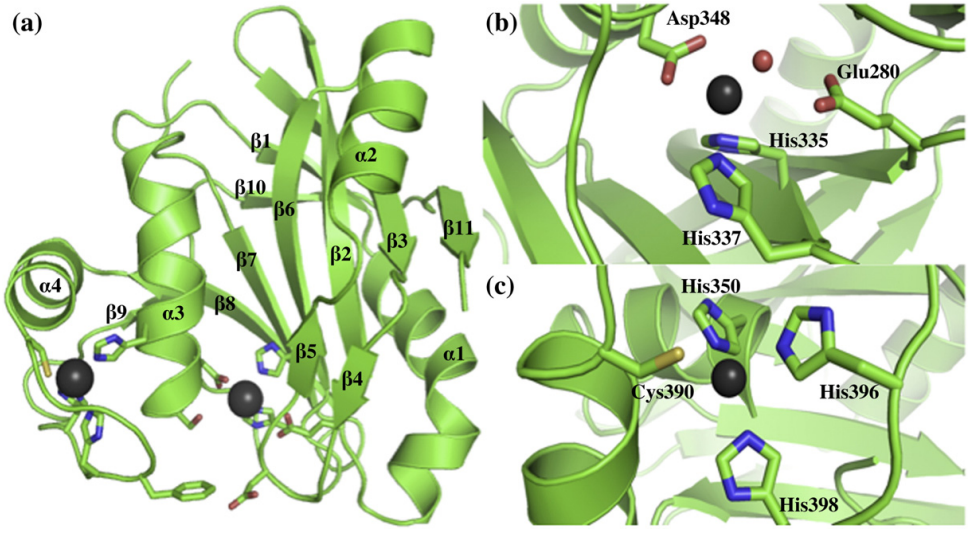

Fig. 2. The structure of the catalytic domain of AMSH. (a) Ribbon representation of the X-ray structure of AMSH244. (b) Expanded view of the active-site zinc coordination. (c) Expanded view of the second zinc coordination site. The coordinating residues are shown as sticks, with carbon shown in green, oxygen shown in red, nitrogen shown in blue and sulfur shown in yellow. Zinc is shown as a gray sphere.

In our efforts to structurally characterize AMSH's recruitment to the ESCRT-0 complex, we generated an N-terminally longer construct of the catalytic domain that has, in addition to AMSH's DUB domain, the peptide sequence that AMSH uses to bind to STAM's SH3 domain.[9] An active-site mutant of this construct, AMSH219^{E280A}, in which Glu280 is mutated to alanine, crystallized in the tetragonal space group $P4_32_12$, with a single molecule in the asymmetric unit, consistent with the monomeric state of AMSH244 found in solution. The structure of this mutant was solved by MR using the structure of AMSH244 as the search probe (Table 1). The overall fold of the two structures is very similar, with a root-mean-square deviation (rmsd) between C^{α} atoms of 0.84 Å. The N-terminal SH3-binding peptide segment was not visualized in the structure perhaps because of disorder in the crystal, suggesting that this peptide segment is flexible and is easily accessible for binding to the SH3 domain of STAM. The catalytic activities of AMSH244 and AMSH219 are similar (Supplementary Fig. 2), suggesting that the SH3-domain-binding peptide segment does not fold onto the catalytic domain, at least not in way to influence diubiquitin binding. We speculate that the flexibility of this segment may allow it to serve as a part of a linker that connects the JAMM domain to the N-terminal portion of the protein. The structure of the mutant does confirm the presence of the E280A mutation; however, clear density in the vicinity of the active-site metal-coordinating residues was still observed, which was interpreted as the density corresponding to a Zn^{2+} (Fig. 3). Thus, despite having lost the catalytic glutamate and consequently the water molecule bound to it, the active-site Zn^{2+} is still present. Further inspection reveals that the side chain of a nearby aspartate, Asp309, has swung by nearly 120° from its position in the wild-type structure, positioning itself such that one of its O^{δ} atoms can coordinate to the zinc, thereby restoring the tetrahedral coordination around it (Fig. 3). As expected, the E280A mutant is still catalytically inactive despite having the zinc in place (Supplementary Fig. 2).

A potential disulfide bond in the catalytic domain of AMSH

The overall structure of AMSH244 and AMSH219^{E280A} is nearly identical; however, further inspection during model building revealed the presence of a potential disulfide bond 7.4 Å away from the catalytic zinc in the latter. Rounds of refinement showed positive density around Cys282 within which we modeled in three alternate conformations, one of which placed this cysteine side chain within disulfide-bonding distance from Cys311 (S^{γ}–S^{γ} distance of 2.0 Å) (Supplementary Fig. 3). The presence of dithiothreitol (DTT) throughout purification and in the crystallization buffer presents a possible reason for the multiple conformations observed in the crystals, preventing the cysteine pair from achieving 100% occupancy in its oxidized form (Supplementary Fig. 3). It is possible that this disulfide may exist in AMSH244 as well, but its observation is precluded because of DTT, whose reducing effect is perhaps more in this construct than in AMSH219^{E280A}. Interestingly, sequence alignment analysis shows that these cysteines are conserved between AMSH and AMSH-LP;[25] however, we do not see the equivalent cysteine pair within disulfide-bonding distance in AMSH-LP (S^{γ}–S^{γ} distance is 4.2 Å in this case). Cys282 is next to the

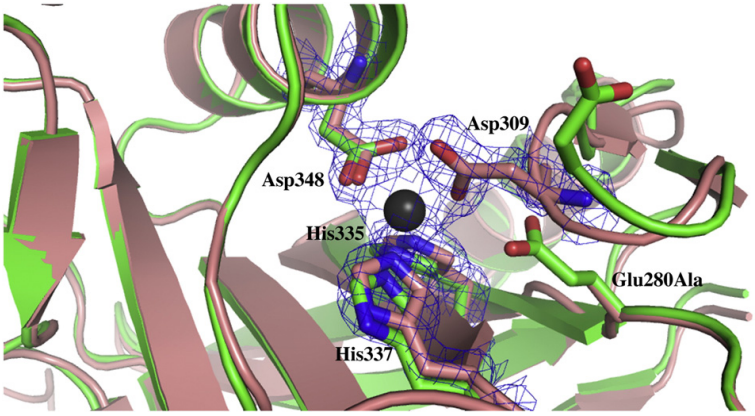

Fig. 3. Superposition of the active sites of AMSH244 and AMSH219^{E280A}. AMSH244 is shown in green, and AMSH219^{E280A}, in pink. The zinc-coordinating residues in AMSH219^{E280A} are outlined in electron density ($2F_{obs}-F_{calc}$) at 1 σ.

active site, and in fact, it makes a van der Waals contact with Leu73 of the distal ubiquitin in the structure of AMSH-LP DUB domain bound to Lys63-linked ubiquitin dimer.[25] In the disulfide orientation, however, as seen in the model of AMSH244 bound to Lys63-linked diubiquitin (please see below), the contact is lost. To probe if the oxidation state of Cys282 is important for the catalytic activity of the enzyme, we created a mutant that would lack the disulfide bond (the Cys282-to-Ala mutant) and prepared the mutant and the wild-type proteins, avoiding DTT all throughout the purification procedure. The catalytic activity of the Cys282Ala mutant is close to the activity seen with the wild-type protein (the mutant retains ~80% of the activity seen with the wild type) (Supplementary Fig. 2).

AMSH diubiquitin recognition

The overall three-dimensional fold of the catalytic domain of AMSH is very similar to that of the previously determined DUB domain of AMSH-LP [Protein Data Bank (PDB) code: 2ZNR[25]] with an rmsd of 1.49 Å of C^{α} atoms as determined by the superposition program SuperPose.[36] The architecture of both the active site and the second zinc-binding site of both the proteins is nearly identical (Fig. 4). To gain insight into how AMSH would recognize Lys63-linked diubiquitin, we generated a model of AMSH244 bound to Lys63-linked ubiquitin dimer by superimposing AMSH244 onto the previously determined X-ray structure of the DUB domain of AMSH-LP^{E292A} bound to Lys63-linked ubiquitin dimer (PDB code: 2ZNV[25]) (Fig. 5). The overall structure of AMSH244 is similar to that of ubiquitin-bound DUB domain of AMSH-LP with an rmsd of 0.93 Å of C^{α} atoms. This level of structural similarity suggests that the mode of diubiquitin binding seen in the model would be preserved in the actual structure of AMSH244 bound to Lys63-linked diubiquitin.

Proximal ubiquitin recognition

The residues that are involved in proximal ubiquitin recognition are completely conserved between AMSH and AMSH-LP (Fig. 6a) (in diubiquitin, a lysine residue of one ubiquitin, called the proximal ubiquitin, is linked by isopeptide bond to the C-terminal carboxylate group of another ubiquitin, called the distal ubiquitin). Fig. 7 shows the superposition of AMSH244 with AMSH-LP's DUB domain, in both its free form and bound to Lys63-linked diubiquitin. The position and orientation of the conserved residues in the proximal site, Phe343, Phe395 and Thr341 of AMSH (Phe355, Phe407 and Thr353 in AMSH-LP) (Fig. 7), which are known to

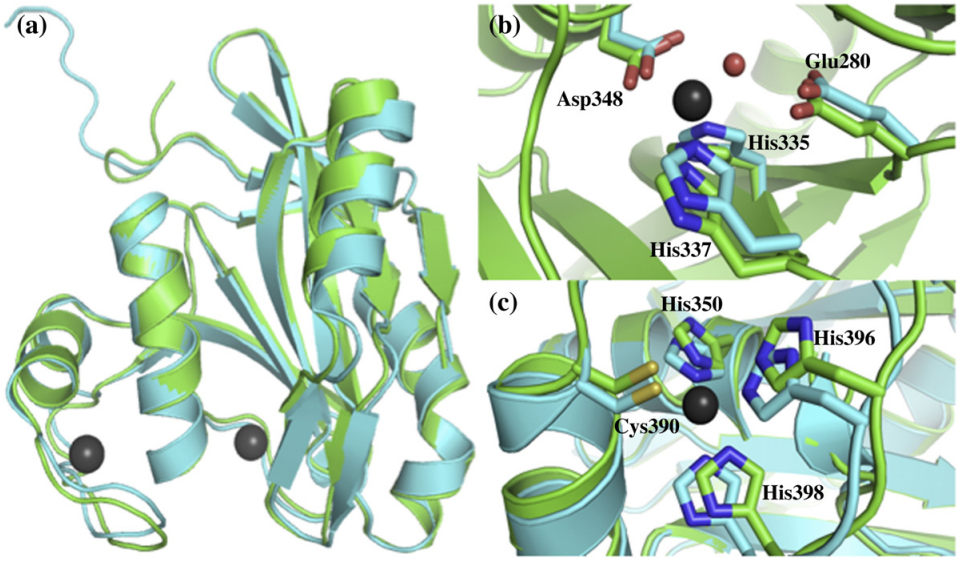

Fig. 4. Structural comparison of the catalytic domains of AMSH and AMSH-LP. (a) Backbone superposition of AMSH (shown in green) and AMSH-LP (shown in cyan). (b) Expanded view of the zinc-coordinating residues in the active site. (c) Expanded view of the residues coordinating the second zinc. The coordinating residues are shown as sticks, with carbon shown in green and cyan, oxygen shown in red, nitrogen shown in blue and sulfur shown in yellow. Zinc is shown as a gray sphere.

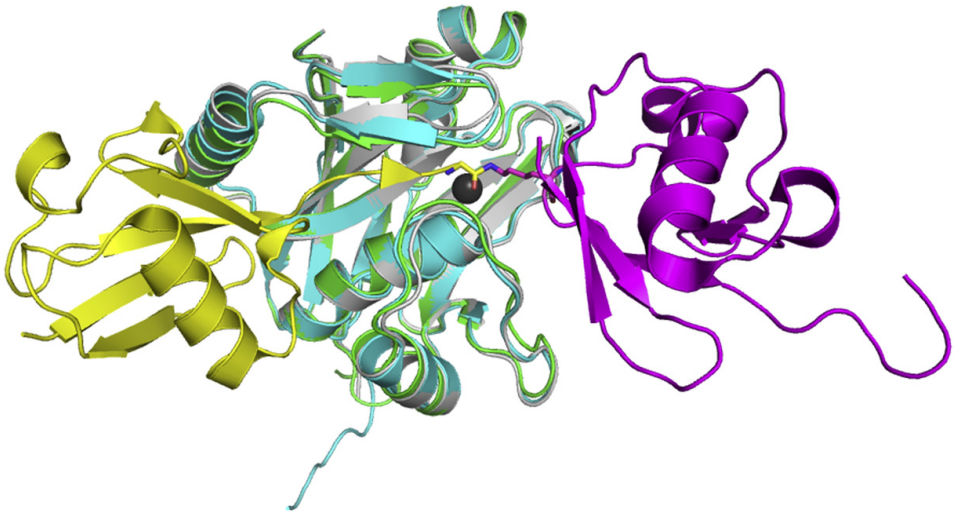

Fig. 5. A model of AMSH244 bound to Lys63-linked ubiquitin dimer. Backbone superposition of AMSH244 (green), the DUB domain of AMSH-LP (cyan) and the DUB domain of AMSH-LP bound to Lys63-linked diubiquitin (gray). The proximal ubiquitin and distal ubiquitin are shown in magenta and yellow ribbon, respectively.

aid in aligning the isopeptide bond and making specific contacts with the two residues flanking Lys63 of proximal ubiquitin, Gln62 and Glu64, are very similar in both the enzymes, consistent with the Lys63-linkage specificity exhibited by both. The only difference seen from the modeling is the orientation of Ser346 (Ser358 in AMSH-LP). The O^{γ} atom of AMSH's Ser346 is pointing away from Glu64 of the proximal ubiquitin (Fig. 7), contrary to the equivalent residue in both free and ubiquitin-bound AMSH-LP, which are at distances of 2.4 Å and 2.6 Å from proximal ubiquitin's Glu64, respectively.

(a)

	341						346	395
AMSH_human	T	A	F	L	S	S		F
AMSH_Rat	T	A	F	L	S	S		F
AMSH_Mouse	T	A	F	L	S	S		F
AMSH_Pig	T	A	F	L	S	S		F
AMSH_Bovine	T	A	F	L	S	S		F
AMSH_Zebrafish	T	A	F	L	S	S		F
AMSH-LP_human	T	A	F	L	S	S		F
Rpn11_human	G	C	W	L	S	G		T

(b)

	312								320	358
AMSH_human	N	T	E	N	E	E	E	L	F	M
AMSH_Rat	H	T	E	N	E	E	E	I	F	M
AMSH_Mouse	H	T	E	N	E	E	E	I	F	M
AMSH_Pig	N	T	E	N	E	E	E	L	F	M
AMSH_Bovine	N	T	E	N	E	E	E	L	F	M
AMSH_Zebrafish	D	T	E	N	E	E	E	L	F	M
AMSH-LP_human	D	M	E	N	V	E	E	L	F	M
Rpn11_human	D	P	V	F	Q	A	K	M	L	L

Fig. 6. Sequence alignment of AMSH from different species including AMSH-LP and RPN11. (a) Sequence alignment comparing the residues implicated in the proximal ubiquitin binding. (b) Sequence alignment comparing the residues implicated in the distal ubiquitin binding.

Distal ubiquitin recognition

Inspection of the model representing AMSH244 bound to Lys63-linked diubiquitin reveals some significant differences from AMSH-LP in the residues that are supposed to be used for interactions with the distal ubiquitin. First, we see that Asp324 of AMSH-LP, which makes hydrogen-bonding and electrostatic interactions with Arg74 of the distal ubiquitin, is replaced by Asn312 in AMSH, which, though may be able to retain the hydrogen-bonding interaction, will lack the electrostatic component, leading probably to weaker binding. While this change can be considered conservative to some extent (Fig. 8), the same cannot be said about the other two substitutions, AMSH's Thr313 and Glu316 in place of the equivalent Met325 and Val328, respectively, in AMSH-LP (Fig. 6b). Met325 and Val328 are making a number of important van der Waals contacts with hydrophobic residues on the C-terminus of the distal ubiquitin in AMSH-LP, particularly with residues Leu73, Val70 and Ile44 (Fig. 8). Threonine is significantly more polar than methionine but can still provide van der Waals

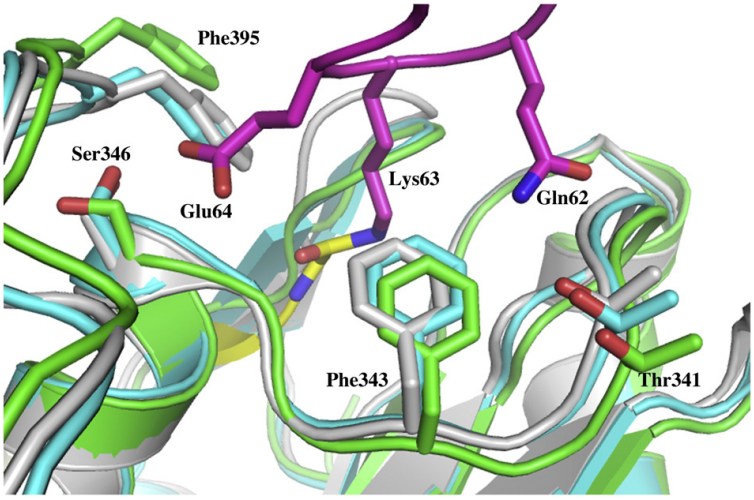

Fig. 7. A view of the residues involved in the proximal ubiquitin recognition. Superposition of AMSH244 (green ribbon), the DUB domain of AMSH-LP (cyan ribbon) and the DUB domain of AMSH-LP bound to Lys63-linked diubiquitin (gray ribbon). Residues from the proximal ubiquitin making contact at the proximal site are shown in magenta.

contact using its $C\gamma H_3$ group. Glutamate, however, cannot substitute readily for valine. On the other hand, Glu316 is appropriately positioned for electrostatic and polar interactions with Arg42 and Gln49 of the distal ubiquitin as seen in our model (Fig. 8). Crystal structure analysis of E280A mutant of AMSH244 bound to Lys63-linked diubiquitin should be sought to verify if such interactions actually occur.

In order to understand the consequences of these substitutions on the kinetic properties of AMSH, we determined the kinetic parameters of AMSH244 and compared them with those of the DUB domain of AMSH-LP. AMSH244 is catalytically less efficient than the DUB domain of AMSH-LP with Lys63-linked diubiquitin as the substrate, with most of the difference being contributed by a k_{cat} that is 7-fold less, but with a slightly better K_m (2-fold lower) (Table 2 and Supplementary Fig. 4). These data suggest that the substitutions in the distal site of AMSH may lead to weaker interactions with the substrate in the transition state of the reaction being catalyzed, whereas the interactions in the ground-state enzyme–substrate complex are relatively less affected.

Table 2. Kinetic parameters

Enzyme	k_{cat} (s^{-1})	K_m (μM)	$k_{cat}/K_m \times 10^{-3}$ (μM^{-1} s^{-1})
AMSH244	1.4 ± 0.1	32.0 ± 5.3	43.8
AMSH-LP DUB	10.3 ± 0.3	66.2 ± 4.8	155.6
	0.860 ± 0.0654[a]	71.8 ± 6.3[a]	12.0[a]

[a] Kinetic parameters reported by Sato *et al.*[25] Differences in the values are presumably due to the difference in substrates used in the activity assay.

Comparison of thermodynamic stability of the catalytic domains of AMSH and AMSH-LP

To explore further the similarity or the lack thereof between the catalytic domains of AMSH and AMSH-LP, we wondered if there would be any difference in thermodynamic stability between the two proteins. The unfolding of the catalytic constructs of both AMSH and AMSH-LP was induced by GdHCl and monitored at 220 nm using circular dichroism (CD) spectroscopy. Both proteins reveal a loss in secondary structure with increasing concentration of GdHCl (Supplementary Fig. 5); however, it was observed that AMSH is less stable toward GdHCl than AMSH-LP, with midpoint of transitions at 2.7 and 3.5 M GdHCl for AMSH and AMSH-LP, respectively (Table 3). Using the linear extrapolation

Table 3. Stability data

	ΔG_{H2O} (kcal mol^{-1})	$[GdHCl]_{0.5}$ (M)	m (kcal mol^{-1} M^{-1})
AMSH244	3.7	2.7	−1.4
AMSH-LP DUB	4.9	3.5	−1.4

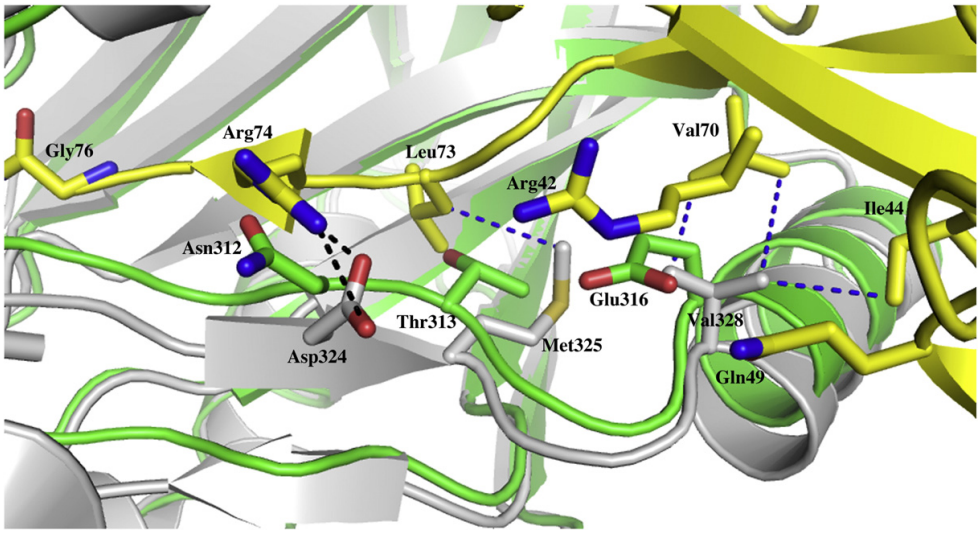

Fig. 8. A view of the residues involved in the distal ubiquitin recognition. Superposition of AMSH244 (green ribbon) and the DUB domain of AMSH-LP bound to Lys63-linked diubiquitin (gray ribbon). The distal ubiquitin is shown in yellow. Hydrogen-bonding interactions are shown as black dashes, and van der Waals interactions are shown as blue dashes.

method described previously,[37] we found ΔG_{H2O} of AMSH244 to be 1.2 kcal mol^{-1} less than that of the DUB domain of AMSH-LP, indicating that the former is thermodynamically less stable than the latter (Fig. 9 and Table 3). We propose that this difference in stability implies a difference in flexibility between the catalytic domains of the two proteins. A more stable protein is likely to have better close packing of side chains, making it more rigid, whereas a less stable protein, presumably because it has lesser amount of close packing, can tend to be more plastic, a property that may make AMSH more suitable for working in the context of a number of different types of protein–protein complexes, such as ESCRT-0 and ESCRT-III. Whether this has anything to do with the biological differences between the two proteins is worth investigating in the future.

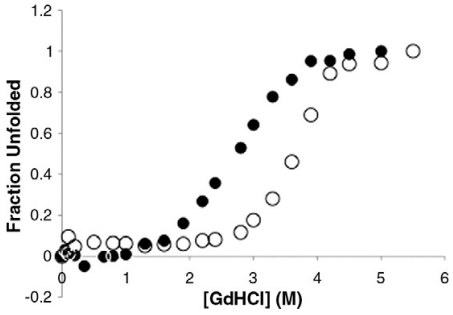

Fig. 9. Fraction unfolded curves comparing the stability of the catalytic domains of AMSH and AMSH-LP with increasing concentrations of GdHCl followed by CD spectroscopy at 220 nm. Data for AMSH244 are shown in filled circles, and those for the DUB domain of AMSH-LP are shown in open circles.

Discussion

AMSH is one of the two DUBs that are employed to regulate the functionality of the ESCRT machinery by counteracting the ubiquitination of cell-surface receptors that are directed toward degradation by the lysosome. Studies have clearly indicated that AMSH is important for receptor turnover and for maintaining free ubiquitin pool within the cell; however, a clearly defined role is yet to be assigned. What is clearly known is that AMSH has specificity toward the Lys63-linked ubiquitin chains.[9,13] DUB specificity for one linkage over another was not understood until the structural basis for Lys63-linked polyubiquitin cleavage was revealed from the crystal structure of the DUB domain of AMSH-LP bound to Lys63-linked ubiquitin dimer.[25] The structure shows how both the proximal and the distal ubiquitins are recognized; however, AMSH-LP's role in the cell is still unknown. Although it shares 54% identity and 75% similarity in its JAMM domain with AMSH,[26] AMSH-LP is not functionally redundant, based on its inability to bind to the

ESCRT complex.[9,26] The study presented here seeks to compare the catalytic domains of AMSH and AMSH-LP structurally and thermodynamically to provide further insight into AMSH's sole specificity within the ESCRT machinery.

We have determined the structure of two constructs representing the catalytic domain of AMSH, AMSH244 and AMSH219^{E280A}. The structure of AMSH244 confirms that AMSH is indeed a zinc metalloprotease of the JAMM family of DUBs with two zinc ions, one at active site and the other playing a structural role in supporting the placement of ubiquitin-binding residues in Ins-2 in a position appropriate for isopeptide bond recognition. The structure of AMSH219^{E280A} provided a surprising observation. We anticipated the loss of the active-site zinc due to the E280A mutation because Glu280, according to the known mechanism of thermolysin-type zinc-dependent metalloproteases, is responsible for holding a water molecule, the one that functions as the nucleophile, at a position such that it is able to serve as the fourth ligand in the coordination sphere of the catalytic zinc. Instead, we see clear density for the zinc. Asp309, on an adjacent loop (from Ins-1), has moved in place to become the fourth residue to coordinate the zinc (Fig. 3). The ability of the enzyme to counteract the loss of the glutamate by still retaining its zinc suggests a form of structural plasticity, allowing for conformational freedom. A similar mutation was incorporated in AMSH-LP for the purpose of co-crystallization with diubiquitin, and the authors stated that they do not see any electron density corresponding to the active-site zinc.[25] Interestingly, Asp309 and its equivalent residue in AMSH-LP have to have a certain amount of flexibility; otherwise, the active site will not be accessible for the diubiquitin substrate. The question that if the observation pertaining to Asp309 in AMSH219^{E280A} is due to more flexibility of Ins-1 in AMSH than in AMSH-LP cannot be answered from the data presented here. It is possible that the same rearrangement of the equivalent aspartate in AMSH-LP might have been observed in the structure of ubiquitin-free AMSH-LP^{E292A}.

Another interesting finding we see from the structure of AMSH219^{E280A} is the presence of a potential disulfide bond adjacent to the active site (Supplementary Fig. 3). It should be noted that a disulfide bond next to the putative active-site zinc was also observed in the structure the JAMM-domain protein *Af*JAMM, a cytosolic protein from *Archaeoglobus fulgidus*.[32] The possibility that the cysteine pair in AMSH is capable of existing in reduced and oxidized forms, reduced when in cytosol and oxidized when associated with endosomes, cannot be ruled out. This feature may contribute to or result from the structural plasticity of the enzyme. However, we cannot say with any degree of certainty if this reversible disulfide bridge is unique to AMSH and, if it is, whether it contributes to the biological difference between AMSH and AMSH-LP, two very similar proteins. It is not clear why the DUB domain of AMSH, not AMSH-LP, should have a disulfide, or is it common to both of them (DTT was also present in the crystallization buffer and throughout purification in the case of the AMSH-LP DUB domain). If it happens to be unique to AMSH, it could perhaps be linked to its association with endosomes, which have been shown to be oxidizing.[38]

Moving forward, we sought to directly compare the catalytic domains of AMSH and AMSH-LP structurally and thermodynamically. It is expected that homologous proteins that share 75% sequence similarity have a similar fold and overall architecture. On par with this expectation, the catalytic domains of AMSH and AMSH-LP have a nearly identical fold and superimposable zinc coordination sites (Fig. 4). Furthermore, AUC experiments confirmed that both the proteins are globular and monomeric in solution (Fig. 1). Thus, structurally, we cannot separate the two proteins from one another. Thermodynamically, however, we see a difference between the two. Chaotrope-induced unfolding with GdHCl indicates that the catalytic domain of AMSH is thermodynamically less stable than that of AMSH-LP (Fig. 9). Analysis of primary sequences of the proteins does reveal some differences in certain key positions, such as in the hydrophobic core (residues Val259, Val363 and Phe376 in AMSH are substituted by residues Leu271, Ile375 and Ile388 in AMSH-LP, respectively), which could contribute to the difference in thermodynamic stability; however, this needs to be investigated in future.

We have sought to obtain structural insight into AMSH's ability to recognize Lys63-linked diubiquitin through modeling. Only recently was Lys63-linkage specificity understood from the structural analysis of the DUB domain of AMSH-LP bound to Lys63-linked diubiquitin.[25] This structure reveals interactions between the enzyme and both the distal and the proximal ubiquitins, but the basis for specificity arises from residues in the proximal site of the enzyme interacting with the proximal ubiquitin, despite a more extensive interaction with the distal ubiquitin (a significantly more accessible surface area is buried upon interaction with distal than proximal ubiquitin).[25] Overall, AMSH adopts very similar interactions when modeled according to the ubiquitin-bound structure of AMSH-LP. As indicated by our model, the proximal binding site is highly conserved between the two proteins (Fig. 6 and 7), consistent with Lys63-linkage specificity of AMSH as well. The only noticeable difference is the orientation of a critical serine residue, Ser346, which we propose will be

induced to adopt an orientation seen in AMSH-LP upon binding to ubiquitin in the proximal site, consistent with the proposed plasticity of the enzyme.

Seeing that AMSH may have specific interactions with the proximal ubiquitin means that this enzyme will be unable to cleave a monoubiquitinated receptor because the last ubiquitin moiety is directly attached to the receptor, which is unlikely to have the same three-residue peptide sequence that occurs in ubiquitin and in the same conformation. Our analysis therefore seems to indicate that AMSH would only be a chain-modifying enzyme, having the ability to shorten a Lys63-linked polymeric chain, leaving the last ubiquitin still attached to the substrate. However, it has been proposed that AMSH acts to oppose E3-ligase activity on the receptor through deubiquitination, presumably by the complete removal of ubiquitin tag, at an early stage of endosomal sorting process, thereby promoting recycling of the receptor.[9] Consistent with this model, small interfering RNA-mediated knockdown of AMSH leads to increased rate of EGFR degradation, presumably due to enhanced targeting to the lysosomal pathway.[13] This implies that AMSH is able to completely deubiquitinate EGFR, since monoubiquitinated EGFR can still be targeted to lysosome.[9] This apparent paradox can be resolved if we allow for a rearrangement of the active site of the enzyme, aided once again by its structural plasticity, brought about by its binding partners on the ESCRT machinery. Further studies are needed to confirm AMSH's ability to cleave a monoubiquitinated substrate to provide clarity to this hypothesis.

Our analysis reveals a difference in the distal-site residues between the two enzymes. The rather nonpolar face of the distal site in AMSH-LP is replaced by a polar one in AMSH (Fig. 8). Considering the high level of overall similarity between the two proteins, this difference is striking. Our kinetic data appear to indicate that the distal-site differences may translate into a reduced affinity between the enzyme and the substrate in the transition state of the reaction rather than in the Michaelis complex, making the catalytic domain of AMSH less efficient than that of AMSH-LP. More work needs to be done in the future to see if the difference in kinetic properties we are observing here is related to the biological difference between AMSH and AMSH-LP. It should be noted that AMSH undergoes activation upon recruitment to the ECSRT complex,[9] the functional significance of which has not been understood yet. If this activation is important for its biological function, one may speculate that the substitution seen in AMSH's distal site is "designed" to keep the enzyme in a latent state.

In conclusion, we have determined the structure of the catalytic domain of the endosome-associated DUB AMSH and found that though structurally nearly identical with the catalytic domain AMSH-LP, it possesses significantly less thermodynamically stability than the latter, an observation we propose implies greater structural plasticity for the catalytic domain of AMSH. This property may, in addition to having a functional SH3-binding motif and MIT domain, endow the enzyme with ability to take part in the ESCRT-mediated functions.

Materials and Methods

Cloning, expression and purification

The DNA encoding AMSH244 was amplified by PCR using a plasmid that contained full-length DNA as the template (pGEX-6P1-AMSH, a kind gift from Sylvie Urbe, University of Liverpool, UK) and was subcloned into pGEX-6P1 (GE Biosciences) by using standard cloning protocols. The resulting N-terminally fused glutathione *S*-transferase (GST)-tagged protein was expressed in *Escherichia coli* Rosetta cells (Novagen) and purified with a glutathione-Sepharose column (GE Biosciences) following the manufacturer's instructions. After removal of the tag by PreScission protease (GE Biosciences), the protein was further purified by size-exclusion chromatography (SEC) using a Superdex S75 column (GE Biosciences).

AMSH219 was subcloned into a pGEX-6P1 expression vector as described above. The Glu280Ala mutation was introduced into the gene by site-directed mutagenesis using QuikChange Site-Directed Mutagenesis Kit (Stratagene) following the manufacturer's protocol. DNA sequencing confirmed the presence of the mutation. AMSH219^{E280A} was purified using standard GST affinity followed by SEC (Superdex S200 column). The DUB domain of AMSH-LP (a kind gift from Prof. Shuya Fukai, The University of Tokyo, Japan) was purified as described in Ref. 25.

Crystallization and structure determination

Crystals of AMSH244 were grown at room temperature by the sitting-drop vapor diffusion method from a mother liquor containing 0.2 M sodium malonate (pH 7.0), 20% polyethylene glycol (PEG) 3350 and 5% PEG 400. Crystals of AMSH219^{E280A} were grown at room temperature by the sitting-drop vapor diffusion method from a mother liquor containing 0.1 M 4-morpholineethanesulfonic acid (pH 6.5), 15% PEG 6000 and 5% methyl-2,4-pentanediol. Crystals were briefly soaked in cryoprotectant solution (20% ethylene glycol) and then plunged into liquid nitrogen for flash cooling. X-ray diffraction data were collected at 100 K on a Mar300 CCD detector (Mar USA) at beamline 23-ID-D at the Advanced Photon Source at Argonne National Laboratory. The data were processed using HKL2000.

The crystal structure of AMSH244 was solved by MR using a homology model of the catalytic domain of AMSH, built based on the crystal structure of the catalytic domain of AMSH-LP using the SWISS-MODEL homology modeling server,[39] as the search model. Refinement and

multiple rounds of model building were carried out using PHENIX[29] and Coot,[40] respectively, yielding a final model with a crystallographic *R*-factor (R_{crys}) of 19.3% and a free *R*-factor (R_{free}) of 22.9%. Residues Thr250 of chain C, Ile251 of chain D, Pro402 of chain E and Glu314, Asn315 and Glu316 of chain G are within disallowed regions of the Ramachandran plot. All of these residues were in weak or no density at 1 σ except Glu314 and Thr250. The structure of AMSH219^{E280A} was also determined by MR using AMSH244 structure as the search model. Refinement and model building were carried out in the same method as described above, yielding an R_{crys} of 18.0% and an R_{free} of 20.5% (Table 1). Graphical analysis was carried out using PyMOL (DeLano Scientific).

Analytical ultracentrifugation

To characterize the oligomeric state of AMSH and AMSH-LP, we conducted sedimentation velocity experiments at 50,000 rpm using both the Beckman Coulter XLI and XLA. (Beckman Coulter, Fullerton, CA, USA). The samples were monitored by both absorbance and interference optics at 280 and 675 nm, respectively. The proteins were dialyzed in 50 mM Tris–HCl (pH 7.6), 50 mM NaCl and 1 mM DTT. Three concentration series were conducted to evaluate the formation of higher-order species, AMSH244 at 30, 60 and 120 μM and AMSH-LP at 25, 47 and 94 μM. The sedimentation coefficients and apparent molecular weights were calculated from size distribution analyses [*c*(*s*)] using SEDFIT v. 12.0 [41,42]. The solvent density, viscosity and partial specific volume of the proteins were calculated using SEDNTERP v. 1.09†.

Guanidine melt using CD spectroscopy

The stability of the folded state of AMSH244 and AMSH-LP toward GdHCl was determined using 8-M stock concentrations of GdHCl (Sigma). Varying concentrations of GdHCl were added to the protein (0. 2 mg mL^{-1}) diluted in 100 mM phosphate buffer, pH 7.4, and allowed to sit at room temperature overnight to allow for complete equilibration. Changes in the folded state of the proteins were monitored using CD by following changes in ellipticity at 220 nm. CD spectra were recorded in a Jasco J-810 Spectropolarimeter in the far-UV region (195–260 nm) in a 0. 1-cm-path-length cuvette. Each spectrum was averaged over four scans (50 nm min^{-1} scan speed, with an 8-s time constant) and corrected by subtraction of a spectrum of the buffer alone. Mean residue molar ellipticity values were calculated using the following equation:

$$[\theta] = \frac{\theta \times 100 \times M}{C \times l \times n}$$

where θ is the ellipticity in degrees, *l* is the optical path in centimeters, *C* is the concentration in milligrams per milliliter, *M* is the molecular mass and *n* is in the number of residues in the protein.

The mean residue molar ellipticity [θ] is given in degree per centimeter squared per decimole. Unfolding curves were analyzed using a two-state unfolding model, using linear extrapolation to obtain the Δ*G* value in the absence of GdHCl.[37]

Determination of kinetic parameters and DUB assay

Human ubiquitin was subcloned into pGEX-6P1 and purified using GST affinity chromatography, and the GST tag was removed by PreScission Protease. The protein was further purified using SEC (Superdex S75 column). Lys63-diubiquitin was enzymatically synthesized from ubiquitin using ATP, human E1 and the E2 complex (Ubc13 and Uev1a) following previously reported procedures.[25] The reaction was incubated at 37° for 4 h and then quenched by dilution with buffer A (50 mM sodium acetate, pH 4.5). The quenched reaction mixture was subjected to ion-exchange chromatography on a Mono-S column (GE Biosciences) to obtain Lys63-diubiquitin.

The *in vitro* DUB assay was carried out by incubating AMSH244, wild-type AMSH219, wild-type AMSH219 expressed and purified in the absence of DTT (AMSH219^{-DTT}), AMSH219^{C282A} (expressed and purified in the absence of DTT) and AMSH219^{E280A} to a final enzyme concentration of 100 nM with 20 μM Lys63-diubiquitin in a total reaction volume of 20 μL. All reactions were carried out in reaction buffer [50 mM Tris–HCl (pH 7.0), 25 mM KCl, 5 mM $MgCl_2$ and 1 mM DTT] for 1 h at 20 °C, except AMSH219^{-DTT} and AMSH219^{C282A}, which were incubated in the same reaction buffer without DTT. The reaction was quenched by the addition of 5× SDS-PAGE sample buffer followed by boiling and then analyzed by SDS-PAGE.

The kinetic parameters were determined by incubating the enzyme (100 nM AMSH244 and 25 nM DUB domain of AMSH-LP) with four concentrations of diubiquitin, ranging from 20 to 100 μM, in reaction buffer [50 mM Tris–HCl (pH 7.0), 25 mM KCl, 5 mM $MgCl_2$ and 1 mM DTT]. The reaction was carried out at 20 °C for 15 min for initial velocity measurements. Reaction tubes were quenched by the addition of 5× SDS-PAGE sample buffer followed by boiling. The reaction mixtures were visualized by SDS-PAGE gels and scanned. Bands corresponding to monoubiquitin were integrated using ImageJ software‡. Ubiquitin standards ranging from 4 to 12.3 μg were used to draw a calibration plot, which was used to quantify the amount of ubiquitin produced. Kinetic parameters were calculated by fitting the data in SigmaPlot.

Accession numbers

Coordinates and structure factors have been deposited in the PDB with accession numbers 3RZU (AMSH244) and 3RZV (AMSH219^{E280A}).

Supplementary materials related to this article can be found online at doi:10.1016/j.jmb.2011.08.029

†http://www.rasmb.bbri.org/rasmb/windows/sednterp-philo

‡http://rsb.info.nih.gov/ij/

Acknowledgements

The authors acknowledge Sylvie Urbé (University of Liverpool) for her generous gift of the AMSH full-length plasmid from which we were able to carry out our studies. We thank Prof. Shuya Fukai (University of Tokyo) for providing GST-fused AMSH-LP. We thank Pavel Afonine for his helpful suggestions on refinement and Alex Tuttle for cloning GST-tagged ubiquitin. We also thank Venugopalan Nagarajan and Michael Becker at beamline 23-ID-D of Advanced Photon Source for assistance with data collection. The General Medicine and Cancer Institutes Collaborative Access Team has been funded in whole or in part with Federal funds from the National Cancer Institute (Y1-CO-1020) and the National Institute of General Medical Science (Y1-GM-1104). Use of the Advanced Photon Source was supported by the U.S. Department of Energy, Basic Energy Sciences, Office of Science, under Contract DE-AC02-06CH11357. Financial support from the National Institutes of Health (1R01RR026273) is gratefully acknowledged.

References

1. Maytal-Kivity, V., Reis, N., Hofmann, K. & Glickman, M. H. (2002). MPN+, a putative catalytic motif found in a subset of MPN domain proteins from eukaryotes and prokaryotes, is critical for Rpn11 function. *BMC Biochem.* **3**, 28.
2. Nijman, S. M., Luna-Vargas, M. P., Velds, A., Brummelkamp, T. R., Dirac, A. M., Sixma, T. K. & Bernards, R. (2005). A genomic and functional inventory of deubiquitinating enzymes. *Cell*, **123**, 773–786.
3. Komander, D., Clague, M. J. & Urbe, S. (2009). Breaking the chains: structure and function of the deubiquitinases. *Nat. Rev., Mol. Cell Biol.* **10**, 550–563.
4. Wilkinson, K. D. (2009). DUBs at a glance. *J. Cell Sci.* **122**, 2325–2329.
5. Komander, D. (2010). Mechanism, specificity and structure of the deubiquitinases. *Subcell. Biochem.* **54**, 69–87.
6. Zhu, P., Zhou, W., Wang, J., Puc, J., Ohgi, K. A., Erdjument-Bromage, H. *et al.* (2007). A histone H2A deubiquitinase complex coordinating histone acetylation and H1 dissociation in transcriptional regulation. *Mol. Cell*, **27**, 609–621.
7. Sobhian, B., Shao, G., Lilli, D. R., Culhane, A. C., Moreau, L. A., Xia, B. *et al.* (2007). RAP80 targets BRCA1 to specific ubiquitin structures at DNA damage sites. *Science*, **316**, 1198–1202.
8. Avvakumov, G. V., Walker, J. R., Xue, S., Finerty, P. J., Jr, Mackenzie, F., Newman, E. M. & Dhe-Paganon, S. (2006). Amino-terminal dimerization, NRDP1–rhodanese interaction, and inhibited catalytic domain conformation of the ubiquitin-specific protease 8 (USP8). *J. Biol. Chem.* **281**, 38061–38070.
9. Clague, M. J. & Urbe, S. (2006). Endocytosis: the DUB version. *Trends Cell Biol.* **16**, 551–559.
10. Wollert, T. & Hurley, J. H. (2010). Molecular mechanism of multivesicular body biogenesis by ESCRT complexes. *Nature*, **464**, 864–869.
11. Saksena, S., Sun, J., Chu, T. & Emr, S. D. (2007). ESCRTing proteins in the endocytic pathway. *Trends Biochem. Sci.* **32**, 561–573.
12. Wright, M. H., Berlin, I. & Nash, P. D. (2011). Regulation of endocytic sorting by ESCRT-DUB-mediated deubiquitination. *Cell Biochem. Biophys.* **60**, 39–46.
13. McCullough, J., Clague, M. J. & Urbe, S. (2004). AMSH is an endosome-associated ubiquitin isopeptidase. *J. Cell Biol.* **166**, 487–492.
14. Sierra, M. I., Wright, M. H. & Nash, P. D. (2010). AMSH interacts with ESCRT-0 to regulate the stability and trafficking of CXCR4. *J. Biol. Chem.* **285**, 13990–14004.
15. Kyuuma, M., Kikuchi, K., Kojima, K., Sugawara, Y., Sato, M., Mano, N. *et al.* (2007). AMSH, an ESCRT-III associated enzyme, deubiquitinates cargo on MVB/late endosomes. *Cell Struct. Funct.* **31**, 159–172.
16. Ma, Y. M., Boucrot, E., Villen, J., Affar el, B., Gygi, S. P., Gottlinger, H. G. & Kirchhausen, T. (2007). Targeting of AMSH to endosomes is required for epidermal growth factor receptor degradation. *J. Biol. Chem.* **282**, 9805–9812.
17. Herrera-Vigenor, F., Hernandez-Garcia, R., Valadez-Sanchez, M., Vazquez-Prado, J. & Reyes-Cruz, G. (2006). AMSH regulates calcium-sensing receptor signaling through direct interactions. *Biochem. Biophys. Res. Commun.* **347**, 924–930.
18. Reyes-Ibarra, A. P., Garcia-Regalado, A., Ramirez-Rangel, I., Esparza-Silva, A. L., Valadez-Sanchez, M., Vazquez-Prado, J. & Reyes-Cruz, G. (2007). Calcium-sensing receptor endocytosis links extracellular calcium signaling to parathyroid hormone-related peptide secretion via a Rab11a-dependent and AMSH-sensitive mechanism. *Mol. Endocrinol.* **21**, 1394–1407.
19. Hislop, J. N., Henry, A. G., Marchese, A. & von Zastrow, M. (2009). Ubiquitination regulates proteolytic processing of G protein-coupled receptors after their sorting to lysosomes. *J. Biol. Chem.* **284**, 19361–19370.
20. Hasdemir, B., Murphy, J. E., Cottrell, G. S. & Bunnett, N. W. (2009). Endosomal deubiquitinating enzymes control ubiquitination and down-regulation of protease-activated receptor 2. *J. Biol. Chem.* **284**, 28453–28466.
21. Carlton, J. G. & Martin-Serrano, J. (2007). Parallels between cytokinesis and retroviral budding: a role for the ESCRT machinery. *Science*, **316**, 1908–1912.
22. Morita, E., Sandrin, V., Chung, H. Y., Morham, S. G., Gygi, S. P., Rodesch, C. K. & Sundquist, W. I. (2007). Human ESCRT and ALIX proteins interact with proteins of the midbody and function in cytokinesis. *EMBO J.* **26**, 4215–4227.
23. Mukai, A., Mizuno, E., Kobayashi, K., Matsumoto, M., Nakayama, K. I., Kitamura, N. & Komada, M. (2008). Dynamic regulation of ubiquitylation and deubiquitylation at the central spindle during cytokinesis. *J. Cell Sci.* **121**, 1325–1333.
24. Tanaka, N., Kaneko, K., Asao, H., Kasai, H., Endo, Y., Fujita, T. *et al.* (1999). Possible involvement of a novel STAM-associated molecule "AMSH" in intracellular

signal transduction mediated by cytokines. *J. Biol. Chem.* **274**, 19129–19135.
25. Sato, Y., Yoshikawa, A., Yamagata, A., Mimura, H., Yamashita, M., Ookata, K. *et al.* (2008). Structural basis for specific cleavage of Lys 63-linked polyubiquitin chains. *Nature*, **455**, 358–362.
26. Kikuchi, K., Ishii, N., Asao, H. & Sugamura, K. (2003). Identification of AMSH-LP containing a Jab1/MPN domain metalloenzyme motif. *Biochem. Biophys. Res. Commun.* **306**, 637–643.
27. Nakamura, M., Tanaka, N., Kitamura, N. & Komada, M. (2006). Clathrin anchors deubiquitinating enzymes, AMSH and AMSH-like protein, on early endosomes. *Genes Cells*, **11**, 593–606.
28. Agromayor, M. & Martin-Serrano, J. (2006). Interaction of AMSH with ESCRT-III and deubiquitination of endosomal cargo. *J. Biol. Chem.* **281**, 23083–23091.
29. Adams, P. D., Grosse-Kunstleve, R. W., Hung, L. W., Ioerger, T. R., McCoy, A. J., Moriarty, N. W. *et al.* (2002). PHENIX: building new software for automated crystallographic structure determination. *Acta Crystallogr., Sect. D: Biol. Crystallogr.* **58**, 1948–1954.
30. Pena, V., Liu, S., Bujnicki, J. M., Luhrmann, R. & Wahl, M. C. (2007). Structure of a multipartite protein–protein interaction domain in splicing factor prp8 and its link to retinitis pigmentosa. *Mol. Cell*, **25**, 615–624.
31. Zhang, L., Shen, J., Guarnieri, M. T., Heroux, A., Yang, K. & Zhao, R. (2007). Crystal structure of the C-terminal domain of splicing factor Prp8 carrying retinitis pigmentosa mutants. *Protein Sci.* **16**, 1024–1031.
32. Ambroggio, X. I., Rees, D. C. & Deshaies, R. J. (2004). JAMM: a metalloprotease-like zinc site in the proteasome and signalosome. *PLoS Biol.* **2**, 113–119.
33. Tran, H. J., Allen, M. D., Lowe, J. & Bycroft, M. (2003). Structure of the Jab1/MPN domain and its implications for proteasome function. *Biochemistry*, **42**, 11460–11465.
34. Gupta, S. P. (2007). Quantitative structure–activity relationship studies on zinc-containing metalloproteinase inhibitors. *Chem. Rev.* **107**, 3042–3087.
35. Lipscomb, W. N. & Strater, N. (1996). Recent advances in zinc enzymology. *Chem. Rev.* **96**, 2375–2434.
36. Maiti, R., Van Domselaar, G. H., Zhang, H. & Wishart, D. S. (2004). SuperPose: a simple server for sophisticated structural superposition. *Nucleic Acids Res.* **32**, W590–594.
37. Pace, C. N. (1986). Determination and analysis of urea and guanidine hydrochloride denaturation curves. *Methods Enzymol.* **131**, 266–280.
38. Austin, C. D., Wen, X., Gazzard, L., Nelson, C., Scheller, R. H. & Scales, S. J. (2005). Oxidizing potential of endosomes and lysosomes limits intracellular cleavage of disulfide-based antibody–drug conjugates. *Proc. Natl Acad. Sci. USA*, **102**, 17987–17992.
39. Arnold, K., Bordoli, L., Kopp, J. & Schwede, T. (2006). The SWISS-MODEL workspace: a web-based environment for protein structure homology modelling. *Bioinformatics*, **22**, 195–201.
40. Emsley, P., Lohkamp, B., Scott, W. G. & Cowtan, K. (2010). Features and development of Coot. *Acta Crystallogr., Sect. D: Biol. Crystallogr.* **66**, 486–501.
41. Brown, P. H. & Schuck, P. (2006). Macromolecular size-and-shape distributions by sedimentation velocity analytical ultracentrifugation. *Biophys. J.* **90**, 4651–4661.
42. Schuck, P. (2000). Size-distribution analysis of macromolecules by sedimentation velocity ultracentrifugation and lamm equation modeling. *Biophys. J.* **78**, 1606–1619.

Bioorganic & Medicinal Chemistry Letters 22 (2012) 3900–3904

Contents lists available at SciVerse ScienceDirect

Bioorganic & Medicinal Chemistry Letters

journal homepage: www.elsevier.com/locate/bmcl

The co-crystal structure of ubiquitin carboxy-terminal hydrolase L1 (UCHL1) with a tripeptide fluoromethyl ketone (Z-VAE(OMe)-FMK)

Christopher W. Davies [a], Joseph Chaney [a], Gregory Korbel [b], Dagmar Ringe [c], Gregory A. Petsko [c], Hidde Ploegh [b], Chittaranjan Das [a,*]

[a] Department of Chemistry, Purdue University, West Lafayette, IN, USA
[b] Whitehead Institute for Biomedical Research, Cambridge, MA, USA
[c] Rosenstiel Basic Medical Sciences Research Center, 415 South Street, MS-029, Waltham, MA, USA

ARTICLE INFO

Article history:
Received 8 February 2012
Revised 25 April 2012
Accepted 27 April 2012
Available online 4 May 2012

Keywords:
Ubiquitin hydrolase
Deubiquitinating enzymes
Fluoromethyl ketone
Enzyme inhibitors

ABSTRACT

UCHL1 is a 223 amino acid member of the UCH family of deubiquitinating enzymes (DUBs), found abundantly and exclusively expressed in neurons and the testis in normal tissues. Two naturally occurring variants of UCHL1 are directly involved in Parkinson's disease (PD). Not only has UCHL1 been linked to PD, but it has oncogenic properties, having been found abnormally expressed in lung, pancreatic, and colorectal cancers. Although inhibitors of UCHL1 have been described previously the co-crystal structure of the enzyme bound to any inhibitor has not been reported. Herein, we report the X-ray structure of UCHL1 co-crystallized with a peptide-based fluoromethylketone inhibitor, Z-VAE(OMe)-FMK (VAEFMK) at 2.35 Å resolution. The co-crystal structure reveals that the inhibitor binds in the active-site cleft, irreversibly modifying the active-site cysteine; however, the catalytic histidine is still misaligned as seen in the native structure, suggesting that the inhibitor binds to an inactive form of the enzyme. Our structure also reveals that the inhibitor approaches the active-site cleft from the opposite side of the crossover loop as compared to the direction of approach of ubiquitin's C-terminal tail, thereby occupying the P1′ (leaving group) site, a binding site perhaps used by the unknown C-terminal extension of ubiquitin in the actual in vivo substrate(s) of UCHL1. This structure provides a view of molecular contacts at the active-site cleft between the inhibitor and the enzyme as well as furnishing structural information needed to facilitate further design of inhibitors targeted to UCHL1 with high selectivity and potency.

UCHL1, a protein normally expressed exclusively in the brain and testis, is a member of the ubiquitin carboxy-terminal hydrolase (UCH) family of enzymes, a subclass of a larger group of enzymes collectively called deubiquitinases (DUBs).[1,2] DUBs catalyze the hydrolysis of isopeptide or peptide bonds between ubiquitin and target proteins, or between monomers in polymeric chains of ubiquitin.[3–6] Although the exact in vivo substrate(s) for this enzyme is not known, biochemical studies have shown that UCHL1 is active only towards ubiquitin conjugates with small leaving groups at the C-terminus of ubiquitin.[7,8] There are five classes of DUBs, four of which are cysteine proteases including the UCH family, the fifth class being zinc metalloproteases.[4–6,9] UCHL1, like its other family members, UCHL3, UCHL5, and BAP1, contains a catalytic triad consisting of a cysteine (Cys90), a histidine (His161), and an aspartate (Asp176). The X-ray crystal structure of the enzyme is known and reveals a misaligned catalytic triad with a Cys-His distance of ~8 Å, much further than a catalytically competent distance of ~4 Å for a cysteine protease.[10] However, upon binding to ubiquitin, as revealed in the co-crystal structure of this enzyme with the ubiquitin-based suicide substrate, ubiquitin vinylmethylester (UbVME), the catalytic triad adopts a productive arrangement as seen in other active cysteine proteases.[11]

The physiological function of UCHL1 is not known; however, abnormal expression of UCHL1 is observed in many forms of cancers, including colorectal, lung and pancreatic cancers.[12–14] UCHL1 transgenic mice are prone to malignancy, primarily lymphomas and lung tumors,[15] and the gad (gracile axonal dystrophy) mouse exhibits severe neurologic defects.[16] UCHL1's role in disease makes it a possible target for design of therapeutics in the form of small-molecule inhibitors. Many other cysteine proteases have been so targeted, because elevated and uncontrolled levels of protease

Abbreviations: Z-VAD-FMK, benzyloxycarbonyl-Val-Ala-Asp fluoromethylketone; Z-VAE(OMe)-FMK, benzyloxycarbonyl-Val-Ala-Glu(γ-methoxy) fluoromethylketone; BAP1, BRCA associated protein-1; CMK, chloromethyl ketones; DUBs, deubiquitinases; FMKs, fluoromethylketones; gad, gracile axonal dystrophy; MR, molecular replacement; UCHL1, ubiquitin carboxy-terminal hydrolase L1; UCHL3, ubiquitin carboxy-terminal hydrolase L3; UCHL5, ubiquitin carboxy-terminal hydrolase L5; UbVME, ubiquitin vinylmethyl ester.

* Corresponding author. Address: Department of Chemistry, Purdue University, Brown Laboratory of Chemistry, 560 Oval Drive, West Lafayette, IN 47907, USA. Tel.: +1 765 494 5478; fax: +1 765 494 0239.
E-mail address: cdas@purdue.edu (C. Das).

0960-894X/$ - see front matter © 2012 Elsevier Ltd. All rights reserved.
http://dx.doi.org/10.1016/j.bmcl.2012.04.124

activity can result in physiological imbalance, leading to the onset of several diseases.[17,18] One of the most studied cysteine protease targets for inhibition is the caspase family of cysteine proteases, the members of which are covalently inactivated by peptide halomethyl ketones such as Z-VAD-FMK (benzyloxycarbonyl-Val-Ala-Asp fluoromethylketone).[19] FMKs (fluoromethylketones) are irreversible inhibitors of cysteine proteases by virtue of their ability to alkylate the active-site thiol, leading to the displacement of the halide group by the catalytic cysteine to form a thioether bond between the cysteine and the inhibitor.[18,20]

Here we report the X-ray co-crystal structure of UCHL1 with a tripeptide fluoromethylketone, Z-VAE(OMe)-FMK (benzyloxycarbonyl-Val-Ala-Glu(γ-methoxy) fluoromethylketone),[21] at 2.35 Å resolution. The co-crystal structure reveals that the inhibitor binds in the active-site cleft, irreversibly modifying the active-site cysteine. However, the catalytic histidine is still misaligned as seen in the native structure,[10] suggesting that the inhibitor binds to an inactive form of the enzyme. Our structure also reveals that the inhibitor approaches the active-site cleft from the opposite side of the crossover loop as compared to the direction of approach of ubiquitin's C-terminal tail thereby occupying the P1′ site, a binding site perhaps used by the unknown C-terminal extension of ubiquitin in the actual in vivo substrate(s) of UCHL1. Our structure provides both the first view of molecular contacts at the active-site cleft between an inhibitor and this enzyme as well as the structural information needed to facilitate further design of inhibitors toward UCHL1 with high selectivity and potency.

Z-VAE(OMe)-FMK (hereafter referred to as simply VAEFMK) was synthesized as described previously.[21] We identified VAEFMK as an inhibitor of UCHL1 during a screen of inhibitors for the viral DUB, UL36 (of herpes simplex virus type 1). During that screen, which included several CMK (chloromethyl ketone) and FMK based putative cysteine protease inhibitors, it was observed that some of these molecules inhibited UL36 both in lysates and in cell culture (unpublished data). The assay employed here relied on the ability of the DUB to react with HA (hemagglutinin)-tagged ubiquitin vinylmethyl ester (HA-UbVME). Curiously, we found one particular compound, VAEFMK, effectively inhibited UCHL1's reaction with HA-UbVME at the concentration of 100 μM; however, there was no effect on UCHL3 and UCHL5 at that concentration. On the other hand, a related compound, Z-VAD-FMK, was unable to inhibit UCHL1 activity even at 440 μM concentration (Supplementary Fig. 2). VAEFMK was co-crystallized with wild-type UCHL1 (upon covalent modification of the enzyme's thiol, the fluoride group is lost (see mechanism below), therefore, the fluoride group is not seen in the structure and the actual adduct we crystallized should be referred to as UCHL1-VAE thioether). The co-crystal structure was solved by molecular replacement (MR) using the structure of UCHL1 (Protein Data Bank (PDB) code: 2ETL) as the search model. After MR, the electron density map ($2F_O$–F_C) was inspected for presence of positive density that could correspond to bound inhibitor. Inspection of the map indeed revealed positive density corresponding to the inhibitor within the active-site cleft. Using ProDrug Server,[22] we generated a model of the inhibitor and placed the molecule within the positive density and carried out rounds of restrained refinement combined with rounds of model building, which resulted in a final free R (R_{free}) and a crystallographic R (R_{crys}) of 25.0 and 19.7%, respectively (Table 1). The final refined model contains the complete 223 amino acids of the wild-type UCHL1 with a single molecule of bound inhibitor. The pentapetide fragment carried over from the GST (glutathione S-transferase) expression tag after cleavage by PreScission Protease (GE Biosciences, USA) was disordered and therefore not modeled. Similarly to the native UCHL1 crystal, the model contains a dimer in the asymmetric unit, with each monomer in the asymmetric unit containing one copy of the inhibitor.

Table 1
Crystallographic table of statistics

	UCHL1-VAE
Residues	1–223
Data collection	
Space group	$P\,42_12$
Cell dimensions	
a, b, c (Å)	110.0, 110.0, 78.7
α, β, γ (°)	90, 90, 90
Resolution (Å)	50.0–2.35 (2.43–2.35)
[*]R_{sym}	5.1 (49.9)
I/σ I	48.5 (2.1)
Unique reflections	19259
Completeness (%)	98.1 (89.6)
Redundancy	12.9 (7.8)
Refinement	
Resolution	34.9–2.35 (2.43–2.35)
[1]R_{crys}/R_{free}	19.7/25.0
Number of atoms	3589
DRG Molecules	2
rmsd	
Bond lengths (Å)	0.005
Bond angles (°)	1.0
Ramachandran plot	
Most favored (%)	91.4
Additionally allowed regions (%)	7.3
Generously allowed regions (%)	0.3
Disallowed (%)	1.0
Bfactors (Å²)	
Protein	76.7
Solvent	59.4
DRG	93.6

[*]$R_{sym} = \Sigma_{jl}\, I(h)_j - \langle I(h)\rangle|/\Sigma_j\, I(h)_j$, where $I(h)_j$ is the scaled observed intensity of the jth observation of reflection h, and $\langle I(h)\rangle$ is the mean value of corresponding symmetry-related reflections.
[1]$R_{crys} = \Sigma\, ||F_{obs}| - |F_{calc}||/\Sigma\, |F_{obs}|$ and $R_{free} = \Sigma\, ||F_{obs}| - |F_{calc}|/\Sigma\, |F_{obs}|$, where R_{free} and R_{crys} are calculated using a randomly selected test set of 5% of the data and all reflections excluding the 5% test data, respectively. Numbers in parentheses are for the high-resolution shell.

VAEFMK is a peptide-based inhibitor that resembles the well-known caspase inhibitor Z-VAD-FMK (Fig. 1a). The usual mechanism of FMK inhibitors proceeds via a two-step addition followed by collapse/migration/displacement mechanism. Fluorine being a highly electron withdrawing group combined with the inductive effects of the carbonyl carbon oxygen makes the carbonyl carbon more electrophilic than the alpha carbon where the substitution ends up. Covalent modification proceeds by an initial nucleophilic attack on the carbonyl carbon by the reactive thiol from the enzyme, followed by the collapse of the carbonyl, migration of the thiol to the alpha carbon, and subsequent displacement of the

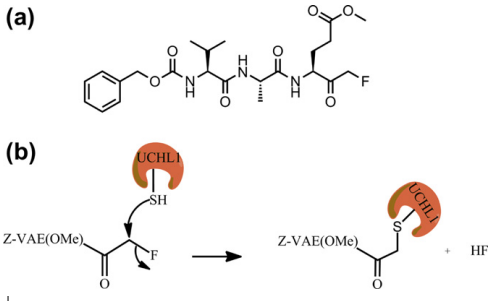

Figure 1. VAEFMK. (a) Structure of Z-VAE(OMe)-FMK (VAEFMK). (b) UCHL1 is irreversibly modified by VAEFMK.

fluorine (the overall reaction is shown in Fig. 1b). Inspection of the electron density map ($2F_O–F_C$) immediately after the MR search showed electron density adjacent to the Cys90 sulfur atom, with continuous density emanating from Cys90. This allowed us to model a covalent bond between the cysteine and the carbon atom of the FMK group, as drawn in Fig. 1. Thus, the co-crystal structure shows that VAEFMK binds to UCHL1 (the compound-bound structure is hereafter referred to as UCHL1-VAE thioether or simply as UCHL1-VAE) via a similar mechanism of action as that known for other FMK inhibitors that inactivate cysteine proteases, including caspases. The inhibitor sits within the solvent-exposed active-site cleft in an extended conformation. The benzyloxycarbonyl group of the inhibitor is exposed to solvent and is relatively disordered as indicated by lack of strong density for the benzylic group, although its position was clearly discernible in our structure (Fig. 2). The Glu(OMe) end of the inhibitor is located next to a pocket adjacent to the catalytic cysteine in the active-site cleft.

Most of the interactions that stabilize the inhibitor within the active site of both the subunits of UCHL1 are between the groups that constitute the oxyanion hole of the enzyme with the backbone of VAEFMK (Fig. 2 and Supplementary Fig. 1). For example, the backbone NH groups of Ser89 and Cys90 hydrogen bond with the backbone carbonyl oxygen atom of the Glu(OMe) residue of the inhibitor. The carbonyl group of the Ala residue of the inhibitor is within hydrogen-bonding distance of the backbone NH groups of Asn88 and the side chain NH_2 group of the oxyanion-stabilizing residue, Gln84. Apart from these hydrogen-bonding interactions, van der Waals interactions also appear to play a role in stabilizing the bound inhibitor. For example, the Cβ atom of the alanine residue in the inhibitor makes a contact with the side chain of Arg178, which seems to have turned around relative to its position in the native structure to accommodate the inhibitor (Figs. 2 and 3). Also, the hydrophobic side chain of Val of VAEFMK is nestled against the side chain of Asn159 (Fig. 2). The inhibitor in one of the subunits appears to be better defined within the active site, perhaps due to additional interactions with two protein-bound water molecules in the active site. Backbone NH of Met6 is hydrogen-bonded to a water molecule, which in turn, hydrogen bonds with the carbonyl group on the side chain of Glu(OMe) residue, and the other water molecule is held in place by hydrogen-bonding with the side chain of Asn159 (Fig. 2). These water molecules were not visualized in the other subunit.

The overall architecture of inhibitor-bound UCHL1 has remained the same as in the native structure,[10] with root mean square deviation (rmsd) of 0.67 Å^2 in Cα atoms of the two structures, suggesting a minimal conformational rearrangement upon binding of the inhibitor. The catalytic triad in the inhibitor-bound structure maintains the orientation seen in the native protein; His161 is still 8 Å away from Cys90, even though the inhibitor covalently modifies the catalytic cysteine (Fig. 3). Since the misaligned active site represents an inactive form of the enzyme, nucleophilicity of the catalytic cysteine does not require the presence of the catalytic histidine in its vicinity (within hydrogen-bonding distance), somewhat surprising considering the widely-held view that the nucleophilicity of the catalytic cysteine in cysteine proteases is due to its existence as an ion-pair with the catalytic histidine (thiolate-imidazolium ion pair).[23]

How does VAEFMK bind to UCHL1? We superimposed the structures of UCHL1-VAE with that of UbVME-bound UCHL1 (UCHL1-UbVME) (PDB code: 3KW5). The crossover loop comprising residues 150–160 can be thought of as a structural feature that divides the active-site cleft into two halves, on its right-hand side lies the P1 subsite (the way it is presented in Fig. 4) and on the left, the P1′ subsite. The C-terminal tail of ubiquitin in the UbVME-bound structure approaches the active-site thiol from the expected P1 side of the active-site cleft, whereas the inhibitor approaches from the other side (Fig. 4). This binding mode may occur because of the bulky nature of the amino acids bearing the FMK moiety. The cleft on the P1 site is narrowest next to the catalytic cysteine, a feature that allows UCHL1 to position the scissile peptide bond right after the C-terminal Gly–Gly motif with exquisite precision. This feature, along with the crossover loop, might have prevented VAEFMK from approaching the catalytic thiol from the P1 side.

Abnormal expression of UCHL1, whose in vivo function remains to be established, has been associated with various forms of cancer, making UCHL1 an attractive target for therapeutics development. Our data may assist future structure-based efforts to design better inhibitors. The structure of UCHL1-VAE shows that VAEFMK targets the active site of UCHL1, as expected, resulting in covalent modification of the catalytic thiol, thereby irreversibly inactivating the enzyme. Although the inhibitor is tethered to the catalytic cysteine covalently, our structure shows additional non-covalent interactions between the inhibitor and atoms in the active-site cleft of the enzyme, mainly between the oxyanion hole groups with the peptide backbone of VAEFMK (Fig. 2).

The co-crystal structure reported here presents a number of interesting observations. It shows intermolecular contacts between the inhibitor and the elements of active site structure of the enzyme. With very little induced fit (except for Arg178), VAEFMK binds to the active site with the Cys–His pair still in misaligned arrangement, as seen in the native structure, suggesting that the catalytic thiol is sufficiently nucleophilic even without forming an ion-pair with the catalytic histidine. Previous studies in papain indicated that the reactivity of the catalytic cysteine is due to formation of an ion-pair with the catalytic histidine,

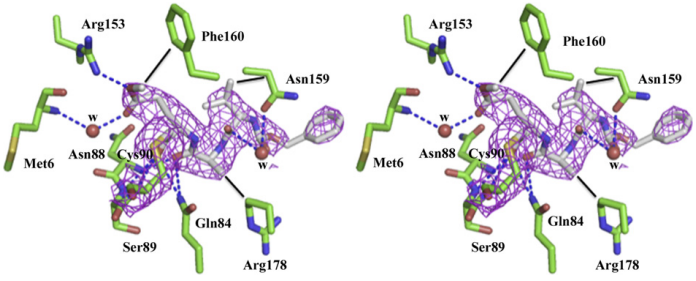

Figure 2. Interactions stabilizing VAEFMK within UCHL1's active site. Stereo view of the active-site residues involved in stabilizing VAEFMK within one subunit of UCHL1's active site. UCHL1 is shown in green sticks and VAEFMK in white sticks encapsulated by magenta mesh electron density map ($2F_O–F_C$) contoured at 0.8σ. The black line represents van der Waals interactions, while blue dotted lines are hydrogen-bonding interactions.

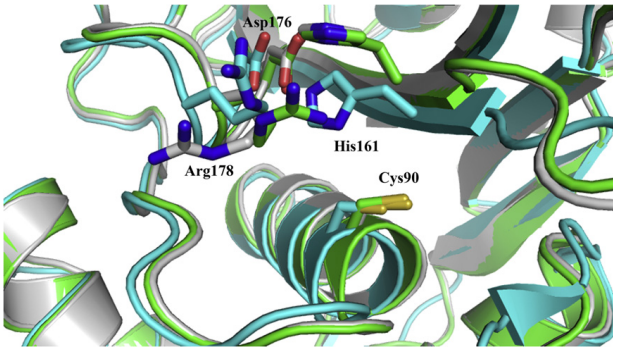

Figure 3. Superposition of wild-type UCHL1, UCHL1-UbVME, and UCHL1-VAE. Active site superposition of UCHL1, UCHL1-UbVME, and UCHL1-VAE showing differences in the spatial arrangement of active-site residues due to UbVME and VAEFMK binding compared to the wild type. Wild-type UCHL1 is shown in green sticks, UCHL1-UbVME in cyan sticks, and UCHL1-VAE in white sticks. Both UbVME and VAEFMK have been removed for clarity.

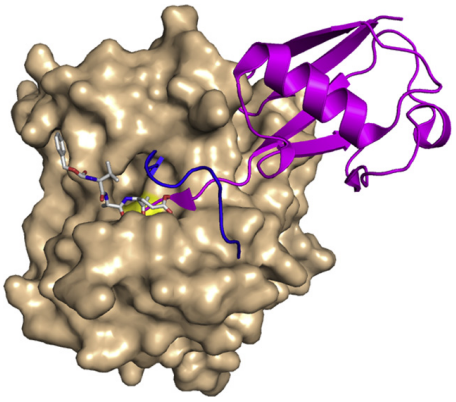

Figure 4. VAEFMK and ubiquitin binding sites within UCHL1. Superposition of UCHL1-UbVME and UCHL1-VAE reveals a novel binding site for VAEFMK, which approaches the active site from the opposite side of the crossover loop as compared to the C-terminal tail of ubiquitin. Ubiquitin is shown in magenta ribbon, VAEFMK in white sticks, and the crossover loop as blue ribbon.

analogous to the activation of the catalytic serine in the eponymous serine proteases by histidine.[24] UCHL1 has been thought to be papain-like in mechanism of action, but our observation suggests that this may not necessarily be the case. The cysteine may be reactive enough without participation by the histidine, perhaps due to a lowered pK_a. However, inspection of the contacts around the catalytic thiol reveals only two nearest neighbors, the backbone NH group of Phe162 and the side-chain NH_2 group of the oxyanion-stabilizing residue Gln84, which are at 4.6 and 5.0 Å from the S^{γ} atom, respectively. It is unclear if these groups, which are located significantly farther than hydrogen-bonding distances, could influence the pK_a of the catalytic thiol. Alternatively, the inhibitor may have been able to exploit proximity to form the covalent bond with a relatively unreactive thiol. It is also possible that fluoride being a good leaving group makes the histidine unnecessary for the reaction to proceed. The fact that the inhibitor seems to bind to a misaligned active site of UCHL1 may turn out to be advantageous from the point of view of specificity, because—among UCH members whose crystal structures have been solved—UCHL1 appears to be unique with its misaligned active-site triad. It may be that the very high intracellular concentration of UCHL1 makes it desirable to have the apoenzyme exist in a form that has little or no activity, and which is only activated by binding of specific substrates.

The co-crystal structure identifies a number of potential contacts that can be exploited for future inhibitor design. The methoxy group on the inhibitor is pointing toward a crevice in the active site that is lined by mostly hydrophobic side chains (Fig. 5). Installation of a hydrophobic side chain in place of the methoxy group might yield tighter-binding analogs. The inhibitor side chain carbonyl group faces a surface that appears to be lined with mostly polar residues. We speculate that installation of a Glu—by removing the methoxy group—will improve the potency of the inhibitor, since Arg153 is poised to make a salt-bridge with the carboxylate group on the inhibitor. Lastly, by superimposing UCHL1-UbVME with UCHL1-VAE structures, we generated a composite view (Fig. 4) that shows how UCHL1 might bind to a ubiquitin conjugate with a C-terminal extension. This composite picture should be viewed as a model representing how UCHL1 could bind to its yet-to-be-identified substrate for hydrolysis. The ubiquitin moiety would bind at the P1 site (as visualized in the UCHL1-UbVME structure). The leaving group attached to it will be threaded through the crossover loop, with part of it perhaps sitting in a similar position in the P1′ site as seen occupied by VAEFMK. With the catalytic histidine in place, oriented correctly upon ubiquitin binding, hydrolysis of the ester or amide linkage between ubiquitin and the C-terminal extension would be executed, leading to the departure of the leaving group from the VAEFMK side of the crossover loop.

Our structural studies have provided the first inhibitor-bound X-ray structure of the deubiquitinase UCHL1 co-crystallized with Z-VAE(OMe)-FMK. Although the inhibitor is seen covalently tethered to the catalytic cysteine through reaction with the FMK group, this group alone is not sufficient. For example, a close structural analog of this compound, Z-VAD-FMK, a well-known caspase inhibitor, does not inhibit UCHL1's activity even at concentrations as high as 440 μM. This suggests that suitable FMK inhibitors can be developed with relatively high selectivity toward UCHL1.

Accession number

Coordinates and structure factors have been deposited in the Protein Data Bank with accession number 4DM9.

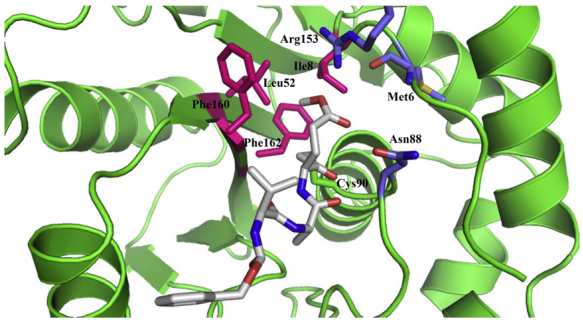

Figure 5. Polar and non-polar pockets within UCHL1's active site. Polar (right) and non-polar (left) pockets within UCHL1's active-site cleft reveal potential interactions that could be exploited for further structural modification of VAEFMK for optimal binding to UCHL1. Residues 154–159 of the crossover loop have been deleted for clarity.

Acknowledgments

We thank the staff at beam line 23-ID-D of Advanced Photon Source for assistance with data collection. The General Medicine and Cancer Institutes Collaborative Access Team has been funded in whole or in part with Federal funds from the National Cancer Institute (Y1-CO-1020) and the National Institute of General Medical Science (Y1-GM-1104). Use of the Advanced Photon Source was supported by the U.S. Department of Energy, Basic Energy Sciences, Office of Science, under Contract DE-AC02-06CH11357. We also thank Nigel Moriarty for his helpful suggestions on creating and editing ligand restrains. Financial support from the National Institutes of Health (1R01RR026273) is gratefully acknowledged.

Supplementary data

Supplementary data associated with this article can be found, in the online version, at http://dx.doi.org/10.1016/j.bmcl.2012.04.124.

References and notes

1. Doran, J. F.; Jackson, P.; Kynoch, P. A.; Thompson, R. J. *J. Neurochem.* **1983**, *40*, 1542.
2. Wilkinson, K. D.; Lee, K. M.; Deshpande, S.; Duerksen-Hughes, P.; Boss, J. M.; Pohl, J. *Science* **1989**, *246*, 670.
3. Wilkinson, K. D. *FASEB J.* **1997**, *11*, 1245.
4. Nijman, S. M.; Luna-Vargas, M. P.; Velds, A.; Brummelkamp, T. R.; Dirac, A. M.; Sixma, T. K.; Bernards, R. *Cell* **2005**, *123*, 773.
5. Love, K. R.; Catic, A.; Schlieker, C.; Ploegh, H. L. *Nat. Chem. Biol.* **2007**, *3*, 697.
6. Komander, D.; Clague, M. J.; Urbe, S. *Nat. Rev. Mol. Cell Biol.* **2009**, *10*, 550.
7. Johnston, S. C.; Riddle, S. M.; Cohen, R. E.; Hill, C. P. *EMBO J.* **1999**, *18*, 3877.
8. Larsen, C. N.; Krantz, B. A.; Wilkinson, K. D. *Biochemistry* **1998**, *37*, 3358.
9. Reyes-Turcu, F. E.; Ventii, K. H.; Wilkinson, K. D. *Annu. Rev. Biochem.* **2009**, *78*, 363.
10. Das, C.; Hoang, Q. Q.; Kreinbring, C. A.; Luchansky, S. J.; Meray, R. K.; Ray, S. S.; Lansbury, P. T.; Ringe, D.; Petsko, G. A. *Proc. Natl. Acad. Sci. U.S.A.* **2006**, *103*, 4675.
11. Boudreaux, D. A.; Maiti, T. K.; Davies, C. W.; Das, C. *Proc. Natl. Acad. Sci. U.S.A.* **2010**, *107*, 9117.
12. Hibi, K.; Liu, Q.; Beaudry, G. A.; Madden, S. L.; Westra, W. H.; Wehage, S. L.; Yang, S. C.; Heitmiller, R. F.; Bertelsen, A. H.; Sidransky, D.; Jen, J. *Cancer Res.* **1998**, *58*, 5690.
13. Yamazaki, T.; Hibi, K.; Takase, T.; Tezel, E.; Nakayama, H.; Kasai, Y.; Ito, K.; Akiyama, S.; Nagasaka, T.; Nakao, A. *Clin. Cancer Res.* **2002**, *8*, 192.
14. Hussain, S.; Zhang, Y.; Galardy, P. J. *Cell Cycle* **2009**, *8*, 1688.
15. Hussain, S.; Foreman, O.; Perkins, S. L.; Witzig, T. E.; Miles, R. R.; van Deursen, J.; Galardy, P. J. *Leukemia* **2010**, *24*, 1641.
16. Saigoh, K.; Wang, Y. L.; Suh, J. G.; Yamanishi, T.; Sakai, Y.; Kiyosawa, H.; Harada, T.; Ichihara, N.; Wakana, S.; Kikuchi, T.; Wada, K. *Nat. Genet.* **1999**, *23*, 47.
17. Rzychon, M.; Chmiel, D.; Stec-Niemczyk, J. *Acta Biochim. Pol.* **2004**, *51*, 861.
18. Palmer, J. T.; Rasnick, D.; Klaus, J. L.; Bromme, D. *J. Med. Chem.* **1995**, *38*, 3193.
19. Slee, E. A.; Zhu, H.; Chow, S. C.; MacFarlane, M.; Nicholson, D. W.; Cohen, G. M. *Biochem. J.* **1996**, *315*(Pt 1), 21.
20. Wang, Z.; Watt, W.; Brooks, N. A.; Harris, M. S.; Urban, J.; Boatman, D.; McMillan, M.; Kahn, M.; Heinrikson, R. L.; Finzel, B. C.; Wittwer, A. J.; Blinn, J.; Kamtekar, S.; Tomasselli, A. G. *Biochim. Biophys. Acta* **1817**, *2010*, 1804.
21. Misaghi, S.; Pacold, M. E.; Blom, D.; Ploegh, H. L.; Korbel, G. A. *Chem. Biol.* **2004**, *11*, 1677.
22. Schuttelkopf, A. W.; VanAalten, D. M. *Acta Crystallogr., Sect. D* **2004**, *60*, 1355.
23. Gul, S.; Hussain, S.; Thomas, M. P.; Resmini, M.; Verma, C. S.; Thomas, E. W.; Brocklehurst, K. *Biochemistry* **2008**, *47*, 2025.
24. Hussain, S.; Pinitglang, S.; Bailey, T. S.; Reid, J. D.; Noble, M. A.; Resmini, M.; Thomas, E. W.; Greaves, R. B.; Verma, C. S.; Brocklehurst, K. *Biochem. J.* **2003**, *372*, 735.

Cell PRESS

Structure
Previews

the extensions showed the opposite resemblance. The authors concluded that recognition of the ground state by M48U1 and M48U7 is more favorable energetically, contributing to their higher affinities. More expansive neutralization studies (180 isolate panel) revealed potent activity against all except those from Clade A/E. The presence of His at position 375 of gp120 of these isolates (instead of the canonical Ser) is interpreted to explain this resistance, because the His partially fills the Phe43 pocket, thereby hindering access of the extensions (but not CD4 or the mimetics lacking the extensions). This is consistent with previous findings that resistance to M48U1 involves the substitution of Ser375 with more bulky residues. The results are discussed in terms of a new mechanism of action of CD4 binding site ligands beyond the previously described avidity (multivalent forms) and avoidance of conformational change (e.g., mAb VRC01), namely optimization of the fitting of the hydrophobic extensions within the interfacial Phe43 cavity.

These new agents and the structural elucidation of the mechanisms underlying their enhanced anti-HIV potencies promise to guide further design of novel neutralizing agents based on optimal fitting of extensions into the Phe43 cavity. The recent ex vivo and nonhuman primate studies with M48U1 as a vaginal microbicide to prevent HIV-1 sexual transmission (Dereuddre-Bosquet et al., 2012) are highly promising for the potential antiviral use of these miniproteins. Structure-guided design and analysis thus continue to pave the way for the development of new CD4 mimetics that not only cap the Phe43 cavity, but also fit energetically favorable extensions deep within its boundaries.

ACKNOWLEDGMENTS

Work in the authors' laboratory is supported in part by the Intramural Program of the NIH, NIAID.

REFERENCES

Acharya, P., Luongo, T.S., Louder, M.K., McKee, K., Yang, Y., Do Kwon, Y., Mascola, J.R., Kessler, P., Loïc, M., and Kwong, P.D. (2013). Structure *21*, this issue, 1018–1029.

Curreli, F., Choudhury, S., Pyatkin, I., Zagorodnikov, V.P., Bulay, A.K., Altieri, A., Kwon, Y.D., Kwong, P.D., and Debnath, A.K. (2012). J. Med. Chem. *55*, 4764–4775.

Dereuddre-Bosquet, N., Morellato-Castillo, L., Brouwers, J., Augustijns, P., Bouchemal, K., Ponchel, G., Ramos, O.H.P., Herrera, C., Stefanidou, M., Shattock, R., et al. (2012). PLoS Pathog. *8*, e1003071.

Dey, B., Pancera, M., Svehla, K., Shu, Y., Xiang, S.H., Vainshtein, J., Li, Y.X., Sodroski, J., Kwong, P.D., Mascola, J.R., and Wyatt, R. (2007). J. Virol. *81*, 5579–5593.

Huang, C.C., Venturi, M., Majeed, S., Moore, M.J., Phogat, S., Zhang, M.Y., Dimitrov, D.S., Hendrickson, W.A., Robinson, J., Sodroski, J., et al. (2004). Proc. Natl. Acad. Sci. USA *101*, 2706–2711.

Kwong, P.D., Wyatt, R., Robinson, J., Sweet, R.W., Sodroski, J., and Hendrickson, W.A. (1998). Nature *393*, 648–659.

Kwong, P.D., Wyatt, R., Majeed, S., Robinson, J., Sweet, R.W., Sodroski, J., and Hendrickson, W.A. (2000). Structure *8*, 1329–1339.

Madani, N., Schön, A., Princiotto, A.M., Lalonde, J.M., Courter, J.R., Soeta, T., Ng, D., Wang, L.P., Brower, E.T., Xiang, S.H., et al. (2008). Structure *16*, 1689–1701.

Martin, L., Stricher, F., Missé, D., Sironi, F., Pugnière, M., Barthe, P., Prado-Gotor, R., Freulon, I., Magne, X., Roumestand, C., et al. (2003). Nat. Biotechnol. *21*, 71–76.

Van Herrewege, Y., Morellato, L., Descours, A., Aerts, L., Michiels, J., Heyndrickx, L., Martin, L., and Vanham, G. (2008). J. Antimicrob. Chemother. *61*, 818–826.

Vita, C., Vizzavona, J., Drakopoulou, E., Zinn-Justin, S., Gilquin, B., and Ménez, A. (1998). Biopolymers *47*, 93–100.

Xiang, S.H., Kwong, P.D., Gupta, R., Rizzuto, C.D., Casper, D.J., Wyatt, R., Wang, L.P., Hendrickson, W.A., Doyle, M.L., and Sodroski, J. (2002). J. Virol. *76*, 9888–9899.

HHARI Is One HECT of a RING

Christopher W. Davies[1] and Chittaranjan Das[1,*]
[1]Department of Chemistry, Purdue University, West Lafayette, IN 47907, USA
*Correspondence: cdas@purdue.edu
http://dx.doi.org/10.1016/j.str.2013.05.003

E3 ubiquitin ligases are the last of an enzyme trio that covalently modifies proteins with ubiquitin, facilitating various cellular functions. In this issue of *Structure*, Duda and colleagues provide the structural basis for the autoinhibited Ariadne-family of E3-ubiquitin ligases.

Ubiquitination, a covalent attachment of the 76-amino-acid polypeptide ubiquitin (Ub) to lysine residues of target proteins, is an important post-translational modification that controls a wide range of cellular processes. Three enzymatic systems facilitate covalent modification of proteins by Ub: E1 activating enzymes, E2 conjugating enzymes, and E3 Ub ligases. First, Ub is activated via adenylation by E1 and is linked subsequently to a cysteine residue on the enzyme as a thioester complex. Ub is then transferred to the catalytic cysteine on an E2 via transthiolation. The final step of the ubiquitination cascade involves the transfer of Ub from the thioester-linked E2 enzyme (E2∼Ub) to a Lys residue of the substrate mediated by an E3 ligase. Two distinct mechanisms exist for ligation of Ub to substrates. A homologous to the E6AP

Structure
Previews

carboxy terminus (HECT)-type E3 ligase, so named because of the presence of a C-terminally located HECT domain, transfers Ub from the active-site cysteine of an E2∼Ub complex to the catalytic cysteine within the HECT domain, forming an E3∼Ub thioester intermediate prior to depositing Ub onto a Lys residue of the substrate. The overwhelming majority of E3 ligases in the human genome, however, are RING E3 ligases, which employ a different mechanism. RING E3s contain a RING domain that coordinates a pair of Zn^{2+} ions, which is used to recruit E2∼Ub (Deshaies and Joazeiro, 2009). Contrary to HECT E3s, RING E3s do not have a catalytic residue. Instead, acting solely as a scaffold, they bring the E2∼Ub complex and substrate together, thereby allowing the direct transfer of Ub from the catalytic cysteine of E2s to Lys residues of the substrate.

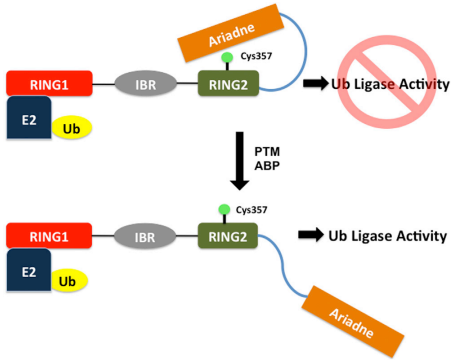

Figure 1. A Cartoon Representation of the Autoinhibited and Active State of the RBR E3 Ligase, HHARI
The C-terminal Ariadne domain of HHARI folds back onto RING2, capping the catalytic cysteine (Cys357), resulting in autoinhibition of ligase activity even when RING1 is bound to Ub∼E2. Ligase activity is presumed to commence upon displacement of Ariadne, likely resulting from either posttranslational modification (PTM) or binding of an unknown Ariadne binding protein (ABP), leaving the catalytic cysteine exposed for Ub transfer.

In the past, eukaryotic E3s have been classified as HECT or RING ligases, with distinct mechanistic features, according to their structure. But recently, in a significant work, Wenzel et al. (2011) provided first evidence in support of a RING-HECT hybrid mechanism used by the novel RING1-in-between-ring (IBR)-RING2 (RBR) ligase human homolog of Ariadne (HHARI), the founding member of a group of conserved eukaryotic ligases. The well-known members of this group now include the Parkinson's disease (PD)-associated protein Parkin, which is linked to autosomal recessive juvenile PD, and linear Ub chain assembly complex (LUBAC), which functions in NF-κB signaling. RBR E3s can be characterized by a canonical RING1 domain, typical of those found in RING E3s, and the presence of additional IBR domain followed by the RING2 domain, which defines them as a unique group of ligases. Like the RING domain of RING E3s, the RING1 domain is known to recruit E2∼Ub, with the proposed HECT type of mechanism arising due to the presence of an invariant cysteine in the RING2 domain, which is thought to form a thioester intermediate with Ub taken from the active-site cysteine of the E2 before ultimately transferring it to a Lys residue on the substrate. Although biochemical evidence supported the RING-HECT hybrid mechanism (Wenzel et al., 2011), structural understanding of this unique class of ligases remained elusive. Structures of RING1, IBR, and RING2 domains from different RBRs have been characterized before, but not together in a full-length construct. Previous biochemical studies with RBRs showed that the full-length proteins are incapable of catalytic activity, but constructs encompassing the RBR core are capable of autoubiquitination, a biochemical read-out of their enzymatic activity. This suggests that full-length RBRs are autoinhibited, but the structural basis of this was not known.

In this issue of *Structure*, Duda et al. (2013) provide the first X-ray crystal structure of full-length HHARI, an Ariadne family of RBR E3 Ub ligases. Like Parkin and HOIP (one of the RBRs of the heterodimeric LUBAC E3), the full-length HHARI remains in an inactive state, but unlike Parkin, HHARI is still capable of binding to E2, suggesting that the protein is in a conformation that prevents its E3 ligase activity. HHARI is an extended 90 Å-long assembly of multiple domains: a UBA-like domain comprised of a three-helix bundle, RING1, a two-helix RING1-to-IBR linker, the IBR, RING2, and the Ariadne domain. The IBR and RING1 domains within the full-length structure are superimposible with previously determined structures. RING2, however, has a novel Zn^{2+}-binding fold containing eight cysteines, seven of which are involved in Zn^{2+} coordination, with the lone unliganded cysteine, Cys357, required for autoubiquitination of HHARI.

The structural basis for HHARI autoinhibition arises from the C-terminal Ariadne domain effectively capping RING2, thus masking the catalytic cysteine, rendering it unable to be ubiquitinated. The Ariadne domain buries 1,000 $Å^2$ of total surface on top of RING2, forming 122 contacts. When the Ariadne domain was deleted from HHARI, a reversal of the autoinhibited state was seen, and a complementary experiment showed that an isolated Ariadne domain also inhibits Ub transfer when added in *trans* to a construct of HHARI lacking the Ariadne domain, suggesting that the release of the Ariadne domain promotes E2-E3 Ub transfer.

The X-ray structure of HHARI reported here by Duda et al. (2013) provides unambiguous evidence showing that the inherent lack of HHARI's E3 ligase activity is hardwired in its structure. A similar mechanism of autoinhibition is perhaps used by other members of the Ariadne family of RBRs as well, although it remains to be demonstrated. Almost coinciding with this report, the X-ray structure of full-length Parkin is also being reported (Trempe et al., 2013). The structure of Parkin reveals one more example of an autoinhibited RBR E3. In Parkin, both the E2 binding site on RING1 and the catalytic site on RING2 are blocked by close packing against other domains unique to this protein (Trempe et al., 2013). Together, these structural studies strongly indicate that autoinhibition may be a common property of RBR E3s, perhaps to avoid autoubiquitination that may render these

Structure
Previews

enzymes susceptible to rapid, untimely degradation by proteasome, as speculated by Duda et al. (2013).

This full-length HHARI structure, like Parkin, drives the field into pondering the mechanism for activation. Parkin undergoes PINK1-dependent phosphorylation to turn into an active form; however, the mechanism is not fully understood (Trempe et al., 2013). Similarly, the Ariadne domain needs to be removed from RING2 to undergo thioester bond formation and subsequent Ub ligase activity, which, as the authors suggest, could be facilitated either by a post-translational modification or an Ariadne binding partner (Figure 1). Future studies will show us the mechanism of catalytic activation of these intriguing ligases. The structures of HHARI and Parkin lay the foundation of an exciting array of further structural work that will reveal mechanistic details of RING-HECT hybrid catalysis of Ub transfer.

ACKNOWLEDGMENTS

Financial support from the American Heart Association Predoctoral fellowship (12PRE12060249) to C.W.D. is gratefully acknowledged, and financial support from the National Institutes of Health (1R01RR026273) is gratefully acknowledged.

REFERENCES

Deshaies, R.J., and Joazeiro, C.A. (2009). Annu. Rev. Biochem. *78*, 399–434.

Duda, D.M., Olszewski, J.L., Schuermann, J.P., Kurinov, I., Miller, D.J., Nourse, A., Alpi, A.F., and Schulman, B.A. (2013). Structure *21*, this issue, 1030–1041.

Trempe, J.F., Sauve, V., Grenier, K., Seirafi, M., Tang, M.Y., Menade, M., Al-Abdul-Wahid, S., Krett, J., Wong, K., Kozlov, G., et al. (2013). Science. Published online May 9, 2013. http://dx.doi.org/10.1126/science.1237908.

Wenzel, D.M., Lissounov, A., Brzovic, P.S., and Klevit, R.E. (2011). Nature *474*, 105–108.

Analytical Biochemistry 440 (2013) 71–77

Contents lists available at SciVerse ScienceDirect

Analytical Biochemistry

journal homepage: www.elsevier.com/locate/yabio

High-throughput compatible fluorescence resonance energy transfer-based assay to identify small molecule inhibitors of AMSH deubiquitinase activity

Jamie L. Arnst [a], Christopher W. Davies [b], Srikumar M. Raja [a], Chittaranjan Das [b], Amarnath Natarajan [a,c,d,*]

[a] Eppley Institute for Cancer Research and Allied Diseases, University of Nebraska Medical Center, Omaha, NE 68198, USA
[b] Brown Laboratory of Chemistry, Department of Chemistry, Purdue University, West Lafayette, IN 47907, USA
[c] Department of Genetics, Cell Biology and Anatomy, University of Nebraska Medical Center, Omaha, NE 68198, USA
[d] Department of Pharmaceutical Sciences, University of Nebraska Medical Center, Omaha, NE 68198, USA

ARTICLE INFO

Article history:
Received 25 October 2012
Received in revised form 17 May 2013
Accepted 23 May 2013
Available online 5 June 2013

Keywords:
HTS
FRET
Deubiquitinase assay
AMSH

ABSTRACT

Deubiquitinases (DUBs) play an important role in regulating the ubiquitin landscape of proteins. The DUB AMSH (associated molecule with the SH3 domain of STAM) has been shown to be involved in regulating the ubiquitin-dependent down-regulation of activated cell surface receptors via the endolysosomal degradative pathway. Therefore, small molecule AMSH inhibitors will be useful chemical probes to study the effect of AMSH DUB activity on cell surface receptor degradation. Currently, there are no known selective inhibitors of AMSH or high-throughput compatible assays for their identification. We report the development and optimization of a novel fluorescence resonance energy transfer (FRET)-based add-and-read AMSH DUB assay in a 384-well format. In this format, the optimal temperature for a high-throughput screen (HTS) was determined to be 30 °C, the assay tolerates 5% dimethyl sulfoxide (DMSO), and it has a *Z*-score of 0.71, indicating HTS compatibility. The assay was used to show that AMSH selectively cleaves Lys63-linked diubiquitin over Lys48- and Lys11-linked diubiquitin. The IC_{50} value of the nonspecific small molecule DUB inhibitor *N*-ethylmaleimide was 16.2 ± 3.2 μM and can be used as a qualitative positive control for the screen. We conclude that this assay is high-throughput compatible and can be used to identify novel small molecule inhibitors of AMSH.

Ubiquitination of proteins has been implicated in numerous biological pathways, including (but not limited to) cell cycle regulation, DNA damage, and endocytosis [1–4]. Ubiquitin molecules are ligated to their target proteins as both mono- and polyubiquitin chains. The diversity in the linkages (eight different linkages) in the polyubiquitin chains facilitates the relay of a variety of signals [4,5]. Deubiquitinases (DUBs)[1] cleave the isopeptide bond in the polyubiquitin chain or the protein–ubiquitin linkage to further regulate ubiquitin-mediated signaling [4,6]. DUBs are part of multiprotein complexes and have both enzymatic and scaffolding functions. Their knockdown not only eliminates the enzymatic function but also disrupts the scaffolding functions, resulting in the dysfunction of the entire complex. DUB activity-specific small molecule inhibitors will provide the precision to specifically study the role of enzymatic functions within these multiprotein complexes. Recent studies have also implicated DUBs in several diseases, particularly cancer, and targeting DUBs for therapeutic intervention is an emerging theme [7,8].

AMSH (associated molecule with the SH3 domain of STAM) plays a key role in regulating receptor sorting at the endosome through its function as a DUB [9–11]. AMSH belongs to the JAMM (JAB1/MPN/MOV34) DUB family and specifically cleaves Lys63-linked polyubiquitin [12,13]. Through interactions at multiple points in endocytic cargo sorting, AMSH plays a critical regulatory role in cell surface receptor down-regulation [14,15]. Down-regulation is accomplished through the recognition of specific ubiquitination patterns on internalized receptors, specifically multi-monoubiquitination and Lys63 polyubiquitination [3,11]. Spatial and temporal dysregulation of AMSH-mediated deubiquitination of internalized ubiquitinated cell surface receptors affects their sorting to the lysosome. Consistently, knockdown of endogenous AMSH or overexpression of catalytically inactive AMSH mutants has been shown to promote the lysosomal degradation of epidermal growth factor receptor (EGFR) as well as other cell surface receptors [16–22]. Small molecule inhibitors of AMSH will be valuable chemical probes for dissecting endocytic cargo sorting.

* Corresponding author at: Eppley Institute for Cancer Research and Allied Diseases, University of Nebraska Medical Center, Omaha, NE 68198, USA. Fax: +1 402 559 8270.
E-mail address: anatarajan@unmc.edu (A. Natarajan).

[1] *Abbreviations used:* DUB, deubiquitinase; AMSH, associated molecule with the SH3 domain of STAM; EGFR, epidermal growth factor receptor; HTS, high-throughput screen; FRET, fluorescence resonance energy transfer; DTT, dithiothreitol; RFU, relative fluorescence units; DMSO, dimethyl sulfoxide; NEM, *N*-ethylmaleimide.

0003-2697/$ - see front matter © 2013 Elsevier Inc. All rights reserved.
http://dx.doi.org/10.1016/j.ab.2013.05.017

Currently, there are no known inhibitors of AMSH and no report of a high-throughput compatible assay for the identification of potential inhibitors.

AMSH alone has been shown to have DUB activity in cell-free assays, making it suitable for high-throughput screens (HTSs) [13,23–25]. There are many assay types used in high-throughput formats to identify inhibitors of enzymes such as proteases [26,27]. The ease of execution and cost per well has made fluorescence-based assays a popular choice in the HTS community. Our laboratory previously reported the development of fluorescence polarization assays and HTSs to identify inhibitors of protein–protein interactions [28–30]. Because it is known that AMSH cleaves Lys63 ubiquitin chains, we chose to explore a fluorescence resonance energy transfer (FRET)-based system [13,23–25]. In a typical FRET assay, the donor and acceptor/quencher are spaced by a suitable linker that, when cleaved, results in the loss of FRET/gain in fluorescence. The catalytic domain of AMSH and a Lys63-linked diubiquitin probe labeled with a donor and a quencher on different ubiquitins was used in this study. The development and optimization of a FRET-based high-throughput compatible AMSH assay is reported. Importantly, this assay can be easily modified for other DUBs that demonstrate linkage-specific cleavage, which might not readily cleave other commercially available ubiquitin probes.

Materials and methods

General reagents

All FRET-labeled diubiquitin probes were purchased from BostonBioChem (R&D) and were stored in 50 mM Hepes (pH 7.5), 150 mM NaCl, and 2 mM dithiothreitol (DTT). The catalytic domain of AMSH (residues 219–424) was expressed and purified as described previously and stored in 50 mM Tris (pH 7.4), 50 mM NaCl, and 1 mM DTT [24]. All concentrations shown in parentheses are final assay concentrations. Anti-ubiquitin antibody (P4D1) was obtained from Cell Signaling.

DUB assay

All measurements were made on 384-well, low-volume, black, round-bottom polystyrene NBS microplates (Corning) using a SpectraMax M5 plate reader (MDS). All reactions were done in reaction buffer (50 mM Hepes [pH 7.0], 25 mM KCl, 5 mM $MgCl_2$, and 1 mM DTT) in a final volume of 20 μl [24]. Measurements were taken at an excitation wavelength of 544 nm and an emission wavelength of 572 nm, and the cutoff was set at 570 nm. The reported fluorescence values (relative fluorescence units, RFU) are a ratio of total fluorescent signal to the background obtained from the probe alone. All experiments were performed at least twice and each time as duplicates.

Dose–response and time-dependent studies of AMSH and K63POS1 probe

AMSH was titrated (15.6–250 nM) into a constant concentration of K63POS1 probe (500 nM), and the DUB reaction was monitored over time at 15-min intervals for 2 h at 30 °C. The optimal probe concentration was determined by titrating K63POS1 probe (200–600 nM) while holding the concentration of AMSH constant at 125 nM. The plate was read following a 90-min incubation. The relationship between product formation and fluorescence was determined by incubating 10 μM K63POS1 probe with 5 μM AMSH overnight at room temperature. Cleaved probe was then diluted 2-fold in reaction buffer followed by fluorescent measurements.

DMSO tolerance

Increasing concentrations of dimethyl sulfoxide (DMSO, 0.5–25% of the assay volume, 20 μl) was added to AMSH (125 nM), and the mixture was incubated for 30 min. K63POS1 probe (500 nM) was then added to the reaction mixture and incubated for an additional 90 min at 30 °C, and measurements were made. Statistics were performed using a Student's *t* test.

NEM inhibition assay

Increasing concentrations of *N*-ethylmaleimide (NEM, 0.8–500 μM) were added to AMSH (125 nM) with a 1:9 ratio of volumes and incubated at room temperature for 30 min. Then 10 μl of K63POS1 probe (500 nM) was added to bring the assay volume to 20 μl. Fluorescence measurements were made after a 90-min incubation at 30 °C. The data were fitted and the IC_{50} values were derived using nonlinear least squares fit to a single site-binding model (SigmaPlot 11.0). NEM time-dependent inhibition was performed by incubating AMSH (125 nM) with 15 or 30 μM NEM for 1 h, 45 min, 30 min, or 15 min at room temperature. The K63POS1 probe was then added and incubated for 90 min at 30 °C.

The effect of NEM on the K63POS1 probe fluorescence was determined by incubating cleaved or uncleaved probe with NEM (0–500 μM) for 90 min at 30 °C. Cleaved probe for this study was generated as described in the "Dose–response and time-dependent studies of AMSH and K63POS1 probe" section above.

Z-Score

AMSH (125 nM) was incubated for 30 min with or without 25 μM NEM at room temperature. K63POS1 probe (500 nM) was then added to AMSH, AMSH + NEM, and buffer-only wells for 90 min at 30 °C before taking fluorescence measurements. Plates were then sealed and incubated at 4 °C overnight for the 24-h measurement. Data from the 384-well plates were collected on separate days, with 48 data points for each condition per day. The *Z*-score was calculated using AMSH + K63POS1 probe as the negative control and K63POS1 probe alone as the positive control.

Results and discussion

Selective cleavage of Lys63-linked diubiquitin probe by AMSH

Several DUBs have been shown to possess linkage-specific cleavage, including members of the JAMM family [5]. AMSH has been shown to selectively cleave Lys63-linked polyubiquitin chains [13,23–25]. The catalytic domain of AMSH and a diubiquitin FRET probe in which the donor and quencher are placed on different ubiquitins linked by the Lys63 isopeptide bond was used to establish the AMSH assay. To identify a suitable probe and demonstrate AMSH's cleavage selectivity, the catalytic domain of AMSH was incubated with five different diubiquitin probes (K11POS4, K48POS1, K48POS3, K63POS1, and K63POS3) that have three different linkages (Lys11, Lys48, and Lys63) (Fig. 1A–C, respectively). Fig. 1 shows the distance between the closest and farthest Lys residues on adjacent ubiquitins. Cleavage of the probes was assessed by the change in fluorescence following a 1-h incubation with AMSH (Fig. 2). The cleavage was also confirmed by sodium dodecyl sulfate–polyacrylamide gel electrophoresis (SDS–PAGE; see Fig. S1 in Supplementary material). No change was observed in the fluorescence reading in the presence of AMSH (Fig. 2, gray bars) with K11POS4, K48POS1, and K48POS3 probes compared with probe alone (Fig. 2, black bars), indicating that AMSH did not cleave the Lys11- or Lys48-linked probes. Approximately 4- and 3-fold

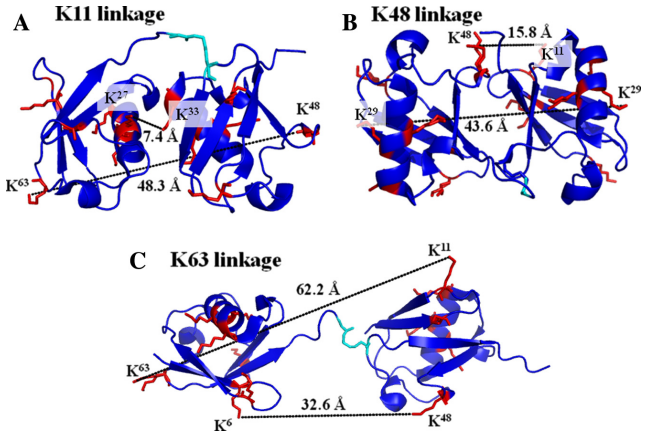

Fig.1. Diubiquitin structures. Shown are structures of K11 diubiquitin (A), K48 diubiquitin (B), and K63 diubiquitin (C), with the lysine residues (red) and the isopeptide bond (cyan) shown as sticks. The largest and smallest distances between lysine residues on the proximal and distal ubiquitins are shown. (For interpretation of the references to color in this figure legend, the reader is referred to the Web version of this article.)

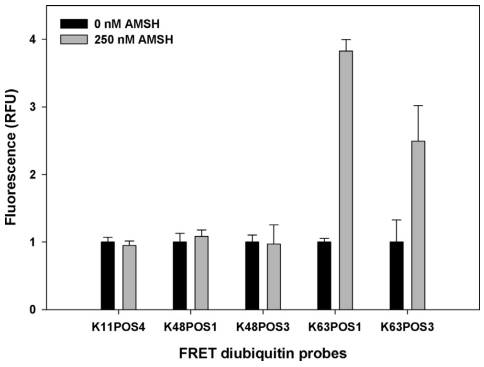

Fig.2. AMSH probe selection. Diubiquitin probes of different linkages (final concentration of 500 nM) were incubated with (gray bars) or without (black bars) 250 nM AMSH for 30 min at 30 °C ($n = 2$).

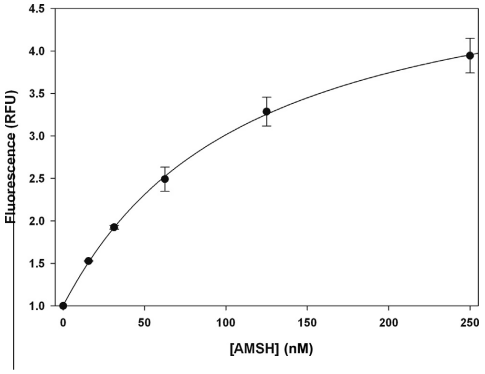

Fig.3. The fluorescence signal is dose dependent. AMSH was titrated (0–125 nM) into 500 nM K63POS1 probe and incubated for 2 h at 30 °C ($n = 2$).

increases in the fluorescence were observed with the K63POS1 and K63POS3 probes, respectively. This increase in fluorescence demonstrates that Lys63-linked diubiquitin is cleaved by AMSH. The difference in the fold change between the two Lys63 probes is likely due to the different positions of the donor/quencher pair, where POS3 may interfere with cleavage by AMSH (Fig. 1C). K63POS1 probe had the larger signal window and, therefore, was used as the probe for all subsequent studies. The selectivity of substrate from the FRET study was consistent with the observed cleavage by Western blot analysis and previously reported studies showing that AMSH preferentially cleaves Lys63-linked polyubiquitin chains over Lys48-linked polyubiquitin chains [13–15,23–25].

AMSH FRET assay optimization

Next, to optimize the concentration of reagents and time of incubation to be used for a screen, we conducted dose–response and time-dependent studies. A dose-dependent increase in the fluorescence was observed with increasing concentrations of AMSH (0–250 nM), with the signal beginning to saturate at 250 nM (Fig. 3). For subsequent studies, we selected 125 nM AMSH because this provided a reasonable signal window while minimizing reagents. The time-dependent increase in the cleavage of the K63POS1 probe was monitored over 2 h (Fig. 4). The fluorescent signal was linear up to 90 min, after which it began to plateau due to complete consumption of K63POS1 probe. Therefore, for the above concentrations of enzyme and substrate, we concluded that an incubation time of 90 min will yield the largest signal window while still in the linear range. Next, we performed a dose-dependent study with the K63POS1 probe. We observed increased signal with increasing K63POS1 probe concentrations, which plateaued at 500 nM at 90 min (Fig. 5A, gray bars). To determine whether this saturation was an artifact of the detection system, the K63POS1 probe was incubated with AMSH overnight to generate cleaved ubiquitin, which was then titrated in reaction buffer,

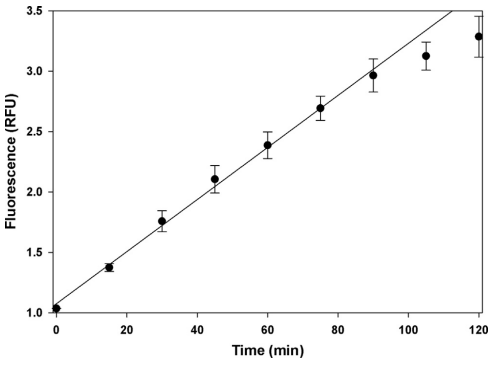

Fig.4. The fluorescence signal is time dependent. AMSH (125 nM) was incubated with 500 nM K63POS1 probe at 30 °C. The signal was monitored over 2 h ($n = 2$).

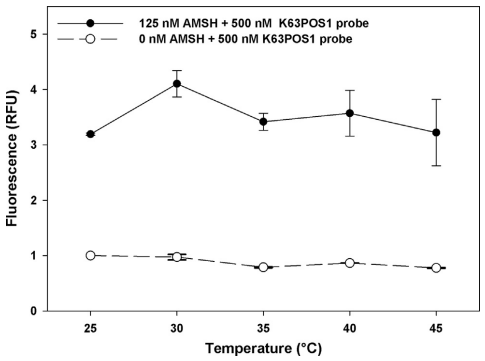

Fig.6. Temperature dependence of AMSH DUB activity. K63POS1 probe (500 nM) was incubated either with or without AMSH (125 nM) for each temperature. For each temperature, measurements were taken following a 90-min incubation of AMSH and probe ($n = 2$).

and fluorescence was measured. We observed a linear relationship between probe concentration and fluorescence (Fig. 5B), suggesting that the saturation observed in Fig. 5A is not an artifact of the detection system. In this study, we also observed a smaller dose-dependent increase in the noise with increasing K63POS1 probe concentrations (Fig. 5A, black bars). Although the best signal to noise (~4) was observed at both 200 and 500 nM of the K63POS1 probe, for subsequent studies we selected the 500-nM concentration because it provided a larger screening window (~9 vs. ~3).

Temperature dependence

Screening large libraries takes several days to complete, and there are always fluctuations despite the best climate-controlled environment; therefore, we next assessed the effect of temperature on the stability of this assay. This was accomplished by incubating the K63POS1 probe with and without AMSH at five different temperatures (25–45 °C) for 90 min (Fig. 6). With increasing temperatures, we observed a significant increase in the variability of the AMSH + K63POS1 fluorescent signal, particularly at temperatures above 40 °C, but little change in probe alone. This indicates that temperatures should not exceed 40 °C during an HTS. In addition, we observed variation in the signal window, with the largest window seen at 30 °C. Although at 25 °C we observed less fluctuation in the signal with AMSH, we conclude that 30 °C is optimal because it results in a larger screening window in this assay format.

DMSO tolerance

DMSO is a widely used solvent for small molecules, and commercially available chemical libraries used in screening campaigns are commonly shipped as DMSO solutions. Thus, the effect of DMSO on the assay was assessed. Increasing concentrations of DMSO were titrated into a constant concentration of AMSH and incubated for 30 min. The K63POS1 probe was then added, and the resulting mixture was incubated for an additional 90 min (Fig. 7). We observed a small but significant increase in the background at 5% DMSO, with much larger effects at higher DMSO concentrations (Fig. 7, black bars). In addition, a significant decrease in the signal at 10% DMSO (Fig. 7, gray bars) was observed. This suggests that DMSO has a significant effect on the assay, particularly as it relates to the screening window. Based on these observations,

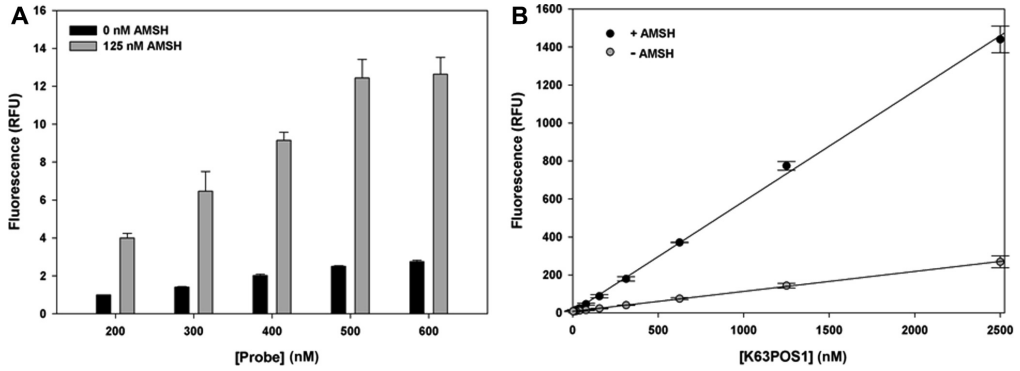

Fig.5. (A) Optimization of K63POS1 probe concentration. AMSH concentration was held constant at 125 nM, and K63POS1 probe was titrated in and incubated at 30 °C for 90 min ($n = 2$). (B) Linear relationship between monoubiquitin formation and fluorescence. K63POS1 probe (10 μM) was incubated with or without 10 μM AMSH overnight. Cleaved probe was then titrated in buffer (2.5–2.5 μM) ($n = 2$).

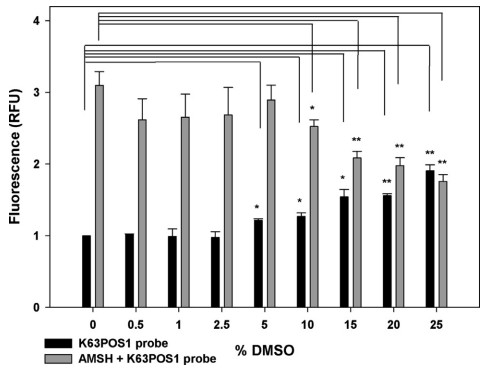

Fig.7. Assay stability in the presence of increasing DMSO concentrations. Increasing concentrations of DMSO were added to AMSH (125 nM) and incubated for 30 min before the addition of K63POS1 probe (500 nM). After a 90-min incubation with K63POS1 probe, fluorescence measurements were taken. $^{*}P \leqslant 0.035$; $^{**}P \leqslant 0.008$ ($n = 2$).

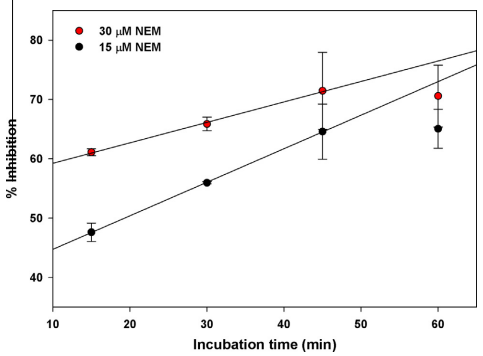

Fig.9. Time-dependent inhibition by NEM. AMSH (125 nM) was incubated with either 15 or 30 μM NEM for 1 h, 45 min, 30 min, or 15 min, followed by the addition of K63POS1 probe (500 nM). Fluorescent measurements were taken following a 90-min incubation at 30 °C ($n = 2$).

we conclude that the assay does not tolerate DMSO above 5% and that during an HTS DMSO concentrations should be kept to a minimum and should not exceed 5%.

Inhibition studies

Currently, there are no known selective inhibitors of AMSH; however, a positive control is desirable for a high-throughput screening campaign. A previous study showed that the nonselective Michael acceptor, NEM, inhibits AMSH, possibly by reacting with Cys282 near the active site [13]. Therefore, to demonstrate that small molecules can inhibit AMSH in this FRET-based assay format, we determined the effects of NEM in the AMSH FRET assay (Fig. 8). AMSH was incubated with different concentrations of NEM (5-fold dilutions) for 30 min at room temperature. The K63POS1 probe was then added, and the mixture was incubated for an additional 90 min at 30 °C. Fluorescence measurements revealed a dose-dependent decrease with increasing concentrations of NEM, indicating inhibition of AMSH (Fig. 8). The IC_{50} value (16.2 ± 3.1 μM) for NEM was determined by curve fitting the data.

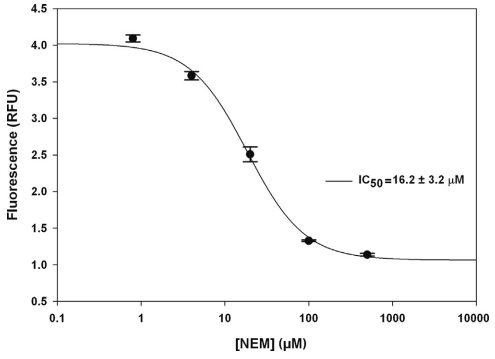

Fig.8. Inhibition by NEM. Fivefold dilutions of NEM were incubated with AMSH (125 nM) for 30 min at room temperature, followed by the addition of K63POS1 probe (500 nM). The plate was then read following a 90-min incubation at 30 °C. IC_{50} = 16.2 ± 3.1 μM ($n = 2$).

We also observed a time-dependent effect of AMSH inhibition by NEM at 15 μM (~IC_{50}) and 30 μM (~2 × IC_{50}) (Fig. 9). Increasing inhibition by NEM was observed up to 45 min of incubation with AMSH, after which saturation was observed. This is likely due to all available NEM having reacted with AMSH at these concentrations. In addition, to confirm that NEM was not affecting the FRET signal of the K63POS1 probe, we incubated increasing concentrations of NEM (0–500 μM) with cleaved or uncleaved K63POS1 probe (Fig. 10). We observed no significant effects on the fluorescent signal in the presence of NEM. Because AMSH belongs to the JAMM family of DUBs that are Zn metalloproteases, the chelation agents phenanthroline and 2,2′-bipyridine were also tested in this assay (data not shown). To our surprise, we observed inhibition of AMSH only at very high concentrations (>1 mM) of the compounds. Based on these findings, we suggest NEM as a qualitative positive control for high-throughput screening campaigns to identify reversible inhibitors. To identify hits from a high-throughput screening campaign, fluorescence values that are 3 standard deviations (99% confidence) from the mean of the negative control (DMSO) should be used and validated in subsequent dose–response studies.

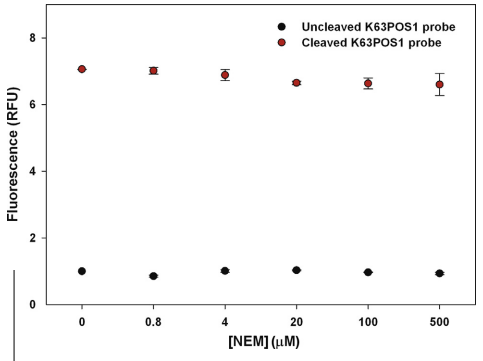

Fig.10. Effect of NEM on K63POS1 probe fluorescence. Increasing concentrations of NEM (0–500 μM) were incubated for 90 min at 30 °C with cleaved or uncleaved K63POS1 probe before fluorescent measurements were taken ($n = 2$).

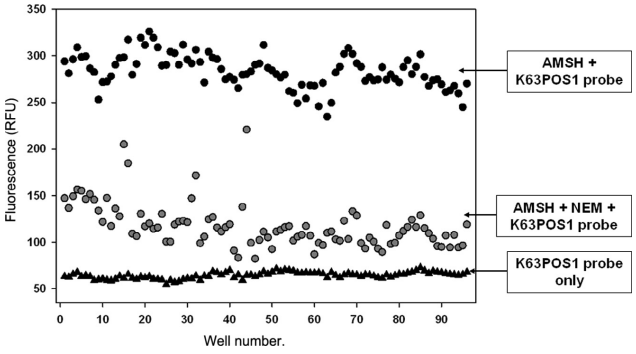

Fig.11. *Z*-score determination. K63POS1 probe was incubated with either buffer, AMSH, or AMSH + 25 μM NEM on separate days and plates. An overall *Z*-score of 0.71 was calculated. Well numbers 1–48 are from day 1, and well numbers 49–96 are from day 2 ($n = 2$).

Z-Score

The suitability of an assay for high-throughput screening is established by the non-unit statistical parameter *Z*-score [31]. It is generally accepted that the *Z*-score reflects reproducibility, robustness, and reliability of an assay for high-throughput screening. The *Z*-score for a given assay ranges from 0 to 1, with 1 being ideal and a score $\geqslant 0.5$ generally considered as suitable for high-throughput screening. To determine the *Z*-score and inter- and intra-plate variability for this assay, measurements were made with K63POS1 probe only, AMSH + K63POS1 probe, and AMSH + K63-POS1 probe treated with 25 μM NEM for 120 min (Fig. 11) on separate days in different 384-well plates. The average *Z*-score was 0.71, indicating that the assay is reproducible, robust, and reliable and thus is high-throughput compatible. In addition, following a 24-h incubation at 4 °C, the plates were reread (data not shown). There was no significant difference in the overall *Z*-score of the plates; however, there were increases in the fluorescence of AMSH + K63POS1 probe and AMSH + K63POS1 probe treated with NEM wells by approximately 9% and 30%, respectively. These increases in fluorescence are likely due to the cleavage of K63POS1 probe by AMSH over time even in the presence of inhibitor. Due to the potential variability in incubation times of plates during an HTS, internal plate controls should be used to normalize for AMSH activity.

In summary, using a FRET-based system, we showed that AMSH selectively cleaves Lys63-linked diubiquitin over Lys48- and Lys11-linked diubiquitin. The FRET AMSH assay was miniaturized to a 384-well format, with the optimal temperature for the screen determined to be 30 °C, and the maximum DMSO concentration tolerated was determined to be 5%. Furthermore, the *Z*-score for this assay was 0.71, which indicates high-throughput compatibility. Lastly, the reagents for this assay can be readily generated for an HTS, with the major expense being the linkage-specific FRET probe.

Acknowledgments

We thank Elizabeth C. Blowers for editing the manuscript. Funding was provided in part by the Eppley Cancer Center, the Nebraska Research Initiative, and a GAANN (Graduate Assistance in Areas of National Need) predoctoral fellowship (to J.L.A.). S.M.R. acknowledges support from the Nebraska Center for Nanomedicine–Center for Biomedical Research Excellence (NCN–COBRE) seed Grant. An American Heart Association predoctoral fellowship to C.W.D. and Grant 1R01RR026273 to C.D. are gratefully acknowledged.

Appendix A. Supplementary data

Supplementary data associated with this article can be found, in the online version, at http://dx.doi.org/10.1016/j.ab.2013.05.017.

References

[1] K. Wickliffe, A. Williamson, L. Jin, M. Rape, The multiple layers of ubiquitin-dependent cell cycle control, Chem. Rev. 109 (2009) 1537–1548.
[2] T.E. Messick, R.A. Greenberg, The ubiquitin landscape at DNA double-strand breaks, J. Cell Biol. 187 (2009) 319–326.
[3] D. Mukhopadhyay, H. Riezman, Proteasome-independent functions of ubiquitin in endocytosis and signaling, Sci. Signal. 315 (2007) 201–205.
[4] D. Komander, M. Rape, The ubiquitin code, Annu. Rev. Biochem. 81 (2012) 203–229.
[5] D. Komander, The emerging complexity of protein ubiquitination, Biochem. Soc. Trans. 37 (2009) 937–953.
[6] D. Komander, M.J. Clague, S. Urbé, Breaking the chains: structure and function of the deubiquitinases, Nat. Rev. Mol. Cell Biol. 10 (2009) 550–563.
[7] J. Fraile, V. Quesada, D. Rodríguez, J. Freije, C. López-Otín, Deubiquitinases in cancer: new functions and therapeutic options, Oncogene 31 (2011) 2373–2388.
[8] B. Nicholson, J.G. Marblestone, T.R. Butt, M.R. Mattern, Deubiquitinating enzymes as novel anticancer targets, Future Oncol. 3 (2007) 191–199.
[9] N. Tanaka, K. Kaneko, H. Asao, H. Kasai, Y. Endo, T. Fujita, T. Takeshita, K. Sugamura, Possible involvement of a novel STAM-associated molecule "AMSH" in intracellular signal transduction mediated by cytokines, J. Biol. Chem. 274 (1999) 19129–19135.
[10] M.J. Clague, S. Urbé, Endocytosis: the DUB version, Trends Cell Biol. 16 (2006) 551–559.
[11] M.H. Wright, I. Berlin, P.D. Nash, Regulation of endocytic sorting by ESCRT–DUB-mediated deubiquitination, Cell Biochem. Biophys. 60 (2011) 39–46.
[12] S. Nijman, M. Luna-Vargas, A. Velds, T.R. Brummelkamp, A.M.G. Dirac, T.K. Sixma, R. Bernards, A genomic and functional inventory of deubiquitinating enzymes, Cell 123 (2005) 773–786.
[13] J. McCullough, M.J. Clague, S. Urbé, AMSH is an endosome-associated ubiquitin isopeptidase, J. Cell Biol. 166 (2004) 487–492.
[14] M. Kyuuma, K. Kikuchi, K. Kojima, Y. Sugawara, M. Sato, N. Mano, J. Goto, T. Takeshita, A. Yamamoto, K. Sugamura, AMSH, an ESCRT-III associated enzyme, deubiquitinates cargo on MVB/late endosomes, Cell Struct. Funct. 31 (2006) 159–172.
[15] M. Nakamura, N. Tanaka, N. Kitamura, M. Komada, Clathrin anchors deubiquitinating enzymes, AMSH and AMSH-like protein, on early endosomes, Genes Cells 11 (2006) 593–606.
[16] Y.M. Ma, E. Boucrot, J. Villén, S.P. Gygi, H.G. Göttlinger, T. Kirchhausen, Targeting of AMSH to endosomes is required for epidermal growth factor receptor degradation, J. Biol. Chem. 282 (2007) 9805–9812.
[17] I.M.J. Meijer, W. van Rotterdam, E.J.J. van Zoelen, J.E.M. van Leeuwen, Recycling of EGFR and ErbB2 is associated with impaired Hrs tyrosine phosphorylation and decreased deubiquitination by AMSH, Cell. Signal. 24 (2012) 1981–1988.

[18] B. Hasdemir, J.E. Murphy, G.S. Cottrell, N.W. Bunnett, Endosomal deubiquitinating enzymes control ubiquitination and down-regulation of protease-activated receptor 2, J. Biol. Chem. 284 (2009) 28453–28466.
[19] F. Herrera-Vigenor, R. Hernández-García, M. Valadez-Sánchez, J. Vázquez-Prado, G. Reyes-Cruz, AMSH regulates calcium-sensing receptor signaling through direct interactions, Biochem. Biophys. Res. Commun. 347 (2006) 924–930.
[20] J.N. Hislop, A.G. Henry, A. Marchese, M. Von Zastrow, Ubiquitination regulates proteolytic processing of G protein-coupled receptors after their sorting to lysosomes, J. Biol. Chem. 284 (2009) 19361–19370.
[21] A.P. Reyes-Ibarra, A. García-Regalado, I. Ramírez-Rangel, A.L. Esparza-Silva, M. Valadez-Sánchez, J. Vázquez-Prado, G. Reyes-Cruz, Calcium-sensing receptor endocytosis links extracellular calcium signaling to parathyroid hormone-related peptide secretion via a Rab11a-dependent and AMSH-sensitive mechanism, Mol. Endocrinol. 21 (2007) 1394–1407.
[22] M.I. Sierra, M.H. Wright, P.D. Nash, AMSH interacts with ESCRT-0 to regulate the stability and trafficking of CXCR4, J. Biol. Chem. 285 (2010) 13990–14004.
[23] M.S. Kim, J.A. Kim, H.K. Song, H. Jeon, STAM–AMSH interaction facilitates the deubiquitination activity in the C-terminal AMSH, Biochem. Biophys. Res. Commun. 351 (2006) 612–618.
[24] C.W. Davies, L.N. Paul, M.I. Kim, C. Das, Structural and thermodynamic comparison of the catalytic domain of AMSH and AMSH-LP: nearly identical fold but different stability, J. Mol. Biol. 413 (2011) 416–429.
[25] J. McCullough, P.E. Row, Ó. Lorenzo, M. Doherty, R. Beynon, M.J. Clague, S. Urbé, Activation of the endosome-associated ubiquitin isopeptidase AMSH by STAM, a component of the multivesicular body-sorting machinery, Curr. Biol. 16 (2006) 160–165.
[26] J. Inglese, R.L. Johnson, A. Simeonov, M. Xia, W. Zheng, C.P. Austin, D.S. Auld, High-throughput screening assays for the identification of chemical probes, Nat. Chem. Biol. 3 (2007) 466–479.
[27] S.J. Goldenberg, J.L. McDermott, T.R. Butt, M.R. Mattern, B. Nicholson, Strategies for the identification of novel inhibitors of deubiquitinating enzymes, Biochem. Soc. Trans. 36 (2008) 828–832.
[28] G. Lokesh, A. Rachamallu, G. Kishore Kumar, A. Natarajan, High-throughput fluorescence polarization assay to identify small molecule inhibitors of BRCT domains of breast cancer gene 1, Anal. Biochem. 352 (2006) 135–141.
[29] E.A. Kumar, C.D. Charvet, G. Lokesh, A. Natarajan, High-throughput fluorescence polarization assay to identify inhibitors of Cbl (TKB)–protein tyrosine kinase interactions, Anal. Biochem. 411 (2011) 254–260.
[30] A. Simeonov, A. Yasgar, A. Jadhav, G. Lokesh, C. Klumpp, S. Michael, C.P. Austin, A. Natarajan, J. Inglese, Dual-fluorophore quantitative high-throughput screen for inhibitors of BRCT–phosphoprotein interaction, Anal. Biochem. 375 (2008) 60–70.
[31] J.H. Zhang, T.D. Chung, K.R. Oldenburg, A simple statistical parameter for use in evaluation and validation of high throughput screening assays, J. Biomol. Screen. 4 (1999) 67–73.

Mechanism of Recruitment and Activation of the Endosome-associated Deubiquitinase AMSH

AUTHOR INFORMATION

*Christopher W. Davies‡, Lake N. Paul‡†, Chittaranjan Das**

Present Addresses

Department of Chemistry, Purdue University, West Lafayette, IN 47907

†Bindley Biosciences Center, Discovery Park, Purdue University, West Lafayette, IN 47907

‡These authors contributed equally.

***Corresponding Author**

Email address: cdas@purdue.edu

765-494-5478 (office)

765-494-0239 (fax)

Funding

This work was funded by the National Institutes of Health (1R01RR026273). CWD thanks the American Heart Association Predoctoral Fellowship (12PRE12060249).

ABBREVIATIONS

AMSH, associated molecule with a Src homology 3 domain of STAM; AMSH-LP, AMSH-like protein; AUC, analytical ultracentrifugation; CD, circular dichroism; DUBs, deubiquitinating

enzymes; ESCRT, endosomal sorting complexes required for transport; ITC, isothermal titration calorimetry; STAM, signal transducing adaptor molecule; MIC-CAP, microcephaly malformation syndrome; UBPY/USP8, ubiquitin specific protease 8.

ABSTRACT

AMSH, a deubiquitinating enzyme (DUB) with exquisite specificity for Lys63-linked polyubiquitin chains, is an endosome-associated DUB that regulates sorting of activated cell-surface signaling receptors to lysosome, a process mediated by the members of the endosomal sorting complexes required for transport (ESCRT) machinery. Whole-exome sequencing of DNA samples from children with microcephaly capillary malformation (MIC-CAP) syndrome identified recessive mutations encoded in the AMSH gene causatively linked to the disease. Herein, we report a number of important observations that significantly advance our understanding of AMSH within the context of the ESCRT machinery. First, we performed mutational and kinetic analysis of the putative residues involved in diubiquitin recognition and catalysis with a view to better understanding the catalytic mechanism of AMSH. Our mutational and kinetic analysis reveals that recognition of the proximal ubiquitin is imperative for the linkage specificity and catalytic efficiency of the enzyme. The MIC-CAP disease mutation, Thr313Ile, shows a substantial loss of catalytic activity without any significant change in thermodynamic stability of the protein, indicating that its perturbed catalytic activity is the basis of the disease. The catalytic activity of AMSH is stimulated upon binding to the ESCRT-0 member STAM, however, the precise mechanism and its significance are not known. Based on a number of biochemical and biophysical analysis, we are able to propose a model for activation according to which activation of AMSH is enabled by facile, simultaneous binding to two

ubiquitin groups in a polyubiquitin substrate, one by the catalytic domain of the DUB (binding to the distal ubiquitin) and the other (the proximal ubiquitin) by the ubiquitin interacting motif (UIM) from STAM. Such a mode of binding would stabilize the ubiquitin chain in a productive orientation, resulting in an enhancement of the activity of the enzyme. These data together provide a mechanism for understanding the recruitment and activation of AMSH at ESCRT-0, providing biochemical and biophysical evidence in support of a role for AMSH when it is recruited to the initial ESCRT complex: it functions to facilitate transfer of ubiquitinated receptors (cargo) from one ESCRT member to the next by disassembling the polyubiquitin chain while leaving some ubiquitin groups still attached to the cargo.

AMSH (associated molecule with a Src homology 3 domain of signal transducing adaptor molecule, STAM) is a member of the JAMM (JAB1/MPN/MOV34) family of deubiquitinating enzymes (DUBs) (*1*), which regulates ubiquitin signaling by catalyzing the hydrolysis of isopeptide (or peptide) bonds between ubiquitin and target proteins or within polymeric chains of ubiquitin. The JAMM family, being one of the five families of mammalian DUBs, are metalloproteases, whereas the others, UCHs, USPs, OTUs, and MJDs) are cysteine proteases (*2-4*). Members of the JAMM family show substantial variation in their overall amino-acid sequence, but share, as the name suggests, a conserved JAMM motif as the catalytic domain. Mechanistically, they share distinct similarities to the extensively studied metalloprotease, thermolysin. Like thermolysin, theses enzymes have a Zn^{2+} in their active site, which is involved in their mechanism of catalysis. The Zn^{2+} ion is coordinated within the active site usually by two histidines, an acidic residue (aspartic acid or glutamic acid), and a water molecule that eventually is used as the nucleophile for attacking the scissile peptide bond. This catalytic water is held in

place by Zn^{2+} and another acidic residue (glutamic acid in AMSH), which provides a hydrogen bond stabilizing the water. Sequence analysis of the members of the JAMM family reveals that only 7 of 14 proteins have the conserved zinc binding capabilities (*5*), while only 6 of those 7 exhibit isopeptidase activity toward ubiquitin and ubiquitin-like proteins, AMSH, AMSH-LP (AMSH like protein), BRCC36, RPN11 (POH1), MYSM1, and CSN5 (*5-7*).

AMSH is one of the two DUBs, the other being UBPY (also known as ubiquitin specific protease 8, USP8) (*8*) known to be important regulators of the ESCRT (endosomal sorting complexes required for transport) complexes (*9*). The ESCRT machinery consist of four protein-protein complexes (ESCRT-0, -I, -II, -III) and the AAA ATPase Vps4 (*10, 11*) that serve several important functions within the cell: endosomal sorting, trafficking, viral budding, cytokinesis, transcriptional regulation, and autophagy (*12*). The ESCRTs were initially discovered in yeast in the context of their role in endosomal sorting and trafficking of cell-surface receptors to lysosome for degradation, as a means for down-regulating their signals (*11*). These receptors are first ubiquitinated, and then, shuttled through the ESCRT machinery, until their internalization within endosomes, which then can fuse with the lysosome delivering the receptors for proteolysis (*11*).

Of the four complexes, only ESCRT-0 and ESCRT-III can specifically recognize DUBs (*9*). The ESCRT-0 recognition is carried out through the binding of the SH3 binding motif (SBM) of DUBs to the SH3 domain of the ESCRT-0 member STAM (*13*), while the ESCRT-III recognition is via the MIT (microtubule interacting and transport) domain of DUBs binding to the C-terminal MIT interacting motifs (MIMs of charged multivesicular body proteins (CHMPs) (*9*). Previous studies have shown that once AMSH binds to STAM, its activity is enhanced (*13, 14*), however, the precise mechanism is not known (*13*). The x-ray crystal structure of the MIT

domain of AMSH bound to the C-terminal MIM fragment of the ESCRT-III member CHMP3 has been determined (*15*). The structure reveals that the AMSH-CHMP3 complex is stabilized mainly by polar interactions, manifesting into tight binding between the two proteins, with a dissociation constant (K_D) of 60 nM, the highest reported K_D for an ESCRT-III MIM -MIT interaction (*15*).

A clear role for AMSH has not been identified yet, however, whole-exome sequencing analysis has shown that recessive mutations in AMSH leads to microcephaly-capillary malformation (MIC-CAP) syndrome (*16*). MIC-CAP is discovered at or shortly after birth in which children diagnosed with the disease have severe microcephaly with progressive cortical atrophy, intractable epilepsy, profound developmental delay and multiple small capillary malformations on the skin (*16-19*). The microcephaly phenotype is attributed to the accumulation of ubiquitinated proteins, suggesting a lost of enzymatic function as was seen in knock-out mice studies (*20*). Out of the ten patients that were screened, six had missense mutations, two had nonsense mutations, two translational frameshift mutations, and three intronic mutations (*16*). Interestingly, five out of the six missense mutations were found within the MIT domain of AMSH, and the sixth, Thr313Ile, found within the JAMM domain (*16*).

Although the exact *in vivo* function of AMSH is not well understood, its exquisite specificity for Lys63-linked polyubiquitin chains, the same type of chain used for endosomal-lysosomal targeting, is well characterized (*21*). The structural basis for this recognition was elucidated with the homologous protein, AMSH-LP, bound to Lys63-linked dimer of ubiquitin (*22*). This structure reveals that the specificity arises from a tri-peptide sequence within the proximal ubiquitin (Gln62, Lys63, and Glu64) interacting directly with a threonine, two phenylalanines, and a serine residue (*22*) on the proximal binding site of the enzyme (in a

diubiquitin motif, the proximal ubiquitin is defined as the one that contributes a Lys residue to be linked to Gly76 of the other ubiquitin, defined as the distal ubiquitin). AMSH and AMSH-LP share 54% identity and 73% sequence similarity, however, AMSH-LP does not have a functional SBM (*9, 23*) nor MIT domain (*24*), therefore, not having the ability to bind to the members of the ESCRT machinery. We recently determined the x-ray crystal structure of the catalytic domain of AMSH, and found that the catalytic domains of AMSH and AMSH-LP are structurally very similar, however, much to our surprise, AMSH is thermodynamically less stable than AMSH-LP, which was attributed to structural plasticity of the former (*25*). This idea of structural plasticity is supported by the second x-ray crystal structure of the catalytic domain of AMSH bearing the active-site glutamate to alanine mutation, which was expected to cause the release of the active-site Zn^{2+}. The structure, however, shows that the tetrahedral coordination around the active-site Zn^{2+} in this mutant is still maintained by a nearby aspartate residue moving in to provide the fourth ligand for the metal in place of the lost water (*25*). Though AMSH and AMSH-LP are able to localize to the endosomes in a similar manner through their ability to bind to clathrin (*13, 26*), the differences between them arising out of AMSH-LP's inability to bind to any of the ESCRT complexes suggests that AMSH and AMSH-LP are not functionally redundant. Moreover, the active-site cleft of AMSH features three substitutions relative to AMSH-LP, substitutions of residues that are predicted to be used for ubiquitin binding. One of them, Thr313, which in AMSH-LP corresponds to Met325, is also the site of a MIC-CAP mutation.

In the present study, we aim to further establish a role for AMSH as an important regulator of the ESCRT machinery. We have carried out extensive mutational and kinetic analysis of residues within the catalytic domain of AMSH to understand their role in ubiquitin

binding to better understand the enzyme's catalytic mechanism. Also, we have studied the effect of the Thr313Ile mutation found in children with the MIC-CAP syndrome on the activity and thermodynamic stability of AMSH with hopes of understanding the molecular basis of the disease. Our results confirmed that residues within the proximal ubiquitin recognition site of AMSH are the basis of specificity for Lys63-linked polyubiquitin chain. Furthermore, we found that of the three residue differences between AMSH and AMSH-LP in the distal ubiquitin-binding site, Thr313 and Glu316 had the most significant effects on AMSH activity. Finally, using the minimal domains required for AMSH activation, we have shed light on the mechanism of AMSH recruitment and activation at ESCRT-0; we found that AMSH is activated due to an intact SBM-SH3 interaction and an intact UIM from STAM. Based on our results, we have proposed a mechanism and role for AMSH in the context of ESCRT-0.

Materials and Methods

Cloning, Expression, and Purification

The DNA encoding the catalytic domain of AMSH was amplified by PCR using a plasmid that contained full-length DNA as the template (pGEX-6p1-AMSH, a kind gift from Sylvie Urbé, University of Liverpool, UK) and was subcloned into pGEX-6p1 (GE Biosciences) by using standard cloning protocols. The resulting N-terminally fused glutathione S-transferase (GST)-tagged protein was expressed in *Escherichia coli* Rosetta cells (Novagen) and purified with a glutathione-Sepharose column (GE Biosciences) following manufacturer's instructions. After removal of the tag by PreScission protease (GE Biosciences), the protein was further purified by size-exclusion chromatography (SEC) using Superdex S75 column (GE Biosciences).

The series of individual point mutations were introduced into the AMSH catalytic domain gene by site-directed mutagenesis using QuikChange Site-Directed Mutagenesis Kit (Stratagene) following manufacturer's protocol. DNA sequencing confirmed the presence of the mutations. The resulting proteins were purified using standard GST-affinity chromatography followed by SEC (Superdex S75 column).

The DNA encoding the SH3 and UIM-SH3 domains was amplified by PCR using a plasmid that contained the full-length DNA as the template (pGW1Myc2c-STAM2, a kind gift from Craig Blackstone, National Institutes of Neurological Disorders and Stroke (NINDS) at the National Institutes of Health (NIH)) and was subcloned into pGEX-6p1 (GE Biosciences) using standard cloning protocols. The resulting N-terminally fused GST-tagged protein was expressed in *E. coli* Rosetta cells (Novagen) and purified with a glutathione-Sepharose column (GE Biosciences) following manufacturer's instructions. After removal of the tag by PreScission protease (GE Biosciences), the protein was further purified by size-exclusion chromatography (SEC) using Superdex S75 column (GE Biosciences).

The A176G mutation was introduced into the UIM-SH3 gene by site-directed mutagenesis using QuikChange Site-Directed Mutagenesis Kit (Stratagene) following manufacturer's protocol. DNA sequencing confirmed the presence of the mutations. The resulting proteins were purified using standard GST-affinity chromatography followed by SEC (Superdex S75 column).

Human ubiquitin was subcloned into pGEX-6p1 and purified using GST affinity chromatography, and the GST tag was removed by PreScission Protease. The protein was further purified using SEC (Superdex S75 column). Lys63-diubiquitin was enzymatically synthesized from ubiquitin using ATP, human E1, and the E2 complex (Ubc13 and Uev1a)

following previously reported procedures (*22*). The reaction was incubated at 37°C for 2 h and then quenched by dilution with buffer A (50mM sodium acetate, pH 4.5). The quenched reaction mixture was subjected to ion-exchange chromatography on a Mono-S column (GE Biosciences) to obtain Lys63-diubiquitin.

Determination of kinetic parameters and DUB assay

The kinetic parameters were determined by incubating the enzymes (25 nM T313A, 100 nM C282A, N312A, E317A, and F320A, 2 μM E316A and F395A, 3 μM T341A and S346A, and 10 μM F343A and S345A) with four concentrations of diubiquitin, ranging from 20 to 177 μM, in reaction buffer (50 mM TRIS-HCl (pH 7.0), 20 mM KCl, 5 mM $MgCl_2$ and 1 mM DTT). The reaction was carried out at 20°C for 10-75 min depending on activity for initial velocity measurements. Reaction tubes were quenched by the addition of 5X SDS-PAGE sample buffer followed by boiling. The reaction mixtures were visualized by SDS-PAGE gels and scanned. Bands corresponding to monoubiquitin were integrated using Image J software (http://rsb.info.nih.gov/ij/). Ubiquitin standards ranging from 4 to 12.3 μg were used to draw calibration plots, which were used to quantify the amount of ubiquitin produced. Kinetic parameters were calculated by fitting the data in SigmaPlot (Systat Software, San Jose, CA).

The *in vitro* DUB assay was carried out by incubating AMSH (residues 219-424) to a final enzyme concentration of 100 nM with 1μM of the SH3 domain of STAM2 or UIM-SH3 gene of STAM2, and 20 μM Lys63-diubiquitin in a total reaction volume of 20 μL. All reactions were carried out in reaction buffer (50 mM TRIS-HCl (pH 7.0), 25 mM KCl, 5 mM $MgCl_2$, and 1 mM DTT) for 5 h at 20°C. The reaction was quenched by the addition of 5X SDS-PAGE sample buffer followed by boiling and then analyzed by SDS-PAGE.

Analytical Ultracentrifugation

Sedimentation velocity experiments were conducted at 50,000 rpm using the Beckman Coulter XLA and XLI (Beckman Coulter, Fullerton, CA, USA). The samples were monitored by both interference and absorbance optics at 254 and 280 nm. The proteins were dialyzed in 50 mM TRIS-HCl pH 7.6, 50 mM NaCl. Three concentration series for AMSH (residues 219-424) were conducted to evaluate the formation of higher-order species at 24, 48, and 96 μM. The AMSH-SH3 complex was characterized using a constant concentration of 23.5 μM of AMSH and three concentrations of SH3 at 24, 47, and 70 μM. The AMSH-UIM-SH3 complex was characterized using a constant concentration of 23.5 μM of AMSH and three concentrations of 48, 144, and 288μM. The AMSH-ubiquitin complex was characterized using a constant concentration of 23.5 μM of AMSH and two concentrations of ubiquitin at 23 and 92 μM. The AMSH-diubiquitin complex was characterized using a constant concentration of 23.5 μM of AMSH and three diubiquitin concentrations at 24, 48, and 96 μM. The solvent density (1.00170 $g.ml^{-1}$), viscosity (0.01022 poise), and the partial specific volumes that were used for the analyses, 0.73387 $ml.g^{-1}$ (AMSH219), 0.71870 $ml.g^{-1}$ (AMSH-SH3), 0.71701 $ml.g^{-1}$ (AMSH-UIM-SH3), 0.72934 $ml.g^{-1}$ (AMSH-diubiquitin), and 0.72479 $ml.g^{-1}$ (AMSH-ubiquitin), were calculated by SEDNTERP v. 20120828 BETA (http://bitcwiki.sr.unh.edu/index.php/Main_Page) (*27*). The sedimentation coefficients and apparent molecular weights were calculated from size distribution analyses [c(s)] using SEDFIT v. 14.3e (*28, 29*). The figures were prepared using GUSSI v. 1.0.7b beta with the sedimentation coefficients standardized to $s_{20,w}$ and the data was normalized to the peak area of the complexes.

Sedimentation equilibrium experiments were conducted at 20°C using a 6-channel centerpiece in an AN-60 Ti rotor spun at speeds of 13,200, 29,900, and 42,000 rpm for the AMSH-ubiquitin complex and 11,600, 21,000, and 36,000 rpm for the AMSH-diubiquitin

complex. The molar ratios of the AMSH-ubiquitin complex were: 1:2, 1:4, and 1:8, and the molar ratios of the AMSH-diubiquitin complex were: 1:2, 1:4, and 1:5, to determine the molecular weight of the complexes. Absorbance scans at 280 nm were taken every 2 hours for 60 hours. The samples were tested for equilibrium using Sedfit (*28, 29*). Calculations of the molecular weights were done by SEDPHAT v. 10.58d (*30-35*) using the Species Analysis and Species Analysis with Mass Conservation Constraints. Errors were calculated using 1-dimensional error surface projections. Final figures were generated in GUSSI.

Isothermal Titration Calorimetry

To determine the K_Ds of AMSH binding to ubiquitin, ITC experiments were conducted using the MicroCal ITC200 (GE Healthcare Life Sciences). The proteins were dialyzed in the same buffer as was used for AUC. For the AMSH-diubiquitin experiment, 10 μM AMSH was in the cell and 500 μM of diubiquitin was in the syringe. The AMSH-ubiquitin titration had 100 μM AMSH in the cell, and 1 mM ubiquitin in the syringe. The F320A mutant of AMSH with ubiquitin had 100 μM of the enzyme in the cell, and 1 mM of ubiquitin in the syringe. These experiments were done at 20°C, 18 total injections of 1.4 μL per injection, with 180 seconds in between injections to allow for a return to baseline before the subsequent injection. The data was then baseline corrected by NITPIC (*36*) and loaded into SEDPHAT (*30-35*) for global analysis and fitting using a 1:1 model. Figures were prepared using GUSSI. To determine the K_D for the AMSH-SH3 interaction, 50 μM of AMSH was in the cell and 750 μM of the SH3 domain was in the syringe. K_D of AMSH-UIM-SH3 interaction was determined using 100 μM AMSH in the cell and 1 mM UIM-SH3 in the syringe. AMSHK238T-UIM-SH3 experiment was conducted using 50 μM of the enzyme in the cell and 1 mM of UIM-SH3 in the syringe. Characterization of ubiquitin binding to UIM-SH3 was done using 50 μM UIM-SH3 was in the

cell and 3.1 mM ubiquitin in the syringe. This data was fit to a two-site model. Confirmation of SH3-ubiquitin binding was done with 100 μM of SH3 in the cell and 3.0 mM ubiquitin in the syringe. The UIM-SH3-Lys63-diubiquitin experiment had 50 μM of UIM-SH3 in the cell and 750 μM diubiquitin in the syringe.

Guanidine Melt using circular dichroism spectroscopy

The stability of the folded state of AMSH244 and AMSH-LP towards GdHCl was determined using 8M stock concentrations of GdHCl (Sigma). Varying concentrations of GdHCl were added to the protein (0.2 $mg.mL^{-1}$) diluted in 100 mM phosphate buffer pH 7.4 and allowed to sit at room temperature overnight to allow for complete equilibration. Changes in the folded state of the proteins were monitored using circular dichroism by following changes in ellipticity at 220 nm. CD spectra were recorded in a Jasco J-810 Spectropolarimeter in the far UV region (195-260 nm) in a 0.1 cm path length cuvette. Each spectrum was averaged over 4 scans (50 $nm.min^{-1}$ scan speed, with a 8 second time constant) and corrected by subtraction of a spectrum of the buffer alone. Mean residue molar ellipticity values were calculated using the following equation:

$$[\theta] = \frac{\theta * 100 * M}{C * l * n}$$

Where θ is the ellipticity in degrees, l is the optical path in cm, C is the concentration in mg/ml, M is the molecular mass and n is in the number of residues in the protein.

The mean residue molar ellipticity [θ] is given in $deg.cm^2.dmol^{-1}$. Unfolding curves were analyzed using a two-state unfolding model, using linear extrapolation to obtain the ΔG value in the absence of GdHCl (*37*).

RESULTS

Mutational and kinetic analysis of the catalytic domain of AMSH

Previous modeling studies investigating the differences between the ability of AMSH and AMSH-LP to bind and cleave Lys63-linked diubiquitin revealed some interesting results. The active site and proximal ubiquitin binding residues were identical between the two proteins; however, in the distal ubiquitin-binding site, AMSH has three residue differences compared to AMSH-LP. Based on this analysis, we sought to carry out an extensive mutational and kinetic analysis of the putative residues in AMSH that might be involved in diubiquitin cleavage.

Active site

The active site of AMSH consists of a Zn^{2+} ion, coordinated directly by three residues (Asp348, His 335, and His337) and a water molecule that is hydrogen bonded to Glu280, and a putative oxy-anion stabilizing residue (Ser345) (Figure 1). In order to probe the roles of Asp348 and Glu280, we generated two aspartate mutants (D348A and D348N) and a glutamate mutant (E280A) and, as expected, found that there was no detectable activity in these mutants (Table 1), most likely due to the loss of Zn^{2+} for the aspartate mutations and the loss of the water molecule in the glutamate mutation.

Next, we probed the function of the putative oxy-anion hole-stabilizing residue, Ser345. Mutating serine to alanine resulted in a significantly impaired enzyme with a 1000-fold reduction in k_{cat} (Table 1). As described with other families of hydrolases, the oxy-anion hole-stabilizing residue plays a critical role in donating a hydrogen bond to the negatively charged tetrahedral intermediate formed after the initial nucleophilic attack. Substantial reduction of k_{cat} alone upon mutation to alanine, with K_M remaining nearly the same, is consistent with Ser345 playing the role as the oxy-anion stabilizing residue in AMSH.

In our previous structural analysis, we noted a potential disulfide bridge between Cys282 and Cys311, 7.4Å away from the active-site Zn^{2+} (*25*). Previous studies have shown that N-ethylmaleimide (NEM) inhibits AMSH activity (IC_{50} of 16.2± 3.2 μM) (*21, 38*), presumably by modifying one of these two cysteines, perhaps Cys282 because it is proximal to the active-site cleft. Its modification might introduce some steric hindrance for substrate binding thus explaining the inhibitory effect. We sought to determine if Cys282 has any role in the enzyme's catalytic activity. Previously, when Cys282 was mutated to alanine, we noticed a loss of activity (*25*), however, a more detailed kinetic analysis of this mutant revealed a more significant reduction in activity, a 6-fold loss in k_{cat} (Table 1), which would suggest that Cys282 does indeed have a role in catalysis. Cys282 is seen making a van der Waals contact with Leu73 of the distal ubiquitin, which may explain the reduction in activity observed here.

Proximal ubiquitin site

Modeling of the catalytic domain of AMSH onto the structure of AMSH-LP bound to Lys63-linked diubiquitin revealed four residues within AMSH (Thr341, Phe343, Ser346, and Phe395) that could determine its specificity for Lys63-linked polyubiquitin chains by recognizing the tri-peptide sequence motif Gln62-Lys63-Glu64 within the proximal ubiquitin, which encompasses the acceptor Lys63 and its two immediate flanking residues. Individual point mutants (to alanine) were generated and kinetic analysis was performed to probe the functional significance of these residues. Overall, the four resides within AMSH showed a drastic reduction in k_{cat} with similar K_M values compared to the wild-type enzyme, confirming their utmost importance to the enzyme's catalytic mechanism (Figure 2 and Table 1), especially during the rate-determining step of isopeptide bond hydrolysis.

Distal ubiquitin site

The distal site is where AMSH significantly differs from AMSH-LP in diubiquitin recognition. Three substitutions are found going from AMSH-LP to AMSH: an aspartate to asparagine, a methionine to a threonine, and a valine to glutamate. Two other important residues within the distal site are completely conserved between AMSH and AMSH-LP, a phenylalanine (Phe320, AMSH numbering) and a glutamate (Glu317) (Figure 3). The conserved Phe320 when mutated to alanine exhibited a 4-fold reduction in k_{cat} and 3-fold increase in K_M, whereas, the Glu317Ala mutant exhibits somewhat similar activity to the wild type, with only a modest 2-fold reduction in k_{cat} (Table 1).

Moving forward, individual point mutations of the three substitutions between AMSH and AMSH-LP revealed some interesting results. Mutating Asn312 to alanine yielded only an approximate 3-fold reduction in k_{cat} (Table 1). Surprisingly, a qualitative diubiquitin cleavage assay revealed that Thr313Ala was apparently more active than the wild type (unpublished data), however, detailed kinetic analysis showed simply an approximate 2-fold increase in k_{cat}, with a ~3-fold loss in K_M (Table 1).

Mutating the Glu316 to alanine proved to cause the most significant change in enzymatic activity amongst the distal site residues. Glu316Ala showed a substantial 74-fold reduction in k_{cat} (Table 1). This k_{cat} effect differs strikingly from the distal site residues of AMSH-LP whose mutation to Ala showed a loss primarily in K_M (*22*). The effect of the glutamate mutation in AMSH mirrors that of residues from the proximal site. Inspection of the AMSH-diubiquitin model reveals that Glu316 is within hydrogen-bonding distance from two distal ubiquitin residues: Arg42 is within 3.1Å (εN of Arg42 and εO of Glu316), and Gln49 is within 2.8Å, if the side chain is flipped by 180° (Figure 3). A significant loss in k_{cat} but not in K_M is consistent with

these hydrogen-bonding interactions contributing to the stabilization of the transition state, perhaps by playing a role in orienting the scissile peptide bond for nucleophilic attack.

Kinetic and thermodynamic characterization of the effect of the MIC-CAP-associated mutation, Thr313Ile

To better understand the molecular basis of the MIC-CAP syndrome, the Thr313Ile (T313I) mutant was generated and analyzed both for its catalytic activity towards Lys63-diubiquitin and its thermodynamic stability. In the absence of a structure, a modeled AMSH-diubiquitin structure suggests that the side-chain hydroxyl from threonine is hydrogen bonded to the backbone NH group of Leu73 in the distal ubiquitin (Fig. S1). The T313I mutant was found to suffer a 6-fold reduction in k_{cat}, with a comparable K_M (Table 1). In terms of its thermodynamic stability, T313I was somewhat less stable than the wild type with a ΔG_{H20} of 2.9 kcal.mol^{-1} compared to 3.6 kcal.mol^{-1} for the wild type (Fig. S2 and Supplementary Table 1). This result indicates that the reduced catalytic activity of the mutant could lead to a loss of function of AMSH translating into the disease state.

Biophysical characterization of ubiquitin binding to the catalytic domain of AMSH

Mutational and kinetic analyses prompted us to seek a better understanding of AMSH-ubiquitin complex formation in solution. Using isothermal titration calorimetry (ITC), we analyzed the binding of Lys63-linked diubiquitin and the catalytic domain of AMSH (AMSH 219-424^{E280A}, an inactive mutant to ensure diubiquitin is not hydrolyzed), and obtained an equilibrium dissociation constant (K_D) of 19 ± 4 μM (Figure 4b and Table 2). As a control, ubiquitin and the catalytic domain of AMSH was analyzed and it was determined that it binds AMSH with similar affinity of 19 ± 3 μM (Figure 4a and Table 2). Both sedimentation velocity

and sedimentation equilibrium experiments using analytical ultracentrifugation (AUC) confirmed the ITC results (Fig. S3, Fig. S4, and Supplementary Table 2). Almost identical binding affinities between diubiquitin and ubiquitin to the catalytic domain of AMSH suggest that there is only one binding site for ubiquitin. To probe which ubiquitin binding site is used, another ITC experiment was done with $AMSH^{Phe320Ala}$ (Phe320 at the distal site is mutated to Ala) and ubiquitin. We observed a ~4-fold decrease in affinity (K_D of 81 ± 15 μM) (Figure 4c and Table 2), consistent with what was observed from kinetics, suggesting that the distal ubiquitin makes the most significant contribution to diubiquitin binding, and the single binding site observed in our ITC experiments with ubiquitin corresponds to binding at the distal site. These data suggest that AMSH alone cannot discriminate between its polyubiquitin substrate and its ubiquitin product.

The intact minimal STAM construct UIM-SH3 is necessary for AMSH activation

The I44 patch, a hydrophobic surface centered on the Ile44 residue in ubiquitin, is ubiquitously used by proteins that specifically bind to ubiquitin, including DUBs. Inspection of our structural model representing AMSH-diubiquitin complex reveals that the I44 patch of the distal ubiquitin is satisfied, with the Ile44 residue engaged in van der Waals interaction with Phe320; however, Ile44 of the proximal ubiquitin is unoccupied (Fig. S5). Looking at the domain structure of the ESCRT-0 member, STAM, one finds a UIM (ubiquitin-interacting motif) N-terminally adjacent to its SH3 domain (Fig. S6). We sought to understand if the UIM, separated from the SH3 domain by a short linker, could act as an adaptor to AMSH by interacting with the proximal ubiquitin while AMSH engages the distal one. To probe this, we used a combination of biophysical techniques and biochemical assays to assess three individual events: (1) AMSH recruitment to STAM via the SH3 domain and a longer STAM segment in

which the UIM is fused to the SH3 domain (UIM-SH3), (2) ubiquitin binding to UIM-SH3, and finally, (3) the ternary complex of the catalytic domain of AMSH, UIM-SH3, and Lys63-linked diubiquitin.

AMSH binds to the SH3 domain of STAM2

To confirm that we have the minimal domains required for the AMSH-STAM interaction we carried out ITC and AUC experiments. We determined that the SH3 domain of STAM binds the catalytic domain of AMSH ($AMSH219^{E280A}$) with a K_D of 1.4 ± 0.04 μM (Table 2 and Fig. S7). Using the longer UIM-SH3 construct, we obtained an identical K_D of 1.9 ± 0.1 μM (Table 2 and Fig. S7), both of which are consistent with a previous ITC study, which showed that a peptide representing the SBM of AMSH binds the SH3 domain with 7 μM affinity (*14*). Using an orthogonal and complementary technique, we confirmed complex formation by sedimentation velocity experiments using AUC and determined that the catalytic domain of AMSH forms a 1:1 complex. The respective $s_{20,w}$ values of 2.5S and 2.6S for the SH3 domain and UIM-SH3 (Figure 5a and b) suggest that the UIM has no role in AMSH recruitment to STAM, as expected.

Both SH3 domain and UIM of STAM bind ubiquitin independently

Secondly, we characterized ubiquitin binding to the UIM of STAM. Since UIMs are only 30-residue domains, much too small for bacterial expression, we used UIM-SH3 to investigate UIM-ubiquitin binding by ITC. Somewhat surprisingly, we found that both the UIM and SH3 domains bind ubiquitin independently. This observation was based on two pieces of evidence. (1) The UIM-SH3 construct binds ubiquitin with a K_D of 273 ± 16 μM, in agreement with previous biosensor measurements of a STAM-derived UIM peptide binding to ubiquitin that provided a K_D of 182 μM (*39*). (2) Interestingly, our measurement of SH3-ubiquitin binding by ITC resulted in a K_D of 62 ± 7 μM (Figure 6b and Table 2). It has been shown previously that a

subset of SH3 domains bind ubiquitin (*40, 41*), and a recent study using NMR titration experiments showed that the SH3 domain of STAM does in fact bind ubiquitin, and that this interaction can be competed off by USP8 binding to the SH3 domain of STAM (*42*). Taken together, these data seem to indicate that both the SH3 domain and the UIM bind ubiquitin independently, with the former having higher affinity than the latter, which would explain the overall K_D of 273 ± 15 μM obtained as the binding affinity of the UIM-SH3 construct for ubiquitin. It is possible that the two binding events corresponding to the two binding sites on UIM-SH3 have similar enthalpy of binding, and with binding affinities not drastically different between them, the ITC experiment is unable to resolve them distinctly.

Alternatively, it is possible that the UIM and SH3 domain fold onto each other generating a weaker interface for ubiquitin than either of them alone. This seems unlikely since UIM-SH3 binds to Lys63-linked diubiquitin with a K_D of 54 ± 20 μM (Figure 6c and Table 2), an affinity higher than that of UIM-SH3 for ubiquitin. These results are consistent with the principle of avid binding of polyubiquitin chains at ESCRT-0, thus indicating that both the UIM and SH3 domain in UIM-SH3 are accessible for ubiquitin binding.

UIM and SH3 domains are necessary for stimulating the activity of AMSH

Using the catalytic domain of AMSH, UIM-SH3 and Lys63-linked diubiquitin, we attempted to recapitulate AMSH recruitment to ESCRT-0 *in vitro*. We carried out a Lys63-diubiquitin DUB cleavage assay with the AMSH:UIM-SH3 complex. The initial experiment comparing the enzyme's activity alone and in the presence of the SH3 domain and then, UIM-SH3, revealed a remarkable difference in DUB activity of AMSH. In the presence of UIM-SH3, it turned over nearly all of the Lys63-diubiquitin to ubiquitin, whereas, AMSH alone or in the

presence of simply the SH3 domain had a significant amount of diubiquitin remaining, suggesting a stimulatory role for UIM-SH3 (Figure 7).

Diving deeper into the mechanism of activation, a similar *in vitro* assay was performed, this time using two SBM, and one UIM mutant versions of the UIM-SH3 construct (Figure 8). Two individual point mutations within the SBM of AMSH were introduced (Lys238Ala and Lys238Thr) to obliterate the SH3-SBM interaction. Lys238 is a completely conserved residue in the canonical SBM motif known to bind SH3 domains, mutating this to threonine made AMSH look like AMSH-LP in terms of its SBM. AMSH-LP has the conserved set of residues within its SBM, except the critical Lys replaced by Thr. We confirmed that there was no binding between the AMSH SBM mutants and the SH3 domain using ITC (Fig. S8). Secondly, we introduced a mutation within the UIM of UIM-SH3 (Ala176Gly) to interrupt ubiquitin binding (Figure 8). The Ala to Gly mutation has been shown previously to cause significant reduction in ubiquitin binding (*39*). The diubiquitin cleavage reactions were performed at 37°C for 15 minutes using 1 μM enzyme, 20 μM Lys63-linked diubiquitin as the substrate, and 5μM STAM binding partner (SH3, $UIM^{A176G}SH3$, or UIM-SH3). SDS-PAGE analysis revealed that only in the presence of the wild-type enzyme and UIM-SH3 is diubiquitin completely hydrolyzed to ubiquitin, hence, an intact SBM-SH3 interaction and a functional UIM are necessary for AMSH activation (Figure 8).

Furthermore, we wanted to understand this activation phenomenon in more detail, in terms of k_{cat} and K_M. To this end, we carried out another kinetic assay in which the catalytic domain of AMSH was pre-incubated in the presence of 20-fold excess UIM-SH3 to ensure that equilibrium favors the formation of the AMSH-UIM-SH3 complex. We saw 6-fold activation in AMSH in the presence of UIM-SH3, contributed by a somewhat greater change in k_{cat} than in K_M (Supplementary Table 3). The k_{cat} effect is not entirely surprising because the UIM interacts with

the proximal ubiquitin, and as we have shown in our mutational and kinetic analysis, the proximal site plays a significant role in properly aligning the isopeptide bond within the active site of AMSH, as determined by the significant loss in k_{cat} upon mutating the residues involved in binding.

DISCUSSION

AMSH is one of the two DUBs recruited to the human ESCRT machinery to regulate the endosomal-lysosomal degradation pathway (*9*). It is a JAMM family DUB,(*1*) having exquisite specificity for recognizing and cleaving Lys63-linked polyubiquitin chains (*9*), which serve as signals for ESCRT-mediated sorting to lysosome. However, a clearly defined role for AMSH has yet to be elucidated. A homologous protein, AMSH-LP, sharing 54% identity and 73% sequence similarity (*9, 23*), of the same family of DUBs, has the same ubiquitin linkage specificity, and from our previous work, is structurally almost identical in its catalytic domain to AMSH (*25*). Even though the catalytic domains of AMSH and AMSH-LP are structurally nearly identical, we showed that AMSH is significantly less stable than AMSH-LP, and consequently perhaps conformationally more plastic, and the enzymes differ in their ubiquitin recognition (*25*). As a result of these differences, we sought to further investigate AMSH kinetically and biophysically to advance our understanding of the enzyme with a view to understanding its role in the context of the ESCRT machinery.

Our kinetic analysis using site-directed mutagenesis of conserved residues in the proximal ubiquitin binding site has shown that the specificity of AMSH for Lys63-linked polyubiquitin chains arises from its recognition of the proximal ubiquitin, similar to the case of AMSH-LP (*22*). Lys63-linked chain specificity for AMSH plays a significant role in

understanding its function as an ESCRT-DUB. Since Lys63-linked polyubiquitin chains are targeting signals for ESCRT-mediated degradation, the specific DUB activity of AMSH may play a central role in the persistent functionality of the ESCRT machinery. Mutation of the proximal ubiquitin binding residues causes drastic reduction in k_{cat}, suggesting that recognition of the tri-peptide sequence motif Gln62-Lys63-Glu64 within the proximal ubiquitin plays a significant role in the ability of AMSH to cleave Lys63-linked polyubiquitin chains. Recognition of Lys63 isopeptide bond and its two flanking residues in the proximal ubiquitin would mean that AMSH could only efficiently hydrolyze bonds between successive ubiquitins in a polymeric chain, and not the last ubiquitin directly attached to a protein receptor (the cargo). This impediment toward completely deubiquitinating a ubiquitinated receptor could have multiple functional implications (discussed below). At the outset, it calls into question the functional role of AMSH when it is recruited to ESCRT-III, where complete deconjugation of a ubiquitinated cargo is the absolute desire, since ubiquitin will otherwise end up in intra-luminal vesicles (ILVs) attached to the cargo and will be subsequently degraded in the lysosome. It seems unlikely that AMSH can have a significant catalytic role with respect to hydrolyzing the last ubiquitin attached to the cargo, yet, AMSH binds to ESCRT-III component CHMP3 with relatively high affinity.

Our data on mutational analysis of the distal ubiquitin binding residues offer some interesting insights. Of the three residues different between AMSH and AMSH-LP, two of them, Glu316 and Thr313, contribute significantly to catalysis playing different roles than the corresponding residues in AMSH-LP. The AMSH residue Glu316 contributes to stabilization of the transition state as indicated by the largely k_{cat} effect when it is mutated to Ala, in contrast to mostly a K_M effect observed when the corresponding residues Val in AMSH-LP mutated to Ala

(*22*). Thr313 in our AMSH-diubiquitin model is seen making a hydrogen bonding contact with the backbone NH group of Leu73 of the distal ubiquitin using its side-chain hydroxyl group and its methyl group is engaged in van der Waals contact with the aliphatic side groups of Leu73 of ubiquitin. Its substitution with Ile as seen in children with the MIC-CAP syndrome is expected to preserve the van der Waals contact but loose the hydrogen bond. Our data show that the substitution of the Thr to an Ile has minimal effect on protein folding and stability, but results in a significantly reduced catalytic efficiency. Going from AMSH to AMSH-LP, the Thr residue is replaced by Met, which could contribute only van der Waals interaction with the substrate. Thus, it appears that the hydrogen-bonding interaction of Thr in AMSH has a unique role whose loss leads to a dramatic effect resulting in a loss of function substantial enough to cause the disease. Overall, these results indicate that subtle differences between very similar enzymes can have profound functional effects.

We found the minimal domain of STAM that is required to stimulate the activity of AMSH. Previous work has shown that STAM has a role in AMSH activation towards Lys63 polymeric chains (*13, 14*); however, these studies were not able to fully elucidate the mechanism of activation. Our study begins to divulge the mechanism underlying activation. This work suggests a simple model invoking simultaneous recognition of two ubiquitin groups in a polyubiquitin chain by AMSH and the UIM of STAM could explain the catalytic activation of the DUB. The UIM of STAM, separated from the SH3 domain by a short linker, could act as an adaptor for AMSH by interacting with the proximal ubiquitin, while AMSH engages the distal one. Such an arrangement would create a more extensive binding interface for diubiquitin in the AMSH:STAM complex than in the enzyme alone, causing catalytic activation. It appears that such activation is necessary since, as our ITC data show, AMSH has no preference for binding to

Lys63-linked diubiquitin, therefore by extrapolation to Lys63-linked polyubiquitin chains over the ubiquitin product.

Prior to activation, AMSH is in a more latent state, but when it is recruited to STAM its full activity is unveiled. AMSH is known to have diverse subcellular localization profiles. Perhaps the free form of the enzyme needs to be in a less-active state so as not to hydrolyze the Lys63 chains that are present in the cytosol other than endosomes. Once it is recruited to the endosomes, its true activity comes alive, as seen by the 6-fold enhancement in activity upon binding to the STAM derived UIM-SH3 construct. A significant implication of this mechanism of activation is that the activation will be absent when AMSH is trying to cleave the last ubiquitin attached to the cargo. While efficiently cleaving between two ubiquitin groups in a Lys63-linked polyubiquitin chain, AMSH might show a severe impediment in hydrolyzing the last ubiquitin attached directly to a cargo, on account of two factors: (1) its high specificity for the Lys63-linked chain between two ubiquitins, which in turn would make it a poor enzyme when ubiquitin is attached to a non-ubiquitin protein, the cargo; and, (2) the lack of an activation effect when cleaving ubiquitin attached to a non-ubiquitin moiety.

Finally, bringing all our data together, we can envision a mechanism for recruitment and activation for AMSH that will ultimately define a function for the enzyme. ESCRT-0 has the defined function of ubiquitinated cargo clustering, capable of harboring up to eight ubiquitin moieties at a time (*43, 44*), which now, with the addition of the SH3 domain could be ten ubiquitins. Our ITC data show that the SH3 domain can actually bind ubiquitin tighter than the UIM. Subsequently, AMSH is recruited to STAM. The AMSH-SH3 binding affinity is stronger than SH3-ubiquitin, making it possible for AMSH to effectively displace ubiquitin from the SH3 domain (the binding interface on SH3 domain for the two proteins show substantial overlap) (*42*)

leading to its recruitment to ESCRT-0. With the UIM from STAM acting as an adaptor to the enzyme, facilitating enzyme activity enhancement, AMSH begins to efficiently disassemble the polyubiquitin chain attached to the cargo. Deubiquitination of the chain will continue until the last ubiquitin directly attached to the cargo. Thus, the recruitment of AMSH at ESCRT-0 will lead to substantial chain trimming but not complete deconjugation of ubiquitin from the cargo. As discussed in the next paragraph, this would promote the cargo's passage from ESCRT-0 to ESCRT-I and subsequent complexes.

Our proposed mechanism defines AMSH as the DUB that facilitates cargo passage from ESCRT-0 onto the next complex. This idea is supported by previous data that shows that avidly bound ubiquitin chains comprise of a binding affinity of ~20 μM affinity (*45*), whereas, ESCRT-I subunit, UBAP1, binds ubiquitin anywhere from 70-140 μM (*46*). The binding affinity of ubiquitin at ESCRT-0 needs to be reduced at least 5-10-fold in order for cargo destined for lysosomal degradation to be transferred to ESCRT-I. When going from Lys63-linked tetra-ubiquitin to diubiquitin, ESCRT-0 has a ~6-fold reduced affinity, and a remarkable, 46-fold reduction in affinity for ubiquitin (*45*). Therefore, we presume that because of the specificity and activation of AMSH, this would be the enzyme that would be most suited for promoting cargo passage, all in support of an idea proposed previously (*47*). By occupying the binding site on ESCRT-0, AMSH will serve to keep USP8 off the initial ESCRT complex. The recruitment of USP8 at ESCRT-0 would be detrimental to cargo's passage to lysosome because USP8 has no hindrance in complete deconjugation. We suggest that USP8's role is specifically at the ESCRT-III level where complete deconjugation is desired.

The main conclusion from our study implies that loss of function mutations in AMSH would lead to impairment of ubiquitin-dependent sorting to lysosome via the ESCRT pathway.

One possible outcome of this impairment is accumulation of ubiquitinated proteins (cargo). Indeed, patient cell lines with AMSH mutation show accumulation of aggregated ubiquitin-protein conjugates (*16*). Furthermore, impairment of ESCRT-mediated endocytic sorting to lysosome is expected to cause hyperactivation of signaling across lipid bilayer. As suggested by the authors of the paper describing MIC-CAP mutations, the capillary abnormalities associated with the syndrome could be a consequence of hyperactive RAS-MAPK signaling induced in humans by impaired AMSH function (*16*). However, because AMSH has several roles within the cell it would be difficult to assign loss of function in one pathway as the exclusive molecular basis of MIC-CAP syndrome.

In summary, using a combination of biochemical and biophysical studies, guided by a structural model, we are able to learn many important aspects of AMSH: (1) The T313I mutation underlying the MIC-CAP syndrome leads to a significant loss of catalytic activity owing to loss of a hydrogen-bonding interaction with ubiquitin. (2) Recognition of proximal ubiquitin contributes significantly to catalysis. (3) Activation of AMSH is enabled by facile, simultaneous binding to two ubiquitin groups in a polyubiquitin substrate, one by the catalytic domain of the DUB (binding to the distal ubiquitin) and the other (the proximal ubiquitin) by the UIM from STAM. (4) Taken together, the above two points strongly indicate that AMSH will suffer a severe loss of catalytic efficiency when cleaving the last ubiquitin attached to cargo compared to a Lys63-linked polyubiquitin chain substrate. These studies provide biochemical and biophysical evidence in support of a hypothesis which postulates that AMSH is recruited to the initial ESCRT complex to facilitate transfer of cargo from one ESCRT member to the next, but not to completely deubiquitinate it (*9*). Its recruitment therefore would facilitate cargo shuttling rather than release from ESCRT and subsequent recycling back to the plasma membrane.

ACKNOWLEDGMENT

We would also like to acknowledge Dr. Myung-il Kim for his help in optimization of the Lys63-linked diubiquitin chain synthesis. Financial support from the American Heart Association Pre-doctoral fellowship (12PRE12060249) to C.W. Davies is gratefully acknowledged. Finally, financial support from the National Institutes of Health (1R01RR026273) to C. Das is gratefully acknowledged.

Supporting Information Available

Cartoon representations of the MIC-CAP-associated mutation and a model of AMSH bound to Lys63-linked diubiquitin. A fraction unfolded GdHCl melting curve and stability data table. ITC thermograms of AMSH binding to the SH3 and UIM-SH3, and AMSHK238T with UIM-SH3. Sedimentation velocity and equilibrium data and data table. AMSH and STAM domain diagram. AMSH activation data table. This material is available free of charge via the Internet at http://pubs.acs.org

REFERENCES

1. Maytal-Kivity, V., Reis, N., Hofmann, K., and Glickman, M. H. (2002) MPN+, a putative catalytic motif found in a subset of MPN domain proteins from eukaryotes and prokaryotes, is critical for Rpn11 function, *BMC Biochem 3*, 28.
2. Komander, D. (2010) Mechanism, specificity and structure of the deubiquitinases, *Subcell Biochem 54*, 69-87.
3. Komander, D., Clague, M. J., and Urbe, S. (2009) Breaking the chains: structure and function of the deubiquitinases, *Nat Rev Mol Cell Biol 10*, 550-563.
4. Wilkinson, K. D. (2009) DUBs at a glance, *J Cell Sci 122*, 2325-2329.
5. Nijman, S. M., Luna-Vargas, M. P., Velds, A., Brummelkamp, T. R., Dirac, A. M., Sixma, T. K., and Bernards, R. (2005) A genomic and functional inventory of deubiquitinating enzymes, *Cell 123*, 773-786.
6. Zhu, P., Zhou, W., Wang, J., Puc, J., Ohgi, K. A., Erdjument-Bromage, H., Tempst, P., Glass, C. K., and Rosenfeld, M. G. (2007) A histone H2A deubiquitinase complex coordinating histone acetylation and H1 dissociation in transcriptional regulation, *Mol Cell 27*, 609-621.

7. Sobhian, B., Shao, G., Lilli, D. R., Culhane, A. C., Moreau, L. A., Xia, B., Livingston, D. M., and Greenberg, R. A. (2007) RAP80 targets BRCA1 to specific ubiquitin structures at DNA damage sites, *Science 316*, 1198-1202.
8. Avvakumov, G. V., Walker, J. R., Xue, S., Finerty, P. J., Jr., Mackenzie, F., Newman, E. M., and Dhe-Paganon, S. (2006) Amino-terminal dimerization, NRDP1-rhodanese interaction, and inhibited catalytic domain conformation of the ubiquitin-specific protease 8 (USP8), *J Biol Chem 281*, 38061-38070.
9. Clague, M. J., and Urbe, S. (2006) Endocytosis: the DUB version, *Trends Cell Biol 16*, 551-559.
10. Wollert, T., Wunder, C., Lippincott-Schwartz, J., and Hurley, J. H. (2009) Membrane scission by the ESCRT-III complex, *Nature 458*, 172-177.
11. Saksena, S., Sun, J., Chu, T., and Emr, S. D. (2007) ESCRTing proteins in the endocytic pathway, *Trends Biochem Sci 32*, 561-573.
12. Roxrud, I., Stenmark, H., and Malerod, L. (2010) ESCRT & Co, *Biol Cell 102*, 293-318.
13. McCullough, J., Row, P. E., Lorenzo, O., Doherty, M., Beynon, R., Clague, M. J., and Urbe, S. (2006) Activation of the endosome-associated ubiquitin isopeptidase AMSH by STAM, a component of the multivesicular body-sorting machinery, *Curr Biol 16*, 160-165.
14. Kim, M. S., Kim, J. A., Song, H. K., and Jeon, H. (2006) STAM-AMSH interaction facilitates the deubiquitination activity in the C-terminal AMSH, *Biochem Biophys Res Commun 351*, 612-618.
15. Solomons, J., Sabin, C., Poudevigne, E., Usami, Y., Hulsik, D. L., Macheboeuf, P., Hartlieb, B., Gottlinger, H., and Weissenhorn, W. (2011) Structural basis for ESCRT-III CHMP3 recruitment of AMSH, *Structure 19*, 1149-1159.
16. McDonell, L. M., Mirzaa, G. M., Alcantara, D., Schwartzentruber, J., Carter, M. T., Lee, L. J., Clericuzio, C. L., Graham, J. M., Jr., Morris-Rosendahl, D. J., Polster, T., Acsadi, G., Townshend, S., Williams, S., Halbert, A., Isidor, B., David, A., Smyser, C. D., Paciorkowski, A. R., Willing, M., Woulfe, J., Das, S., Beaulieu, C. L., Marcadier, J., Geraghty, M. T., Frey, B. J., Majewski, J., Bulman, D. E., Dobyns, W. B., O'Driscoll, M., and Boycott, K. M. (2013) Mutations in STAMBP, encoding a deubiquitinating enzyme, cause microcephaly-capillary malformation syndrome, *Nat Genet 45*, 556-562.
17. Carter, M. T., and Boycott, K. M. (2011) Microcephaly-capillary malformation syndrome: a story of rapid emergence of a new recognizable entity, *Am J Med Genet A 155A*, 2078-2079.
18. Mirzaa, G. M., Paciorkowski, A. R., Smyser, C. D., Willing, M. C., Lind, A. C., and Dobyns, W. B. (2011) The microcephaly-capillary malformation syndrome, *Am J Med Genet A 155A*, 2080-2087.
19. Isidor, B., Barbarot, S., Beneteau, C., Le Caignec, C., and David, A. (2011) Multiple capillary skin malformations, epilepsy, microcephaly, mental retardation, hypoplasia of the distal phalanges: report of a new case and further delineation of a new syndrome, *Am J Med Genet A 155A*, 1458-1460.
20. Suzuki, S., Tamai, K., Watanabe, M., Kyuuma, M., Ono, M., Sugamura, K., and Tanaka, N. (2011) AMSH is required to degrade ubiquitinated proteins in the central nervous system, *Biochem Biophys Res Commun 408*, 582-588.
21. McCullough, J., Clague, M. J., and Urbe, S. (2004) AMSH is an endosome-associated ubiquitin isopeptidase, *J Cell Biol 166*, 487-492.

22. Sato, Y., Yoshikawa, A., Yamagata, A., Mimura, H., Yamashita, M., Ookata, K., Nureki, O., Iwai, K., Komada, M., and Fukai, S. (2008) Structural basis for specific cleavage of Lys 63-linked polyubiquitin chains, *Nature 455*, 358-362.
23. Kikuchi, K., Ishii, N., Asao, H., and Sugamura, K. (2003) Identification of AMSH-LP containing a Jab1/MPN domain metalloenzyme motif, *Biochem Biophys Res Commun 306*, 637-643.
24. Agromayor, M., and Martin-Serrano, J. (2006) Interaction of AMSH with ESCRT-III and deubiquitination of endosomal cargo, *J Biol Chem 281*, 23083-23091.
25. Davies, C. W., Paul, L. N., Kim, M. I., and Das, C. (2011) Structural and thermodynamic comparison of the catalytic domain of AMSH and AMSH-LP: nearly identical fold but different stability, *J Mol Biol 413*, 416-429.
26. Nakamura, M., Tanaka, N., Kitamura, N., and Komada, M. (2006) Clathrin anchors deubiquitinating enzymes, AMSH and AMSH-like protein, on early endosomes, *Genes Cells 11*, 593-606.
27. Laue, T. M., Shah, B. D., Ridgeway, T. M., and Pelletier, S. L. (1992) Analytical Ultracentrifugation in Biochemistry and Polymer Science, *Royal Society of Chemistry*, 90-125.
28. Brown, P. H., and Schuck, P. (2006) Macromolecular size-and-shape distributions by sedimentation velocity analytical ultracentrifugation, *Biophys J 90*, 4651-4661.
29. Schuck, P. (2000) Size-distribution analysis of macromolecules by sedimentation velocity ultracentrifugation and lamm equation modeling, *Biophys J 78*, 1606-1619.
30. Balbo, A., Minor, K. H., Velikovsky, C. A., Mariuzza, R. A., Peterson, C. B., and Schuck, P. (2005) Studying multiprotein complexes by multisignal sedimentation velocity analytical ultracentrifugation, *Proc Natl Acad Sci U S A 102*, 81-86.
31. Dam, J., and Schuck, P. (2005) Sedimentation velocity analysis of heterogeneous protein-protein interactions: sedimentation coefficient distributions c(s) and asymptotic boundary profiles from Gilbert-Jenkins theory, *Biophys J 89*, 651-666.
32. Dam, J., Velikovsky, C. A., Mariuzza, R. A., Urbanke, C., and Schuck, P. (2005) Sedimentation velocity analysis of heterogeneous protein-protein interactions: Lamm equation modeling and sedimentation coefficient distributions c(s), *Biophys J 89*, 619-634.
33. Houtman, J. C., Brown, P. H., Bowden, B., Yamaguchi, H., Appella, E., Samelson, L. E., and Schuck, P. (2007) Studying multisite binary and ternary protein interactions by global analysis of isothermal titration calorimetry data in SEDPHAT: application to adaptor protein complexes in cell signaling, *Protein Sci 16*, 30-42.
34. Vistica, J., Dam, J., Balbo, A., Yikilmaz, E., Mariuzza, R. A., Rouault, T. A., and Schuck, P. (2004) Sedimentation equilibrium analysis of protein interactions with global implicit mass conservation constraints and systematic noise decomposition, *Anal Biochem 326*, 234-256.
35. Schuck, P. (2003) On the analysis of protein self-association by sedimentation velocity analytical ultracentrifugation, *Anal Biochem 320*, 104-124.
36. Keller, S., Vargas, C., Zhao, H., Piszczek, G., Brautigam, C. A., and Schuck, P. (2012) High-precision isothermal titration calorimetry with automated peak-shape analysis, *Anal Chem 84*, 5066-5073.
37. Pace, C. N. (1986) Determination and analysis of urea and guanidine hydrochloride denaturation curves, *Methods Enzymol 131*, 266-280.

38. Arnst, J. L., Davies, C. W., Raja, S. M., Das, C., and Natarajan, A. (2013) High-throughput compatible fluorescence resonance energy transfer-based assay to identify small molecule inhibitors of AMSH deubiquitinase activity, *Anal Biochem*.
39. Fisher, R. D., Wang, B., Alam, S. L., Higginson, D. S., Robinson, H., Sundquist, W. I., and Hill, C. P. (2003) Structure and ubiquitin binding of the ubiquitin-interacting motif, *J Biol Chem 278*, 28976-28984.
40. He, Y., Hicke, L., and Radhakrishnan, I. (2007) Structural basis for ubiquitin recognition by SH3 domains, *J Mol Biol 373*, 190-196.
41. Stamenova, S. D., French, M. E., He, Y., Francis, S. A., Kramer, Z. B., and Hicke, L. (2007) Ubiquitin binds to and regulates a subset of SH3 domains, *Mol Cell 25*, 273-284.
42. Lange, A., Ismail, M. B., Riviere, G., Hologne, M., Lacabanne, D., Guilliere, F., Lancelin, J. M., Krimm, I., and Walker, O. (2012) Competitive binding of UBPY and ubiquitin to the STAM2 SH3 domain revealed by NMR, *FEBS Lett*.
43. Mayers, J. R., Fyfe, I., Schuh, A. L., Chapman, E. R., Edwardson, J. M., and Audhya, A. (2010) ESCRT-0 assembles as a heterotetrameric complex on membranes and binds multiple ubiquitinylated cargoes simultaneously, *J Biol Chem*.
44. Wollert, T., and Hurley, J. H. (2010) Molecular mechanism of multivesicular body biogenesis by ESCRT complexes, *Nature 464*, 864-869.
45. Ren, X., and Hurley, J. H. (2010) VHS domains of ESCRT-0 cooperate in high-avidity binding to polyubiquitinated cargo, *EMBO J*.
46. Agromayor, M., Soler, N., Caballe, A., Kueck, T., Freund, S. M., Allen, M. D., Bycroft, M., Perisic, O., Ye, Y., McDonald, B., Scheel, H., Hofmann, K., Neil, S. J., Martin-Serrano, J., and Williams, R. L. (2012) The UBAP1 subunit of ESCRT-I interacts with ubiquitin via a SOUBA domain, *Structure 20*, 414-428.
47. Hurley, J. H. (2011) Nipped in the bud: how the AMSH MIT domain helps deubiquitinate lysosome-bound cargo, *Structure 19*, 1033-1035.

Table 1. Kinetic Parameters of AMSH Mutants

[a]No observed activity up to 10 μM of protein per 20 μL reaction over 4 hours at 20°C.

Site	Protein	k_{cat} x 10^{-3} (s^{-1})	K_M (μM)
	Wild type	1400 ± 100	32 ± 5
Active site			
	Glu280Ala	NA[a]	NA[a]
	Cys282Ala	230 ± 140	45 ± 7
	Ser345Ala	1.4 ± 0.1	38 ± 15
	Asp348Ala	NA[a]	NA[a]
	Asp348Asn	NA[a]	NA[a]
Proximal			
	Thr341Ala	24 ± 1	15 ± 3
	Phe343Ala	5 ± 3	21 ± 4
	Ser346Ala	13 ± 3	23 ± 8
	Phe395Ala	22 ± 8	18 ± 9
Distal			
	Asn312Ala	430 ± 60	19 ± 2
	Thr313Ala	2600 ± 600	82 ± 5
	Glu316Ala	19 ± 4	31 ± 9
	Glu317Ala	750 ± 200	19 ± 7
	Phe320Ala	370 ± 20	98 ± 15
MIC-CAP			
	Thr313Ile	225 ± 39	21 ± 5

Protein	Titrant	K_D (μM)	ΔH (kcal.mol^{-1})	ΔS (cal.mol^{-1}.K^{-1})	N
AMSH	Ub	19 ± 3	19.3 ± 7.8	86.4	1
AMSH	DiUb	19 ± 4	13.7 ± 1.8	67.7	1
AMSHF320A	Ub	81 ± 15	2.6 ± 0.4	27.5	1
AMSH	SH3	1.4 ± 0.04	-15.1 ± 0.1	-23.7	1
AMSH	UIM-SH3	1.9 ± 0.1	-15.8 ± 0.1	-26.9	1
AMSHK238A	SH3	NA[a]	NA[a]	NA[a]	NA[a]
AMSHK238T	SH3	NA[a]	NA[a]	NA[a]	NA[a]
SH3	Ub	62 ± 7	-4.1 ± 0.2	5.3	1
UIM-SH3	Ub	273 ± 16	-18.2 ± 1.0	-44.7	2
UIM-SH3	DiUb	54 ± 21	-13.0 ± 6.6	-23.9	1

Table 2. Thermodynamic Parameters Deduced from ITC Data

[a]No observed binding at 50 μM of enzyme and 1 mM of UIM-SH3

Figure Legends

Figure 1. The DUB domain of AMSH. (a) Ribbon diagram of the crystal structure of the catalytic domain of AMSH (PDB ID: 3RZU). The active site is highlighted by the black square. (b) An expanded view of the active-site residues of AMSH. The black spheres represent Zn^{2+}, and the red sphere the active-site water molecule.

Figure 2. Residues involved in proximal ubiquitin recognition within the catalytic domain of AMSH. AMSH residues are shown as pink sticks, proximal ubiquitin residues as green sticks, and the distal ubiquitin residues as cyan sticks.

Figure 3. Residues involved in distal ubiquitin recognition within the catalytic domain of AMSH. AMSH residues are shown as pink sticks, proximal ubiquitin residues as green sticks, and the distal ubiquitin residues as cyan sticks.

Figure 4. Isothermal titration calorimetry (ITC) thermograms of ubiquitin binding to the catalytic domain of AMSH. (a) ITC thermogram of ubiquitin binding to the catalytic domain of AMSH revealing a K_D of 19 ± 3 μM. (b) ITC thermogram of Lys63-linked diubiquitin binding to the catalytic domain of AMSH revealing a K_D of 19 ± 4 μM. (c) ITC thermogram of a Phe320Ala mutant of the catalytic domain of AMSH binding to ubiquitin revealing a K_D of 81 ± 15 μM.

Figure 5. c(s) distributions of the catalytic domain of AMSH binding to (a) the SH3 domain of STAM and (b) UIM-SH3. Three concentration series were used to assess the formation of the

AMSH:SH3 and AMSH:UIM-SH3 complexes revealing 1:1 complexes at 2.5S and 2.6S, respectively. Excess SH3 and UIM-SH3 are present at 1.3S. The data for both c(s) distributions were normalized to the peak area of the complexes. (C) Overlay of AMSH, AMSH:SH3, and AMSH:UIM-SH3 revealing changes in s-value of the AMSH:SH3 and AMSH:UIM-SH3 complexes compared to AMSH alone at 2.2S. The c(s) distributions were normalized to the peak area of the complexes.

Figure 6. ITC thermograms of ubiquitin binding to UIM-SH3 of STAM. (a) Thermogram of ubiquitin binding to UIM-SH3 revealing a K_D of 273 ± 16 μM. (b) Thermogram of ubiquitin binding to the SH3 domain of STAM revealing a K_D of 62 ± 7 μM. (c) Thermogram of Lys63-linked diubiquitin binding to UIM-SH3 revealing a K_D of 54 ± 21 μM.

Figure 7. DUB activity assay by monitoring diubiquitin cleavage. SDS-PAGE gel comparing the activity of the catalytic domain of AMSH alone and in the presence of the SH3 domain and UIM-SH3 of STAM. Only the lane with UIM-SH3 reveals activation. The asterisk indicates ubiquitin contamination in the diubiquitin purification.

Figure 8. Catalytic activation of AMSH in presence of UIM-SH3. (a) Domain diagram of the minimal AMSH and STAM proteins, indicating the locations of the introduced mutations. (b) SDS-PAGE investigating the effects of mutants on the catalytic activation of AMSH. Only in the presence of the wild-type enzyme and wild-type UIM-SH3 is the activity of AMSH enhanced, indicated by complete disappearance of the diubiquitin substrate (black arrow). All lanes have Lys63-linked diubiquitin.